Next-Gen Runway Capacity Modelling

An evaluation of Time-Based Separation and RECAT-EU-PWS across Spanish airports

Álvaro Lanza Rausell

Delft University of Technology

TU Delft

Next-Gen Runway Capacity Modelling

An evaluation of Time-Based Separation and RECAT-EU-PWS across Spanish airports

by

Álvaro Lanza Rausell

to obtain the degree of Master of Science

at the Delft University of Technology,

to be defended publicly on Friday May 8, 2026 at 13:00.

Student number:	5067251	
Project duration:	June 17, 2025 – May 8, 2026	
Thesis committee:	Dr. A. Bombelli	TU Delft, Chair
	Dr. M.J. Ribeiro	TU Delft, External Examiner
	Ir. P.C. Roling	TU Delft, Supervisor
	Ir. M. de Bernardo Atienza	INECO, Supervisor

Cover:	Created by the author using Gemini 3 Flash
Style:	TU Delft Report Style, with modifications by Daan Zwaneveld

An electronic version of this thesis is available at `http://repository.tudelft.nl/`.

TU Delft

Preface

Coincidence or not, at the time of writing this preface in mid-April 2026, it has been exactly seven years since I received one of the most important emails of my life: I had passed the entrance exams and been admitted to study Aerospace Engineering at TU Delft, one of the world's leading universities in the field.

Back then, I could never have imagined all the wonderful people I would meet along the way. Friends, professors, teaching assistants, colleagues... this journey has given me far more than I ever expected, and I could not be happier that I made that decision years ago.

Looking back on all this time, I can confidently say that studying abroad, and especially studying in Delft, has been the experience of a lifetime. Yes, there was hard work, constant pressure, and the challenge of always trying to do our best. But thanks above all to the friends I made there, it could not have been more enjoyable. It would be impossible to mention everyone, but I would especially like to thank Marco, Paula, Juan, Paloma, Diego, Paola, Mikel and Mario for their support and for all the memories we have shared. Whether it was long days (and nights) studying together in the library or pulse, having " a few " beers at Bouwpub or ID, wandering through the food stalls at Markt Square on a random Thursday, clubbing untill sunrise at one of the many Fiesta Macumbas we went to, enjoying a sunny day in Scheveningen, or travelling together, every moment became special because of the people I shared it with. No matter where life takes us, I know we will always be able to count on one another.

I have to express my sincere gratitude to all the lecturers and professors who guided us throughout these years. In particular, I would like to thank Marta Ribeiro and Alessandro Bombelli for agreeing to be part of my graduation committee. I would also like to say a very big thank you to my university supervisor, Paul Roling, not only for his guidance, the learning, and the many interesting conversations we shared during our bi-weekly meetings, but also for planting the seed of my interest in airports a few years ago, when I took part in the "Airport of the Future" minor, which he coordinated. That interest grew strong enough for me to choose airport planning for my internship and, ultimately, this topic for my master's thesis, truly closing the circle.

I would also like to thank everyone I had the pleasure of meeting during my time at the company: colleagues, friends and supervisors. Throughout my internship and thesis, I had the opportunity to work on very interesting and exotic projects that greatly enriched my experience. Beyond the professional experience, I will always remember the personal moments we shared: the "endless" afterworks, the very interesting conversations about any topic during breakfast, the laughs, and even that adventure trip to Melilla with work friends. All of these moments made my time at the company very fun and memorable. I am especially thankful to Miguel de Bernardo for kindly and generously accepting the role of company supervisor, and for all his support throughout this project. He was also one of my supervisors during my internship at INECO, and I cannot fully express how much I have learned from him. In many ways, Miguel has been the bridge between my first professional experience and the final stage of my university journey.

My thanks also go to my friends from Valencia, from summer, from Ribadesella, and from Madrid, for putting up with me during this thesis process, even when we saw each other less and I was often worried or stressed.

I am also grateful to those experts who directly helped me with this thesis, providing with their invaluable knowledge in the topic. Thanks to Javier Vázquez, Jaime del Molino and Massimiliano Zanin.

To my family, my cousins, uncles and aunts: thank you for your constant support, encouragement, and love.

Finally, thank you to my father and mother. For everything. For teaching me never to give up. For showing me how to endure and keep going. For making me grow into the man (and engineer) I am today. For buying me toy airplanes when I was a kid. For all those hours spent near airports while your son took photos of some exotic aircraft from who knows where. For giving me the opportunity to leave Spain and study in one of the best places I could have dreamed of. For being two role models I have always looked up to with admiration and inspiration. Above all, for your endless love and affection. Gracias Papá. Gracias Mamá.

Álvaro Lanza Rausell
Delft, April 2026

Abstract

As airports approach the limits of their runway systems, increasing capacity through infrastructure expansion is not always feasible due to economic, environmental, and operational constraints. Consequently, there is growing interest in operational measures that improve the use of existing infrastructure. Two such concepts are Time-Based Separation (TBS), which reduces the loss of arrival capacity due to headwinds by dynamically adjusting separations, and RECAT-EU-PWS, which refines wake turbulence separation minima through a more detailed pairwise categorisation scheme. However, no openly available macro-level analysis currently evaluate the capacity gains associated with these concepts across different airport environments and operating conditions.

This thesis investigates to what extent the implementation of TBS and RECAT-EU-PWS can increase airport peak runway capacity. To address this question, ARCAS (Airport Runway Capacity Assessment Software) was developed as a discrete-event simulation model in Python. The model builds on previous runway dependency logic and was implemented in a flexible and modular framework capable of representing multiple runway configurations, traffic mixes, weather conditions, and separation schemes. Embedded within a Monte Carlo approach, ARCAS estimates peak capacity, generates capacity envelopes, and evaluates the effects of TBS and RECAT-EU-PWS under a range of representative scenarios.

The model was applied to several Spanish airport case studies representing single mixed, parallel segregated, intersecting, and converging/diverging runway systems. Verification and validation showed that the model provides a credible macro-level representation of runway performance, with Monte Carlo estimates stabilising at around 500 runs and peak-capacity deviations of up to 2% in when compared to other runway capacity models.

The results show that runway capacity is limited by different dominant bottlenecks depending on runway configuration. In single mixed and parallel segregated runways, the main drivers are traffic composition and weather, with the proportion of heavy aircraft emerging as the most significant source of capacity loss and headwind also exerting a strong influence. In intersecting and converging runway systems, by contrast, the dominant constraints are runway geometry and runway-blocking constraints. TBS was found to be technically beneficial only above configuration dependent headwind thresholds, with meaningful gains appearing at approximately 12 kts for single mixed runways, 4 kt for parallel segregated systems, 15 kts for intersecting layouts, and 25 kts for converging layouts. RECAT-EU-PWS likewise showed scenario specific effects: in single mixed operations, gains were observed across the entire analysed range of heavy aircraft shares, while in parallel segregated, intersecting, and converging layouts, meaningful benefits emerged only above heavy-aircraft shares of approximately 11%, 5%, and 5%, respectively.

A limitation of this work is that the analysis is intentionally restricted to a macro-level, runway-centred assessment of TBS and RECAT-EU-PWS. The current framework adopts a fixed categorical implementation of the 20-category wake turbulence scheme, does not explicitly represent complementary concepts such as ROCAT, and considers meteorological effects mainly through headwind conditions in the application of TBS. In addition, the model evaluates runway throughput once aircraft are already established in the approach stream, without accounting for upstream sequencing concepts such as Point Merge. The case-study validation is also limited to several Spanish airports, which can constrain the generalisation of the results, particularly for the intersecting-runway case where the selected scenario is not fully representative of typical operations. Finally, although the datasets used are of generally high quality, some parameters, such as departure runway occupancy times and departure speed profiles, had to be derived from previous work rather than obtained directly from local operational data.

Acronyms

ACC	Area Control Center
AENA	Aeropuertos Españoles y Navegación Aérea
AIAA	American Institute of Aeronautics and Astronautics
ANS	Air Navigation Services
ANSP	Air Navigation Services Provider
ARCAS	Airport Runway Capacity Assessment Software
ASDA	Accelerate-Stop Distance Available
ASMA	Arrival Sequencing and Metering Area
ATC	Air Traffic Control
ATIS	Automatic Terminal Information Service
ATM	Air Traffic Management
DBS	Distance-Based Separation
DC	Declared Capacity
DES	Discrete Event Simulation
FAA	Federal Aviation Authority
FAF	Final Approach Fix
FTDi	Final Target Distance indicator
IAF	Initial Approach Fix
IAT	Inter Arrival Time
IATA	International Air Transport Association
ICAO	International Civil Aviation Organization
IDT	Inter Departure Time
IFR	Instrument Flight Rules
ILS	Instrument Landing System
IMC	Instrumental Meteorological Conditions
INECO	Ingeniería y Economía del Transporte
LOS	Level Of Service
LVNL	Luchtverkeersleiding Nederland
LVP	Low Visibility Procedures
LDA	Landing Distance Available
MAP	Missed Approach Point
METAR	Meteorological Aerodrome Report
MMC	Marginal Meteorological Conditions
mov	Movements
MRS	Minimum Radar Separation
MTC	Maximum Throughput Capacity
MTOM	Maximum Takeoff Mass
MTOW	Maximum Takeoff Weight
NOZ	Normal Operating Zone
NTZ	No Transgression Zone
ops	Operations

PAOAS	Parallel Approach Obstacle Assessment Surface
PHC	Peak Hourly Capacity
PICAP	Programa de Investigación de Capacidad de Pistas
POH	Pilot's Operating Handbook
RCAP	Runway Capacity Discrete Event Simulation
RECAT	European Wake Vortex Recategorisation
RECAT-EU-PWS	European Pairwise Wake Vortex Recategorisation
RMC	Roll Moment Coefficient
ROCAT	Optimised Runway Occupancy Time Spacings for Arrivals
ROT	Runway Occupancy Time
RSC	Runway System Capacity
RVR	Runway Visual Range
RWC	Reasonable Worst-Case (conditions)
RWY	Runway
SBR	Standard Busy Rate
SC	Sustainable Capacity
SESAR	Single European Sky ATM Research
SID	Standard Instrument Departure route
TAS	True Airspeed
TBS	Time-Based Separation
THR	Threshold
TODA	Take-Off Distance Available
TORA	Takeoff Run Available
TPHP	Typical Peak-Hour Passenger
TRB	Transportation Research Board
TWR	Tower
VFR	Visual Flying Rules
VMC	Visual Meteorological Conditions
WISA	Wake Impact Severity Assessment
WMO	World Meteorological Organization
WTC	Wake Turbulence Category
WVE	Wake Vortex Encounter

Contents

Part I

Scientific Paper

Enhancing runway capacity: A Discrete-Event Simulation evaluation of Time-Based Separation and RECAT-EU-PWS

Álvaro Lanza Rausell* and Paul C. Roling†
Faculty of Aerospace Engineering, Delft University of Technology, the Netherlands

Miguel de Bernardo Atienza‡
Department of Planning and Sustainable Mobility, INECO, Madrid, Spain

As airports approach the capacity limits of their runway systems, increasing capacity through infrastructure expansion is not always feasible because of economic, environmental, and operational constraints. This creates strong interest in operational techniques that improve the use of existing infrastructure. Two procedures are especially relevant in this context: Time-Based Separation (TBS), which mitigates headwind-related arrival capacity loss by dynamically adjusting approach spacing, and RECAT-EU-PWS, which replaces broad wake turbulence categories with more detailed pairwise separation minima. Despite their practical relevance, openly available macro-level studies comparing the capacity gains from these solutions across different airport environments remain limited.

This paper investigates to what extent the implementation of TBS and RECAT-EU-PWS can increase airport peak runway capacity. To do so, ARCAS (Airport Runway Capacity Assessment Software) was developed as a discrete-event simulation model in Python. The model builds on earlier runway dependency logic and was implemented in a flexible modular framework able to represent multiple runway configurations, traffic mixes, weather conditions, and separation schemes. ARCAS estimates peak runway capacity, generates capacity envelopes, and evaluates the effects of TBS and RECAT-EU-PWS under several representative operational scenarios.

Verification and validation using Spain's busiest airports showed that the model provides a credible macro-level representation of peak runway capacity, with peak-capacity deviations of up to 2% relative to compared models. Results show that the dominant runway bottlenecks differ substantially by layout. In single mixed and parallel segregated systems, the main drivers are fleet composition and wind, with heavy-aircraft share producing the greatest capacity loss and headwind exerting a strong secondary influence. In intersecting and converging systems, by contrast, the primary limitations are geometric and blocking constraints between runways. TBS is beneficial only above configuration-dependent headwind thresholds, with benefits appearing under comparatively moderate headwind conditions in segregated layouts but requiring substantially stronger winds in more constrained runway systems such as converging or intersecting. RECAT-EU-PWS similarly produces capacity gains dependent on runway layout and traffic, with some configurations benefiting across a broad range of heavy-aircraft shares and others only when the proportion of heavy aircraft becomes sufficiently high.

Overall, TBS and RECAT-EU-PWS should not be treated as universal capacity solutions, but as airport-specific deployment options. Each Air Navigation Services Provider should first assess the dominant runway bottlenecks, local wind exposure, and fleet-mix characteristics of the airports it manages in order to determine whether TBS, RECAT-EU-PWS, or a combination of both would increase peak runway capacity.

*MSc student, Air Transport Operations
†Lecturer / researcher, Air Transport Operations. AIAA member
‡Senior Airport Planner

I. Nomenclature

A	=	arrival
D	=	departure
c_i, c_j	=	wake or aircraft category of follower aircraft i and leader aircraft j
$\bar{c}$	=	controller communication buffer
$D(\cdot,\cdot)$	=	common-path distance function for a SID pair
D_D	=	common-path distance between two consecutive departures
D_{ij}	=	applicable RECAT-EU-PWS arrival separation distance for leader–follower pair (i, j)
D_{MAP}	=	missed-approach protection distance
D_{MIN}	=	minimum blocking-distance parameter used in coupled-runway constraints
G_{ij}	=	baseline wake-turbulence time separation for departure leader–follower pair (i, j)
G_{ij}^{SID}	=	effective SID-dependent time separation
$G_{ij}^{\text{SID,same}}$	=	SID-dependent time separation for two consecutive departures assigned to the same SID
$G_{ij}^{\text{SID,diff}}$	=	SID-dependent time separation for two consecutive departures assigned to different SIDs
H	=	headwind component
$IADT$	=	inter-arrival-departure time
$IDAT$	=	inter-departure-arrival time
IDT_{ij}	=	inter-departure time between leader j and follower i
R_A	=	arrival runway occupancy time
R_D	=	departure runway occupancy time
$R_{D,j}$	=	runway occupancy time of leading departure j
$R_{A,int}$	=	runway occupancy time of arrival until intersection
$R_{D,int}$	=	runway occupancy time of departure until intersection
$R_{A,com}$	=	runway occupancy time of arrival until touchdown
s_i, s_j	=	SID assigned to follower aircraft i and leader aircraft j
S_{ij}	=	required distance-based separation between leader j and follower i
S_{ij}^{base}	=	baseline arrival wake-separation distance under distance-based separation
S_{ij}^{TBS}	=	headwind-adjusted arrival separation distance under TBS
t_i	=	threshold-crossing time of leader aircraft i
$t_j^{\min}$	=	earliest feasible threshold-crossing time of follower aircraft j
t_{A_i}	=	threshold-crossing time of leading arrival i
$t_{A_j}^{\min}$	=	earliest feasible threshold-crossing time of following arrival j
v	=	time-equivalent spacing imposed by common-path departure coupling
V_i	=	ground speed of leader aircraft i on final approach
$V_{D,i}$	=	departure ground speed i
$V_{j,\text{adj}}$	=	headwind-adjusted approach ground speed of follower aircraft j
$V_{j,\text{nom}}$	=	nominal approach speed of follower aircraft j

II. Introduction

Global demand for air travel continues to grow, and Spain reflects the same trend. IATA reports that worldwide passenger traffic in 2025 rose by 5.3% compared with 2024 and exceeded pre-pandemic 2019 levels by 9.3%. In Spain, Aena recorded 321 million passengers in 2025, a 4% increase over 2024. This figure is expected to almost double up to 600 million annual passengers by 2050. Both short-term outlooks and long-term projections all point towards the same direction: continued growth.

As airports move towards the limits of their runway systems, there is a clear need to increase effective runway capacity. In principle, this can be achieved either through infrastructure expansion, such as the construction of new runways and exit taxiways, or through operational and procedural changes that extract more throughput from the existing infrastructure [1]. In practice, large infrastructure projects are often constrained by cost, land availability, environmental impact, and politics. For that reason, procedures that maximise the use of current runway infrastructure are increasingly important in airport planning and air traffic management.

Literature shows that runway capacity is not a fixed number but the outcome of several interacting factors. These include runway layout and geometry, runway mode of operation, weather conditions, aircraft performance, fleet mix, and ATC procedures [1, 2]. Across these factors, one of the most important operational bottlenecks is the wake vortex separation that must be maintained between leading and following aircraft. Wake turbulence separation, radar minima, runway occupancy times, and runway-crossing constraints all influence how closely successive movements can be scheduled and therefore directly affect peak throughput.

Two procedures are particularly relevant in this context. The first is Time-Based Separation (TBS), which aims to preserve landing throughput under varying headwind conditions by replacing fixed Distance-Based Separation (DBS) on final approach with equivalent time spacing derived from zero wind conditions [3]. Under conventional distance-based separation, stronger headwinds reduce aircraft ground speed and therefore increase the time interval between successive arrivals, lowering runway throughput even when wake safety margins are unchanged. TBS mitigates that mechanism and is therefore especially relevant for improving capacity resilience in poor wind conditions.

The second is RECAT-EU-PWS, a refined wake-turbulence categorisation and static pairwise wake turbulence scheme developed to reduce the over-conservatism embedded in the legacy ICAO wake categories [4]. By distinguishing aircraft more precisely and assigning separation minima at a more granular pairwise level, RECAT-EU-PWS can reduce unnecessary spacing for certain leader and follower combinations while maintaining safety. Its potential value is particularly relevant at airports where wake-related separations form a substantial share of the active runway bottleneck.

Despite the relevance of these two methods in maximising peak runway capacity, there are no openly available macro-level analyses describing the extent to which these are effective.

This paper proposes a new runway capacity model, ARCAS, which is based on the runway dependencies identified by van der Klugt [5], and extended by incorporating SID sequencing, TBS, and RECAT-EU-PWS functionality within a common simulation framework. ARCAS is implemented as a discrete-event simulation model in Python and is designed to evaluate peak runway capacity across multiple runway configurations, traffic mixes, wake categorisation schemes and weather conditions.

The research question addressed in this paper is therefore: ***To what extent can the implementation of Time-Based Separation and the wake categorisation scheme RECAT-EU-PWS increase an airport's peak runway capacity?*** The analysis answers this question through representative Spanish airport case studies covering single mixed, parallel segregated, intersecting, and converging/diverging runway systems.

The remainder of the paper is structured as follows. Section III covers the current state of the art of runway capacity methods. Section IV presents the ARCAS model and its simulation architecture. Section V summarises the methodological approach and explains how TBS and RECAT-EU-PWS are represented. Section VI introduces the case scenarios. Section VII discusses the main results, with emphasis on TBS improvement by configuration, RECAT-EU-PWS implementation thresholds, and sensitivity analysis. Section VIII concludes the paper, and Section IX provides recommendations for future work.

III. State of the Art

The state of the art in runway capacity assessment has evolved from simplified deterministic approximations toward simulation-based and data-driven approaches capable of representing the stochastic and context-specific nature of airport operations. Early research focused on analytical and queueing-based formulations of runway throughput, with foundational work by Blumstein [6] and Newell [7] establishing the relationship between separation minima, runway occupancy, demand, and delay. As aviation demand increased and airport systems became more complex, practical "fast planning" tools such as the FAA lookup table and spreadsheet [8] were developed to provide fast, standardized estimates for common runway configurations. These table-based tools remain useful for preliminary planning, but their applicability is limited by fixed assumptions regarding traffic mix, runway layout, and meteorological conditions.

Subsequent research introduced more advanced analytical and empirical methods. Analytical models improved fidelity by incorporating aircraft performance, ATC rules and runway geometry [9, 10]) and weather dependence[11]. Empirical approaches such as Gilbo's Pareto frontier [12] and later censored-regression models attempted to infer capacity directly from observed operations [13] . These methods improved understanding of the feasible region of arrival and departure tradeoff and the effects of operational factors, but they generally remain constrained when multiple interacting

dependencies must be represented simultaneously, particularly under unsaturated demand or highly airport-specific operating conditions.

On the other hand, simulation models can reproduce detailed aircraft operations within the airfield and surrounding airspace [14, 15]. DES is particularly suitable for runway capacity modelling because runway operations are event-driven and resource-constrained: aircraft arrive, land, vacate, line up, and depart according to sequencing rules, separation constraints, and runway availability [16]. Examples of commercial and research tools include SIMMOD [17, 18] and RCAP 1.0 [5] and 2.0 [19]. Compared with other methods, these models can simulate local runway dependencies, mixed arrival–departure interactions, traffic variability, fleet heterogeneity, and stochastic delay formation more realistically.

Table 1 summarizes the abovementioned runway capacity models from classifies them by type: table-based, analytical, simulation, or empirical.

Table 1 Literature overview

Model	Year	Table-Based	Analytical	Simulation	Empirical
Blumstein [6]	1959		✓		
SIMMOD [17]	1978			✓	
Newell [7]	1979		✓		
FAA Lookup Table [8]	1983	✓			
FAA Spreadsheet [8]	1983	✓			
Gilbo [12]	1993				✓
Lee et al. [20]	1998		✓		
TAAM [18]	1998			✓	
Hansen [21]	2004				✓
AIRTOP	2006			✓	
TRB ACS [22]	2012	✓			
Kicinger et al. [11]	2012		✓		
RCAP 1.0 [5]	2012			✓	
Kim et al. [13]	2015				✓
RCAP 2.0 [19]	2016			✓	
Di Mascio et al. [23]	2020		✓		
Cheung et al. [9]	2021		✓		

Literature also shows that runway capacity does not solely depend on a single factor, but is instead the outcome of several interdependent operational factors. These include runway mode of operation, runway system geometry, meteorological conditions, wake turbulence separation requirements, aircraft performance, fleet mix and Runway Occupancy Time (ROT) [5]. Among these, one of the most important bottlenecks is aircraft separation. Capacity is strongly constrained by the minimum spacing that must be maintained between leader and a follower aircraft, whether in distance or time, on approach or departure. Wake turbulence separations are especially important in this regard, because they directly govern how closely aircraft of different types can be sequenced on arrival or departure while preserving safety [24].

Recent advances in the field therefore focus not only on modelling runway systems more accurately, but also on improving operational efficiency through enhanced separation techniques. Two of the most relevant are Time-Based Separation, TBS, and RECAT-EU-PWS. TBS addresses the loss of arrival capacity under headwind conditions by replacing fixed distance minima with time-equivalent separations, thereby obtaining a more constant runway throughput in poor wind conditions [3]. RECAT-EU improves on previous ICAO and RECAT-EU wake categories by using a more refined scheme which can be applied based on 20 different categories or even at a pairwise level. This increased granularity reduces unnecessary conservatism for many leader and follower pairs and thus reduces wake separation of frequent aircraft pairs, which increases capacity [4].

IV. Simulation Model

ARCAS was developed to provide a macro-level assessment of peak runway capacity under different runway configurations and separation concepts. The model focuses on the runway system rather than full gate-to-gate airport performance: aircraft are assumed to already be established in the arrival and departure streams, and the objective is to estimate feasible runway schedules subject to same-runway and cross-runway constraints.

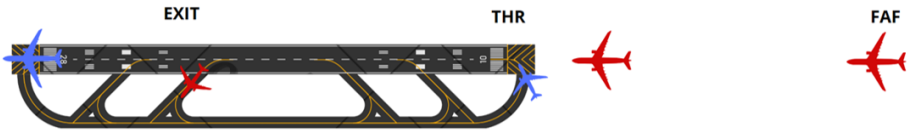

Fig. 1 DES representation of runway operations

The model is implemented as a discrete-event simulation, in which runway operations are represented by the key events at which constraints become active. The discrete-event simulation model is structured around two operational queues: an arrival queue and a departure queue. Figure 1 shows this discretized sequence. For arrivals (depicted as red aircraft), the Final Approach Fix (FAF) serves as the generator and the point at which aircraft enter the sequence. The next event is the aircraft crossing the threshold (THR), just before touchdown. The final event, or sink, is EXIT, where the aircraft vacates the runway via an exit taxiway. In specific runway layouts where blocking constraints make it necessary, two more events are added to the simulation: aircraft touch-down, and aircraft crossing the intersection with other runway.

The departure sequence begins at the threshold, where the aircraft initiates its take-off roll (the generator), and ends when the aircraft rotates and climbs out of the runway (the sink). This process is depicted in Figure 1 as blue aircraft. Again, if the departure sequence includes intersection or time blocking constraints, a third event where the departing aircraft crosses an intersecting runway is added. Aircraft movement through STARs and IAF is not simulated. Movement through SIDs is not simulated but considered to produce more realistic departure separations. Between such events, the system state is assumed unchanged [16]. This approach is well suited to runway-capacity analysis because throughput depends primarily on the timing relationships between successive operations.

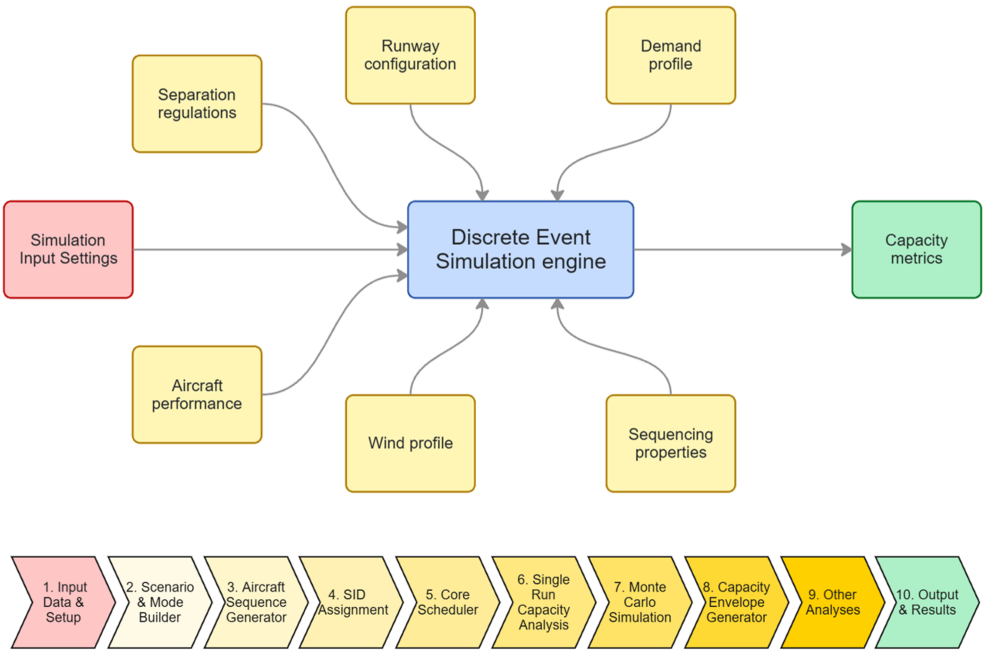

Fig. 2 ARCAS general working

As shown in Figure 2, each run starts from a scenario definition containing runway layout, mode of operation, separation scheme, fleet composition, wind assumptions, and operational parameters such as runway occupancy times, missed-approach protection distances, and common-path distances. The model then generates arrival and departure sequences and passes them to a scheduler that constructs the earliest feasible timetable while respecting all applicable constraints. The same parameter structure is used across single mixed, parallel segregated, intersecting, and converging/diverging runway systems, allowing airport-specific geometry and procedures to be represented without changing the underlying model logic.

The input structure is modular. Depending on the scenario, wake separations are represented either through ICAO-based matrices or by RECAT-EU-PWS pairwise separation data. runway occupancy times and nominal speeds are also included, so that fleet composition affects both wake constraints and runway blocking behaviour. For departure operations, Standard Instrument Departures (SIDs) can be assigned probabilistically, allowing the model to distinguish between same-SID and different-SID interactions where relevant.

A central feature of ARCAS is the stochastic generation of aircraft sequences. Since peak capacity depends not only on average fleet mix but also on the ordering of aircraft, arrivals and departures are repeatedly sampled according to the traffic mix of each scenario. This avoids relying on a single deterministic sequence, which could overestimate or underestimate runway performance.

The scheduler is the core of the model. For each generated sequence, it computes the earliest feasible threshold-crossing and runway-vacated times. In single-runway mixed-mode operations, the next aircraft is scheduled at the earliest time allowed by wake separation and ROT constraints. In multi-runway configurations, additional cross-runway logic is applied to account for dependencies between operations on different runways. This includes, for example, the earliest touchdown time of an arrival following a departure on another runway, or the earliest departure release after a conflicting arrival. For coupled operations, the scheduler compares candidate next movements and applies a short receding-horizon rollout to select the locally most efficient sequencing choice.

To obtain statistically robust capacity estimates, the scheduling process is embedded in a Monte Carlo loop. For each scenario, sequences are regenerated and simulated many times, and the resulting capacities are aggregated. This reduces sensitivity to favourable or unfavourable aircraft sequencing and allows convergence to be checked through the coefficient of variation. For the simulated scenarios, 500 runs were found sufficient for stable estimates.

Beyond single operating points, ARCAS also generates capacity envelopes. For a range of arrival shares, the Monte Carlo procedure is repeated and the resulting arrival and departure throughputs are recorded. This produces an arrival–departure tradeoff curve for each scenario, which is useful because concepts such as TBS and RECAT-EU-PWS do not necessarily affect all operating regimes equally.

The main outputs of the model are peak hourly capacity, arrival and departure throughput, and the capacity envelope of each runway configuration. In addition, the framework supports sensitivity analyses and KPI-based parameter ranking. ARCAS therefore serves not only as a throughput estimator, but also as a diagnostic tool for identifying the dominant bottlenecks in runway performance and for screening the potential benefits of operational concepts before more detailed studies are undertaken.

V. Methods

The methodological framework combines analytical runway-dependency logic with discrete-event simulation. Previously developed dependency relationships from van der Klugt [25] and subsequent work were used as the conceptual basis, and the present contribution extends those relationships into a Python-based flexible simulation environment capable of representing multiple runway configurations, weather assumptions, and separation schemes. Because that prior work already established much of the runway-dependency formulation, this paper does not re-derive every dependency relation in detail. Instead, the focus is placed on how those relationships are integrated into a broader comparative assessment of TBS and RECAT-EU-PWS.

A. Representation of runway operations

In order to represent single, parallel, converging-diverging and intersecting runways, in all of their possible modes of operation and with their interdependencies, the equations developed by van der Klugt [5] are utilized. These equations

determine the scheduling times for both arrival and departure operations on the considered runways while respecting same-runway and cross-runway constraints.

Although the model implemented in RCAP 1.0 already contains some SID (Standard Instrument Departures) modelling, the realism is extended by implementing two different approaches: a Common Path method and a Specific Matrix method. It should be noted that SIDs are not simulated as full trajectories; rather, they are taken into account to determine the additional time spacing required between consecutive departures so that separation is preserved, particularly in cases where a slower leading aircraft may be followed by a faster follower.

The Common Path method links each pair of departure procedures to an effective common-path distance and combines this with the speed differential between leader and follower aircraft, the set of SIDs available on the runway, and their utilisation. Based on this information, the additional buffer time required between consecutive departures is calculated. In contrast, the Specific Matrix method directly embeds SID-related constraints within the departure time-based separation matrix, such that procedure-specific effects are represented as explicit separation requirements.

1. Common Path Method

To represent SID-dependent departure interactions, ARCAS assigns each departure an SID according to a scenario-specific probability distribution. The interaction between two consecutive departures is then determined through a common-path matrix, whose elements specify the shared-route distance between every leader-follower SID pair. For a leading aircraft j and a following aircraft i, this is written as

$$D_D = D(s_j, s_i) \tag{1}$$

where $D(\cdot, \cdot)$ is the SID-pair matrix and D_D denotes the distance over which both departures remain coupled before diverging. If no airport-specific SID matrix is available, a default common-path distance may be adopted.

The inter-departure time is governed by runway occupancy, wake-turbulence separation, and the additional spacing required along the shared departure path. It is defined as

$$IDT_{ij} = \max\left(R_{D,j},\ G_{ij},\ v\right) + \bar{c} \tag{2}$$

where $R_{D,j}$ is the runway occupancy time of the leading departure, G_{ij} is the applicable wake-turbulence time separation, $\bar{c}$ is a controller communication buffer, and v is the time-equivalent spacing imposed by the common path.

Let S_{ij} denote the required distance-based separation and $V_{D,j}$, $V_{D,i}$ the ground speeds of the leading and following aircraft. Then

$$v = \begin{cases} \dfrac{S_{ij}}{V_{D,j}}, & D_D \le S_{ij} \text{ or } V_{D,j} \ge V_{D,i} \\ \dfrac{D_D}{V_{D,j}} - \dfrac{D_D - S_{ij}}{V_{D,i}}, & D_D > S_{ij},\ V_{D,j} < V_{D,i} \end{cases} \tag{3}$$

This formulation allows the model to capture how different SID combinations influence departure spacing and runway throughput without explicitly simulating trajectories after take-off.

2. Specific Matrix Method

As an alternative to the common-path method, ARCAS can represent SID effects through airport specific departure time-separation matrices. This approach assumes that the local ANSP has already embedded SID interactions into calibrated departure separations, so that no explicit common path distance needs to be modelled. SID effects are therefore introduced directly through separation matrices instead of through a common-path term. This is the approach commonly applied in Spanish airports.

Let

$$G_{ij} = G(c_j, c_i) \tag{4}$$

denote the baseline departure wake-turbulence time separation for a leader-follower category pair (c_j, c_i). In addition,

two airport-specific SID-aware matrices are defined:

$$G_{ij}^{\text{SID,same}} = G^{\text{SID,same}}(c_j, c_i) \tag{5}$$

$$G_{ij}^{\text{SID,diff}} = G^{\text{SID,diff}}(c_j, c_i) \tag{6}$$

where the first applies when two consecutive departures follow the same SID, and the second when they follow different SIDs.

Given the SID labels s_j and s_i of the leader and follower, the effective SID-dependent separation is selected as

$$G_{ij}^{\text{SID}} = \begin{cases} G_{ij}^{\text{SID,same}}, & s_j = s_i \\ G_{ij}^{\text{SID,diff}}, & s_j \neq s_i \end{cases} \tag{7}$$

To ensure that these local values never relax the baseline wake-turbulence requirement, the model applies the most restrictive separation:

$$\tilde{G}_{ij} = \max\left(G_{ij},\, G_{ij}^{\text{SID}}\right) \tag{8}$$

The resulting inter-departure time is then

$$IDT_{ij} = \max\left(R_{D,j},\, \tilde{G}_{ij}\right) + \bar{c} \tag{9}$$

where $R_{D,j}$ is the runway occupancy time of the leading departure and $\bar{c}$ is the controller communication buffer.

B. Implementation of Time-Based Separation

Time-Based Separation (TBS) is implemented in ARCAS to represent the reduction in arrival throughput that occurs when fixed distance-based separation is applied under headwind conditions. In conventional distance-based operations, wake minima are expressed in nautical miles and remain constant regardless of wind. However, when aircraft encounter headwind on final approach, their ground speed decreases and the time required to fly a given separation distance increases. As a result, the same nominal wake distance translates into a larger temporal spacing, reducing the achievable arrival rate. TBS addresses this effect by dynamically reducing the applied distance separation so that the resulting time interval remains equivalent to the no-wind reference case. Figures 3 and 4 illustrate both concepts. In the model, this concept is applied exclusively to arrival-arrival interactions; departure separations and mixed arrival-departure constraints are kept unchanged.

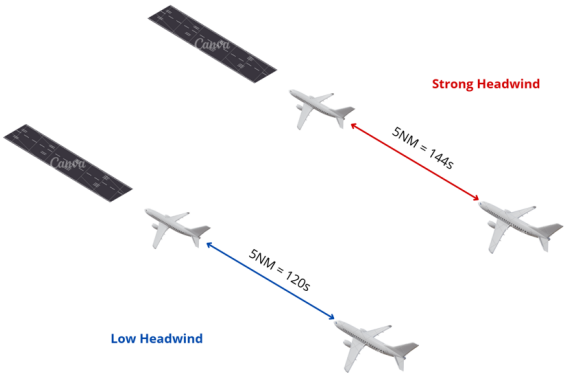

Fig. 3 Distance-Based Separation

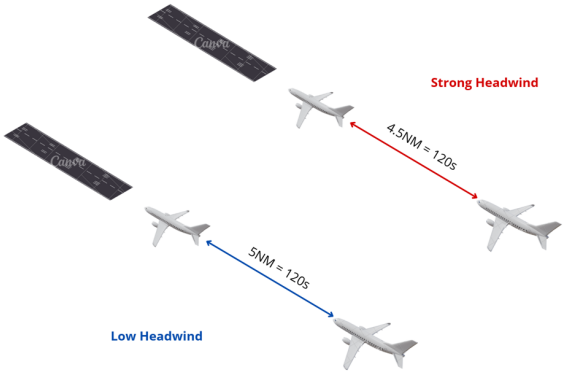

Fig. 4 Time-Based Separation

For each arriving follower aircraft j, the adjusted ground speed is defined as

$$V_{j,\text{adj}} = V_{j,\text{nom}} - H \tag{10}$$

where $V_{j,\mathrm{nom}}$ is the nominal approach speed and H is the headwind component. The baseline wake distance S_{ij}^{base} for leader–follower pair (i, j) is then rescaled as

$$S_{ij}^{\mathrm{TBS}} = S_{ij}^{\mathrm{base}} \frac{V_{j,\mathrm{adj}}}{V_{j,\mathrm{nom}}} \tag{11}$$

so that the wake matrix becomes dynamic and wind dependent. This scaling is applied consistently to both ICAO and RECAT-EU-PWS separation matrices.

The adjusted separation replaces the baseline value throughout the arrival sequencing logic, including threshold spacing, chaining at the final approach fix, and missed-approach protection. The minimum threshold-crossing time for a following arrival is therefore

$$t_{A_j}^{\min} = t_{A_i} + \frac{S_{ij}^{\mathrm{TBS}}}{V_i} 3600 \tag{12}$$

where V_i is the leader ground speed. The formulation assumes steady headwind conditions and does not account for gusts or windshear.

C. Implementation of RECAT-EU-PWS

RECAT-EU-PWS is implemented by replacing the legacy ICAO wake categories with a twenty-category pairwise separation framework. In practical terms, this means that both arrival and departure separations are read from finer-grained separation matrices, allowing the model to represent a much wider range of leader-follower combinations than the ICAO scheme. Each simulated aircraft is assigned a RECAT class together with category-specific performance parameters, including approach and departure speeds and ROTs. The rest of the modelling remains identical to that of ICAO. Arrival separations are defined in nautical miles, whereas departure separations are defined directly in time. To preserve operational realism, any arrival separation below 3 NM is replaced by the Minimum Radar Separation (MRS), which is assumed independent of wake-turbulence effects.

For arrivals, the pairwise wake minimum between leader i and follower j is converted into a threshold-time constraint. If the leader crosses the threshold at time t_i, the earliest feasible threshold time of the follower is

$$t_j^{\min} = t_i + \frac{D_{ij}}{V_i} \cdot 3600 \tag{13}$$

where D_{ij} is the applicable RECAT-EU-PWS distance minimum and V_i is the leader ground speed on final approach. This formulation reflects that wake protection depends on the motion of the leader aircraft. For departures, the RECAT-EU-PWS minima are already time-based and are therefore applied directly within the inter-departure scheduling logic.

Traffic sequences are generated according to a predefined fleet mix associated with the RECAT categories, and the scheduler evaluates feasible arrival and departure times while enforcing wake separations, runway occupancy, SID interactions, and any cross-runway blocking constraints. Capacity is then estimated through repeated Monte Carlo simulation and compared against the corresponding ICAO-based scenarios, with and without TBS. This implementation therefore enables a direct comparison between ICAO and RECAT-EU-PWS under identical runway geometry, traffic mix, and scheduling logic. Aircraft belonging to the same RECAT-EU-PWS category are assumed to share identical performance parameters.

VI. Case Scenarios

Five Spanish airports were selected to cover a broad range of runway layouts, traffic mixes, and operational environments. Alicante-Elche represents the single mixed-runway case. Palma de Mallorca represents a segregated parallel system. Barcelona-El Prat runways 02 and 06R represent an intersecting-runway layout. Madrid-Barajas runways 32R and 36L represent a converging/diverging runway system with partial interdependence between flows. In addition, Tenerife Norte and Palma de Mallorca were used as targeted RECAT-EU-PWS case studies to analyse how modest changes in fleet composition can shift runway capacity.

The selection of Spanish airports is primarily driven by the need for a consistent and reliable basis for model implementation and comparison. Evaluating the impact of Time-Based Separation and RECAT-EU-PWS requires

detailed operational inputs and parameters, that are not always publicly available in a homogeneous format. In this study, such information was provided by ENAIRE for Spanish airports, enabling the modelling framework to be applied with a common data standard across all case studies.

The specific airports were then selected to represent a range of high-traffic conditions and runway configurations. Collectively, they cover four common runway layout categories found at many airports worldwide, which supports the broader relevance of the results beyond the Spanish context. These, together with the most relevant parameters for capacity calculation, are summarized in Table 2.

Table 2 Representative case scenarios

Airport	ICAO Code	Configuration	Runway-limiting parameters
Alicante	LEAL	Single mixed	R_A, R_D, D_{MAP}
Palma de Mallorca	LEPA	Segregated parallel	R_A, R_D, D_{MAP}
Barcelona-El Prat	LEBL	Intersecting A+D	R_A, R_D, D_{MAP}, R_A, int, R_D, int
Madrid-Barajas	LEMD	Converging/diverging A+D	R_A, R_D, D_{MAP}, R_A, com, D_{MIN}
Tenerife-Norte	GCXO	Single mixed	R_A, R_D, D_{MAP}

VII. Results

A. Verification and validation

Verification was conducted through four complementary approaches. First, the code, parameters, and data structures were systematically inspected to identify possible errors in constants, units, matrix definitions, and indexing. Second, individual simulation runs were exported and visually examined using operational timelines and Gantt charts in order to verify sequencing logic, event timing, and the absence of runway conflicts. Third, dedicated verification functions were developed to recalculate selected simulation outputs directly from run variables, allowing the mathematical consistency of the implemented equations to be checked independently of the full simulation process. Fourth, model outputs were compared with those from RCAP 1.0 and, where applicable, ENAIRE's capacity tool PICAP. Throughout all scenarios, peak capacity results kept general consistency with variations around 1% between ARCAS and the other models, reaching a maximum of 2%.

Calculation verification addressed the statistical uncertainty associated with the Monte Carlo approach. Convergence was evaluated through the coefficient of variation of peak hourly capacity as a function of the number of simulation runs. In all four scenarios, the coefficient of variation alternated rapidly during the first iterations and then stabilised, with convergence reached at approximately 500 runs. Figure 5 shows the example for the segregated runways mode. This value was therefore adopted as a tradeoff between computational time and statistical robustness. In most cases, RECAT-EU-PWS showed slightly higher residual variability than the ICAO scheme, likely due to the greater sensitivity introduced by the finer categorisation of aircraft performance and separations. The intersecting-runway case was the only exception, where RECAT-EU-PWS produced slightly more stable outcomes than ICAO.

Validation was performed by comparing the simulated capacity envelopes with observed hourly runway throughput from 2025 operations for the selected airport scenarios. The objective was not to reproduce every observed operating point exactly, but to assess whether the model yields realistic estimates of peak capacity. Because actual throughput may remain below runway capacity due to external constraints such as terminal limitations, stand availability, or surrounding airspace restrictions, the comparison was interpreted as a consistency check rather than a one-to-one fit.

Figure 6 shows the comparison for Palma de Mallorca (ICAO, DBS) scenario in calm conditions. ARCAS (green envelope) and RCAP 1.0 (red envelope) show near-identical capacity envelopes, with identical arrival performance and only marginally higher ARCAS estimates. The PICAP peak capacity point (in yellow) lies close to both envelopes, but still converges to the same value of 95 ops/h as ARCAS. The observed 2024 throughput, represented by the blue crosses, remains below the theoretical frontier, indicating that Palma operates relatively near capacity but still below peak theoretical limits. Differences between the three models remain below 1%.

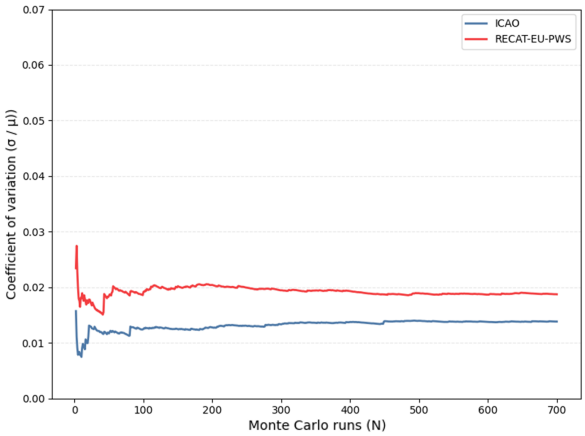

Fig. 5 Coefficient of variation. Segregated runways

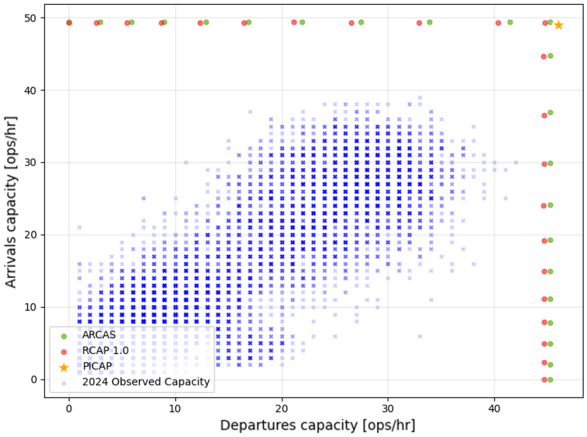

Fig. 6 Palma models & throughput comparison

B. Improvement of TBS by configuration

This section presents the simulation results for the implementation of time-based separation. In the scope of the selected scenarios to represent each of the most common runway geometric layouts, the effectiveness of TBS implementation is mainly affected by two factors: i) each airport's headwind profile and ii) the runway layout and mode of operation. Figure 7 represents the capacity improvement of TBS over DBS throughout multiple headwind speeds across the different runway layouts. It was obtained through 500 Monte Carlo simulations per runway layout scenario and headwind speed. It shows that the effect of TBS differs strongly by runway configuration. This is a central result of this work. As headwind velocity increases, the decaying effect it has on runway capacity becomes greater. As such, TBS, being able to mitigate the negative effect of headwind on runway capacity, should have a greater effect with greater headwinds. The single point on each line represents the heavy-aircraft mix threshold above which TBS yields a capacity gain of at least one additional arrival or departure slot.

For a single mixed runway configuration (represented by Alicante), TBS mainly benefits pure arrivals and balanced operating points because it acts directly on arrival-arrival spacing and only indirectly affects departures through the propagation of inter-arrival-departure times and inter-departure-arrival times.

As headwind increases, total capacity under ICAO gradually deteriorates, whereas TBS partly neutralises that loss. The resulting benefit ranges from 0% to roughly 6%, with realistic meaningful gains emerging only once headwind reaches 12 knots.

In a segregated parallel system, the logic is cleaner because arrivals and departures are effectively de-coupled. Departures remain unchanged, and TBS acts entirely through the arrival flow. Because the runways are independent, the effect of TBS is more direct and meaningful. In the mixed runway case, separation between two arrivals is not as limiting, as when a departure is inserted in between, other time constraints, such as departure ROT, IADT and IDAT can become limiting. This is not seen however in the decoupled segregated case, where the flow of arrivals is not interrupted. This is one of the reasons why TBS shows its best results in this configuration.

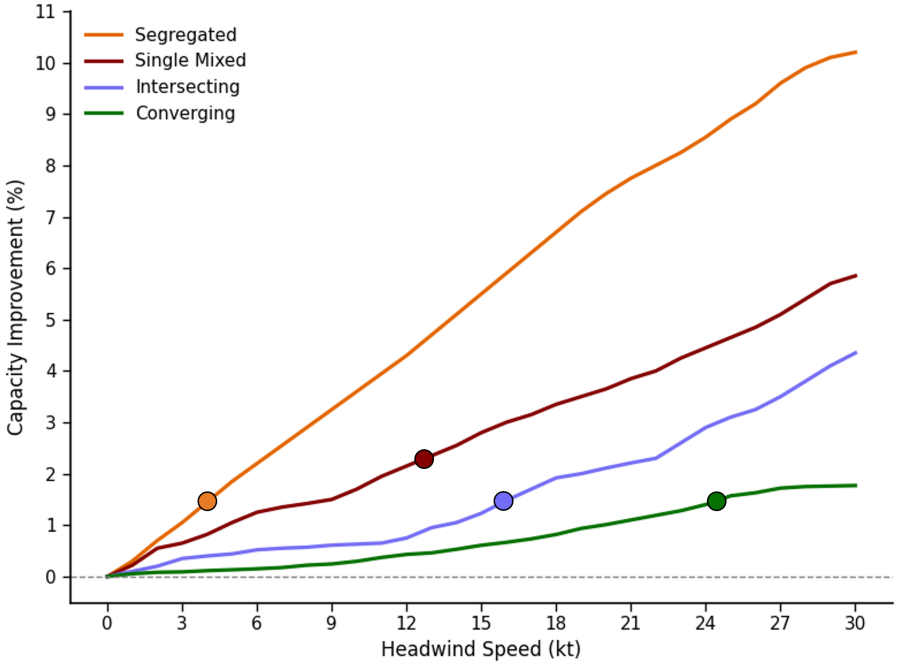

Fig. 7 TBS capacity improvement per runway configuration

As seen in Figure 7, the gain in capacity when implementing TBS can reach up to 11% under a 30 kts headwind, and realistic capacity gains begin to be observed at a headwind speed of 4 kts. This is arguably the clearest best-case deployment setting for TBS within the analysed airports: arrival capacity is weather-sensitive, but there is little geometric coupling to absorb the recovered spacing.

Interestingly, the intersecting runway layout, with dedicated arrivals and departures runways, shows an overall poorer and more inconsistent behaviour, with capacity gains reaching less than 5% at the maximum tested headwind, and realistic capacity increases beginning at a speed of 15 kts.

This lower effectiveness of TBS on increasing capacity is explained by the use of cross-runway blocking constraints, which define forbidden time windows in which departures cannot take place; when an arrival is less than a distance D_{MIN} and until the arrival has crossed the point of intersection. These blocking windows remain largely unaffected by TBS, and as such are still the primary constraints in this type of operation.

A similar situation occurs with the converging open-v runways, modelled through Madrid's runways 32R and 36L. Due to the time-blocking constraints imposed to avoid the interaction between missed approaches and departures on the projected point of intersection of both runways, it shows the lowest practical sensitivity to TBS. The geometry and blocking logic dominate performance, so improvements only become meaningful at much stronger headwinds, around 25 kts.

C. Improvement of RECAT-EU-PWS and implementation thresholds

RECAT-EU-PWS also produces configuration-dependent gains, but the relevant trigger is not headwind; it is traffic composition, especially heavy-aircraft share. In the scope of the selected scenarios to represent each of the most common runway geometric layouts, the effectiveness of RECAT-EU-PWS implementation is mainly affected by two factors: i) each airport's unique traffic composition and ii) the runway layout and mode of operation.

Figure 8 was obtained through multiple simulations comparing both wake turbulence schemes, per runway layout scenario and varying proportion of heavy aircraft in the traffic mix. It shows that the effect of pairwise RECAT differs strongly by runway configuration. This is a central result of the thesis work. It becomes evident that as the amount of heavy aircraft in the peak hour increases, the required wake separations increase, and so do the runway occupancy times.

As such, using a finer scheme allows an increase in capacity. The single point on each line represents the heavy-aircraft mix threshold above which RECAT-EU-PWS yields a capacity gain of at least one additional arrival or departure slot.

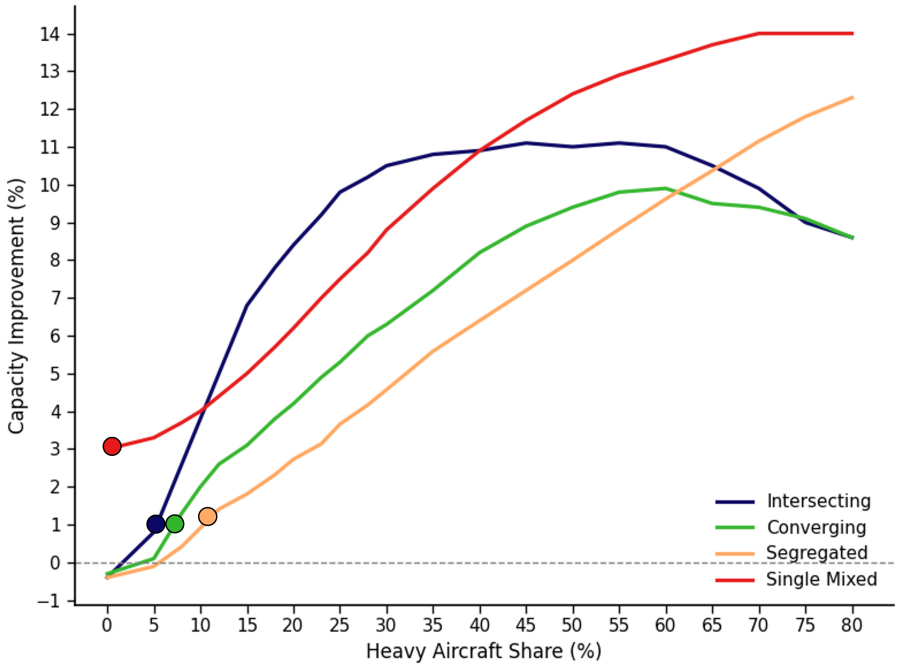

Fig. 8 RECAT-EU-PWS capacity improvement per runway configuration

In the single mixed-runway configuration, RECAT-EU-PWS delivers the greatest capacity gains across the entire analysed range of heavy-aircraft proportions, varying from 3% to more than 14%. As such, RECAT-EU-PWS implementation is technically viable at all heavy traffic compositions for a mixed runway.

For the remaining two-runway systems (Intersecting, Converging and Segregated) ICAO performance initially outperforms slightly that of RECAT-EU-PWS. This occurs because at these low percentages of heavy aircraft, almost all leading-following aircraft combinations in the mix happen to be Medium "M" category in ICAO, or D1 in RECAT-EU-PWS, which are floored to the Minimum Radar Separation of 3 NM. Without these reductions in separation, and caused by the added variability of ROTs and speed profiles, RECAT-EU-PWS provides a more refined capacity estimate which can be lower than ICAO due to the narrowing down of the categories.

For segregated parallel runways, RECAT-EU-PWS only becomes meaningfully beneficial once heavy-aircraft share reaches 11%. Below that threshold, the legacy ICAO structure is already sufficiently well matched to the fleet composition and the additional granularity of RECAT yields only limited benefit. Above the threshold, the refined pairwise structure prevents capacity from degrading as sharply, especially on the arrival runway. As the heavy aircraft composition increases, the frequency of heavy and medium leader/follower combinations also increases. In this case, ICAO applies a 5NM separation while RECAT-EU-PWS applies 4 or 3.5 NM, depending on whether the leader is in the B1 or B2 category. Similarly, towards the end of the range, when the majority of combinations are between two heavy aircraft (B1 or B2 in pairwise RECAT), a reduction in 1 NM can be observed between both schemes, which allows for continuous improvement.

The dedicated RECAT-EU-PWS case studies reinforce this interpretation. Two additional applications, at Tenerife-Norte (Figure 9) and Palma de Mallorca (Figure 10), were used to test whether the scheme can capture capacity changes caused by relatively small variations in fleet composition within the same broad ICAO wake category. In both airports, increasing the share of turboprop aircraft led to a measurable reduction in peak runway capacity under RECAT-EU-PWS, whereas the capacity metrics under ICAO remained unchanged. This occurs because turboprops, although classified as a medium aircraft in the ICAO scheme, have operational characteristics that are more penalising for runway throughput,

particularly in approach speed and climb performance. The effect was more pronounced at Tenerife-Norte, where turboprop traffic forms a larger share of peak hour flights, but the same trend was also observed at Palma. These case studies therefore show that small changes in the proportions of specific aircraft categories, particularly those associated with turboprop and regional traffic, can shift peak capacity even when aggregate ICAO category shares appear similar. This is an important observation: capacity screening based only on L/M/H percentages may overlook cases in which a finer wake-separation scheme is valuable for planning purposes.

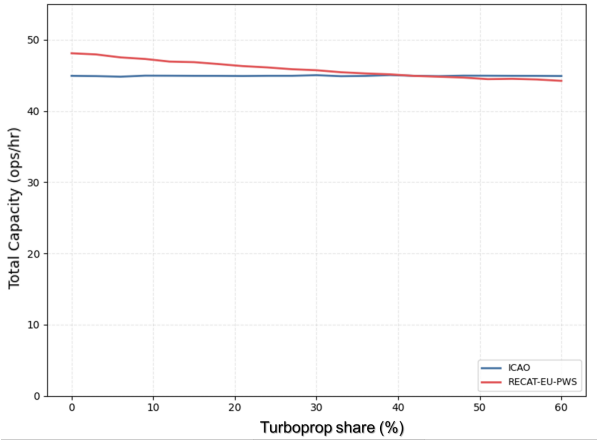

Fig. 9 RECAT-EU-PWS variation with turboprops. Tenerife Norte

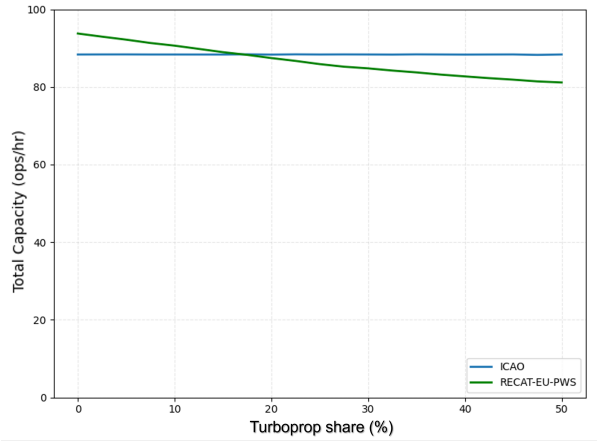

Fig. 10 RECAT-EU-PWS variation with turboprops. Palma

In the intersecting runways case, ICAO remains slightly better up to roughly 4-5% heavy traffic, after which RECAT becomes advantageous. As the composition of heavy aircraft increases, the capacity improvement increases until reaching a maximum of 10% in the 40 to 60% heavy traffic mix. Beyond this proportion, the improvement, despite still existing, is lower. This decline, starting at these percentage levels occurs due to the time-blocking windows caused by the intersection constraints. The existence of these strict intersection runway blocking rules also explain why, under a heavy aircraft proportion between 10 and 35 percent, this runway layout shows the greatest benefit when using pairwise RECAT, as precisely a small reduction in time can be just enough to accommodate an extra arrival or departure before the blocking constraints.

Even though separations between aircraft can be reduced, in the selected scenario, heavier aircraft show significantly larger runway occupancy times in proportion to those by medium aircraft. This amplifies the effect of the runway blocking constraints, which explains that "dip" towards the end of the heavy aircraft explored range. The crossing geometry still limits the extent of achievable gain.

Lastly, the converging/diverging configuration follows a similar logic as the intersecting. An increase in slot capacity appears at only around 5% of heavy-aircraft share. Below that point, geometric coupling remains the primary limitation and a refined wake scheme has relatively little room to improve throughput. Once heavy traffic becomes more prominent, RECAT starts to matter because wake separations become a larger component of the active bottleneck set. Again, a maximum capacity improvement of around 9% is reached at a heavy-aircraft share of 60%. Beyond this point, a dip is observed, again due to the forbidden time-rules being amplified by finer tuning of ROTs and speed profiles.

Table 3 TBS & RECAT-EU-PWS implementation thresholds

Configuration	TBS [headwind speed]	RECAT-EU-PWS [Heavy mix]
Single mixed runway	12 kts	Entire range
Segregated parallel	4 kts	11 %
Intersecting runway	15 kts	5 %
Converging/diverging	26 kts	6 %

To move from technical feasibility to actual deployment relevance, the threshold values identified in the sensitivity analyses and summarized in Table 3 can be combined with airport-specific wind data and traffic mix, both corresponding to peak hour data, as well as capacity projections. For TBS, this comparison shows that Palma de Mallorca is the clearest candidate for implementation, since the required headwind threshold is low (4 kt), exceeded in 34% of observations, and capacity forecasts indicate that the airport may exceed its sustainable capacity within the next five years. By contrast, Alicante appears unfeasible, as headwinds above the relevant 12 kts threshold occur in about 3.1% of observations despite the airport being projected to exceed its sustainable capacity within the next two years. Barcelona's intersecting configuration and Madrid's converging configuration appear less suitable for TBS deployment, because the necessary headwind conditions occur very rarely, below 1% in both scenarios, as well as below their peak and sustainable capacity limits in current forecasts.

For RECAT-EU-PWS, the assessment depends on whether the peak-hour fleet mix exceeds the relevant traffic-composition threshold. Under this criterion, Alicante, Barcelona, and Madrid appear technically favourable for implementation, since gains arise across the full analysed range in the single mixed case, while Barcelona's peak-hour heavy-aircraft share of about 15% exceeds the 5% threshold for the intersecting case and Madrid's 23% exceeds the 5% threshold for the converging case. Palma de Mallorca, however, does not currently justify RECAT-EU-PWS deployment, since its peak-hour heavy-aircraft share of around 2% remains far below the 11% threshold required for meaningful gains, even though long-term forecasts point to increasing capacity pressure.

D. Sensitivity analysis and KPI interpretation

In order to answer why different runway configurations show different behaviour to the implementation of TBS and RECAT-EU-PWS, it is necessary to first address and identify which are the main bottlenecks, or capacity-limiting drivers in each of the scenarios.

To do so, a sensitivity analysis for each scenario is performed by varying the capacity-limiting parameters of D_{MAP}, D_{MIN}, ROTs, headwind, heavy aircraft share and point of intersection, where each applies. This is done not only to demonstrate that the implemented model is robust and that its results vary consistently with expectations, but also to identify the main limiting factors, or capacity bottlenecks, affecting each runway configuration.

The missed approach point distance, D_{MAP}, is relevant because it directly affects the runway-availability time separation constraint. By changing the latest point at which a go-around can be initiated, it alters the minimum separation required to ensure timely runway vacation. In this study, D_{MAP} is varied between 0.3 NM and 1.5 NM in all four scenarios.

Runway occupancy times (ROT) are also analysed, since they determine how long an aircraft occupies the runway before it becomes available for the next operation. Although ROT is often not the primary limiting factor, a sensitivity analysis helps determine the conditions under which it becomes restrictive. For this purpose, both arrival and departure ROTs are varied from −40% to +40% of their nominal values in all scenarios.

The parameter D_{MIN} is important in coupled runway operations because it defines part of the blocking area in which a departure forbids an arrival. Since the parallel segregated runway case consists of de-coupled runways, this analysis is only carried out for intersecting and converging runway configurations, with D_{MIN} varied from 0 to 4 NM.

Finally, for intersecting runways, the location of the intersection point also affects capacity: the closer it is to the thresholds, the higher the achievable capacity. To examine this effect, arrival and departure ROTs at the intersection are varied simultaneously in a two-dimensional sensitivity analysis, exploring all possible points of intersection between two runways.

Results from the sensitivity analysis are obtained and evaluated using two author-developed key performance indicators. These are the Capacity Limitation Indicator (CLI) and the Operational Bottleneck Indicator (OBI).

CLI is defined as the maximum percentage reduction in peak capacity induced by each parameter over the entire range. The resulting scores are normalized within each scenario in order to identify the critical factors. This KPI may be interpreted as a stress test, as it captures the full extent of capacity variation across the entire parameter range, irrespective of the practical realism of the values considered.

OBI is defined as the maximum realistic capacity loss with respect to the baseline parameter ranges. As such, it represents a more scenario-specific KPI, providing a less general but more practically grounded measure than CLI.

Table 4 CLI scores by scenario and parameter

Parameter	Mixed	Segregated	Intersecting	Converging
Intersection	–	–	10.0	–
D_{MIN}	–	–	8.9	10.0
HVY%	10.0	10.0	5.5	5.1
Headwind	5.5	4.7	2.0	1.5
D_{MAP}	4.0	0.8	2.3	1.9
ROT	9.6	1.9	3.1	3.3

The CLI results in Table 4 show that the main capacity drivers differ significantly by runway configuration. In the Mixed and Segregated scenarios, the proportion of heavy aircraft is the dominant factor, with ROT also having a strong influence in the Mixed case. In contrast, capacity in the Intersecting configuration is mainly limited by the intersection constraint and D_{MIN}, while in the Converging scenario D_{MIN} is the primary bottleneck. Overall, the results indicate that fleet composition dominates in conventional runway layouts, whereas blocking and intersection-related constraints are more critical in operationally constrained configurations.

Table 5 OBI scores by scenario and parameter

Parameter	Mixed	Segregated	Intersecting	Converging
Intersection	–	–	10.0	–
D_{MIN}	–	–	2.3	10.0
HVY%	10.0	10.0	4.8	6.5
Headwind	9.5	8.1	1.6	2.1
D_{MAP}	4.7	0.0	1.9	0.7
ROT	3.6	0.0	0.5	1.6

On the other hand, OBI results in Table 5 provide a more scenario-specific assessment by considering only realistic parameter variations around the baseline. Heavy aircraft mix remains the dominant factor in the Mixed and Segregated scenarios, with headwind also showing a strong influence. In the Intersecting configuration, the intersection point is the main limiting factor, while the effect of D_{MIN} is much smaller than in the CLI results. In the Converging scenario, D_{MIN} remains the dominant parameter, with heavy mix also contributing significantly. Overall, the OBI indicates that traffic mix is the most consistent practical driver of capacity, whereas parameters such as D_{MIN} and ROT, which appear important in the CLI, are less influential under realistic operating conditions. Thus, while CLI highlights theoretical worst-case bottlenecks, OBI better reflects the parameters most relevant in practice.

The KPI analysis therefore suggests that capacity loss in conventional layouts is mostly driven by separation and fleet-composition effects; capacity loss in intersecting and converging layouts is mostly driven by geometric interdependence. This distinction is precisely what explains why TBS and RECAT do not produce uniform gains across airports.

From an airport-planning perspective, the results imply that neither TBS nor RECAT-EU-PWS should be treated as a universal capacity enhancers. Instead, each concept should be evaluated first against the dominant bottleneck. TBS is especially attractive where arrival throughput is strongly weather-sensitive and where the runway system is not already limited by geometry. RECAT-EU-PWS is most attractive where a meaningful share of the traffic mix falls into combinations that are penalised by the coarser ICAO categorisation. Conversely, in systems dominated by runway intersections or blocking windows, major gains should not be expected unless these bottlenecks are also varied. A broader analysis of the results is provided in Chapter 7 of the accompanying thesis associated with this work [26].

VIII. Conclusions

This paper evaluated to what extent Time-Based Separation (TBS) and RECAT-EU-PWS can increase airport peak runway capacity under different runway layouts, traffic mixes, weather conditions, and separation concepts. A first

conclusion is that a stochastic, Monte Carlo-based discrete-event approach provides a credible and flexible basis for macro-level runway-capacity assessment. By combining established runway-dependency logic with modular scenario inputs, the built model, ARCAS, is able to represent runway dependencies, operational rules, fleet composition, and separation schemes within a common framework. Verification and validation indicate that the model is sufficiently robust for comparative studies of runway capacity performance.

The second conclusion is that runway capacity is strongly configuration-dependent, and so are the benefits of Time-Based Separation (TBS) and RECAT-EU-PWS. Sensitivity analysis showed that the dominant bottlenecks vary substantially across runway layouts. In single mixed and segregated parallel systems, the main capacity drivers are traffic composition and weather, with heavy-aircraft share emerging as the most important source of capacity loss and headwind as a strong secondary factor. In contrast, intersecting and converging/diverging layouts are mainly constrained by runway geometry and cross-runway blocking effects. As a result, the same operational concept does not produce uniform benefits across airports.

With respect to TBS, the results show that its ability to recover capacity under headwind conditions depends primarily on runway configuration and local wind conditions. Across the analysed cases, meaningful gains only emerged once airport-specific headwind thresholds were exceeded. These were lowest in segregated parallel operations and highest in converging layouts, where geometric blocking constraints dominate performance. TBS should therefore be understood as a targeted solution for wind-sensitive arrival systems rather than as a universally beneficial intervention.

A similar conclusion applies to RECAT-EU-PWS. Its effectiveness depends mainly on runway geometry and local traffic mix, particularly the proportion of aircraft pairs for which the legacy ICAO categorisation is overly conservative. In mixed-runway operations, RECAT-EU-PWS provided benefits across the full analysed range, whereas in parallel, intersecting, and converging layouts meaningful gains appeared only beyond configuration-specific traffic mix thresholds. The targeted case studies at Tenerife-Norte and Palma de Mallorca further showed that RECAT-EU-PWS can detect capacity effects caused by relatively small changes in fleet composition, including changes within the same ICAO wake category. This indicates that the scheme is not only a capacity enhancer, but also a potentially useful planning tool for assessing how future demand distributions may affect runway performance.

Overall, the deployment assessment shows that TBS is most justified at Palma de Mallorca, where the required headwind threshold is relatively low and occurs frequently enough to make implementation technically viable. By contrast, TBS appears difficult to justify at Alicante, Barcelona and particularly Madrid, where the required headwind conditions occur too rarely to produce consistent benefits. For RECAT-EU-PWS, the conclusions are different: Alicante, Barcelona, and Madrid appear to be suitable candidates, as their traffic mix conditions are compatible with meaningful capacity gains, while Palma de Mallorca does not currently justify implementation given its low proportion of heavy aircraft. These conclusions become more relevant in light of capacity forecasts, which indicate increasing pressure in Alicante and Palma, while Madrid's converging and Barcelona's intersecting runways are expected remain significantly below their peak and sustainable capacities.

The results also show that capacity gains must be interpreted in an operational context. Because delay grows non-linearly as demand approaches capacity, even modest throughput improvements from TBS or RECAT-EU-PWS may translate into meaningful delay reductions in highly utilised systems. Conversely, where spare runway capacity already exists, the practical value of such concepts is naturally smaller.

IX. Recommendations

Overall, the study supports a selective implementation strategy. Airports should first identify whether their dominant bottleneck is primarily wake-related, weather-related, runway-occupancy-related, or geometry-related. Only then can TBS and RECAT-EU-PWS be prioritised in a way that is both operationally viable and economically feasible. The key question is therefore not simply whether one of these solutions can increase capacity, but whether it addresses the active constraint of the runway system under consideration.

Several directions for future work follow from this study. First, the current RECAT-EU-PWS implementation could be extended toward more refined pairwise or aircraft-specific representations, allowing additional differences in speed profiles, runway occupancy times, and wake behaviour to be captured more accurately. Second, future research should examine complementary separation concepts such as ROCAT, particularly in scenarios where runway occupancy time becomes the limiting factor after wake minima are reduced, and how headwind affects ROT. Third, the present TBS

formulation could be expanded to include crosswind-sensitive wake transport and decay, since wake behaviour is not determined by headwind alone.

Additional work is also needed at the case-study level. Validation should be extended beyond the current Spanish airport set, especially for intersecting-runway systems, where more representative airports would improve the generalisability of the findings. The integration of upstream sequencing concepts such as Point Merge would also help clarify how the organisation of arrival flows influences the realised benefit of TBS at the runway threshold. Finally, the current runway-centred framework could be developed toward a more holistic gate-to-gate airport model, supported by higher-fidelity local operational data, especially for parameters such as departure runway occupancy times and speed profiles.

In addition to the technical recommendations identified in this study, future work should also address the broader deployment conditions required for the practical implementation of RECAT-EU-PWS and TBS. Although the present thesis demonstrates their potential to improve runway capacity, successful deployment will depend not only on technical performance but also on economic, operational, and institutional feasibility. In this respect, implementation should be analysed across the strategic, tactical, and operational decision-making levels of Air Traffic Management, while simultaneously considering regulatory, personnel, and systems-related dimensions. Consequently, a more comprehensive assessment of deployment feasibility is needed to complement the technical results presented here and to support the realistic adoption of these concepts in operational airport environments.

Acknowledgments

A.L.R. gratefully acknowledges Javier Vázquez Capitán (INECO, *Project Manager in Runway Capacity, Operations and ANSPs*), Jaime del Molino Blanco (IATA, *Head ATM-CNS Europe*) and Massimiliano Zanin (CSIC, *Principal Researcher*) for their guidance and support, and the companies ENAIRE and INECO for providing data, operational expertise, and support during the entire process. The author used artificial intelligence tools for language and grammar checking in selected parts of the document. All content was carefully reviewed and validated by the author.

References

[1] R. de Neufville, and A. Odoni, *Airport Systems Planning, Design and Management*, 2nd ed., McGraw Hill Education, 2013. ISBN:978-0-07-177058-3.

[2] M. Gelhausen, D. Wilken, and P. Berster, *Airport Capacity Constraints and Strategies for Mitigation: A Global Perspective*, Academic Press / Elsevier, London, 2019. ISBN:9780128126585.

[3] F. Rooseleer, and S. Neshevski, "Guidelines on Time-Based Separation (TBS) with Optimised Runway Delivery (ORD) for Final Approach," Tech. Rep. GUID-196, EUROCONTROL, 2024. ISBN:978-2-87497-127-3.

[4] F. Rooseleer, "RECAT-EU-PWS Solution: Optimised Wake Turbulence Categorisation and static Pair-Wise Separation (S-PWS) Minima on Approach and Departure," Tech. rep., EUROCONTROL, Brussels, Belgium, 2023.

[5] J. van der Klugt, P. Roling, R. Hove, and R. Curran, "Calculating capacity of dependent runway configurations: A discrete-event simulation approach for analysing the effect of aircraft sequencing," 2013. https://doi.org/10.2514/6.2013-4353.

[6] A. Blumstein, "The Landing Capacity of a Runway," *Operations Research*, Vol. 7, No. 6, 1959, pp. 752–763. https://doi.org/10.1287/opre.7.6.752.

[7] G. Newell, "Airport Capacity and Delays," *Transportation Science*, Vol. 13, No. 3, 1979, pp. 201–241. https://doi.org/10.1287/trsc.13.3.201.

[8] Federal Aviation Administration, "Airport Capacity and Delay," Advisory circular ac 150/5060-5, Federal Aviation Administration, Washington, D.C., 1983. https://doi.org/10.21949/1513590.

[9] W. Cheung, R. Piplani, S. Alam, and L. Bernard-Peyre, "Dynamic capacity and variable runway configurations in airport slot allocation," *Computers & Industrial Engineering*, Vol. 159, 2021, p. 107480. https://doi.org/10.1016/j.cie.2021.107480.

[10] K. Chen, Anupriya, P. Bansal, R. Anderson, N. Findlay, and D. Graham, "Understanding the capacity of airport runway systems," *Transportation Research Part C: Emerging Technologies*, Vol. 173, 2025, p. 104998. https://doi.org/10.1016/j.trc.2025.104998.

[11] R. Kicinger, J. Krozel, M. Steiner, and J. Pinto, "Airport Capacity Prediction Integrating Ensemble Weather Forecasts," 2012. https://doi.org/10.2514/6.2012-2493.

[12] E. Gilbo, "Airport capacity: Representation, Estimation, Optimization," *IEEE Transactions on Control Systems Technology*, Vol. 1, No. 3, 1993, pp. 144–154. https://doi.org/10.1109/87.251882.

[13] A. Kim, S. Rokib, and L. Yi, "Refinements to a Procedure for Estimating Airfield Capacity," *Transportation Research Record: Journal of the Transportation Research Board*, Vol. 2501, 2015, pp. 18–24. https://doi.org/10.3141/2501-03.

[14] A. Kim, and M. Hansen, "Validation of Runway Capacity Models," *Transportation Research Record: Journal of the Transportation Research Board*, Vol. 2177, 2010, pp. 69–77. https://doi.org/10.3141/2177-09.

[15] B. Bubalo, and J. Daduna, "Airport capacity and demand calculations by simulation—the case of Berlin-Brandenburg International Airport," *NETNOMICS Economic Research and Electronic Networking*, Vol. 12, 2011, pp. 161–181. https://doi.org/10.1007/s11066-011-9065-6.

[16] J. Banks, J. Carson, B. Nelson, and D. Nicol, *Discrete-Event System Simulation*, 5th ed., Prentice Hall, 2009. ISBN:978-0-13-815037-2.

[17] C. Wang, X. Zhang, and X. Xu, "Simulation Study on Airfield System Capacity Analysis Using SIMMOD," 2008, pp. 87–90. https://doi.org/10.1109/ISCID.2008.70.

[18] M. Bazargan, K. Fleming, and P. Subramanian, "A simulation study to investigate runway capacity using TAAM," 2003, pp. 1235 – 1243 vol.2. https://doi.org/10.1109/WSC.2002.1166383.

[19] M. Lamers, "Enhanced Runway Capacity at Airports with Complex Runway Layouts," Master's thesis, Delft University of Technology, Jun. 2016.

[20] D. Lee, C. Nelson, and G. Shapiro, "The Aviation System Analysis Capability Airport Capacity and Delay Models," NASA Contractor Report, RTOP 538-04-14-02, NAS2-14361, Apr. 1998.

[21] M. Hansen, "Post-Deployment Analysis of Capacity and Delay Impacts of an Airport Enhancement: Case of a New Runway at Detroit," *Air Traffic Control Quarterly*, Vol. 12, 2004, pp. 339–365. https://doi.org/10.2514/atcq.12.4.339.

[22] Transportation Research Board and National Academies of Sciences, Engineering, and Medicine, *Evaluating Airfield Capacity*, The National Academies Press, Washington, DC, 2012. https://doi.org/10.17226/22674.

[23] P. Di Mascio, G. Rappoli, and L. Moretti, "Analytical Method for Calculating Sustainable Airport Capacity," *Sustainability*, Vol. 12, No. 21, 2020. https://doi.org/10.3390/su12219239.

[24] International Civil Aviation Organization (ICAO), *Procedures for Air Navigation Services – Air Traffic Management (PANS-ATM), Doc 4444*, International Civil Aviation Organization, Montréal, Quebec, Canada, sixteenth ed., 2016. ISBN 978-92-9258-081-0.

[25] J. van der Klugt, "Calculating Capacity of Dependent Runway Configurations," Master's thesis, Delft University of Technology, Nov. 2012.

[26] A. Lanza Rausell, "Next-Gen Runway Capacity Modelling: An evaluation of Time-Based Separation and RECAT-EU-PWS across Spanish airports," Master's thesis, Delft University of Technology, May 2026.

Part II

Master Thesis

1

Introduction

Air transport continues to play a central role in global connectivity, tourism, trade, and economic development. This importance is reinforced by the continued growth in demand: worldwide passenger traffic in 2025 increased by 5.3% compared with 2024 values, and in Europe more than 11 million flights took to the skies, representing a 4% increase from the previous year. As passenger volumes and aircraft movements increase, many airports face growing pressure to accommodate demand within limited physical space and increasingly complex operational environments. In this context, airport capacity becomes a strategic concern. However, airport capacity is not determined by a single element: it emerges from the interaction of multiple subsystems, including runways, taxiways, aprons, terminals, and airspace. Among these, runway capacity is often the most critical constraint, as it directly limits the number of aircraft arrivals and departures that can be handled within a given period.

When an airport approaches the limits of its runway system, decision-makers are generally confronted with a two-tier choice. On the one hand, capacity can be increased through infrastructure expansion, for example by constructing additional runways, rapid exit taxiways, or other supporting airside elements. On the other hand, the existing infrastructure can be used more efficiently through operational improvements that reduce separations, optimise sequencing, or mitigate capacity losses under adverse conditions. While infrastructure expansion may provide long-term relief, it is often constrained by cost, land availability, environmental impact, and politics. As a result, there is strong interest in techniques that can "squeeze" additional capacity from existing runway systems while maintaining safety.

This challenge is particularly relevant because runway capacity is influenced by a large number of interdependent factors. These include runway geometry, mode of operation, wake turbulence separation requirements, aircraft performance characteristics, fleet mix, air traffic control procedures, and meteorological conditions. These factors do not act independently. Instead, they interact in a way that makes runway capacity a dynamic and scenario specific concept rather than a fixed value. For that reason, airport and air navigation stakeholders require tools that go beyond simplified static estimates and are capable of representing real operational variability. Allocating landing and takeoff slots based on inaccurate RSC estimates can lead to either under or over-utilisation of available capacity, which can directly result in inefficiencies or congestion.

Two operational concepts have gained particular relevance in this context. The first is Time-Based Separation (TBS), which adjusts arrival separation dynamically as a function of headwind conditions, thereby reducing the capacity loss that otherwise occurs when strong headwinds increase the time needed to fly a fixed distance-based separation. The second is RECAT-EU-PWS, a more refined wake turbulence categorisation and separation framework that replaces broader legacy categories with more detailed pairwise minima. Both concepts offer the possibility of increasing peak runway capacity and reducing delay without major infrastructure expansion. Yet, up to this day, there are currently no openly available macro-level analyses that evaluate the extent to which TBS and, separately, RECAT-EU-PWS can increase peak runway capacity across different airports and operational conditions.

This thesis work addresses that gap by investigating the extent to which these two concepts can improve runway performance across Spanish airports. More specifically, the central research question is:

To what extent can the implementation of Time Based Separation and the wake categorisation scheme RECAT-EU-PWS increase an airport's peak runway capacity?

To answer this question, the thesis work includes the development of ARCAS (Airport Runway Capacity Assessment Software), a discrete-event simulation model implemented in Python. The model builds on earlier runway dependency logic while extending it into a flexible framework capable of representing multiple runway geometries, traffic mixes, weather conditions, different separation schemes and with TBS and RECAT-EU-PWS functionality.

The remainder of this thesis is structured as follows. Chapter 2 provides the background and problem definition, introducing the concept of runway capacity, the main metrics used to define it, and the principal factors that affect it. It also reviews existing methods for runway capacity estimation and discusses the role of runway geometry, weather, aircraft characteristics, and wake turbulence separation. Chapter 3 identifies the research gap and presents the main research question together with the corresponding subquestions. Chapter 4 develops the methodological framework and formulates the runway dependencies and separation concepts required for the model, including the implementation of TBS and RECAT-EU-PWS. Chapter 5 presents the simulation model itself and explains its Python implementation, operational logic, and Monte Carlo structure. Chapter 6 introduces the airport scenarios and case studies used in the analysis. Chapter 7 presents the results, together with verification, validation, and sensitivity analyses. Finally, Chapter 8 summarises the main conclusions, reflects on the limitations of the work, and offers recommendations for future research and possible deployment considerations.

2

Background & Problem Definition

2.1. What is Runway Capacity?

Airport capacity refers to the maximum number of aircraft operations and passengers an airport can accommodate within a given timeframe. It is not determined by a single variable, but instead by the combined performance of multiple subsystems, each having its own operating constraints. These include runway capacity, taxiway capacity, apron capacity, and terminal capacity. The overall effectiveness of an airport depends on how well these components work together and the weakest element often becomes the bottleneck.

The combination of multiple factors is what determines an airport's platform capacity. The available capacity is maximized when each factor is used at its optimal level; however, increasing capacity in one area can reduce overall effectiveness if not matched in others (e.g., increasing runway throughput without sufficient apron capacity or an efficient turnaround process) [1].

Runway capacity is often the most critical constraint, as it governs the number of aircraft departures and arrivals an airport can handle in an hour. Factors such as the number of runways, their configuration, separation requirements, and weather conditions all influence this capacity. A more detailed discussion is provided in the following section. However, once aircraft are on the ground, taxiway capacity becomes essential. Inefficient taxiway design or bottlenecks can lead to ground congestion, delays, and extended runway occupancy times, reducing the effective throughput of the airfield.

Beyond airside operations, apron or stand capacity determines how many aircraft can be parked and serviced at the same time. This includes contact gates at terminals and remote stands. Lack of available stands can force arriving aircraft to wait or be towed to distant areas, disrupting schedules. Finally, terminal capacity governs the flow of passengers through the airport. From check-in and security screening to baggage claim and customs, the speed and efficiency of terminal processes can impact directly the number of passengers an airport can handle during peak hours.

Additionally, airport capacity can be classified into nominal and peak capacity. Off-peak or nominal periods are essential for recovering from over-demand during peak hours. For example, when delays cause aircraft or passengers to accumulate beyond expected levels [1].

In essence, airport capacity is a function of its most constrained subsystem. Even if a runway can support 60 movements per hour, if the terminal can only process 40 arrivals' worth of passengers, the effective airport capacity will be limited to 40.

Runway System Capacity (RSC) can and has been defined in multiple ways over the years. Typically, it can be broken down into practical hourly capacity, maximum throughput capacity, sustained capacity, and declared capacity. Odoni and de Neufville [2] define them in the following terms:

The Maximum Throughput Capacity (MTC) is defined as the expected number of movements that can be performed in one hour on a runway system without violating ATM rules, assuming continuous aircraft demand. Proposed by the FAA in the late 1960s, Practical Hourly Capacity (PHC) is defined as the expected number of movements in an hour on a runway system with an average delay per movement of 4 minutes. This indicator

assumes a certain level of service (LOS) and states that maximum capacity is reached once the average delay exceeds 4 minutes. Values typically range between 80-90% of MTC [2].

In contrast, Declared Capacity (DC) is defined as the number of aircraft movements per hour that an airport can accommodate at a reasonable LOS. Values typically range between 85-90% of MTC. Here, delay is used as the principal indicator of LOS. The concept of declared capacity has been widely implemented worldwide and forms the basis for international practices such as schedule coordination and slot allocation.

Finally, Sustained Capacity (SC) is defined as the number of movements per hour that can be reasonably sustained over several hours. This refers mainly to the workload of the ATM system and air traffic controllers. Depending on weather conditions, SC ranges from 90-100% of MTC [2].

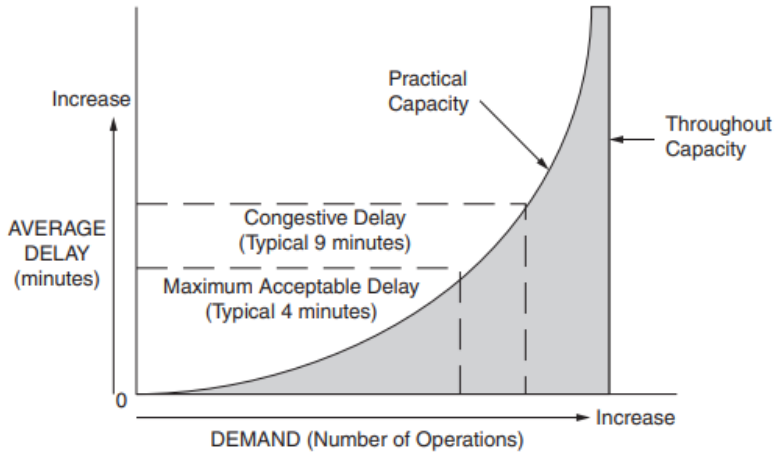

Figure 2.1: Delay as a function of capacity and demand [3]

2.2. Runway System Capacity Estimation

The study of airport and runway system capacity (RSC) has evolved considerably over the past six decades, at the same time as evolution in air traffic demand, computing capabilities, and modeling methodologies. In the early 1960s and 1970s, initial studies focused on understanding airfield capacity through basic queueing theory and empirical observation [4] [5]. These first studies were mainly driven by the need to quantify runway throughput under different traffic conditions, often with simplistic assumptions.

As commercial aviation grew rapidly in the 1980s and 1990s, especially at large hub airports, the U.S. Federal Aviation Administration (FAA) and international agencies developed practical tools, such as capacity handbooks and tabular reference guides to support planners and air traffic controllers [6] [7]. These tools were designed to offer quick and standard assessments based on typical runway configurations and traffic mixes.

The early 1990s also marked the introduction of more defined analytical and empirical techniques, such as the Pareto frontier model proposed by Gilbo [8], which offered a visual way to evaluate feasible combinations of arrival and departure rates. Over time, thanks to growing computational power and data availability, simulation-based approaches became more prominent in the 2000s, which allowed for higher fidelity modeling of airfield operations [9] [10]. More recently, statistical learning and model based methods, including censored regression and clustering, have been used to estimate capacity under real-world conditions [11] [12].

To frame this previous work, the different methodologies can be classified into four categories [13]:

1. Table-based and spreadsheet approaches
2. Analytical models
3. Simulation-based methods
4. Empirical estimation approaches

2.2.1. Table-Based and Spreadsheet Methods

These methods are among the most straightforward, and typically use predefined combinations of categorical variables, such as runway configuration, fleet mix, and meteorological conditions, to produce RSC estimates [6] [7]. While suitable for early-stage or high-level planning because of their simplicity, these models are constrained by fixed assumptions. Differences with those assumptions can lead to non-representative or inaccurate results. They are however, useful in providing a fast and preliminary estimate.

Table 2.1: Spreadsheet & Lookup Table methods literature overview

Model	Year	Description	Reference
FAA Lookup Table	1983	Estimate of an airport's hourly runway capacity based on three key factors: the runway configuration (single, parallel, or intersecting runways), the aircraft mix ratio, and the weather conditions. Provides simple yet fast estimates.	[6]
FAA Spreadsheet	1983	More detailed than the lookup table, also based on: location of runway exits, percentage of arrivals, and percentage of touch-and-go operations. As with the lookup table, the inputs only vary in pre-specified categories.	[6]
TRB ACS	2012	Takes into account more complex factors such as arrival runway occupancy time, average aircraft approach speed, separation requirements for arrivals and departures, and the arrival gap spacing buffer. However, only works with pre-specified runway configurations; customization level is low but provides a good first estimate.	[7]

2.2.2. Analytical Methods

Analytical approaches model runway operations by the use of mathematical equations, either in closed form or as numerically solvable models [2]. These are more specific than lookup tables as more detailed operational

inputs are used. However, these models are generally fixed to specific configurations, such as single, parallel, or intersecting runways, and often exclude important factors like taxiway or airspace constraints.[5][14].

Table 2.2: Analytical methods literature overview

Author	Year	Description	Reference
Blumstein	1959	Considered the first rigorous quantitative model for runway capacity. Estimates the capacity of a single runway using a queueing approach based on inputs like runway occupancy times (ROT) and separation minima.	[4]
Newell	1979	Represents the runway as a service system linking runway capacity with arrival & departure demand. Quantifies how exceeding nominal capacity generates delays and provides a throughput–delay tradeoff.	[5]
Lee et al.	1998	Estimates runway and airport capacity using ATC rules, aircraft performance, and runway configurations. Generates capacity curves to represent the tradeoff between arrivals and departures for different weather and operational scenarios.	[15]
Kicinger et al.	2012	The Integrated Airfield Capacity Model is an analytical method which integrates deterministic weather forecasts in airport capacity modelling.	[16]
Cheung et al.	2021	Analytical model to estimate runway capacity for any optimized sequence of arrivals and departures. Accurately handles mixed-mode operations, allowing testing of scenarios and comparison of sequencing algorithms.	[17]
Di Mascio et al.	2020	Calculates specific runway capacity and compares it to sustainable and saturation capacity. Provides maximum potential capacity of the infrastructure under given hypotheses.	[14]

2.2.3. Simulation-Based Methods

Simulation models can reproduce detailed aircraft operations within the airfield and surrounding airspace [10][18]. These models often have the ability to simulate actual operational conditions at specific airports, giving researchers a realistic foundation for developing and testing new concepts. The software's ability to model different runway configurations and scenarios ensures that findings are relevant to real-world applications. Discrete event simulation (DES), a common technique in this field, is especially effective in reproducing the sequential nature of aircraft movements and operational delays. Although powerful, these models require extensive input data and computer resources. Examples range from AirTOP, developed by TRANSOFT, to runwaySimulator [19], developed by MITRE and used by the FAA. The role and advantages of DES when modeling runway capacity will be further discussed in the following sections.

Table 2.3: Simulation methods literature overview

Model	Year	Description	Reference
AIRTOP	2006 (c.u)	Developed by Transoft solutions, this is a fast-time gate-to-gate simulation . AirTOP is capable of simulating runway capacity, terminal movements, apron and ground movements as well as en-route flows. It provides a highly customizable simulation framework	
SIMMOD	1978 (c.u)	SIMMOD, the FAA airport and airspace simulation model, is a DES planning tool used to study and improve enroute and terminal-area air traffic, as well as airport and airline ground operations. It represents the air and ground system as a series of nodes connected by links. Airport and airspace nodes exist, which allows flexibility in the level of detail: from a specific ground movement at an airport to airport-to-airport routes.	[20]
TAAM	1998	Fast time simulation model developed by Boeing-Jeppesen for the analysis of capacity and delay in an airport's terminal area and at the airport itself. It is widely used across the industry and in similar fashion to AIRTOP, provides gate-to-gate simulation capacity. It can be used to analyse a large range of airport related problems and is one of the commonly used software by airports and airlines. The advantage of TAAM is that includes a lot of output. Next to capacity and delay, the model can be used to create noise contours, calculate the amount of fuel burned, and calculate costs. TAAM is therefore a rather complete model, which is one of the most used simulation packages in the industry.	[9]
RCAP 1.0	2012	Uses Discrete Event Simulation to calculate the capacity of any given runway system with varying runway layouts, traffic mixes and operational conditions.	[21][22]
RCAP 2.0	2016	Continuation of Van der Klugt´s RCAP 1.0, Introduces RECAT-EU wake separation scheme.	[23]

2.2.4. Empirical Estimation Methods

Empirical models derive RSC using observed throughput data. A simple assumption is that this throughput under saturated demand reflects actual capacity, while below saturated conditions it represents only a lower bound. An example approach is the Pareto Frontier method [8], which defines a convex boundary of feasible arrival and departure combinations. While insightful, this method becomes infeasible due to the exponential growth of required scenario frontiers.

Recent literature has introduced censored regression methods to overcome data limitations [11] [12]. These methods conceptualize capacity as a latent variable, censored when actual demand is below system limits. Typically, operational data are clustered into separate groups, and a regression is fit to each cluster. These models offer improvements in handling measurement error and data censoring, but are inflexible in more complex settings and may omit confounding factors like air traffic control restrictions that influence capacity. Consequently, they might result in inaccurate estimates.

Table 2.4: Empirical methods literature overview

Author	Year	Description	Reference
Gilbo	1993	Introduces a Pareto-based model to address the maximum feasible combinations of arrival and departure rates for a given airport system. This outputs the boundary between feasible and infeasible operating points. Requires observations as input, as well as runway configuration and meterological conditions. Model is determenistic and not robust to missing data.	[8]
Hansen	2004	Model utilizes censored regression. Requires observed airport throughput as an input, and assumes continuous demand (demand exceeds capacity). Model helps in identification of how RSC varies with airport operational factors, however estimate is only valid when demand exceeds capacity.	[11]
Kim et Al	2015	Model utilizes censored regression to analyse refined data from past operations and segregate by weather, runway, type, which are all given as inputs. This statistical model accounts for missing data, however has limited reach in accounting for multiple operational factors.	[12]

2.2.5. Peak hour calculation

The concept of a representative peak hour is very important in airport capacity evaluation and performance measurement. The design hour should represent periods of continuous operational stress rather than peaks, while also representing the demand conditions under which the performance of infrastructure becomes important. There are several techniques available for the identification of a representative hour, and the airport operator chooses the one that best suits the characteristics of their operation. The techniques can be used with either natural hours (fixed clock hours) or rolling hours.

One of the simplest techniques available is the peak or busiest hour, which is the hour with the highest traffic volume recorded in a year [24]. While this technique is very simple to calculate, it is also very susceptible to exceptional circumstances and may therefore result in overestimation of capacity needs.

To overcome the above drawback, rank based techniques are generally preferred. The 30th peak hour, also known as the Standard Busy Rate (SBR), is the hour with the 30th highest traffic volume recorded in a year (some airports use the 40th busiest hour instead) [2]. A related concept is the 5% peak hour, defined as the traffic level above which the cumulative traffic accounts for only 5% of annual movements [3]. Similarly, the 95th percentile busy hour identifies the hour that exceeds 95% of hourly traffic observations in the dataset [25].

Operationally driven methodologies are also employed. The peak hour of the *IATA Busy Day* is equivalent to the busiest hour of the second busiest day in an average week during the peak month [26]. This definition seeks to capture the recurring seasonal congestion rather than annual peak events. Another performance-driven metric is the Peak Service Rate, which is described by EUROCONTROL as the 99th percentile of movements per hour calculated from a rolling 5-minute distribution [27]. This rate is an approximation of the theoretical maximum achievable rate under optimal operating conditions and sufficient demand, and is usually calculated within the operational day (e.g., 06:00-23:00 local time).

Although the interest of this thesis is peak hourly movements, passenger based methodologies are also described. In the Design Hour Rate, passenger flow rate in the chosen hour is greater than the flow rate in the hours that carry 97-99% of annual passenger traffic, with an adjustable percentage to local conditions [26]. Similarly, the FAA describes the Typical Peak-Hour Passenger (TPHP) demand as roughly the 85th percentile utilization of throughput capacity [24].

The selection of the design hour therefore depends on whether the objective is infrastructure sizing, operational planning, or performance benchmarking.

From now onwards in this thesis, the peak hour in the context of runway capacity will be reffered to as the average of the hours with the highest density of arrivals and departures. This definition is adopted because the objective is not infrastructure sizing but the analysis of operational capacity. Consequently, emphasis is placed on peak demand conditions rather than sustained conditions.

2.3. Discrete Event Simulation

Discrete Event Simulation (DES) is a time-based modeling technique used to simulate dynamic, stochastic systems where changes occur at specific points in time. The system evolves through the sequence of events, which are instantaneous occurrences that change the state of the system. This approach is effective for modeling complex and constrained environments like airports, where the timing and sequencing of operations are critical.

A DES system consists of interacting entities such as aircraft and resources (e.g., runways), whose properties and interactions are captured in a model. Which is an abstract representation containing the system's state, entities, attributes, events and delays.

A DES event is a change in the system state. For runway operations, typical events include an aircraft entering the Final Approach Fix (FAF), reaching the runway threshold, vacating the runway, or lifting off. These events affect the state of the aircraft and the overall system. The simulation advances by maintaining an event list (a time ordered queue of event notices representing scheduled events). Rather than progressing continuously, the simulation clock jumps from one event time to the next, focusing only on state changes.

As the simulation runs, entities (aircraft) are generated based on scheduled timetables or historical data. Once created, these entities interact with system resources. If a required resource is unavailable, the aircraft joins a list (or queue), such as a first come, first served waiting line. Once a resource becomes available, the entity begins an activity (e.g., landing or takeoff) for a specified time, after which the resource is released and the next event is triggered. Any idle time spent waiting for resources is considered a delay, which may be defined explicitly or left indefinite, depending on system conditions [28].

Figure 2.2 shows a possible discretized arrival and departure sequence. For arrivals (depicted as red dots), the Final Approach Fix (FAF) serves as the generator, or the point at which aircraft enter the sequence. The next event is the aircraft crossing the threshold (THR), just before touchdown. The final event, or sink, is EXIT, where the aircraft vacates the runway via an exit taxiway.

In contrast, the departure sequence begins at the threshold, where the aircraft initiates its take-off roll (the generator), and ends when the aircraft rotates and climbs out of the runway (the sink).

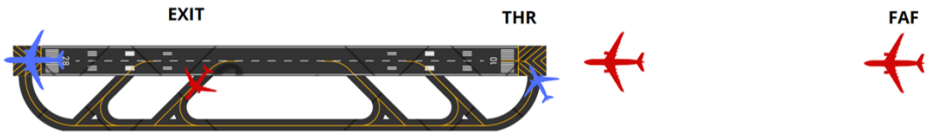

Figure 2.2: DES representation of runway operations

DES also supports the use of decision nodes, which can model operational rules like assigning runways based on aircraft type, wind direction, or time of day. After completing their operations, aircraft reach sinks, which remove them from the system, representing, for example, aircraft reaching the gate or departing the airspace.

In addition to well-established commercial tools such as AirTOP (developed by Transoft Solutions) and the runwaySimulator (developed for the FAA by MITRE), several research-driven tools have adopted DES as their core simulation methodology. Notably, RCAP 1.0, developed by J. van der Klugt [22] [21], and its successor RCAP 2.0, developed by M.F. Lamers [23], implement discrete event logic to analyse runway capacity under different runway configurations, traffic scenarios and separation schemes. More about these models will be explained in chapter 4.

2.4. Factors affecting Runway Capacity

Several related factors affect runway capacity, often varying based on airport infrastructure, traffic patterns, weather conditions, and operational procedures. Knowing these factors is of great importance in order to accurately model runway performance. The following subsections describe each of these factors in detail.

2.4.1. Runway mode of operation

Runway modes of operation determine how traffic is distributed across an airport's available runways and shape both capacity and efficiency.

The two main modes are mixed operations, where individual runways handle both arrivals and departures, and segregated operations, where specific runways are dedicated exclusively to one type of movement.

According to theoretic studies, the maximum capacity can be obtained when operating parallel runways in mixed mode. However, and as explained in this section, multiple other factors come into play. This is a reason why in some cases only when adopting fully segregated operations will maximum capacity be reached. Firstly, it eliminates the requirement for separate monitoring controllers, simplifying staffing and coordination. Secondly, by separating arriving and departing aircraft onto different runways, it removes the potential for direct interaction between them, which can help reduce the number of missed approaches. Additionally, this separation can lead to a less complex air traffic control (ATC) environment, easing the workload for both radar approach and aerodrome controllers.

In the context of parallel runways, ICAO Doc.9643 [29] further specifies four modes:

1. **Independent parallel approaches**. Simultaneous approaches to precision or non-precision instrument runways, where there are no separation minima constraints between aircraft on different runways. A centerline separation (i.e., the distance between the centerlines of two parallel runways) of at least **1035 m** is required.

   However, centerline separation is not the only requirement for independent parallel approaches. According to EU Regulation 2017/373 ATS.TR.225 [30], the following additional requirements must be met:

   (a) An Automatic Terminal Information System (ATIS) broadcaster informing on the mode of operation in use.

   (b) Precision approaches on all involved runways.

   (c) Existence of a Normal Operations Zone (NOZ), which acts as a buffer zone allowing aircraft to recover the approach path in case of deviation.

   (d) Existence of a 610 m Non-Transgression Zone (NTZ) between both runways.

   (e) Monitoring controllers assigned to each runway.

   (f) Evasive maneuver procedures in case of NTZ intrusion.

   (g) Existence of a Parallel Approach Obstacle Assessment Surface (PAOAS).

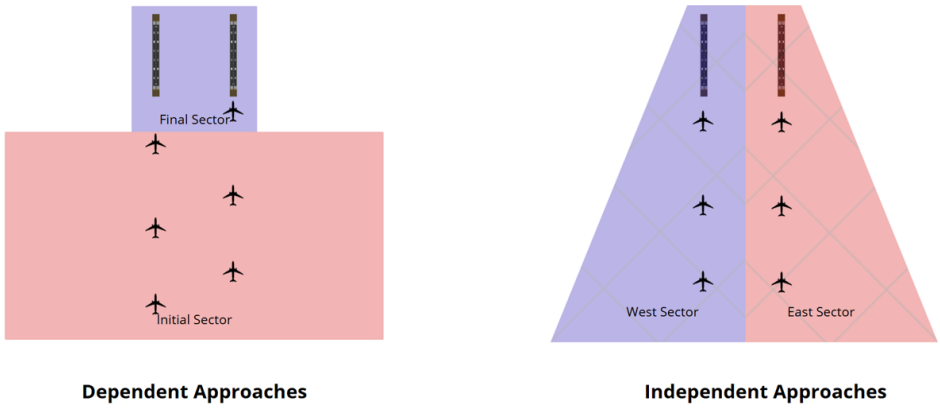

Figure 2.3: Comparison of dependent vs. independent parallel approach operations

This also results in a sectorization system based on traffic flow (in contrast to dependent approaches, where sectors are divided into initial and final phases), with independent ATC units assigned to each runway, and a single approach controller per runway.

2. **Dependent parallel approaches**. Simultaneous approaches to precision or non-precision instrument runways, where separation minima constraints exist between aircraft on different runways, require a centerline separation of at least **915 m**. Depending on the centerline separation, varying degrees of diagonal (horizontal) separation must be provided. This is detailed in Figure 2.4 and Table 2.5

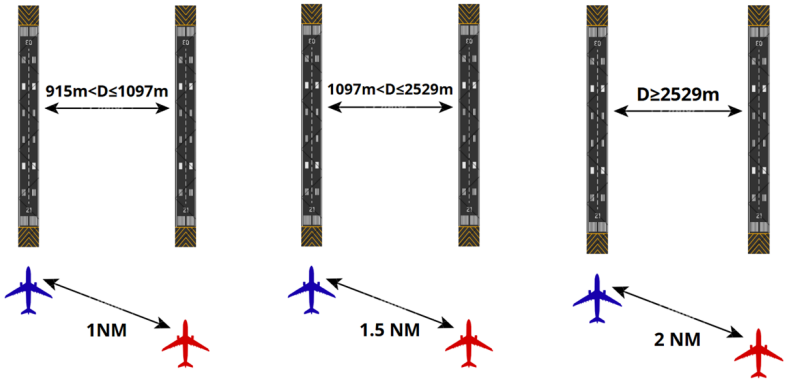

Figure 2.4: Diagonal separation between aircraft in dependent parallel approaches

3. **Independent parallel departures**. Parallel runways can be used for independent instrument departures if one of the following conditions is met:

   (a) Both runways are used exclusively for departures.

   (b) Semi-mixed operations: one runway is used for departures, while the other operates in a mixed mode (arrivals and departures).

   (c) Fully mixed operations on both runways.

   If the centerline separation is less than **760 m**, the runways shall be operated as a single runway.

4. **Segregated parallel operations**. As explained above, in this mode each runway is dedicated exclusively to one type of movement. Segregated parallel operations are allowed whenever runway centerlines are separated by a distance greater than 760m and when the nominal departure tracks diverges by more than 30° from the missed approach path. If centerline separation is below 760m, both runways shall operate as a single runway.

Mode	Type	Spacing	Diag Sep
1	AA	$1035 \leq S < 1310\,\text{m}$	–
	AA	$1310 \leq S < 1525\,\text{m}$	–
	AA	$S \geq 1525\,\text{m}$	–
2	AA	$915 < S \leq 1097\,\text{m}$	1 NM
	AA	$1097 < S \leq 2529$,m	1.5 NM
	AA	$S \geq 2529\,\text{m}$	2 NM
3	DD	$S \geq 760\,\text{m}$	–
	DM	$S \geq 760\,\text{m}$	–
	MM	$S \geq 760\,\text{m}$	2 NM (A+A) only
4	AD	$S \geq 760\,\text{m}$	–
	AM	$S \geq 760\,\text{m}$	–
	DM	$S \geq 760\,\text{m}$	2 NM (A,A)

Table 2.5: Parallel runways spacing & diagonal separations

Additionally, the runways can be staggered. Staggering refers to displacing the thresholds of parallel runways so they are not longitudinally aligned. In this context, one runway threshold is positioned ahead of, or behind the other, relative to the direction of arriving aircraft. The main advantage of staggering is that it increases the effective separation between aircraft without requiring greater physical centerline distance.

For every 150 m of stagger toward the arriving aircraft, the required minimum centerline separation can be reduced by 30 m. Conversely, for every 150 m of displacement away from the arriving aircraft, an additional 30 m must be added to the centerline separation.

2.4.2. Runway system geometry

From a conceptual point of view, an ideal airport layout would feature multiple runways functioning entirely independently, allowing total capacity to simply reflect the sum of each runway's throughput [23]. However, achieving the necessary centerline separation requires vast expanses of land, which are often limited by environmental constraints, urban development, and even political considerations. As a result, various forms of interdependence between runways exist, and each introducing its own operational limitations and procedures. These built-in dependencies reduce the total efficiency and restrict how much traffic an airport can handle at any given time. The following dependencies have previously been identified and explained in existing literature, namely by van der Klugt [22] [21] , and Stomatopoulos [31] amongst others.

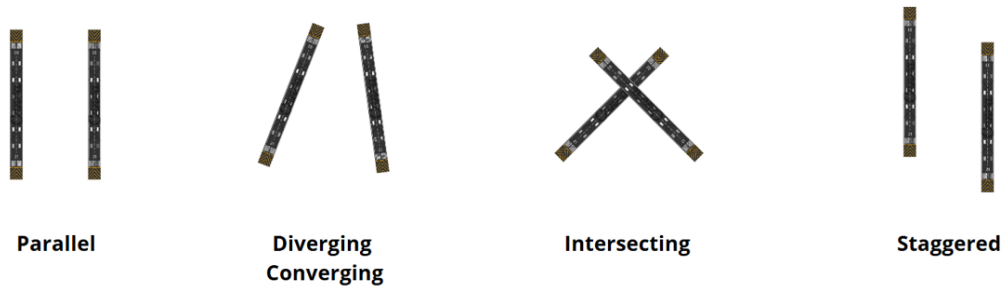

Figure 2.5: Runway layouts

Parallel runways

In parallel runway operations, numerous dependencies exist and these depend on the mode of operation (dependent, independent, segregated or opposite direction) as well as the centerline separation between runways.

1. **Segregated operations**. As explained above, in segregated operations each runway adopts landing or takeoff operations. However, dependencies still exist to avoid the simultaneous operation of departure and arrival in the missed approach track. As such, in coupled operations a departure may only be released once the arrival has completed its landing on the other runway or when the arrival is a sufficient distance D_{min} from the threshold. To account for cases where the minimum distance may be insufficient, the departure should rotate no later than the moment the arrival reaches the Missed Approach Point (MAP), avoiding a missed approach procedure.
2. **Dependent operations**. There exist four types of dependencies, all of which are explained in the table below.

No.	Type	Description
1	$A \rightarrow D$	Arrival on RWY1 followed by departure on RWY2: Departure is cleared when arrival exits the runway, with runway occupancy time $R_{A,\text{com}}$
2	$D \rightarrow D$	Interdeparture time between both departures is approximately G_{ij}
3	$A \rightarrow A$	Diagonal separation D_D imposed between aircraft arriving on both runways. Depends on centerline separation
4	$D \rightarrow A$	RWY1 departure is only cleared if the arriving aircraft is at least a minimum distance D_{min} from RWY2 threshold

3. **Independent operations** Independent Approaches see no additional dependencies, whilst independent departures have the sole requirement of specific track divergence of 30 degrees to avoid encounters

It must be noted than near parallel runways are those that have no intersection, and whose extended centerlines have an angle of divergence of 15° or less. The main consideration in designing procedures for simultaneous operations on near-parallel runways is the convergence point of their centerlines, which depends on runway alignment (even or staggered) and their angle. It is also important to assess whether the runways are used in converging or diverging directions. Independent approaches are typically not feasible in diverging configurations with intersecting paths, but diverging departures or segregated operations benefit from natural lateral separation. All operational modes should be carefully reviewed and adjusted to each aerodrome before implementation [29].

Converging and diverging runways

Converging and Diverging runways are those that do not directly intersect, but their projected centerlines do. Consequently, they are converging or diverging to and from each other. The risk in these cases can come from two sources:

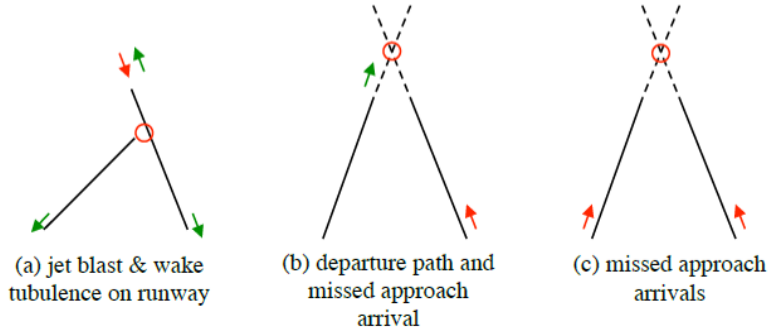

Figure 2.6: Converging Diverging dependency types [22]

1. **Jet blast on the ground**

   The first type of dependency involves the impact of wake turbulence and jet blast generated by operations on one runway affecting the safe use of the adjacent runway. As illustrated in Figure 2.6a, this situation occurs, for example, when an aircraft lines up or begins its takeoff roll in the southwest direction, producing wake turbulence and jet blast that may interfere with operations on the other runway. The extent of this interference depends heavily on the runway layout, particularly the location of the convergence point, the nature of the operations being conducted, and the aircraft types involved. Two main scenarios can be identified:

   a. **Departures on both runways:** In this case, the jet blast and wake turbulence generated by one departing aircraft may affect the departure on the adjacent runway. As a result, simultaneous departures are not permitted. The second aircraft can only be cleared for departure once the first has either cleared the convergence point or passed it on the adjacent runway, depending on the specific layout. In some configurations, even lining up on the runway may be restricted, thereby increasing departure intervals.

   b. **Arrivals and departures:** When a departure is initiated, the arriving aircraft on the other runway must be at a safe minimum distance from the threshold to avoid wake turbulence and jet blast interference. A departure clearance may only be issued once the arrival has passed the convergence point.

      To manage this dependency, four key variables must be considered:

Parameter	Description
t_{lu}	Line-up time per Wake Turbulence Category (WTC)
R_{cl}	Runway Occupancy Time (ROT) until the aircraft clears the convergence point, per WTC
R_{int}	ROT until the aircraft has passed the jet blast point on the adjacent runway (for both arrivals and departures), per WTC
D_{min}	Minimum distance from the arrival to the runway threshold required to safely release a departure

The purpose of maintaining D_{min} is to minimize the risk of a missed approach. This distance must be large enough to allow sufficient time for issuing a landing clearance prior to touchdown.

2. **Missed Approach**

   Figure 2.6b shows the potential conflict between a departure path and the missed approach track of an arrival. To avoid this, a departure is only permitted if the arriving aircraft is at a minimum distance D_{min} from the runway threshold, ensuring the departure is completed before the arrival reaches the threshold.

   Figure 2.6c shows converging arrivals where missed approach paths can intersect. To reduce the risk of simultaneous missed approaches, staggering is applied. This enforces separation between arrivals on different runways: an arrival on runway "X" is only cleared if the aircraft approaching runway "Y" is at least D_{st} from its threshold. The value of D_{st} depends on weather, local conditions, and Wake Turbulence Category (WTC). In some configurations and under good visibility, staggering may not be required.

Table 2.6: Subdependencies in Converging & Diverging operations [22]

Dependency	**Type**	**Regulations**	**Variables**
Jet blast	$D \rightarrow D$	Only one mov. at jet blast point	$t_{lw},\ R_{\text{int}},\ R_{cl}$
Jet blast	$A \rightarrow D$	Only one mov. at jet blast point	$t_{lw},\ R_{\text{int}},\ R_{cl},\ D_{\min}$
Missed approach	$A \rightarrow D$	No simultaneous DEP and ARR	$t_{lw},\ R_{\text{int}},\ R_{cl},\ D_{\min}$
Missed approach	$A \rightarrow A$	Staggering of arrivals	$R_{\text{int}},\ D_{st}$

A = arrival, D = departure

Intersecting runways

Intersecting runways are those that have a point of intersection. An advantage is that a higher wind coverage is provided , as runways face different directions. They have similar behaviour to converging and diverging runways, but in this case the point of interest now lies in the intersection between both runways. The location of this point affects capacity, as the closer it is to the landing and departure thresholds, the greater the capacity.

If two intersecting runways are active at the same time, ATC must closely monitor to avoid risky situations arise. Three different situations can occur: two departures, two arrivals or a departure and an arrival.

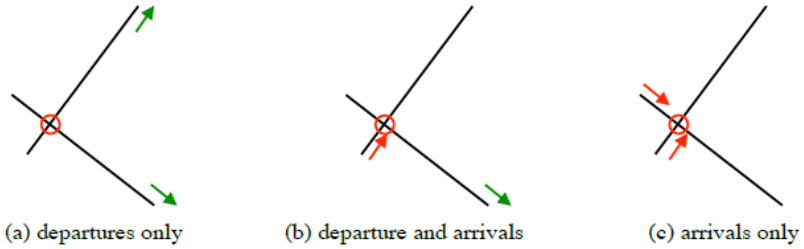

Figure 2.7: Intersecting dependency types [22]

1. **Two Departures**

   When intersecting runways are used exclusively for departures (see Figure 2.6a), it is important that the intersection lies relatively close to the origin point of the departures (as illustrated). If this condition is not met, the resulting wake turbulence may be strong enough to require the application of the minimum inter-departure separation to departures on both runways, which would essentially reduce the capacity of the system to that of a single runway.

   Hence, a departure on RWY 2 may only be cleared once the preceding departure on RWY 1 has crossed the point of intersection. This type of runway occupancy time is referred to as R_{int}.

2. **Departure & Arrival**

   In the case of a departure from RWY 1 followed by an arrival on RWY 2, the arrival should be at least at a distance $D_{\min}$ when the departure is cleared. Conversely, if the arrival precedes the departure, the departure can only be cleared once the arrival has passed the intersection point, again using the occupancy time R_{int}.

3. **Two Arrivals**

   In the case of two simultaneous arrivals, the most favorable scenario is having the intersection located closer to the arrival directions. This secures that the aircraft cross the intersection as quickly as possible. In such situations, a staggering distance D_{st} is imposed.

Table 2.7: Dependent operations on intersecting runways. [22]

Dependency	Type	Regulations	Variables
Intersection (a)	$D \rightarrow D$	Clearance after D passed intersection	R_{int}
Intersection (b)	$A \rightarrow D$	Clearance after A passed intersection or A should be at distance before threshold	$R_{\text{int}},\ D_{\min}$
Intersection (c)	$A \rightarrow A$	Staggering of arrivals	D_{st}

2.4.3. Meteorological conditions

Airport weather conditions have a significant impact on runway capacity, as factors including wind and visibility can affect the spacing and flow of aircraft.

METAR Data

A METAR (Meteorological Aerodrome Report) is a standardized weather report issued at regular intervals, typically every hour, providing current surface weather conditions at an aerodrome. It follows the international format set by the International Civil Aviation Organization (ICAO) and the World Meteorological Organization (WMO). This type of data is of great use for controllers and flight crew as it provides a consistent and short summary of weather conditions.

As shown in Figure 2.8, each METAR begins with the report type (METAR or SPECI) and the ICAO location indicator of the aerodrome. This is followed by the date and time of the observation (UTC) and, where applicable, modifiers such as AUTO for automated reports. The next section provides detailed wind information, including direction in degrees and speed in knots. Gusts are indicated by a "G" followed by the gust speed, and highly variable winds are denoted by "VRB" or by specifying the range of variation.

Visibility is then reported, usually in meters (except in the US). In conditions of low visibility, the Runway Visual Range (RVR) may be included, specifying the distance a pilot can see down a specific runway. This is followed by the "present weather" group, which describes significant phenomena through abbreviations such as rain (RA), snow (SN) or fog (FG). Cloud coverage and ceiling are then reported using codes such as FEW (few), SCT (scattered) or BKN (broken) along with the height of the cloud base in hundreds of feet above ground level.

The temperature and dew point are listed next, separated by a slash, and reported in degrees Celsius. Negative values are indicated with the prefix "M" (minus). The altimeter setting (barometric pressure) follows, expressed in either hectopascals (prefix "Q"). Some METARs also contain a Runway State Group (RSG), providing information about runway contamination type. [32]

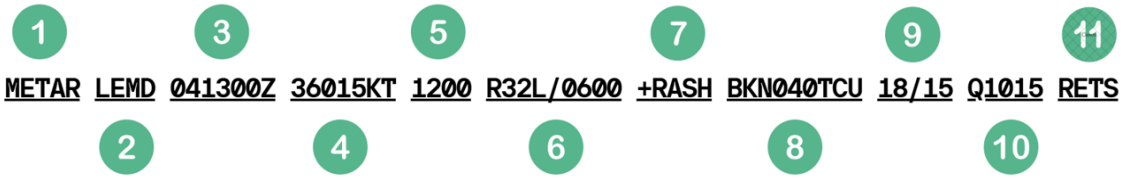

Figure 2.8: Sample METAR

	Description
1	Routine aviation weather observation
2	Reporting station (Madrid-Barajas in this case)
3	Time & day of month of observation
4	Wind direction and speed
5	Visibility in m
6	Runway visual range
7	Heavy rain showers
8	Cloud coverage and ceiling
9	Temperature & dew point
10	Altimeter setting
11	Runway state group

Wind

Wind is also an influential factor affecting runway capacity. The two characteristics of interest are wind speed and wind direction, both of which are typically reported in METAR data. Wind direction relative to the runway heading is decomposed into two components: headwind/tailwind and crosswind.

The headwind component is generally beneficial for aircraft operations, as it increases the relative airflow over the wings, improving lift and reducing the required takeoff and landing distances. Conversely, a tailwind increases the

ground speed required for takeoff and landing. Both components are significant because they directly influence the aircraft's ground speed. A stronger headwind results in a lower ground speed, which increases the time taken to fly the final approach segment along a common arrival path. This extended approach time can, in turn, lead to longer inter-arrival times, reducing the achievable arrival rate and overall runway throughput [22]. This will be further discussed in ongoing sections.

The crosswind component is critical in determining runway usability. Excessive crosswinds can constrain operations, forcing the change of runway configuration or use of alternative runway. The maximum crosswind component is documented in an aircraft's Pilot's Operating Handbook (POH). The crosswind component varies for different aircraft types. For most commercial aircraft, this ranges between 25 and 40 knots.

A runway can only be used if both the tailwind and crosswind remain within specified operational limits. These limits may be imposed by regulatory authorities, airport operators, or individual airlines. If either component exceeds its allowable threshold, the active runway configuration must be changed to align more closely with the prevailing wind.

Visibility

Airports classify visibility into three main categories: good visibility, marginal visibility, and low visibility. In the US, these are defined as Visual Meteorological Conditions (VMC), Marginal Meteorological Conditions (MMC), and Instrument Meteorological Conditions (IMC) [22]. Each category requires different operational procedures. When visibility is marginal or low, airport capacity is usually reduced. During low visibility conditions, specific Low Visibility Procedures (LVP) are implemented, which can involve increasing the minimum separation between aircraft to maintain safety.

Visibility at an airport is characterized by three main factors: the visibility distance, the cloud base height, and the Runway visual range. Each of these factors has defined thresholds that determine the current weather situation at the airport. Visibility distance is important for air traffic controllers and pilots as it affects their ability to see the runway and other aircraft. The height of the cloud base influences whether controllers can visually monitor aircraft from the control tower. When visibility is insufficient, reliance on ground radar increases, which leads to larger separation standards. Additionally, the cloud base affects the decision height for pilots to visually identify the runway during an Instrument Landing System (ILS) approach. The RVR impacts the pilot's runway visibility and also limits taxiway operations.

2.4.4. Wake separation requirements

Wake turbulence separation is, without doubt, the most constraining factor when discussing runway capacity. The subsections below will develop how the phenomena is generated, its effect in runway operations, and the different schemes utilized to properly classify and identify aircraft based on the wake turbulences generated.

Wake turbulence phenomena

A wingtip vortex is a rotating, trailing spiral of air that forms at a wing's tip due to high-pressure air from the wing's lower surface flowing around the tip toward the low-pressure region above the wing, creating a persistent swirling circular motion that extends downstream [33].

Lift is generated thanks to the pressure differential between the lower part of the wing and the upper part. However, this pressure difference between below and above the wing is what generated the roll up of the airflow at the wingtip, generating a wake of two counter-rotatting cylindrical vortices.

The vortex's strength is influenced by the aircraft's weight, speed, wingspan, and the shape of its wing. Additionally, the use of flaps can also alter the vortex formed. Notably, the vortex strength of an aircraft increases proportionally to an increase in its weight or a decrease in its speed. As turbulence-induced decay of wake is accelerated in a "dirty" aircraft configuration, the maximum vortex strength is observed when the aircraft is heavy, clean, and slow [34].

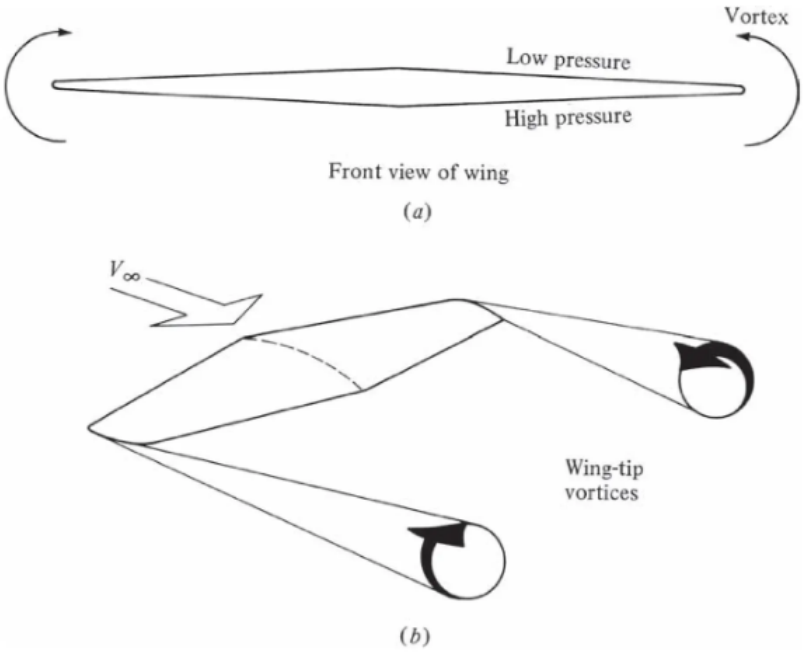

Figure 2.9: Wingtip vortex phenomena [33]

Once generated, vortices descend until they decay (or reach the ground). Decay generally happens rapidly, often within 2 to 3 minutes, and is accelerated in windy and turbulent conditions over land due to increased fluctuations in wind velocity. It also occurs significantly faster in close proximity to the ground, namely called the ground effect. The rate of decay is also influenced by the aircraft's wing features and how the load is distributed. A greater wingspan reduces the decay, whereas a smaller wingspan increases it.

An encounter with the vortex generated by a preceding aircraft is defined as a wake vortex encounter (WVE). These encounters cause severe consequences to the trailing aircraft, such as sudden and uncontrolled rolling motion in both directions, which can lead to the temporary or permanent loss of control of the aircraft. Thus, in order to prevent these encounters during approach or departure, safety separations between leading and trailing aircraft must be imposed. This will be developed in the following subsubsections.

ICAO separation requirements

As explained in the previous subsubsection, aircraft´s wake vortex depend mainly on the aircraft´s weight and wingspan. This will mean that certain combinations of leading and following aircraft will be riskier than others ie a heavy aircraft followed by a light will be more dangerous than a light followed by a heavy. This results in four wake turbulence categories (WTC) separation scheme.

The ICAO document 4444 PANS-ATM [35] classifies aircraft into four different categories: "L" (light), "M" (medium), "H" (heavy) and "S" (super-heavy) [1] based on aircraft maximum take-off weight (MTOW). These are shown in Table 2.8. Table 2.9 further classifies frequent aircraft models into these categories.

Although its decresing occurence, the Boeing 757 is a special case. Due to its unusually slow approach speed and wing design, it produces a significantly greater wake vortex than other aircraft in it´s class. For this reason, it is classified as a Heavy aircraft when in leading position, and as Medium in a trailing position [35].

[1] Airbus A380-800 categorized into newly-created category "Super heavy" S in 2008

Table 2.8: ICAO WTC based on MTOW [35]

WTC	MTOW
L	$MTOW < 7{,}000$ kg
M	$7{,}000$ kg $< MTOW < 136{,}000$ kg
H	$MTOW > 136{,}000$ kg
S	Airbus A380-800

Table 2.9: Representative aircraft in ICAO WTC, ordered by MTOW.

L (Light)		M (Medium)		H (Heavy)	
Aircraft	**MTOW**	**Aircraft**	**MTOW**	**Aircraft**	**MTOW**
Cessna 172	1,100	ATR 72-600	23,000	Boeing 767-200	159,000
Diamond DA42	1,900	CRJ1000	39,000	Boeing 767-300ER	186,900
Pilatus PC-12	4,740	Boeing 737-800	79,000	Airbus A330-300	242,000
Beech King Air 200	5,670	Airbus A321neo	97,000	Airbus A340-600	368,000
Learjet 35A	6,300	Boeing 757-300*	124,000	Boeing 747-400	396,900

In this sense, ICAO defines two types of separations that must be considered. The first is departures Time Based Separation, which specifies the minimum waiting period for a second aircraft after the preceding aircraft has departed. Pilots are responsible for maintaining this separation, which applies to departures from the same runway, intersecting runways, and closely spaced parallel runways. The applicable separation values are provided in Table 2.10. It should be noted that values shown in brackets are not officially defined by ICAO; in such cases, the minimum separation is used, with 60 seconds being the most common value. The starred-values for the super category are not defined by ICAO, but instead by LVNL based on data collection [36].

The second type is Arrivals Distance Based Separation, which must be maintained by aircraft following a common path. This applies to successive departures on the same runway along the shared departure route, up to the point where aircraft diverge as well as to aircraft approaching the same common approach path and depends on the flight speeds of the two aircraft. Distance-based separation is also applied to successive arrivals along the full length of their common approach path. Air traffic controllers manage this separation when directing both incoming and outgoing traffic. The required separation distances are listed in Table 2.11. When no separation is prescribed minimum radar separation (MRS) of 3NM (2.5 in some cases) applies [35].

Table 2.10: ICAO Time-Based Separation for departures [s] [35].

Leading aircraft → **Following aircraft ↓**	**Light**	**Medium**	**Heavy**	**Super**
Light	(60)	120	180	180
Medium	(60)	(60)	120	120
Heavy	(60)	(60)	(60)	120
Super	(60)	(60)	(60)	60*

Table 2.11: ICAO Distance-Based Separation between two consecutive aircraft [NM] [35] [36].

Leading aircraft → **Following aircraft ↓**	**Light**	**Medium**	**Heavy**	**Super**
Light	(3)	6	7	8
Medium	(3)	4	5	6
Heavy	(3)	(3)	(3)	5
Super	(3)	(3)	(3)*	(3)*

RECAT Separation Requirements

ICAO separation regulations are designed to account for the “worst-case scenario” within each aircraft category, which often results in overconservative separations. For example, the Heavy (”H”) category includes both the Boeing 767-300 and the Airbus A340-600, despite a difference in wingspan of over 15 meters and a MTOW difference exceeding 200 tons. A similar situation occurs in the Medium (”M”) category, where aircraft like the Embraer 145 and the A321neo differ by 16 meters in wingspan and 75 tons in MTOW. In these cases, separation distances are safe but overconservative, reducing operational efficiency [37].

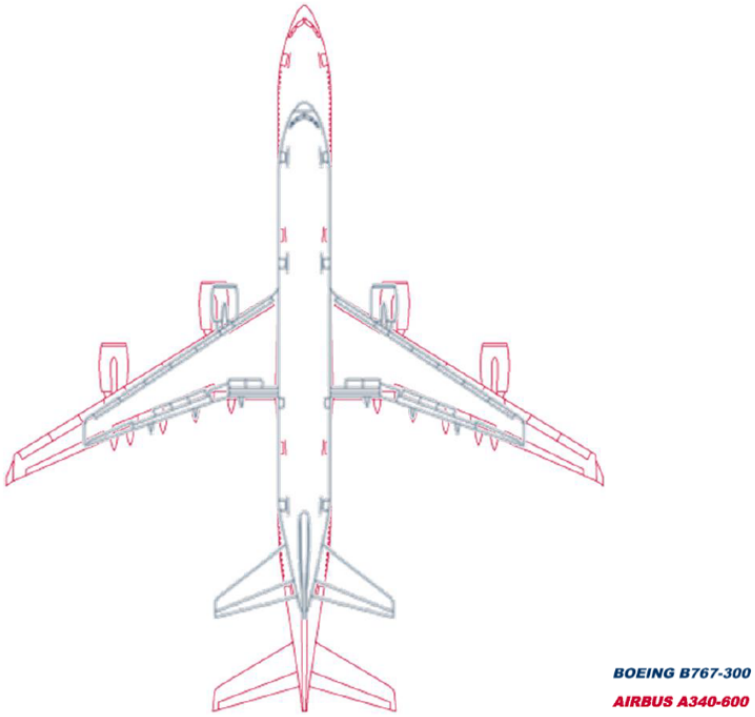

Figure 2.10: Comparison of aircraft size between boeing 767-300 and Airbus A340-600 [37]

To address these inefficiencies, Eurocontrol developed the RECAT-EU scheme [37], based on the FAA’s initial RECAT-1 framework, which was first implemented at Memphis International Airport in 2012. The benefits were significant: according to airport authorities, capacity increased by up to 20%, allowing the airport to accommodate as many as 22 additional arrivals per hour.

This new categorization subdivides the Medium and Heavy categories into Upper and Lower subcategories and introduces a Super Heavy category for aircraft such as the A380-800. By incorporating not only MTOW but also wingspan, RECAT-EU allows for more precise, aircraft-specific separation, reducing unnecessary spacing while maintaining safety.

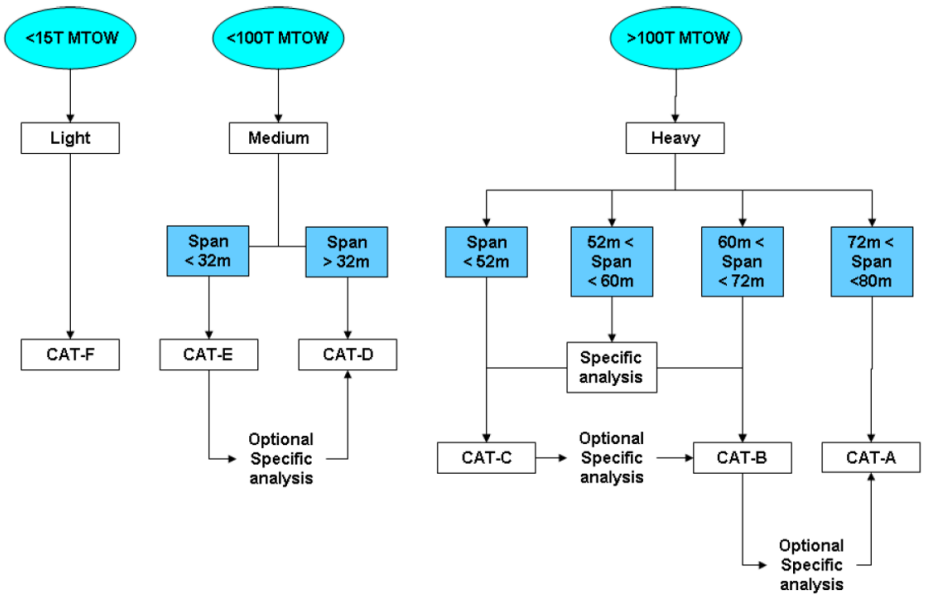

Figure 2.11: Categorisation scheme assigning aircraft to RECAT-EU categories [37]

Table 2.12: RECAT-EU Distance-Based Separation minima on approach and departure [NM] [37].

Following aircraft → Leading aircraft ↓	**Super Heavy A**	**Upper Heavy B**	**Lower Heavy C**	**Upper Medium D**	**Lower Medium E**	**Light F**
Super Heavy A	3	4	5	5	6	8
Upper Heavy B	(3)	3	4	4	5	7
Lower Heavy C	(3)	(3)	3	3	4	6
Upper Medium D	(3)	(3)	(3)	(3)	(3)	5
Lower Medium E	(3)	(3)	(3)	(3)	(3)	4
Light F	(3)	(3)	(3)	(3)	(3)	3

Table 2.13: RECAT-EU Time-Based Separation minima on departure [s] [37].

Following aircraft → Leading aircraft ↓	**Super Heavy A**	**Upper Heavy B**	**Lower Heavy C**	**Upper Medium D**	**Lower Medium E**	**Light F**
Super Heavy A	(60)	100	120	140	160	180
Upper Heavy B	(60)	(60)	(60)	100	120	140
Lower Heavy C	(60)	(60)	(60)	80	100	120
Upper Medium D	(60)	(60)	(60)	(60)	(60)	120
Lower Medium E	(60)	(60)	(60)	(60)	(60)	100
Light F	(60)	(60)	(60)	(60)	(60)	80

The implementation of the RECAT-EU scheme allows the reduction in separation for numerous combinations in leader-follower aircraft. For instance, in the case where a Boeing 767-300 leads and an Airbus A340-600 follows, separation can be reduced 1.5 NM when transitioning from the ICAO scheme to RECAT-EU.

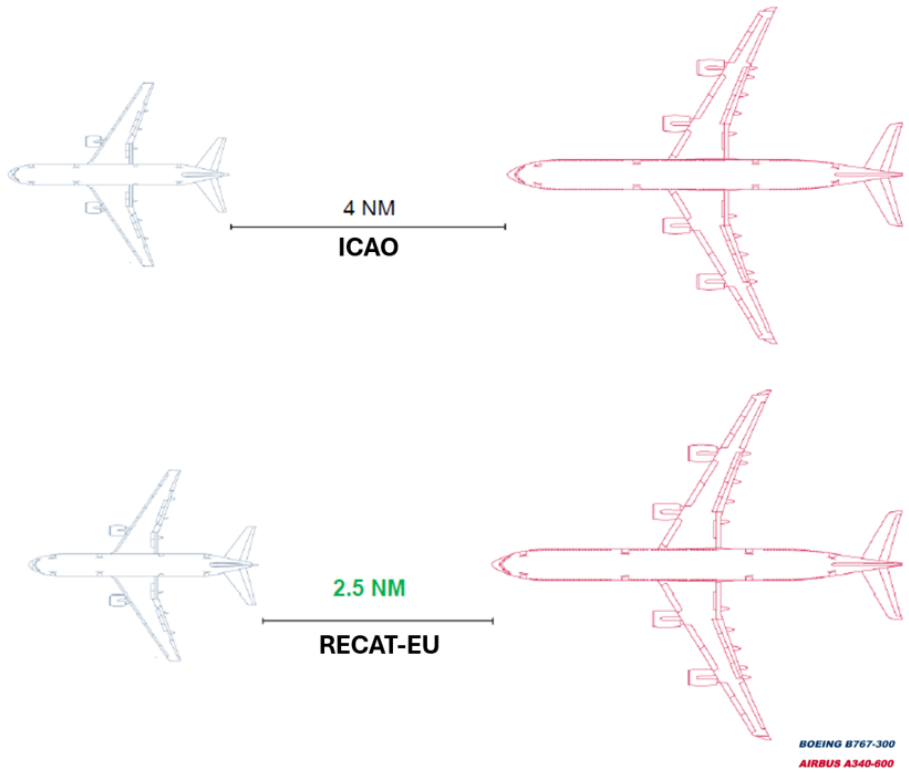

Figure 2.12: Comparison of ICAO and RECAT separations for a leading 767-300 following A340-600 case [37]

Following the implementation of RECAT-EU, airports can realize several immediate benefits, as highlighted by Eurocontrol [37]:

- **Capacity:** Runway throughput can increase by approximately 5% or more during peak hours at the most constrained European airports, with some cases reaching up to 8%.
- **Delay:** The enhanced flexibility provided by RECAT-EU allows for a faster recovery from overall delays.
- **Flight time:** For the same throughput, total flight time can be reduced for a given arrival or departure sequence, providing additional flexibility for air traffic control.

It is important to note that the performance and benefits of RECAT-EU are logically dependent on the specific fleet mix at each airport.

RECAT-EU can be implemented either fully or partially, to update or replace existing local wake separation procedures. Its operational deployment requires minimal modifications to the ATM functional system. This involves updating local flight plan strips, adapting Approach and Tower traffic displays with new wake turbulence categories, and publishing the updated minima.

Air traffic controllers must be trained to manage the six wake categories, which can be conducted using ATC simulations. Flight crews must be briefed on local procedural changes. ICAO phraseology remains unchanged, as “HEAVY” aircraft types are retained [37].

The changes in distance and time minima can be better visualized in the following tables:

Table 2.14: Difference in wake separation minima on approach between ICAO and RECAT-EU schemes [NM] [37].

Following aircraft → **Leading aircraft ↓**	**Super Heavy A**	**Upper Heavy B**	**Lower Heavy C**	**Upper Medium D**	**Lower Medium E**	**Light F**
Super Heavy A	(+0.5)	-2	-1	-2	-1	
Upper Heavy B		-1		-1		+1
Lower Heavy C		-1 (-1.5)	-1	-2	-1	
Upper Medium D						
Lower Medium E					-1	
Light F					(+0.5)	

Table 2.15: Difference in wake separation minima on departure between ICAO and RECAT-EU schemes [s] [37].

Following aircraft → **Leading aircraft ↓**	**Super Heavy A**	**Upper Heavy B**	**Lower Heavy C**	**Upper Medium D**	**Lower Medium E**	**Light F**
Super Heavy A		-20		-40	-20	
Upper Heavy B				-20		+20
Lower Heavy C				-40	-20	
Upper Medium D						
Lower Medium E						-20
Light F						+20

As shown in Table 2.14 and Table 2.15, certain combinations of leading and following aircraft demonstrate that RECAT-EU can, in specific cases, be less efficient than ICAO. For instance, when an Upper Heavy aircraft is followed by a light one.

According to EU Regulation 2017/373 ATMS/ANS Part IV [30]:

"As an alternative to the wake turbulence separation minima prescribed in AMC1 to AMC6 ATS.TR.220, an air traffic services provider may decide to implement RECAT-EU or parts thereof, subject to the approval of the competent authority."

This provision enables the implementation of RECAT-EU/ICAO hybrid systems, allowing the selection of the most advantageous separation minima for each situation.

Another option is to implement a hybrid scheme. Such a scheme could be based on either a 6-CAT or 7-CAT approach, combining RECAT-EU with the ICAO LIGHT WTC. A hybrid 6-CAT solution can be applied without the use of a separation support tool (drawing on existing operational examples with six categories, similar to RECAT-EU, whereas a hybrid 7-CAT solution, being more complex, would require tool-based separation support).

6CAT Hybrid ICAO - RECAT-EU

In this scheme, separation minima for ICAO LIGHT aircraft remain unchanged, following the legacy ICAO WTC values. It is important to note that for aircraft in the LOWER MEDIUM category (MTOM between 7 and 100 tons, with a wingspan below 32 m), no reduction in separation is permitted when following a SUPER (including the A380). In such cases, the 7 NM minimum continues to apply.

The hybrid wake turbulence separation scheme has been implemented in Austria since 2018 [38]. In practice, its application has been restricted to arrival operations, specifically targeting aircraft in the Upper Medium, Lower Heavy, and Upper Heavy categories.

Based on RECAT-EU | Based on ICAO WTC | Based on both

RECAT-EU			CAT-A Super Heavy	CAT-B Upper Heavy	CAT-C Lower Heavy	CAT-D Upper Medium	CAT-E Lower Medium	CAT-F Light
	ICAO legacy		A380	H		M		L
		RECAT-EU 6-CAT hybrid	A380	UH	LH	UM	LM	L
CAT-A	A380	A380		4	5	5	7	8
CAT-B	H	UH		3	4	4	5	6
CAT-C		LH			3	3	5	6
CAT-D	M	UM						5
CAT-E		LM						4
CAT-F	L	L						

Figure 2.13: RECAT-EU Hybrid 6CAT distance minima scheme [37]

7CAT Hybrid ICAO - RECAT-EU

In this scheme, separation minima for LIGHT aircraft remain as the legacy ICAO WTC values. A new category ”SMALL MEDIUMS” is introduced for aircraft with an MTOM between 7 and 15 tons. While these are classified as MEDIUM under ICAO, they fall into the LIGHT category under RECAT-EU. For this group, the standard ICAO legacy separation applicable to ICAO MEDIUM WTC is retained.

The remaining MEDIUM aircraft, with MTOM between 15 and 100 tons and a wingspan of less than 32 m, continue to be classified under the RECAT-EU LOWER MEDIUM category, with the corresponding separation minima applied.

Based on RECAT-EU | Based on ICAO WTC | Based on both

RECAT-EU			CAT-A Super Heavy	CAT-B Upper Heavy	CAT-C Lower Heavy	CAT-D Upper Medium	CAT-E Lower Medium	CAT-F Light	
	ICAO legacy		J	H		M			L
		RECAT-EU 7-CAT	SH	UH	LH	UM	LM	SM	L
CAT-A	J	SH		4	5	5	6	7	8
CAT-B	H	UH		3	4	4	5	5	6
CAT-C		LH			3	3	4	5	6
CAT-D	M	UM							5
CAT-E		LM							4
CAT-F		SM							3
	L	L							

Figure 2.14: RECAT-EU Hybrid 7CAT distance minima scheme [37]

RECAT-EU-PWS

The Pairwise Wake Separation, or ‘S-PWS’, solution for approach and departure, developed under the SESAR2020 programme, is an evolution of the RECAT-EU separation scheme. It allows reductions in separation of up to 1 NM for distance-based operations or up to 30 seconds for departures, while maintaining safety.

There are multiple approaches to implementing the RECAT-EU-PWS scheme. It can be applied on a pairwise basis, typically supported by air traffic control (ATC) separation delivery tools, or through a categorical system, either with or without such tool support. Additionally, a procedural implementation may be adopted for selected aircraft type pairings, enabling targeted improvements to the wake turbulence categorisation scheme and facilitating incremental operational benefits.

RECAT-EU-PWS is based on frequent leader–follower aircraft pairs in European airspace and is designed to tailor

separation distances to the actual aircraft pair rather than broad categories. The system is grounded in detailed wake turbulence risk assessments under reasonable worst-case (RWC) conditions, with safety assurance provided in the EUROCONTROL Safety Case. Minima are anchored to selected pivot aircraft pairs, representing frequent traffic combinations aligned with current ICAO separation standards. Other aircraft pairs are then positioned relative to these pivot pairs based on their wake turbulence severity, measured using the Roll Moment Coefficient (RMC), with margins included to ensure overall risk remains acceptable. This approach slightly increases exposure for lower-severity pairs and reduces it for the most critical pairs, resulting in a balanced distribution of wake turbulence risk. Time-based separations for departures are derived from the same methodology and validated through the Wake Impact Severity Assessment (WISA) flight simulation campaign, confirming that reduced separation does not compromise safety.

Two main components define how the system works: the Pair-Wise Separation matrix and the 20-category (20CAT) scheme.

Pair-Wise Separation (PWS) Matrix

The PWS matrix is the core of RECAT-EU-PWS. It is a lookup table specifying the minimum wake turbulence separation for each aircraft pair. Instead of applying broad rules such as "all heavy aircraft require 4 NM behind a medium aircraft," the PWS matrix defines exact minima for frequent aircraft pairs, e.g., a Boeing 747-400 following an A320.

Dynamic and data-driven, the PWS matrix covers 103 aircraft categories and reflects real-world wake turbulence characteristics. It applies to distance-based separations for arrivals (DBS) and time-based separations for departures (TBS).

	A388	B748	B77L	B77W	A359	A35K	B744	A346	A345	B773	B772	A343
A388	2.5	4	4	4	4	4	4	4	4	4	4	4
B748		2	2	2	2.5	2.5	2	2.5	2.5	2.5	2.5	3
B77L		2	2	2	2.5	2.5	2	2.5	2.5	2.5	2.5	3
B77W		2	2	2	2.5	2.5	2	2.5	2.5	2.5	2.5	3
A359		2	2	2	2.5	2.5	2	2.5	2.5	2.5	2.5	3
A35K		2	2	2	2.5	2.5	2	2.5	2.5	2.5	2.5	3
B744		2	2	2	2.5	2.5	2	2.5	2.5	2.5	2.5	3
A346		2	2	2	2.5	2.5	2	2.5	2.5	2.5	2.5	3
A345		2	2	2	2.5	2.5	2	2.5	2.5	2.5	2.5	3
B773		2	2	2	2	2	2	2	2	2	2	2.5
B772		2	2	2	2	2	2	2	2	2	2	2.5
A343		2	2	2	2	2	2	2	2	2	2	2.5

Figure 2.15: Extract of PWS matrix for DBS arrivals [39]

	A148	B734	B733	B735	E195	E190	GL5T	GLEX	GLF5
A388	160	160	160	160	160	160	160	160	160
B748	110	100	100	100	100	100	110	110	100
B77L	110	100	100	100	100	100	110	110	100
B77W	110	100	100	100	100	100	110	110	100
A359	110	100	100	100	100	100	110	110	100
A35K	110	100	100	100	100	100	110	110	100
B744	110	100	100	100	100	100	110	110	100
A346	110	100	100	100	100	100	110	110	100
A345	110	100	100	100	100	100	110	110	100
B773	110	100	100	100	100	100	110	100	100
B772	110	100	100	100	100	100	110	100	100

Figure 2.16: Extract of PWS matrix for TBS departures [39]

20-Category (20CAT) Scheme

The 20CAT scheme complements the PWS matrix by grouping aircraft into finer categories based on mass, wingspan, and wing aspect ratio. Of the 20 categories, 14 are based on the PWS, while aircraft not included in these categories, such as the A330Neo or Boeing 777X, are assigned through dedicated analysis.

For aircraft types outside the 14 PWS-based categories, the original RECAT-EU 6-category system is utilized, ensuring full coverage of all aircraft types.

An example of aircraft categorised using the 14-CAT scheme is shown in Figure 2.17, where aircraft in black belong to the PWS matrix and the ones in red have been assigned utilizing a specific analysis.

Cat Name	A1	B1	B2	C1	C2	C3	C4	D1	E1	E2	E3	F1	F2	F3
Ac type in 96 list	A388	B77L B77W A351 A359 A358 B744 A346 A345 B778 B779	B773 B772 A343 A332 A333 A342 B788 A338 A339 B78X	MD11 DC10	B764 B762 B763 IL76	A306 A30B A310 A3ST	B752 B753	B739 B738 B737 B736 A321 A320 A318 A319 MD83 MD82 A19N B37M B39M B3XM	A148 B734 B733 B735 E190 GL5T GLEX GLF5 B712 F100 F70 B463 RJ1H RJ85 E170 CRJ7 CRJ9 GLF4	F27 F50 DH8D AT75 AT72 FA7X AT43 AT45 AN32 AT46 AT73 AT76	CRJ2 J328 E145 E135 CL30 F2TH F900 FA50 CL60 GALX C750 CRJ1 E35L E45X	SF34 D328 E120 C680 C68A DHC4	C56X H25C C25C LJ45 LJ40 H25B C560 LJ60 BE40 LJ35 B190 FA20 LJ55 LJ75	B350 C25B PC12 C550 C25A C501 C525 C510 P46T PA34 C10T

Figure 2.17: Aircraft assigned to 14CAT system [39]

	A1	A	B1	B2	B	C1	C2	C3	C4	C	D1	D	E1	E2	E3	E	F1	F2	F3	F
A	3.0	3.0	4.0	4.0	4.0	5.0	5.0	5.0	5.0	5.0	5.0	5.0	6.0	6.0	6.0	6.0	8.0	8.0	8.0	8.0
A1	2.5	3.0	4.0	4.0	4.0	5.0	5.0	5.0	5.0	5.0	5.0	5.0	6.0	6.0	6.0	6.0	7.0	7.0	8.0	8.0
B	2.5	2.5	3.0	3.0	3.0	4.0	4.0	4.0	4.0	4.0	4.0	4.0	5.0	5.0	5.0	5.0	7.0	7.0	7.0	7.0
B1		2.5	2.5	3.0	3.0	3.0	3.5	3.5	3.5	4.0	4.0	4.0	4.5	5.0	5.0	5.0	6.0	6.5	7.0	7.0
B2		2.0	2.0	2.5	2.5	2.5	3.0	3.5	3.5	3.5	3.5	4.0	4.5	5.0	5.0	5.0	5.5	6.5	7.0	7.0
C		2.0	2.0	2.5	2.5	2.5	3.0	3.0	3.0	3.0	3.0	3.0	4.0	4.0	4.0	4.0	5.5	6.0	6.0	6.0
C1		2.0	2.0	2.5	2.5	2.5	3.0	3.0	3.0	3.0	3.0	3.0	4.0	4.0	4.0	4.0	5.0	5.0	6.0	6.0
C3		2.0	2.0	2.0	2.0	2.0	2.0	2.5	2.5	2.5	2.5	3.0	3.5	4.0	4.0	4.0	4.5	5.0	6.0	6.0
C2		2.0	2.0	2.0	2.0	2.0	2.0	2.5	2.5	2.5	2.5	3.0	3.5	3.5	4.0	4.0	4.0	4.5	6.0	6.0
C4		2.0	2.0	2.0	2.0	2.0	2.0	2.0	2.0	2.0	2.0	2.5	2.5	3.0	3.5	3.5	3.5	4.0	6.0	6.0
D												2.5	2.5	2.5	2.5	2.5	3.5	4.0	5.0	5.0
D1												2.5	2.5	2.5	2.5	2.5	3.0	3.5	5.0	5.0
E												2.5	2.5	2.5	2.5	2.5	3.0	3.5	4.0	4.0
E1																		2.5	4.0	4.0
E2																		2.5	4.0	4.0
E3																		2.5	4.0	4.0
F																		2.5	3.0	3.0
F1																		2.5	3.0	3.0
F2																		2.5	3.0	3.0
F3																		2.5	2.5	2.5

Figure 2.18: 20CAT distance-based wake turbulence separation minima for arrivals and departures [39]

	A1	A	B1	B2	B	C1	C2	C3	C4	C	D1	D	E1	E2	E3	E	F1	F2	F3	F
A			100.0	100.0	100.0	120.0	120.0	120.0	120.0	120.0	140.0	140.0	160.0	160.0	160.0	160.0	180.0	180.0	180.0	180.0
A1			100.0	100.0	100.0	120.0	120.0	120.0	120.0	120.0	140.0	140.0	160.0	160.0	160.0	160.0	180.0	180.0	180.0	180.0
B									60.0	60.0	100.0	100.0	120.0	120.0	120.0	120.0	140.0	140.0	140.0	140.0
B1									60.0	60.0	100.0	100.0	110.0	120.0	120.0	120.0	140.0	140.0	140.0	140.0
B2									60.0	60.0	90.0	100.0	110.0	120.0	120.0	120.0	130.0	140.0	140.0	140.0
C									60.0	60.0	80.0	80.0	100.0	100.0	100.0	100.0	120.0	120.0	120.0	120.0
C1									60.0	60.0	80.0	80.0	100.0	100.0	100.0	100.0	120.0	120.0	120.0	120.0
C3									60.0	60.0	60.0	70.0	90.0	100.0	100.0	100.0	110.0	120.0	120.0	120.0
C2									60.0	60.0	60.0	70.0	90.0	90.0	100.0	100.0	100.0	110.0	120.0	120.0
C4									60.0	60.0	60.0	60.0	60.0	70.0	90.0	90.0	90.0	100.0	120.0	120.0
D																	90.0	100.0	120.0	120.0
D1																	70.0	90.0	120.0	120.0
E																			100.0	100.0
E1																			100.0	100.0
E2																			100.0	100.0
E3																			100.0	100.0
F																			80.0	80.0
F1																			80.0	80.0
F2																			80.0	80.0
F3																				

Figure 2.19: 20CAT time-based wake turbulence separation minima for departures [39]

The overall procedure for assigning aircraft to a category is illustrated in Figure 2.24, showing how aircraft types are classified into PWS or non-PWS categories to ensure that appropriate pair-wise minima are consistently applied. It should be noted that if a calculated pairwise separation is less restrictive than the corresponding Runway Occupancy Time or Minimum Radar Separation, the ROT or MRS values still apply and take priority.

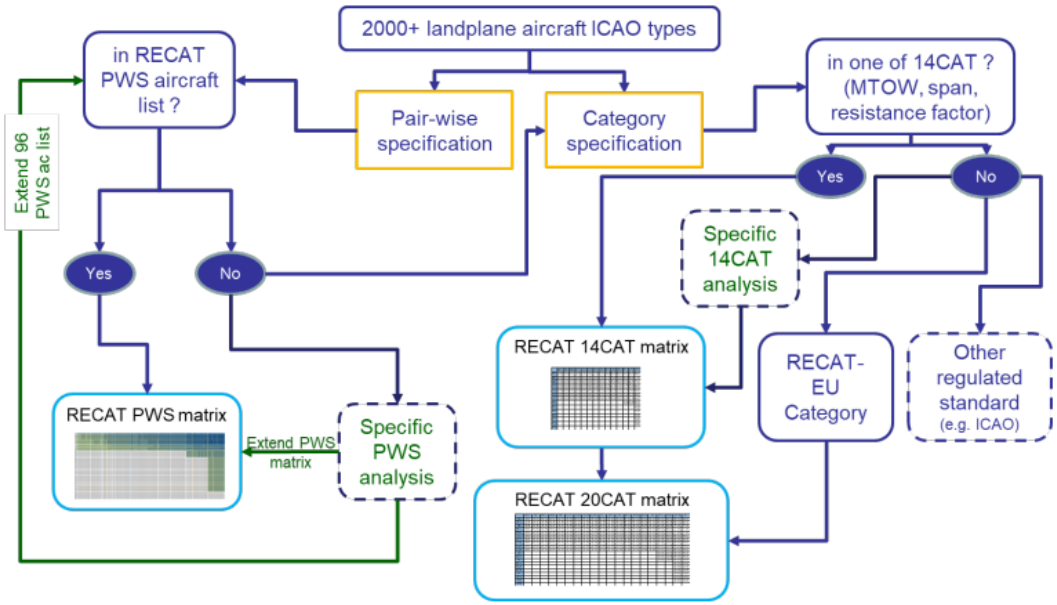

Figure 2.20: Aircraft type assignment logic into the RECAT-EU-PWS scheme [39]

When implemented, runway throughput can be increased by up to 10% compared to the ICAO legacy scheme [39]. However, several operational considerations must be addressed. Air Traffic controlers should be properly trained to manage the new separation requirements. Flight crews should be informed of the locally applicable PWS minima, understand that operations near these minima constitute high-intensity runway operations, and be aware that lower-severity wake turbulence encounters may occur more frequently.

Arrivals Time-Based Separation

Distance-Based Separation (DBS) upon arrivals is effective under calm wind conditions, but becomes limiting when aircraft experience headwinds.

When affected by headwinds, the aircraft's true airspeed (TAS) (the velocity of the airplane relative to the surrounding air) remains constant at the level required for safe flight, but its ground speed decreases because the headwind acts directly against its forward motion over the ground. For instance, an aircraft flying with a TAS of 150 knots into a 30-knot headwind will have a reduced ground speed of 120 knots, meaning it covers less distance across the ground in the same amount of time. This discrepancy between TAS and ground speed under headwind conditions leads to longer intervals between arriving aircraft when separations are based solely on

distance, thereby lowering runway throughput and reducing airport capacity. Time-Based Separation (TBS) addresses this challenge by replacing fixed distance separations with dynamic time intervals that account for wind effects. This can be visualized in Figure 2.21 and Figure 2.22

TBS consists in the separation of aircraft in sequence on the final approach to a runway using time intervals instead of distances. These intervals are established from the equivalent time-to-fly of the distance minima observed in low wind conditions. This enables air navigation service providers (ANSPs) to provide a stable arrival runway throughput across all headwind conditions [40].

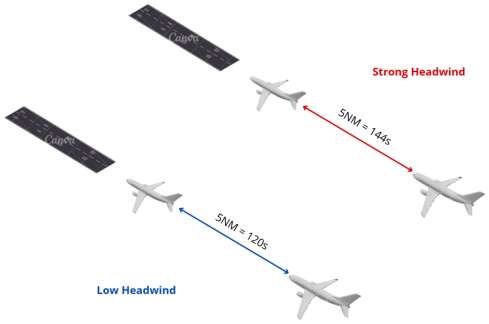

Figure 2.21: Distance-Based Separation

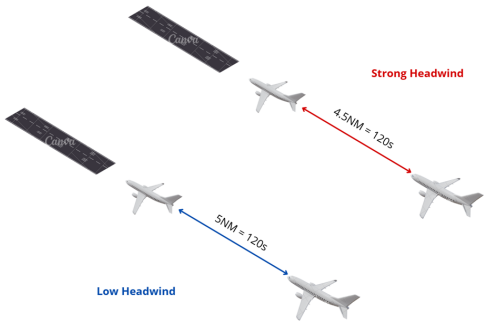

Figure 2.22: Time-Based Separation

The principle of TBS is to maintain equivalent time separation across different wind conditions. This is achieved through a dynamic reduction of the applicable distance separation minima as headwinds increase. The resulting minima are then derived from the distribution of equivalent time-to-fly of the distance-based separation minima in calm wind conditions, and can be verified through the comparison of quantiles (e.g., 1st, 10th and 50th percentiles) of the time separation distribution, as shown in Figure 2.23.

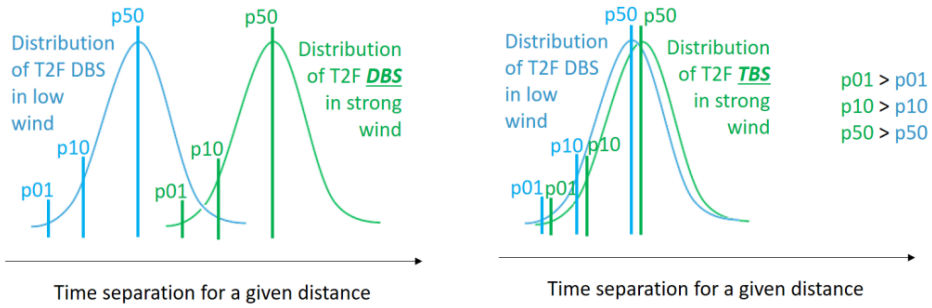

Figure 2.23: Time separation evolution corresponding to a given distance when operating DBS or TBS in low or strong headwind conditions [40].

The TBS system relies on two key inputs: the aircraft sequence, which anticipates speed management and defines the required time separation for each wake category pair, and the wind profile, captured approximately 10 minutes before landing, to set final approach separations. Using this information, TBS software provides controllers with real-time indicators based on aircraft airspeed, ground speed, heading, altitude, and weather conditions, without requiring modifications on board the aircraft. This allows controllers to apply equivalent distance information that reflects the effect of headwinds, maintaining runway capacity even in adverse weather.

Today, Time-Based Separation (TBS) is in daily operation at four major airports: London Heathrow (since 2015), Toronto Pearson (since 2022), Amsterdam Schiphol (since 2023) and London Gatwick (implemented in 2025). At Heathrow, the introduction of time-based minima has delivered a 20% increase in average capacity. In strong wind conditions, the system nearly triples the landing rate, enabling up to 4.2 additional landings per hour compared to distance-based procedures. Each year, this translates into approximately 90,000 minutes of reduced arrival delays, 15 kilotonnes of fuel savings, and a reduction of 47 kilotonnes of CO_2 emissions.

In Europe, besides being deployed at AMS, LGW and LHR, there is interest/plans in a few more airports, such as Copenhaguen, Vienna, Barcelona and Paris Charles de Gaulle amongst others. These are depicted in blue in Figure 2.24

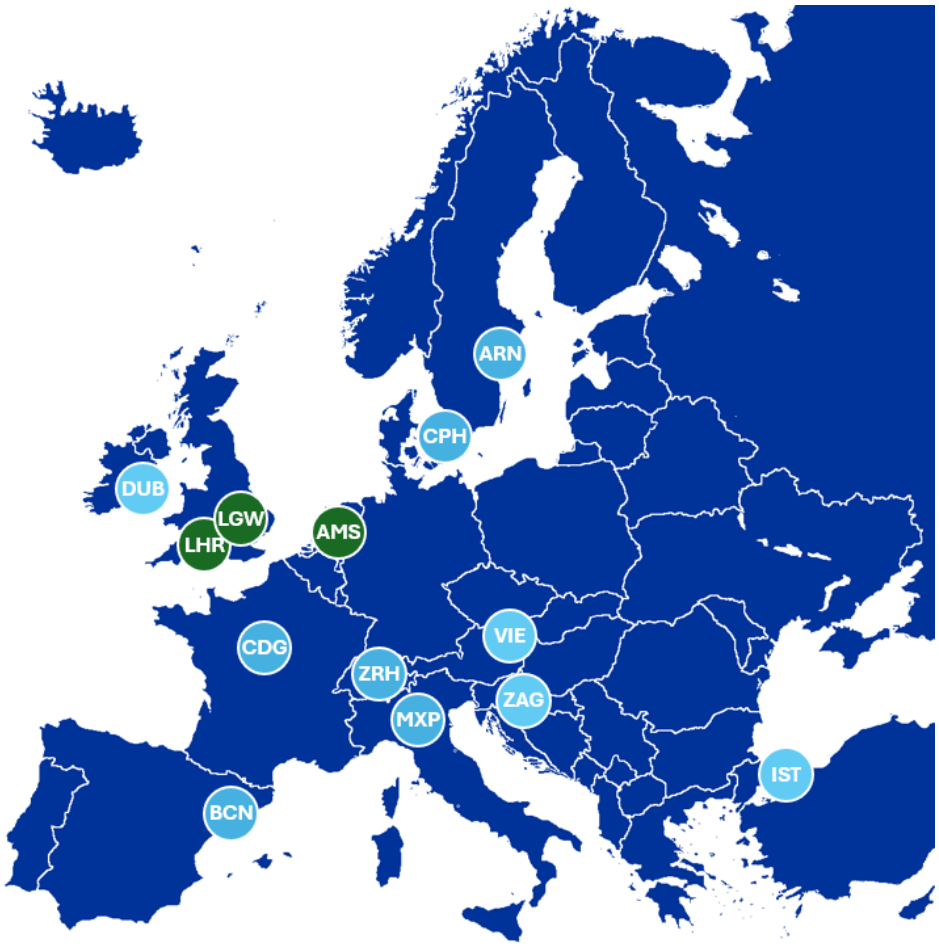

Figure 2.24: Status of TBS implementation in european airports

2.4.5. Aircraft Characteristics

The capacity of a runway system is also determined in large part by aircraft characteristics, such as approach and departure speeds, fleet mix, and runway occupancy times (ROTs).

Aircraft Speed Profile

In addition to the Wake Turbulence Category (WTC), various other aircraft characteristics can affect runway capacity. Two significant aircraft-specific factors are the speed profile and climb capabilities. When the leading aircraft has a slower ground speed than the trailing one, an extra distance buffer at the beginning of the shared path is necessary to maintain compliance with separation standards further along. In a similar manner, a 'closing-case' can occur when two aircraft take off consecutively, but the leading one climbs more slowly than the following aircraft, needing extra spacing [23].

Fleet Mix

Fleet mix refers to the distribution of different aircraft types operating at an airport, ranging from small general aviation aircraft to large long-haul wide-body jets. A diverse fleet mix complicates sequencing and separation requirements due to differences in wake turbulence categories and speeds. Airports dominated by a homogeneous fleet typically experience higher runway throughput than those with a highly heterogeneous fleet mix. For instance, Atlanta Hartsfield-Jackson operates under a highly mixed fleet environment, which influences its capacity. In contrast, airports with more uniform fleets, such as Riga (dominated by A220 and B737 aircraft), can achieve higher throughput.

Runway Occupancy Times (ROTs)

Runway Occupancy Time is defined as the time interval between the aircraft crossing the threshold and its tail vacating the runway [41]. ROT is a key determinant of runway capacity since subsequent arrivals or departures cannot proceed until the preceding aircraft has cleared the active runway. Factors affecting ROT, including aircraft type, final approach speed, runway exit type, airline, and the presence of a trailing aircraft on final approach, were identified by N.P. Meijers [42]:

1. **Aircraft Type** : Heavier aircraft have a larger momentum. As such, they require increased braking forces and a longer braking distance.
2. **Approach Speed**: Similarly to heavier aircraft, faster aircraft have a higher momentum. However, they also travel down the runway faster.
3. **Exit Type**: The exit system greatly affects the ROT. Using exits positioned at the far end of the runway notably increases ROT, whereas utilizing high-speed exits considerably decreases ROT.
4. **Airline**: The choice of the exit used to vacate the runway is also affected by each airline's braking procedures and pilot´s will to reduce aircraft taxi duration, thus impacting ROT.
5. **Following Aircraft**: Finally, the proximity of trailing aircraft on final approach incentivises pilots to vacate the runway earlier and reduces ROT on average.

Shorter ROTs can lead to improved capacity. However, these are not typically bottlenecks in runway system capacity.

2.4.6. Capacity, demand, and delay

Airport runway performance is commonly characterised through the interaction between demand (requested operations) and capacity, with delay representing the primary outcome experienced by users when demand approaches capacity. A key distinction in the capacity literature is between throughput capacity and practical (or sustainable) capacity. Throughput capacity corresponds to the theoretical maximum processing rate that could be achieved under idealised conditions, abstracting from small delays caused by random disturbances and operational imperfections. Practical capacity instead embeds a level of service requirement (e.g., a maximum acceptable average delay), and is therefore the capacity that can be sustained while maintaining an acceptable delay performance. This distinction is important because it connects capacity to service quality: an airport can operate below throughput capacity while still producing substantial delay if it is operating close to its practical limit.

A consistent finding across airport capacity studies is that the capacity–delay relationship is strongly non-linear. Delays may occur well before throughput capacity is reached because stochastic variations in demand and service processes cause temporary overloads and queue formation [2]. As utilisation increases, the system becomes less able to absorb perturbations, and the time required to dissipate accumulated delay increases sharply. This qualitative behaviour is consistent with classical queueing theory results for highly utilised service systems, where expected waiting time rises rapidly as utilisation approaches one.

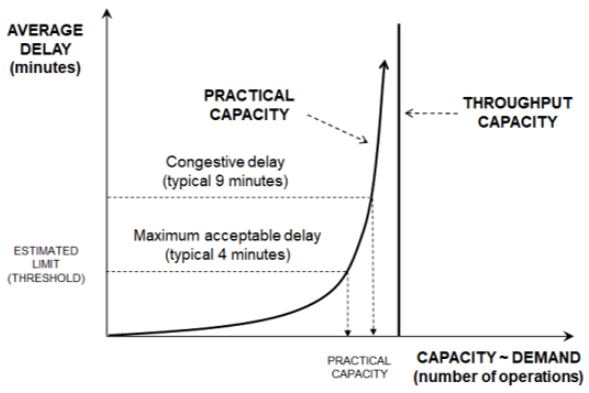

Figure 2.25: Demand, practical and throughput capacity [3]

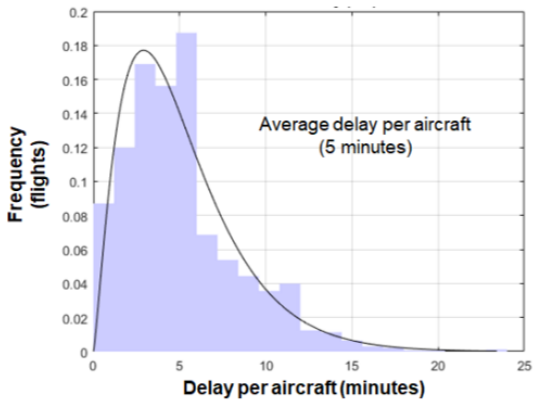

Figure 2.26: Typical probability distribution of aircraft delay [3]

Most analytical approaches reduce the interaction between demand and capacity to a single dimensionless quan-

tity: utilisation. In queueing notation, utilisation is often written as

$$\rho \;=\; \frac{\lambda}{\mu}, \tag{2.1}$$

where λ denotes the average demand rate and μ denotes the average service (capacity) rate. In airport applications, an equivalent operational definition is frequently used, for example departures per hour divided by throughput capacity:

$$U \;=\; \frac{\mathrm{DEP}}{C}. \tag{2.2}$$

In the remainder of this thesis, ρ and U are treated as equivalent utilisation measures expressed using different notation; both quantify how "close" the system operates to its capacity limit.

Rodríguez-Sanz and Rubio Andrada [43] propose an empirical model that maps utilisation to average departure delay. Using the operational utilisation definition in Eq. (2.2), average departure delay δ_t (minutes) is modelled as

$$\delta_t \;=\; \delta_0\big(\exp(U) - \lambda\big), \tag{2.3}$$

where δ_0 controls the magnitude of delay growth and λ shifts the curve to reflect baseline delay under very low traffic conditions. The authors calibrate this relationship using observed delay data from EUROCONTROL's Central Office for Delay Analysis (CODA) and report fitting parameters $\lambda = 1$ and $\delta_0 = 115$

A complementary modelling approach derives utilisation-delay sensitivity from steady-state queueing theory. In this literature, the relationship of capacity and delay can be discussed at different temporal scales: *short-term* delay formation (e.g., peak-hour dynamics) depends on detailed airport-specific processes and variability, whereas *long-term* effects (e.g., season- or year-average) can be approximated using steady-state arguments. A fundamental requirement is that long-run utilisation remains below unity ($\rho < 1$); otherwise queues do not reach equilibrium and expected delay grows without bound [2].

In heavy traffic, a widely used approximation predicts that expected waiting time (and thus delay) scales approximately with $(1-\rho)^{-1}$ as $\rho \to 1^-$ [44]. In comparative terms, this implies an "explosive" rise in delay as demand approaches capacity:

$$\mathbb{E}[W_q] \;\propto\; \frac{1}{1-\rho}. \tag{2.4}$$

Although Eq. (2.4) is a simplification of more general queueing expressions (which can also incorporate variability in arrivals and service), it is widely used for planning and scenario comparison because it requires only utilisation (or equivalently demand and capacity). Practically, it highlights that when utilisation is already high, even small increases in capacity (or small reductions in demand) can lead to disproportionately large reductions in expected delay.

3

Research Question

3.1. Research Gap

When airports operate close to their maximum capacity, difficulties in arrival and departure flows appear, especially during peak traffic periods. An important factor affecting these capacities is wake turbulence separation constraints, which prescribe separation minimas between aircraft to ensure safe operations.

However, these standards have been traditionally applied in a sort of rigid manner, utilizing broad wake turbulence categories (ICAO, RECAT). This results in runway capacity being underutilised, and especially in adverse wind conditions where strong headwind can further impact runway capacity.

Over the past decade, several approaches have been developed to address this issue, among which arrivals time based separation (TBS) and the new wake categorisation scheme RECAT-EU-PWS can be found. TBS changes dynamically the distance separation between arrivals depedning on headwind conditions, reducing the capacity loss that occurs in strong headwinds. In contrast, RECAT-EU-PWS replaces broad category rules with much finer category minimas.

However, no macro level analyses exist that evaluate TBS and RECAT-EU-PWS operations across different wind conditions and diverse airport environments. This gap is particularly interesting at capacity-limited airports, where even a slight increase in peak capacity can have significant operational implications. The objective is to end up with a quantifiable assessment of how the implementation of these approaches can increase capacity and reduce delay.

Besides capacity considerations common concern that is often faced by airport planners and authorities is ”How will the change of equipment of a specific airline affect our runway capacity?”. The legacy categorisation scheme, ICAO, can indeed provide a useful baseline, however, and as mentioned previously is relatively coarse. It cannot capture the subtle differences between aircraft types when these belong to a same WTC (ie an ATR72 and Airbus A321).

This limitation can become even more significant in the future, when considering the next generation of aircraft, many of which could feature novel wing designs, materials and characteristics. In such cases, reliance on broad categorical rules can fail to reflect the ”true” capacity of an runway system.

3.2. Research Question

The goal of this research is to investigate how a tool capable of estimating runway capacity for multiple airports under varying wind conditions optimized through the application of TBS and RECAT-EU-PWS can contribute to improved capacity. Furthermore, the study seeks to assess the potential of such a tool to inform long-term airport planning and strategic decision-making, supporting the development of more resilient and efficient airport operations. Consequently, the research question can be stated as:

Research Question

To what extent can the implementation of Time Based Separation and the wake categorisation scheme RECAT-EU-PWS increase an airport´s peak runway capacity?

In order to fully answer the main research question, it can be divided into smaller, more specific subquestions, grouped into different report chapters.:

Background & Problem Definition

- What is Runway Capacity and what are the metrics used to define it?
- What are the main factors affecting RSC?
- What are the existing methodologies that can be used to calculate it?
- How does Time Based Separation increase runway capacity in headwind conditions?
- What is RECAT-EU-PWS and how does this scheme differ from previous RECAT and ICAO?
- What is the relationship between capacity improvement and delay reduction?

Methodology

- How can the majority of existing runway dependencies be modelled in a mathematical form?
- How can the effect of SID allocation be taken into account in such model?
- How can RECAT-EU-PWS and TBS be modelled mathematically prior implementation in a simulator?

Simulation Model

- How can a discrete event simulation model be built such that it calculates runway capacity, reflects runway dependency and incorporates TBS and RECAT-EU-PWS in python?

Scenarios

- What relevant spanish airports can be used to validate the created simulation model?
- What are the conditions and parameters that characterise this selection of airports?

Results, Verification and Validation

- How does headwind affect runway capacity across different runway configurations? Can the implementation of TBS mitigate this capacity loss?
- To what extent can switching to a RECAT-EU-PWS categorization scheme increase runway capacity across different traffic mixes in different airports?
- How does the variation of other runway operational parameters affect capacity?
- To what extent can delay be reduced as TBS or RECAT-EU-PWS are implemented in the scenarios?
- How do different runway layouts affect capacity?
- In what ways can a RECAT-EU-PWS capacity tool help airport planners in assessing operational impact of specific aircraft on runway capacity?

4

Methodology

As discussed earlier, the numerical model should be capable of calculating Runway System Capacity for multiple runway geometries, varying fleet mix, varying weather conditions and Time-Based Separation and RECAT-EU-PWS functionality so that it can optimize and maximize peak airport capacity, and also assess how changes in traffic mix, headwind, runway mode of operation, equipment, and runway parameters affect both peak capacity and delay reduction/expansion.

4.1. Single Runway Operations

The first thing that this model should be capable of doing is properly simulating runway departure and arrival operations for a variety of runway configurations. These correspond to single runways, parallel runways, converging and diverging runways as well as intersecting runways. The interdependencies ruling over these modes have already been introduced and explained in chapter 2. Here below, the equations developed by van der Klugt [22][21] used to model each of these dependencies and modes will be presented and briefly explained. For the original explanation, please refer to his thesis.

4.1.1. Arrivals Only Capacity

When having arrivals-only mode, the ATC requirements are the following two:

1. **Wake Turbulence & Minimum Radar Separation**: As explained in previous sections, aircraft pairs must be appropriately separated in order to avoid wake-turbulence encounters. This separation must be kept throughout the entire common approach path.
2. **Runway Occupancy Time (ROT)**: The runway can only be occupied by one aircraft at a time.

As explained thoroughly in van der Klugt (2012) [21], the arrival-only capacity is calculated by determining the smallest inter-arrival time IAT possible between two consecutive arrivals. The inter-arrival time is determined by applying the two separation requirements as mentioned above. These requirements are, from a controller's perspective, applied between the entries of two arrivals on the common approach path D_A.

The inter-arrival time between consecutive aircraft is derived from the time separation imposed by air traffic control at the entry point of the common approach path. This imposed separation, denoted by μ, differs from the inter-arrival time IAT, which is measured at the runway threshold. The relationship between these two quantities depends on aircraft speeds and separation constraints along the common approach path, as illustrated in Figure 4.1.

Radar and wake turbulence separation are distance-based constraints that apply over the entire common approach path. Depending on the relative ground speeds of the leading and following aircraft, two situations can be distinguished: a closing case and an opening case.

In the closing case, the leading aircraft j is slower than the following aircraft i ($V_{A,j} < V_{A,i}$). As a result, the following aircraft may reduce the separation during the approach. To prevent this, the distance-based separation

must be satisfied at the end of the common approach path, i.e. at the runway threshold (Figure 4.2). The corresponding minimum time separation imposed by the controller at the entry of the common approach path is given by:

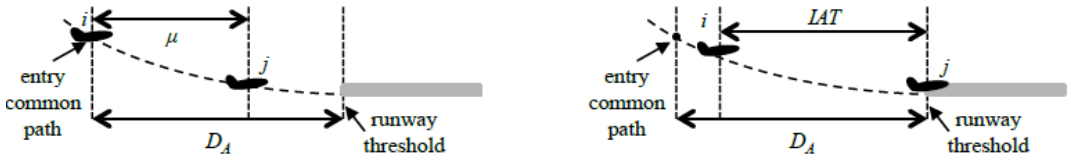

Figure 4.1: Time separation μ imposed throughout common approach path (left) and Inter-Arrival Time (right). [22]

$$\mu_1 = \frac{D_A}{V_{A,j}} - \frac{D_A - S_{ij}}{V_{A,i}} \tag{4.1}$$

where D_A is the length of the common approach path, S_{ij} is the required distance-based separation for the aircraft pair considered, and indices i and j denote the following and leading aircraft, respectively. The expression represents the minimum entry time separation needed to ensure the required distance separation at the runway threshold.

In the opening case, the leading aircraft is faster than or equal in speed to the following aircraft ($V_{A,j} \geq V_{A,i}$). In this situation, the distance between aircraft will not decrease along the approach, allowing the distance-based separation to be imposed at the entry of the common approach path (Figure 4.2). The corresponding imposed time separation is therefore:

$$\mu_1 = \frac{S_{ij}}{V_{A,j}} \tag{4.2}$$

which represents the time required for the leading aircraft to establish the necessary radar and wake turbulence separation at the entry of the common approach path.

Figure 4.2: Closing case, with a slower leader aircraft j and faster follower i (left) and Opening case, with a faster leader j and slower follower i (right). [22]

In addition to approach-path separation requirements, runway availability must be ensured before an arrival clearance can be issued. If the runway is not vacated before the following aircraft reaches the latest point at which a missed approach can be initiated, the arrival clearance is withheld and a missed approach is executed. This introduces an additional constraint that depends on the runway occupancy time of the leading aircraft and the missed approach point distance D_{MAP}.

For both the closing and opening cases, the time separation imposed to satisfy this runway availability constraint is given by:

$$\mu_2 = \frac{D_A}{V_{A,j}} - \frac{D_A - D_{MAP}}{V_{A,i}} + R_{A,j} \tag{4.3}$$

where $R_{A,j}$ denotes the runway occupancy time of the leading aircraft. This expression ensures that the leading aircraft has vacated the runway before the following aircraft reaches the missed approach initiation point (Figure 4.3).

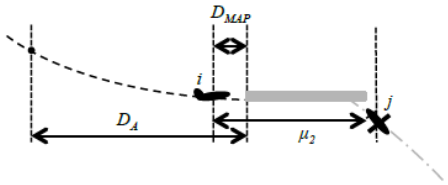

Figure 4.3: Separation required to ensure runway clearance by the leading aircraft before the following arrival reaches the missed approach point D_{MAP}. [22]

The actual time separation imposed by the controller is the most restrictive of the two previously defined separations. Therefore, the effective imposed separation μ is defined as:

$$\mu = \max(\mu_1, \mu_2) \tag{4.4}$$

The resulting inter-arrival time IAT_{ij} between two consecutive aircraft, measured at the runway threshold, is obtained by combining the imposed time separation with the difference in travel times of the two aircraft along the common approach path:

$$IAT_{ij} = \frac{D}{V_{A,i}} - \frac{D}{V_{A,j}} + \mu \tag{4.5}$$

4.1.2. Departures Only Capacity

The inter-departure time IDT is determined using an approach analogous to the inter-arrival time calculation. Several air traffic control separation requirements apply between consecutive departures, including wake turbulence time-based separation, runway occupancy constraints, and potential radar and wake turbulence separation along a common departure path. While most capacity models consider only the first two constraints, separation along a common departure path may significantly affect departure capacity depending on fleet mix and path length.

In addition to separation requirements, an average communication buffer time $\bar{c}$ is included to account for the delay between the issuance of a departure clearance and the actual start of the take-off roll. For consistency, the inter-departure time IDT_{ij} is defined as the time between the start of two consecutive take-off rolls, where the start of the roll corresponds to the clearance time plus the communication buffer.

When no common departure path is considered, the inter-departure time depends only on runway occupancy and wake turbulence separation. In this case, the interval between two take-off rolls is determined by:

$$IDT_{ij} = \max(R_{D,j}, G_{ij}) + \bar{c} \tag{4.6}$$

where $R_{D,j}$ is the runway occupancy time of the leading departing aircraft and G_{ij} is the required time-based separation between the aircraft pair.

If a common departure path is considered (i.e. $D_D > 0$), an additional separation constraint must be satisfied while the following aircraft is airborne and the leading aircraft is still on the common path. This modifies the inter-departure time to:

$$IDT_{ij} = \max(R_{D,j} - R_{D,i} + v, G_{ij}) + \bar{c} \tag{4.7}$$

where v represents the additional time required to maintain radar and wake turbulence separation along the common departure path.

The time increment v depends on the length of the common departure path, the required distance-based separation, and the ground speeds of the departing aircraft.

If the length of the common departure path is less than or equal to the required distance-based separation, the time increment is determined by the time needed for the leading aircraft to establish the required separation:

$$v = \frac{S_{ij}}{V_{D,j}} \tag{4.8}$$

When the common departure path exceeds the distance-based separation, the calculation of v depends on the relative ground speeds of the leading and following aircraft. As in the inter-arrival case, an opening and a closing case can be distinguished, leading to the following definition:

$$v = \begin{cases} \frac{S_{ij}}{V_{D,j}}, & \text{if } V_{D,j} \geq V_{D,i} \\ \frac{D_D}{V_{D,j}} - \frac{D_D - S_{ij}}{V_{D,i}}, & \text{if } V_{D,j} < V_{D,i} \end{cases} \tag{4.9}$$

The resulting time increment v is substituted into Equation 4.7 ,which ensures that the inter-departure time is always equal to or greater than the required wake turbulence time-based separation G_{ij}.

4.1.3. Mixed Mode Operations

A runway is in mixed mode operations when arrivals and departures occur simultaneously, which gives flexibility to the airport depending on arrival or departure peaks. In this case, both inter-arrival and inter-departure separations constraints are applied, in addition to arrival and departure separations, which will be discussed below.

Van der Klugt (2012) [22] identifies that the main thing to avoid in mixed mode operations is the missed approach of the arriving aircraft due to the departing aircraft still occupying the runway. Hence, a departure may only be cleared for take-off if the following conditions are met:

1. The previous arriving aircraft should have vacated the runway with Runway Occupancy Time R_A.
2. The next arrival should be at a distance greater or equal to the minimum distance D_{MM} from runway threshold the moment departure clearance is given.
3. The next arrrival should be at a distance greater or equal to the Missed Approach Point distance D_{MAP} at the moment the departing aircraft lifts off.

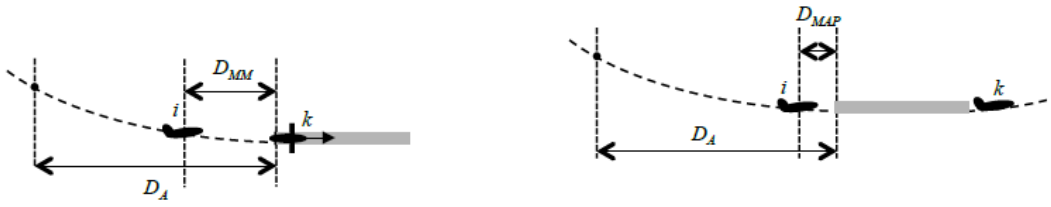

Figure 4.4: Minimum arrival distance from the runway threshold D_{MM} allowing departure take-off, and latest missed-approach point D_{MAP} the arrival must not pass before departure is airborne [22]

Using the above rules, the time windows in which no departures or arrivals are allowed can be defined as the following:

- A new departure can be planned in the following times before or after an arrival:

$$\begin{cases} t_{\max,D} = t_A - \max\left(\frac{D_{MM}}{V_A} - \bar{c}_D,\ \frac{D_{MAP}}{V_A} + R_D\right) \\ t_{\min,D} = t_A + R_A + \bar{c}_D \end{cases} \tag{4.10}$$

- Similarly, a new arrival can be planned in the following times before / after a departure:

$$\begin{cases} t_{\max,A} = t_D - R_A - \bar{c}_D \\ t_{\min,A} = t_D + \max\left(\dfrac{D_{MM}}{V_A} - \bar{c}_D,\ \dfrac{D_{MAP}}{V_A} + R_D\right) \end{cases} \tag{4.11}$$

4.2. Multiple Runway Operations

This section discusses the dependency types which can be found in layouts feauturing more than one runway. These are parallel runways, intersecting runways and converging / diverging runways [22].

4.2.1. Converging & Diverging Runways

As explained in subsection 2.4.2, converging diverging runways are those that do not directly intersect, but their projected centerlines do. Two dependencies are identified: jet blast interference, for converging runways, and missed approach interference in converging (also called open-V) runways.

Jet Blast Interference - Two Departures

Jet blast effects restrict simultaneous or closely spaced departures on diverging runways. To address this, two operational cases are considered: jet blast at a runway intersection and jet blast at a runway threshold. These are shown in Figure 4.5 below.

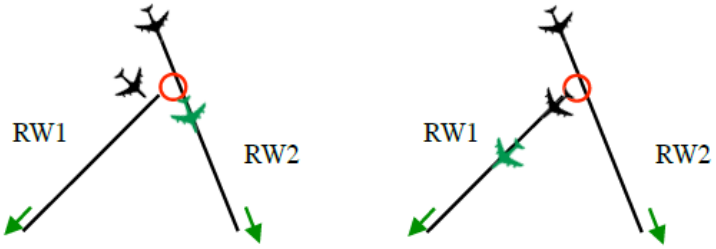

Figure 4.5: Two departures on diverging runways, illustrating intersection and threshold effects. [22]

In the first case, a departure on one runway can generate jet blast that interferes with a departure on another runway at the intersection point. To mitigate this, the aircraft on the affected runway may be required to line up with engines idle until the departing aircraft on the other runway has passed the convergence point.

In the second case, jet blast may occur near the runway threshold. Here, the departure on the second runway must wait until the preceding aircraft has cleared the jet blast area. A time window can be defined around each departure during which no other departure may be initiated.

For a departure on runway 1 relative to a departure on runway 2, the allowable time range is

$$\begin{cases} t_{\max,D1} = t_{D2} - \bar{c}_{D2} - R_{D1,\text{cl}} \\ t_{\min,D1} = t_{D2} + R_{D2,\text{int}} + t_{D1,\text{lu}} + \bar{c}_{D1} \end{cases} \tag{4.12}$$

and, conversely, for a departure on runway 2 relative to runway 1,

$$\begin{cases} t_{\max,D2} = t_{D1} - t_{D1,\text{lu}} - \bar{c}_{D1} - R_{D2,\text{int}} \\ t_{\min,D2} = t_{D1} + R_{D1,\text{cl}} + \bar{c}_{D2} \end{cases} \tag{4.13}$$

Where $R_{D2,\text{int}}$ is the take-off roll time of the first departure until the intersection point, $\bar{c}_{D1}$ represents the communication buffer. $R_{D1,\text{cl}}$ denotes the time required for the aircraft to clear the critical area, $t_{D1,\text{lu}}$ is the line-up time, and $\bar{c}_{D1}$ represents the communication buffer.

Jet Blast Interference - Departure & Arrival

In the same runway configuration, an additional interaction may occur when an arrival operates on one runway while a departure takes place on another. As illustrated in Figure Figure 4.6, a departure may be authorized provided that the arriving aircraft is located at least a minimum distance $D_{\min}$ from the runway threshold.

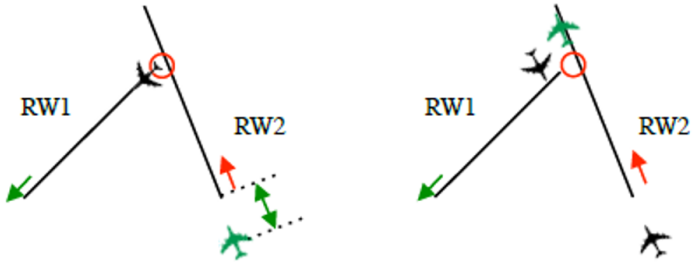

Figure 4.6: Departure and arrival on diverging runways [22]

Under this condition, the arrival is allowed to touch down a defined time after the departure has started its take-off roll. A departure may be cleared to line up and initiate its take-off roll only after the arrival on the intersecting runway has passed the jet blast critical point.

These conditions define time-blocking intervals around scheduled events. For an arrival on runway 2 occurring before or after a departure on runway 1, the admissible time window is

$$\begin{cases} t_{\max,A2} = t_{D1} - R_{A2,\text{int}} - t_{D1,\text{lu}} - \bar{c}_{D1} \\ t_{\min,A2} = t_{D1} - \bar{c}_{D1} + \dfrac{D_{\min}}{V_{A2}} \end{cases} \tag{4.14}$$

while the corresponding time window for a departure relative to an arrival on runway 2 is

$$\begin{cases} t_{\max,D1} = t_{A2} - \dfrac{D_{\min}}{V_{A2}} + \bar{c}_{D1} \\ t_{\min,D1} = t_{A2} + R_{A2,\text{int}} + t_{D1,\text{lu}} + \bar{c}_{D1} \end{cases} \tag{4.15}$$

V_{A2} denotes the arrival ground speed and $\bar{c}_{D1}$ represents the communication buffer.

Missed Approach Interference - Arrival & Departure

A further runway interaction occurs when the missed-approach trajectory of an arriving aircraft intersects the projected departure path. In such cases, sufficient temporal separation between arrival and departure operations is required. As shown in Figure Figure 4.8, a departure may be authorized if the arriving aircraft is still at least a minimum distance $D_{\min}$ from the runway threshold. Once the arriving aircraft is within the distance $D_{\min}$, departures must be delayed until the landing has been completed.

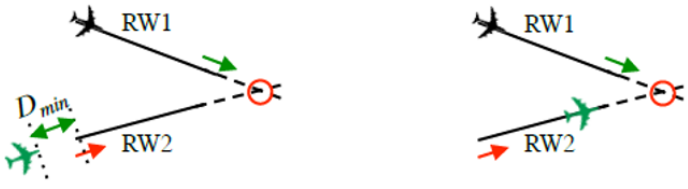

Figure 4.7: Departure and arrival on converging runways [22]

These constraints define a blocking interval for arrivals relative to a departure on runway 1 as

$$\begin{cases} t_{\max,A2} = t_{D1} - R_{A2,\text{com}} - \bar{c}_{D1} \\ t_{\min,A2} = t_{D1} - \bar{c}_{D1} + \dfrac{D_{\min}}{V_{A2}} \end{cases} \tag{4.16}$$

while the admissible time window for a departure relative to an arrival on runway 2 is

$$\begin{cases} t_{\max,D1} = t_{A2} - \dfrac{D_{\min}}{V_{A2}} + \bar{c}_{D1} \\ t_{\min,D1} = t_{A2} + R_{A2,\text{com}} + \bar{c}_{D1} \end{cases} \tag{4.17}$$

where V_{A2} denotes the arrival speed, $\bar{c}_{D1}$ represents the communication buffer and $R_{A2,\text{com}}$ is the required time from touchdown until the aircraft has cleared the ”blocked” area.

Missed Approach Interference - Two Arrivals

The last dependency of converging runways involves the possible conflict, or intersection between the missed approach paths of two simultaneous arrivals. In this case, arrivals have to be staggered by a staggering distance D_{st}.

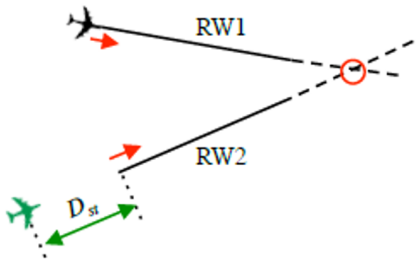

Figure 4.8: Two arrivals on converging runways [22]

An arrival on one runway may be scheduled after an arrival on another runway has touched down, subject to an additional minimum time separation. As this condition applies symmetrically to both arrival sequences, a single blocking interval can be defined for an arrival on runway 2 relative to an arrival on runway 1 as

$$\begin{cases} t_{\max,A1} = t_{A2} - \dfrac{D_{\text{st}}}{V_{A2}} \\ t_{\min,A1} = t_{A2} + \dfrac{D_{\text{st}}}{V_{A1}} \end{cases} \tag{4.18}$$

Where D_{st} represents the required distance separation and V_{A2} is the arrival ground speed. The indices $A1$ and $A2$ may be interchanged to obtain the corresponding time block for arrivals on the opposite runway.

4.2.2. Intersecting Runways

Operations on intersecting runways are governed by separation rules similar to converging runways; however, the *physical runway intersection* is the critical element rather than projected flight or missed-approach paths. Separation dependencies depend on the combination of runway movements.

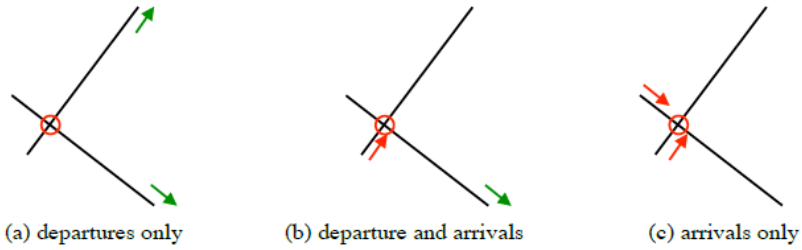

Figure 4.9: Intersecting dependency types [22]

Two Departures

When both runways are used for departures, separation can be ensured either by:

- Allowing the next departure once the previous aircraft has passed the intersection, or
- Applying an increased inter-departure time separation.

For the first case, the minimum time separation is

$$\Delta t_{\min} = R_{D1,\text{int}} + \bar{c}_{D2} \tag{4.19}$$

where $R_{D1,\text{int}}$ is the runway occupancy time (ROT) until the intersection is passed.

The corresponding time block around a departure is

$$\begin{aligned} t_{\max,D2} &= t_{D1} - \bar{c}_{D1} - R_{D2,\text{int}} \\ t_{\min,D2} &= t_{D1} + R_{D1,\text{int}} + \bar{c}_{D2} \end{aligned} \tag{4.20}$$

If an increased inter-departure separation G_{12} is applied (e.g. for wake turbulence), the minimum separation becomes

$$\Delta t_{\min} = G_{12} + \bar{c}_{D2} \tag{4.21}$$

with

$$\begin{aligned} t_{\max,D2} &= t_{D1} - \bar{c}_{D1} - G_{12} \\ t_{\min,D2} &= t_{D1} + G_{12} + \bar{c}_{D2} \end{aligned} \tag{4.22}$$

One Arrival and One Departure

For mixed arrival–departure operations, the arrival must be sufficiently distant from the threshold or have passed the intersection to allow a departure. Additionally, to limit missed-approach risk, the arrival should be beyond the missed-approach point when the departure completes its take-off roll.

The minimum time interval for an arrival after a departure is

$$\Delta t_{\min} = \max\left(\frac{D_{\min}}{V_A} - \bar{c}_D \, \frac{D_{\text{MAP}}}{V_A} + R_{D\text{int}} \right). \tag{4.23}$$

Conversely, the minimum interval for a departure after an arrival is

$$\Delta t_{\min} = R_{A,\text{int}} + \bar{c}_D \tag{4.24}$$

Two Arrivals

For arrival-only operations on intersecting runways, the same staggering conditions apply as for converging approaches. However, the required staggering distance depends on the direction of operation. Approaches toward the intersection generally require smaller separation, while approaches with the intersection beyond the threshold increase runway occupancy time and reduce capacity.

4.2.3. Parallel Runways

Several forms of operations exist on parallel runways. For closely spaced parallel runways, wake vortex interactions between aircraft on both runways must be taken into account.

Dependent Approaches and Departures

For dependent approaches, a diagonal separation distance D_{dia} is applied between two consecutive arrivals on parallel runways. Together with the lateral runway spacing s, the projected in-trail separation S_p between arrivals is given by

$$S_p = \sqrt{D_{\text{dia}}^2 - s^2} \tag{4.25}$$

The required inter-arrival time is then calculated using the same procedure as for single-runway operations, accounting for aircraft ground speeds.

Dependent departures are applicable when the spacing between parallel runways is $s < 760\,\text{m}$. In this case, the standard inter-departure separation rules for a single runway are applied across both runways, treating departures as mutually dependent.

Segregated Operations

In segregated operations, arrivals and departures are assigned to separate parallel runways. Separation rules can be applied to avoid simultaneous arrival-departure interactions on intersecting departure and missed-approach paths.

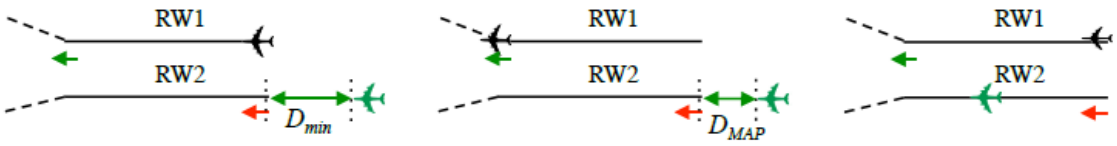

Figure 4.10: Segregated runway dependencies [22]

A departure may only be released when the arrival is simultaneously:

- Securely touched down (typically a fraction of the Runway Occupancy time)
- At a sufficient distance D_{MIN} from the runway threshold
- At the missed approach point (MAP) when the departure rotates.

The minimum time interval for an arrival after a departure is

$$\Delta t_{\min} = \max\left(\frac{D_{\min}}{V_{A2}} - \bar{c}_{D1}\,\frac{D_{\text{MAP}}}{V_{A2}} + R_{D1}\right) \tag{4.26}$$

The minimum time interval for a departure after an arrival is

$$\Delta t_{\min} = R_{A2,\text{com}} + \bar{c}_{D1} \tag{4.27}$$

The corresponding time block around a departure during which no arrival may be planned is

$$\begin{aligned} t_{\max,A2} &= t_{D1} - \max\left(\frac{D_{\min}}{V_{A2}} - \bar{c}_{D1}\,\frac{D_{\text{MAP}}}{V_{A2}} + R_{D1}\right) \\ t_{\min,A2} &= t_{D1} + R_{A2,\text{com}} + \bar{c}_{D1} \end{aligned} \tag{4.28}$$

Conversely, the time block around an arrival during which no departure may be planned is

$$\begin{aligned} t_{\max,D1} &= t_{A2} - \max\left(\frac{D_{\min}}{V_{A2}} - \bar{c}_{D1}\,\frac{D_{\text{MAP}}}{V_{A2}} + R_{D1}\right) \\ t_{\min,D1} &= t_{A2} + R_{A2,\text{com}} + \bar{c}_{D1} \end{aligned} \tag{4.29}$$

4.3. Modelling of SIDs in Departure Operations

Standard Instrument Departures (SIDs) define the initial geometry of aircraft trajectories after take-off. When consecutive departures follow procedures that share a common initial path, aircraft remain exposed to the same wake environment until their trajectories diverge. As a result, wake-based separation constraints may need to be enforced over a longer distance than would be assumed under purely runway-based or time-based separation rules.

This effect is particularly relevant when the follower aircraft is faster than the leader, as insufficient spacing at release may lead to a loss of imposed separation along the shared path. To prevent this, the take-off of the follower is delayed, increasing the minimum inter-departure time. Conversely, procedures that diverge shortly after take-off can reduce or eliminate this additional constraint.

Neglecting SID geometry can therefore underestimate departure separation requirements and lead to an overestimation of runway capacity. To address this, SID dependent constraints can be incorporated into the departure model in the two following ways.

The Common Path method consists of linking each pair of procedures to an effective common-path distance, which determines whether additional spacing must be applied between consecutive departures. In contrast, the Specific Matrix method consists of directly embedding SID constraints within the departure Time-Based matrix, such that procedure-specific effects are represented as explicit time separation requirements.

4.3.1. Common Path Method

Consider two consecutive departures, where aircraft j denotes the leading aircraft and aircraft i the following aircraft.

Each aircraft is characterized by:

- a wake/aircraft category $c \in \mathcal{C}$ (e.g. $\mathcal{C} = \{\mathrm{L}, \mathrm{M}, \mathrm{H}\}$ or a RECAT set)
- a ground speed $V_D > 0$ in kts
- a runway occupancy time $R_D \geq 0$ in seconds

Each departure is assigned a SID label $s \in \mathcal{S}$, where $\mathcal{S}$ is the finite set of SIDs considered.

Let T denote the start time of the take-off roll, defined as the clearance time plus the communication buffer $\bar{c}$.

To represent the diversity of departure procedures, each aircraft is assigned a SID according to a predefined probabilistic model.

A baseline SID mix is given by a probability mass function

$$p(s) = \mathbb{P}(s = s_i) \qquad s \in \mathcal{S} \tag{4.30}$$

such that $p(s) \geq 0$ and $\sum_{s \in \mathcal{S}} p(s) = 1$.

Operational considerations may however introduce dependencies between consecutive assignments. Define a SID length function (in nautical miles)

$$L : \mathcal{S} \to \mathbb{R}_{\geq 0} \qquad L(s) = \text{nominal procedure length of SID } s \tag{4.31}$$

and let $L_{\max} > 0$ denote the threshold above which a SID is classified as long.

Optional constraint: no consecutive long SID when the aircraft category changes. If $L(s_j) > L_{\max}$ and $c_i \neq c_j$, the same SID is not assigned consecutively. The admissible SID set for aircraft i becomes

$$\mathcal{S}_i = \begin{cases} \mathcal{S} \setminus \{s_j\}, & \text{if } L(s_j) > L_{\max}\ c_i \neq c_j \\ \mathcal{S} & \text{otherwise.} \end{cases} \tag{4.32}$$

The conditional probability of assigning SID s is therefore

$$\mathbb{P}(s_i = s \mid s_j, c_i, c_j) = \frac{p(s)\,\mathbf{1}\{s \in \mathcal{S}_i\}}{\sum_{r \in \mathcal{S}_i} p(r)} \tag{4.33}$$

This introduces a first-order dependence between consecutive SID assignments while preserving the marginal mix whenever the exclusion is inactive.

SIDs influence separation because different procedures may share a common segment after take-off before diverging. This interaction is represented through a pairwise common departure path length

$$D_D = D(s_j, s_i) \tag{4.34}$$

where $D(s_j, s_i)$ denotes the distance over which the trajectories associated with SIDs s_j and s_i remain coupled.

A constant fallback value $\bar{D}_D > 0$ may be used when SID pairing information is unavailable.

Departure separation is determined using:

- A time-based wake turbulence separation requirement

$$G_{ij} = G(c_j, c_i) \tag{4.35}$$

- A distance-based separation parameter used to derive equivalent time constraints when departures share a common path

$$S_{ij} = S(c_j, c_i) \tag{4.36}$$

The inter-departure time IDT_{ij} can then be defined as the time between the start of two consecutive take-off rolls. Incorporating runway occupancy, wake turbulence separation, and the SID-dependent common path leads to the constraint

$$IDT_{ij} = \max(R_{D,j}, G_{ij}, v) + \bar{c} \tag{4.37}$$

Distance-to-time constraint

The additional time increment v depends on the relationship between the common departure path length D_D and the required distance-based separation S_{ij}.

Short common-path ($D_D \leq S_{ij}$): If the procedures diverge before the required distance separation becomes binding, the increment reduces to:

$$v = \frac{S_{ij}}{V_{D,j}} \tag{4.38}$$

Long common-path ($D_D > S_{ij}$): When the common path exceeds the required separation, the value of v depends on the relative ground speeds of the aircraft:

$$v = \begin{cases} \frac{S_{ij}}{V_{D,j}}, & \text{if } V_{D,j} \geq V_{D,i} \\ \frac{D_D}{V_{D,j}} - \frac{D_D - S_{ij}}{V_{D,i}}, & \text{if } V_{D,j} < V_{D,i} \end{cases} \tag{4.39}$$

Substituting v into Eq. (4.37) ensures that the inter-departure time always satisfies runway occupancy, wake turbulence separation, and SID-induced common-path constraints.

4.3.2. Specific Matrix Method

The common-path approach described previously reconstructs the effect of SIDs by modelling the shared departure path distance explicitly and translating the distance-based requirement S_{ij} into an equivalent time increment. An alternative approach (utilized in most spanish airports [45]) is to assume that the airport (or ANSP) has already embedded SID effects into a calibrated TBS scheme for departures. In this case, the SID dependence is not introduced through a geometry term D_D, but rather through a SID-conditioned time-separation matrix applied directly in the inter-departure time constraint.

Baseline time separation The matrix

$$G_{ij} = G(c_j, c_i) \tag{4.40}$$

denotes the baseline wake-turbulence time separation for a leader–follower category pair (c_j, c_i). This term captures the minimum controller-applied release interval under standard assumptions (e.g. generic procedure divergence, nominal surveillance environment).

Airport-specific SID-aware TBS matrices. We introduce two additional time-separation tables (in seconds), each indexed by the same category set $\mathcal{C}$:

$$G_{ij}^{\mathrm{SID,same}} = G^{\mathrm{SID,same}}(c_j, c_i) \tag{4.41}$$

$$G_{ij}^{\mathrm{SID,diff}} = G^{\mathrm{SID,diff}}(c_j, c_i) \tag{4.42}$$

These matrices are intended to be *airport specific* and to account implicitly for the typical distance-based wake/radar constraints encountered in the local terminal airspace when: (i) successive departures follow the *same* SID, or (ii) successive departures follow *different* SIDs.

Given the SID labels s_j and s_i for the leader and follower, define the SID pairing indicator

$$\delta_{ji} \;=\; \mathbf{1}\{s_j = s_i\} \tag{4.43}$$

The SID-conditioned time separation is then selected as

$$G_{ij}^{\mathrm{SID}} \;=\; \delta_{ji}\, G_{ij}^{\mathrm{SID,same}} \;+\; (1-\delta_{ji})\, G_{ij}^{\mathrm{SID,diff}} \tag{4.44}$$

To ensure that the airport-specific SID-aware separations do not relax baseline wake-turbulence minima, the effective time-based requirement is taken as the elementwise maximum

$$\tilde{G}_{ij} \;=\; \max\!\big(G_{ij},\, G_{ij}^{\mathrm{SID}}\big) \;=\; \delta_{ji}\, \max\!\big(G_{ij}, G_{ij}^{\mathrm{SID,same}}\big) + (1-\delta_{ji})\, \max\!\big(G_{ij}, G_{ij}^{\mathrm{SID,diff}}\big) \tag{4.45}$$

This enforces that, for every category pair (c_j, c_i), the model adopts the most conservative separation available between the departures separation minima and the locally calibrated SID-dependent values.

Under this second approach, SID effects are applied *directly* through $\tilde{G}_{ij}$, and no explicit common-path distance D_D (or pairwise $D(s_j, s_i)$) is required in the departure constraint. The minimum inter-departure time is therefore written as

$$IDT_{ij} \;=\; \max\!\big(R_{D,j},\, \tilde{G}_{ij}\big) + \bar{c} \tag{4.46}$$

where $R_{D,j}$ is the leader runway occupancy time and $\bar{c}$ is the communication buffer previously defined such that T denotes the start time of the take-off roll.

Finally, the departure schedule is generated through the same recursive threshold-time constraint,

$$T_i \;\geq\; T_j + IDT_{ij} \tag{4.47}$$

for each consecutive leader–follower pair (j, i).

4.4. Time-Based Separation upon Arrivals

Time-Based Separation (TBS) is implemented in the simulator to mitigate the reduction in maximum runway throughput caused by headwind conditions and the associated increase in effective spacing. Instead of enforcing a fixed distance between consecutive arrivals, TBS dynamically adjusts the separation distance so that the resulting time spacing remains equivalent to the no-wind reference case.

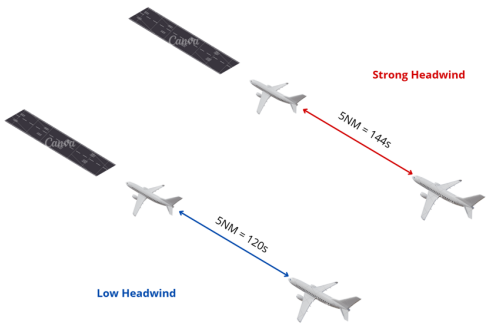

Figure 4.11: Distance-Based Separation

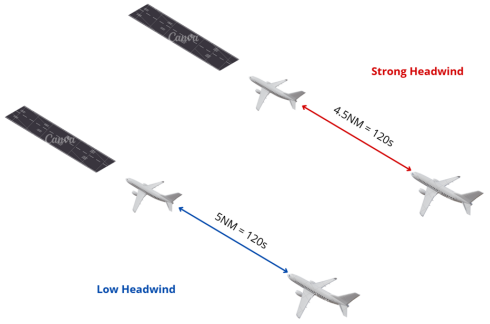

Figure 4.12: Time-Based Separation

In the model, TBS applies *exclusively* to arrival–arrival interactions. Departure separations and mixed arrival–departure constraints remain unchanged.

Arrival Ground Speed Adjustment

TBS relies on modified arrival ground speeds that account for headwind effects. For each arrival aircraft type j, the adjusted ground speed is defined as

$$V_{j,\text{adj}} = V_{j,\text{nom}} - H \tag{4.48}$$

where $V_{j,\text{nom}}$ is the nominal approach speed and H is the headwind component (kt). This adjustment is applied to arrivals only; departure speeds are unaffected by wind.

Baseline separations correspond to distance-based wake minima at the runway threshold, denoted S_{ij}^{base}, where i is the leader and j the follower. When TBS is enabled, these distances are rescaled according to the follower's ground speed:

$$S_{ij}^{\text{TBS}} = S_{ij}^{\text{base}} \cdot \frac{V_{j,\text{adj}}}{V_{j,\text{nom}}} \tag{4.49}$$

It should be noted that the TBS formulation produces a dynamic separation matrix. For each leader-follower pair (i, j), the separation S_{ij}^{TBS} is individually recomputed according to the follower's adjusted ground speed. Consequently, the wake separation matrix is no longer static but varies with wind conditions and aircraft performance, resulting in a pair-specific, wind-dependent separation requirement.

It also ensures that when headwind reduces the follower's ground speed, the required distance separation is proportionally reduced, while higher ground speeds lead to increased distances. The scaling is applied consistently for both ICAO wake categories and RECAT-EU-PWS matrices.

Integration into the Scheduler

The TBS-adjusted separation distance S_{ij}^{TBS} replaces the baseline distance throughout the arrival sequencing logic and affects the entire common approach path, including:

- Minimum spacing at the runway threshold,
- Chaining of arrivals at the final approach fix (FAF), and
- Missed-approach protection constraints.

The minimum threshold spacing between two arrivals is enforced as

$$t_{A_j}^{\min} = t_{A_i} + \frac{S_{ij}^{\text{TBS}}}{V_i} \cdot 3600 \tag{4.50}$$

where V_i is the leading aircraft ground speed. Missed-approach protection is additionally ensured by considering the missed-approach distance and runway occupancy time of the leader.

The final threshold crossing time of an arrival corresponds to the maximum of all applicable constraints, including A-A separation, arrival–departure dependencies, and runway vacancy requirements.

To provide an illustrative example, a 25 kt headwind scenario is considered. Light, Medium and Heavy aircraft are assumed to fly final approach indicated airspeeds of 142 kt, 152 kt and 154 kt respectively.

The ICAO distance-based separation minima implicitly ensure a given time spacing between a leader–follower pair. When a headwind is present, aircraft ground speeds decrease and the same temporal spacing can be maintained at a shorter distance. The matrix on the right therefore represents the time-equivalent distance separations under a 25 kt headwind, i.e. the leader–follower distances that provide the same time separation as the nominal ICAO matrix in no headwind conditions.

It must be noted that matrix entries shown in parentheses correspond to the Minimum Radar Separation (MRS). These values are surveillance-limited rather than wake-turbulence-limited and are therefore independent of wind conditions. Consequently, they are not affected by Time-Based Separation (TBS) and remain unchanged in the headwind-adjusted matrix.

Table 4.1: TBS example calculation

Table 4.2: Arrivals Static DBS Matrix

Leader → Follower ↓	**Light**	**Medium**	**Heavy**
Light	(3)	6	7
Medium	(3)	4	5
Heavy	(3)	(3)	(3)

Table 4.3: Arrivals Headwind adjusted DBS Matrix

Leader → Follower ↓	**Light**	**Medium**	**Heavy**
Light	(3)	4.94	5.77
Medium	(3)	3.34	4.18
Heavy	(3)	(3)	(3)

To illustrate the equivalence, consider a Medium leader followed by a Medium follower. For the nominal ICAO distance $D_0 = 4$ NM and approach speed $V_0 = 152$ kt the time spacing is

$$t_0 = \frac{D_0}{V_0} \times 3600 = \frac{4}{152} \times 3600 \approx 94.7 \text{ s}.$$

Under a 25 kt headwind the ground speed becomes $V_{HW} = 127$ kt and the same 4 NM distance corresponds to a larger time,

$$t_{HW,DBS} = \frac{4}{127} \times 3600 \approx 113.4 \text{ s}.$$

Applying Time-Based Separation (TBS) preserves the original temporal spacing by reducing the distance to

$$D_{TBS} = D_0 \frac{V_{HW}}{V_0} = 4 \cdot \frac{127}{152} \approx 3.34 \text{ NM},$$

and thus

$$t_{HW,TBS} = \frac{D_{TBS}}{V_{HW}} \times 3600 \approx 94.7 \text{ s} \approx t_0.$$

Hence the right-hand matrix reports the time equivalent distances under the 25kt headwind.

The following assumptions are taken into account:

1. Environmental effects other than steady headwind are neglected. TBS Modelling does not contemplate windshear nor sudden changes in wind gusts.
2. Minimum Radar Separation cannot be reduced by TBS
3. Wake interaction depends solely on leader motion

4.5. Implementation of RECAT-EU-PWS

In addition to the baseline ICAO Light/Medium/Heavy wake turbulence separation scheme, the simulation model was extended to support the RECAT-EU-PWS separation framework. The objective of this implementation is to evaluate runway throughput differences when a refined wake turbulence categorisation is applied instead of the conventional ICAO scheme. The implementation replaces the ICAO separation matrices by pairwise separations while keeping the scheduling logic of the simulator unchanged. Consequently, any observed capacity variation originates exclusively from the separation scheme and not from modifications to the runway allocation algorithm.

In order to derive category specific operational parameters such as approach speed and runway occupancy time, representative aircraft observed in all five scenarios are assigned to each RECAT-EU-PWS category. These representative aircraft, shown in Table A.1, are assumed to characterise the typical performance of all aircraft belonging to the respective category and are therefore used to parameterise the simulation model. Categories for which no representative aircraft is listed correspond either to aircraft types that do not operate at the studied scenarios or occur with a negligible frequency. Consequently, these categories are not included, as the contribution to runway capacity would be statistically insignificant. A broader and general categorisation is also provided in section A.2,

Table 4.4: RECAT-EU-PWS scenario categorisation

A	A1	B	B1	B2	C	C1	C2	C3	C4
-	A388	-	A359	A332	-	DC10	762	A306	752
			A35K	A333		MD11	763	A30B	753
			A346	A338			764	A310	
			744	A339					
			748	788					
			77L	789					
			77W	78X					
				772					
				773					
D	**D1**	**E**	**E1**	**E2**	**E3**	**F**	**F1**	**F2**	**F3**
E290	A319	-	CRX	AT76	CR2	-	C680	C56X	B350
E295	A320		CR9	AT46	CL60		E120	LJ35	C25A
	A321		E190		E145			G150	C550
	A20N		E195					H25B	PA34
	A21N		734					PC24	PC12
	737		GLEX						
	738								
	739								
	B38M								
	BCS1								
	BCS3								

The pairwise RECAT scheme defines an expanded set of aircraft categories and provides pairwise leader–follower separation minima for both arrivals and departures. Each aircraft in the simulated traffic sequence is assigned a class together with associated performance parameters, including nominal approach speed. Arrival separations are defined in nautical miles, whereas departure separations are defined in time. To preserve operational realism, a minimum surveillance constraint is enforced such that any separation smaller than 3 NM is replaced by 3 NM. This value represents the Minimum Radar Separation (MRS) and is considered independent of wake turbulence effects.

As explained in the previous section, wake constraints are applied by converting distance separations into time separations at the runway threshold. If a leader aircraft i crosses the runway threshold at time t_i, the earliest feasible threshold time of the follower j is computed as

$$t_j^{\min} = t_i + \frac{D_{ij}}{V_i} \cdot 3600,$$

where D_{ij} is the prescribed separation and V_i is the ground speed of the leader aircraft on final approach expressed in knots. This formulation reflects that wake turbulence protection ensures a minimum wake age at a fixed spatial location and therefore depends on the leader motion rather than the follower motion. For departures, the separations are already defined in time and are applied directly. When multiple operational constraints apply simultaneously, including wake turbulence, runway occupancy and SID interaction, the most restrictive constraint determines the feasible spacing between aircraft.

Traffic sequences are generated according to a predefined fleet mix associated with the RECAT-EU-PWS classes. For each aircraft, performance parameters are assigned based on its category and the runway scheduler computes feasible arrival and departure times while enforcing wake turbulence separation, runway occupancy constraints, SID interaction constraints and crossing runway blocking constraints. Monte Carlo simulations are then performed by repeatedly sampling traffic sequences and evaluating the resulting throughput. Capacity metrics such as hourly throughput and rolling peak demand are computed and compared between ICAO and pairwise scenarios, both with and without TBS.

It is assumed that aircraft within the same RECAT-EU-PWS category share identical performance parameters

4.6. Delay impacts from capacity changes

Since the primary aim is to quantify relative impacts between scenarios (rather than absolute minute-by-minute delay prediction), the analysis adopts a queueing-based heavy-traffic approximation, which captures the strongly non-linear growth of delay as utilisation approaches unity [2].

The approach is most consistent with long-run or averaged operating conditions (e.g., design-hour averages or full-day averages), where demand and capacity can be treated as approximately stationary. Short-term delay formation is not explicitly modelled.

4.6.1. Inputs and utilisation

For each scenario $s \in \{1, 2\}$ the following quantities are defined:

- D: operations per hour (demand), assumed fixed across scenarios for comparative analysis;
- C_s: throughput capacity (operations per hour) under scenario s.

Scenario utilisation is computed as

$$U_s \;=\; \frac{D}{C_s}. \tag{4.51}$$

When utilisation is presented using queueing notation, ρ is used equivalently (i.e., $\rho \equiv U$).

While equation 2.3 provides a direct mapping to delay in minutes, applying it in a scenario-based assessment requires calibrated parameter values that are consistent with the operational context, delay reporting conventions, and time period of the scenarios being evaluated. Because scenario-specific fitting values (or airport-specific calibration data) are not available in this study, the exponential model is reviewed in the literature but is not used to generate the main comparative results.

A steady-state heavy-traffic approximation is applied in which expected delay is proportional to $(1 - U)^{-1}$ as utilisation approaches unity [44]. Defining a dimensionless delay index as

$$\tilde{\delta}(U) \;=\; \frac{1}{1 - U}, \tag{4.52}$$

the ratio of expected delay between the improved and baseline scenarios is

$$\frac{\tilde{\delta}_2}{\tilde{\delta}_1} \;=\; \frac{(1 - U_2)^{-1}}{(1 - U_1)^{-1}} \;=\; \frac{1 - U_1}{1 - U_2}, \tag{4.53}$$

and the percentage change is

$$\%\Delta\tilde{\delta} \;=\; \left(\frac{1 - U_1}{1 - U_2} - 1\right) \times 100. \tag{4.54}$$

This formulation highlights the non-linear “blow-up” of congestion as utilisation approaches one and provides a simple means to compare the relative delay impacts of capacity changes across scenarios.

The heavy-traffic model is used to evaluate how the implementation of Time-Based Separation (TBS) for arrivals and RECAT-EU-PWS affects expected delay across the airport scenarios considered in this thesis. For each scenario pair, the analysis reports U_1, U_2, and the implied change in the delay index $\%\Delta\tilde{\delta}$ from Eq. (4.54).

5

Simulation Model

5.1. General Principles

The RCAP software, in versions 1.0 [22] and 2.0 [23], already has computational capabilities for runway capacity analysis. These implementations contain a scheduling engine with the analytical runway dependency formulations that were developed in the RCAP methodology. Nevertheless, these implementations are written in Visual Basic. As a contribution to this thesis, the ARCAS *"Airport Runway Capacity Analysis Software"* simulation model has been developed from scratch, keeping the mathematical runway interaction and separation equations described in RCAP. The aim was not to replace the methodology but to re-implement a part of the logic in Python, in a flexible and modular simulation framework.

Discrete Event Simulation is used to analyse the runway capacity problems studied in this thesis. DES is appropriate for this problem because aircraft movements can be represented as a sequence of discrete operational events in time while the system state remains unchanged between events. Rather than modelling continuous aircraft trajectories, the simulation focuses on those moments where separation constraints become binding, which are the points relevant for runway capacity assessment. The engine receives a set of operational inputs which describe the airport and traffic scenario. These include the runway configuration, separation regulations, aircraft performance characteristics, wind conditions, traffic demand profile and sequencing assumptions. Based on these inputs, it produces chronologically ordered runway operations from which multiple capacity metrics are obtained.

The overall workflow of the simulator is illustrated in Fig. 5.1.

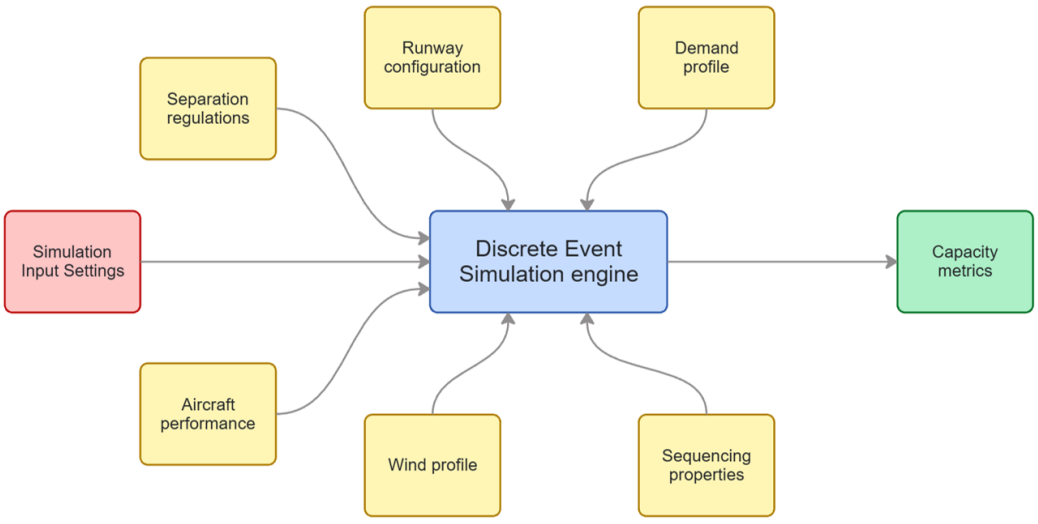

Figure 5.1: ARCAS general working

The simulator implements four different runway layouts: a single mixed-mode runway, segregated parallel runways, converging runways and intersecting runways. In the segregated configuration one runway is dedicated to arrivals and the other to departures, whereas in the converging and intersecting configurations both runways may serve arrivals and departures subject to interaction constraints.

Different wake turbulence separation schemes are applied, including ICAO separations and RECAT-EU-PWS although further schemes can be implemented with ease. Time Based Separation is also used. Aircraft performance data and fleet composition determine the operational variation, while wind conditions affect the aircraft approach speeds, which can be used to scale down wake separations when TBS is enabled. The same simulation engine is used for all configurations; only the applicable constraint relationships differ.

5.1.1. Montecarlo Simulation

To account for operational variability, the simulator operates within a Monte-Carlo framework as illustrated in Fig. 5.2.

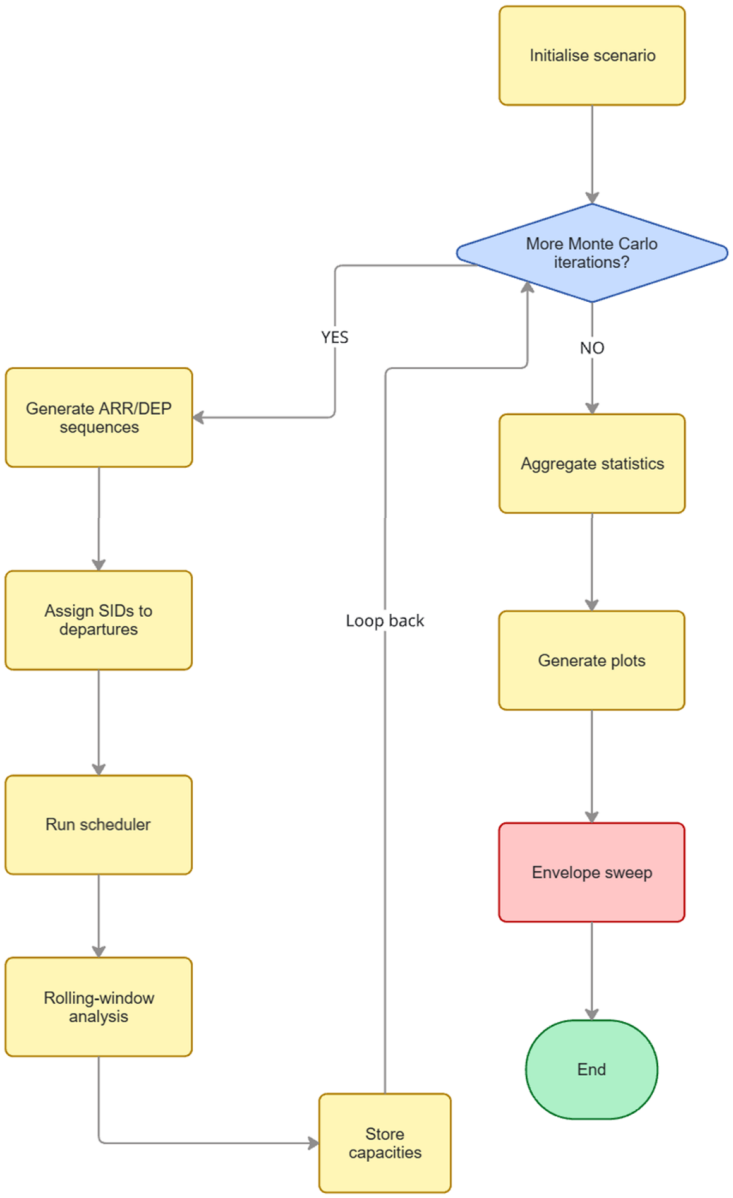

Figure 5.2: Monte Carlo section flowchart

For a defined scenario, arrival and departure sequences are repeatedly generated and simulated. Each iteration represents a possible operational realisation under identical statistical assumptions but different random draws of aircraft sequencing outcomes. After each run, the resulting capacity measures are stored. Once the specified number of iterations has been completed, the results are aggregated to obtain statistically stable estimates of runway throughput.

5.1.2. Capacity Envelope Analysis

Beyond analysing a single traffic composition, the simulator can evaluate capacity across different arrival-departure ratios. This process is illustrated in Fig. 5.3.

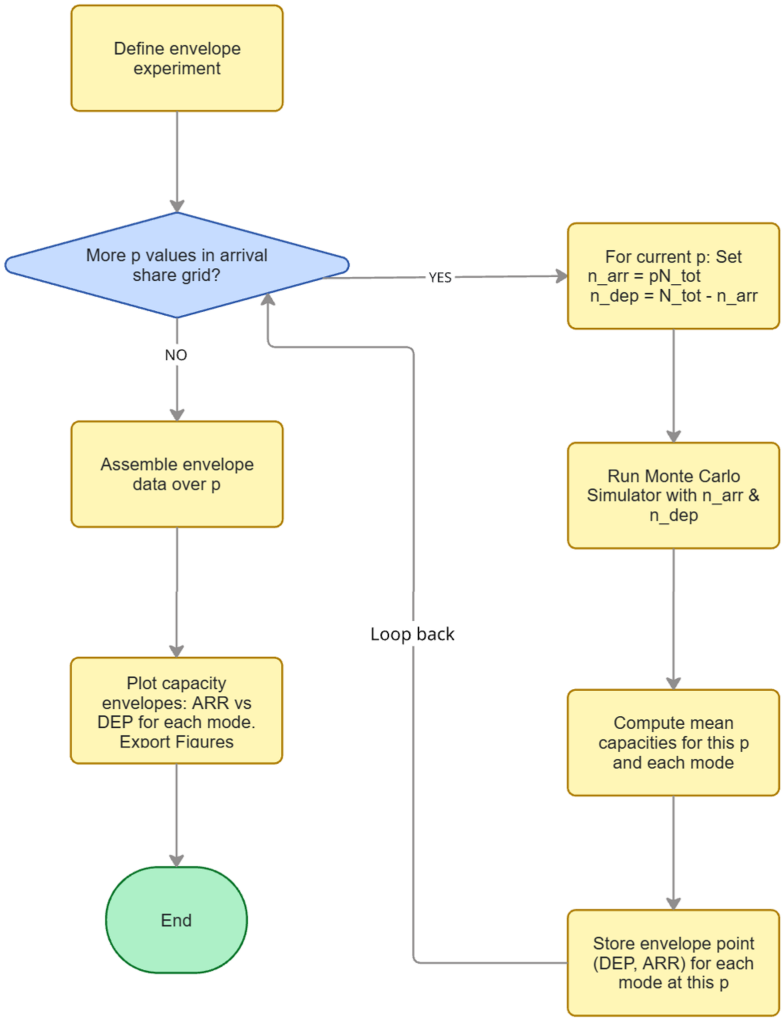

Figure 5.3: Capacity envelope sweep flowchart

For a range of arrival-share values, the Monte-Carlo procedure is executed and the corresponding mean arrival and departure throughputs are recorded. Each traffic mix therefore produces one operating point in the arrival-departure capacity plane. Collectively, these points form the capacity envelope for the considered runway configuration and separation scheme.

The envelope representation allows direct comparison of operational concepts by illustrating the trade-off between arrival and departure throughput rather than relying on a single scalar capacity value.

5.2. Python Implementation

As it can be seen in Figure 5.4, the python code is divided into ten ”blocks”. In the following subsections, a detailed description of what is done in each, including key functions and parameters is included.

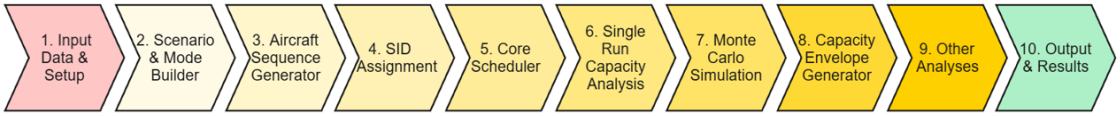

Figure 5.4: Code block structure

5.2.1. Input Data and Parameterisation

The simulation framework is implemented in Python as a discrete-event model of runway operations. All four runway configurations considered in this thesis (single mixed-mode, segregated parallel, converging and intersecting) share a common pattern of input data and parameterisation. In the segregated parallel case, which is representative of the overall structure, the user specifies a wake separation scheme (either ICAO L/M/H or RECAT-EU-PWS with twenty categories), as well as whether Time Based Separation (TBS) is enabled. For ICAO, the model uses flat two-dimensional separation tables such as `icao_arr_nm_flat` for arrival separations and `icao_dep_time_flat` for departure time separations. For the RECAT-EU-PWS case, nested dictionaries from `recat20.py` (for example `r20.LANDING_SEP_NM_20` and `r20.DEP_SEP_T_20`) provide the pairwise separations between the twenty classes.

Operational parameters are also introduced at this stage. These include the approach distance from the final approach fix to the runway threshold, defined as D_A and represented by the constant `DA`, the minimum missed-approach protection distance `DMAP`, and the minimum cross-runway blocking distance `DMIN` when runways are coupled. Typical runway occupancy times (ROT) for each wake or RECAT category are defined in dictionaries such as `icao_arr_params` and `icao_dep_params` for the ICAO case, or `r20.ARR_PARAMS` and `r20.DEP_PARAMS` for the RECAT case. Additional safety margins, such as the Controller buffer time τ and, where applicable, cross-runway blocking parameters for the case of intersecting, converging and coupled segregated runways, are also specified.

As explained in chapter 4, the traffic mix is encoded via probability distributions. For ICAO, the proportions of light, medium and heavy traffic are stored in `ICAO_MIX`, while for RECAT the proportions of the twenty classes are taken from `r20.FLEET_MIX_20` or from modified mixes created for sensitivity studies. Finally, the user defines simulation knobs such as the number of operations to be simulated, the headwind experienced by arrivals, whether common-path DBS (distance-based separation) is active, the look-ahead depth of the rollout optimiser, and the number of Monte Carlo iterations.

5.2.2. Scenario and Mode Builder

Once the input data is fed by the user and ”read”, a scenario and mode builder assembles the effective parameters required to run a simulation. The program takes a scenario label (for example `"ICAO_noTBS"`, `"ICAO_TBS"`, `"RECAT20_noTBS"` or `"RECAT20_TBS"`) and returns a consistent set of performance parameters and separation matrices. For ICAO configurations, this involves constructing arrival and departure parameter sets, optionally applying headwind corrections to arrival speeds, and building the associated distance- and time-based separation matrices, including SID-dependent adjustments. For RECAT-EU-PWS configurations, the builder retrieves the corresponding RECAT parameter tables, enforces minimum separations where required, and, if TBS is active, rescales the arrival separation matrix using headwind-adjusted ground speeds before incorporating the RECAT SID-dependent departure constraints.

The key functions involved in this process are:

- `_build_mode_model_for_run()`: Central scenario builder that takes a scenario label and assembles all performance and separation data into a single dictionary used by the simulator.
- `adjust_speeds_with_headwind()`: Applies a specified headwind to nominal approach speeds to obtain ground speeds for each aircraft category.

- `apply_tbs_nm()`: Rescales baseline separation matrices in nautical miles so that they are consistent with Time Based Separation, using the follower's ground speed.
- `apply_minimum_to_matrix()`: Enforces a minimum allowed separation element-wise on a given matrix, for both flat and nested representations.
- `combine_sep_matrices_max()`: Merges multiple separation matrices by taking the element-wise maximum, ensuring that the most restrictive constraint is applied whenever several rules are in force.

5.2.3. Aircraft Sequence Generation

The process of generating traffic sequences for each runway is stochastic and driven by the fleet mixes specified by the user. For the ICAO case, a specific generator creates a list of length n where each element stores only the wake category type (L, M or H). This generator uses the mix tuple (p_L, p_M, p_H) given by `ICAO_MIX` and a scalar seed to initialise the pseudo-random number generator, and is applied separately to arrival and departure streams, with different seeds for each.

For RECAT-EU-PWS, a more general generator is used. In this case, a mapping from each RECAT class (e.g. `"B1"`, `"D1"`, `"E2"`) to a probability, together with a deterministic ordering of the classes, is converted into a cumulative distribution function from which n independent samples are drawn, again producing a list of type-only records.

The type-only sequences produced by these generators are then expanded into full aircraft performance records in a separate step, which iterates over the sequence, looks up each type in the appropriate parameter dictionary, and returns a new list where each element includes the type, the relevant speed and the runway occupancy time. These are assigned to a departure or arriving runway, when multiple runways of dedicated use, or, in the case of a mixed runway, the operation type "A" or "D" is also appended in the sequence dictated by the probability of arrival, p

When multiple systems are compared in the same experiment (for example, ICAO versus RECAT, or TBS versus no TBS), the same random seeds `seed_arr` and `seed_dep` are used for all modes. This ensures that the chronology of arrival and departure types is shared across modes, making the comparison more fair.

The corresponding implementation functions are:

- `generate_sequence_icao()`: ICAO-specific sequence generator that samples wake categories $L/M/H$ according to `ICAO_MIX` and a given seed.
- `generate_sequence_from_mix()`: Generic RECAT-EU-PWS sequence generator that samples arbitrary type labels based on a probability mapping and an explicit ordering of the classes.
- `expand_sequence()`: Converts a type-only sequence into full aircraft records (ROTs, speeds, SID logic..) by attaching the corresponding speed and runway occupancy time from the chosen parameter dictionary.

5.2.4. SID Assignment to Departures

Each departure is assigned a SID label that influences the applicable departure separation. The SID assignment procedure operates on the expanded departure sequence and uses a target SID utilisation mix provided by the user (for example through `SID.SID_MIX`) and an interaction matrix `SID.matrix` containing information such as diagonal lengths and pairwise interaction effects.

In a first step, the user-provided SID mix is reconciled with the SIDs actually present in the interaction matrix: aliases are resolved, unsupported SIDs are discarded, and the remaining probabilities are renormalised so that they sum to one. In a second step, the algorithm iterates over the departure list and draws a SID for each aircraft using a pseudo-random sampler initialised with a fixed seed. The selected SID is then attached to the departure record under the key `"SID"` and is later used by the departure separation logic to distinguish between same-SID and different-SID cases.

The corresponding implementation functions are:

- `_normalized_sid_mix()`: Preprocesses the user-specified SID mix by checking aliases, removing SIDs not present in `SID.matrix`, and renormalising the probabilities if necessary.
- `assign_sids_to_departures()`: Assigns a SID to each departure based on the cleaned mix and the interaction matrix, (optionally enforces the no consecutive long SID rule for followers of a different type)

and stores the selected SID in each departure record.

5.2.5. Core Scheduler

The core of the simulation model is the scheduler, which takes the arrival and departure sequences and constructs a feasible schedule of threshold and vacated times, respecting all applicable constraints. These are both same-runway and cross-runway, in the case where coupled segregated runways are used, as well as intersecting or converging & diverging runways

The scheduler applies same-runway wake and runway occupancy constraints using several helper functions. For arrivals, `calc_m1_m2()` computes two candidate inter-arrival times m_1 and m_2, one representing a pure wake-based separation and the other incorporating missed-approach protection with D_{MAP}. The function then returns their maximum, which is used to propagate the time from one arrival at the final approach fix to the next. For departures, `calc_inter_departure_time_generic()` calculates the minimum inter-departure time by comparing runway occupancy of the leading departure, time-based separations G_{ij} obtained via `get_dep_time_sep()`, and distance-based separation constraints along the common departure path obtained via `get_nm_sep()` and the DBS matrix.

Cross-runway interactions are modelled through two additional functions. For example, for coupled segregated runways, the function `arr_min_touchdown_after_departure()` computes a lower bound on the touchdown time of an arrival following a departure on the parallel runway, enforcing both a minimum distance D_{MIN} along the missed-approach path and the protection distance D_{MAP}. Conversely, `dep_min_start_after_arrival()` determines the earliest time when a departure can be initiated after an arrival, based on the arrival runway occupancy and an additional buffer.

When simulating more than one runway, the constraints are combined into an optimisation routine that, at each step, computes the earliest feasible time for scheduling the next arrival and the next departure. To choose between them, a receding-horizon rollout optimiser is employed: the function `score_rollout()` simulates a short sequence of future decisions for each candidate (arrival or departure first), using the same constraint logic, and evaluates a local density metric (operations per unit time). The scheduler then selects the candidate that maximises this metric, commits it to the schedule, and repeats the process until all aircraft are scheduled or a time limit is reached.

For the single mixed-mode runway model the structure is similar in terms of constraint evaluation, but there is no cross-runway coupling and therefore no need for a rollout optimiser. In that case the scheduler simply chooses the next aircraft by earliest feasible time, using wake and runway occupancy constraints only. This makes the choice basically deterministic given the arrival/departure queue.

5.2.6. Single Run Capacity Analysis

Once a schedule has been produced, the simulator performs a single run capacity analysis by ”inspecting” the temporal distribution of arrival and departure events. The key quantity is the maximum rolling hourly throughput, which is obtained by sliding a one hour time window over the sequence of operations and counting how many fall within each window.

For scenarios where only a single stream is of interest (for example, arrivals only), `rolling_capacity()` takes a list of event times and computes the maximum number of events in any interval of length 1h, returning both the corresponding equivalent hourly rate and the start time of the best window. When both arrivals and departures are present, the function `rolling_capacity_with_mix()` is used. It considers 1 hour windows that contain both arrivals and departures, computes the total number of operations in each, and imposes an additional constraint on the arrival share $p = A/(A + D)$, which must lie within a tolerance `tol` of a user-specified target p_{target}. Among these windows, the one with the largest throughput is selected. The helper function `_count_in_window()` is used internally to count the number of events in each candidate window.

Additional summary statistics for a single run are produced by `_stats()`, which takes the list of scheduled movements (arrivals or departures) and computes the average inter-departure or inter-arrival time, the corresponding approximate rate, and the makespan (time between the first and last runway usage). These statistics, together with the detailed schedule, are written to an Excel file via `save_to_excel()`. For visual inspection and verification of a particular run, the function `plot_two_runways()` produces a Gantt plot of runway occupancy for the arrival and departure runways.

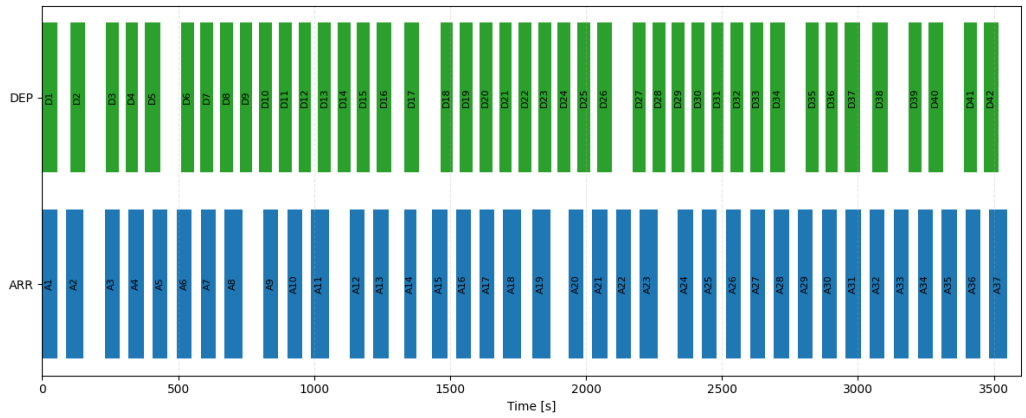

Figure 5.5: Single run gantt chart (example)

5.2.7. Monte Carlo Simulator

Now, single-run capacity estimates are biased due to the random allocation of aircraft types and SIDs. To obtain statistically robust results, the simulator implements a Monte Carlo simulation in which many independent runs are performed under the same high-level scenario but with different random seeds.

The function `montecarlo_XXXX()` where XXXX stands for each of the simulators (mixed, segregated, intersection or convdiv) first constructs the set of modes to compare. Depending on the flags `compare_systems` and `include_tbs`, these will include both wake schemes with and without TBS. For each mode, the function calls `_build_mode_model_for_run()` to obtain a mode-specific parameter set. Then, for each Monte Carlo iteration, it generates new random seeds for the arrival and departure sequences, and for each mode in turn calls the helper function `_simulate_once_for_mode()`. This helper function draws the aircraft type sequences using `_draw_sequences_for_mode()`, expands them using `expand_sequence()`, optionally assigns SIDs using `assign_sids_to_departures()`, and finally invokes `simulate_XXXX()` followed by the rolling capacity analysis. It returns the combined, arrival-only and departure-only capacities for that run and mode.

The results of all runs and modes are stored in a `pandas` DataFrame and processed to produce summary statistics. An option exists to detect and remove outliers using the function `_iqr_mask()`, which applies an interquartile range rule to flag values that fall outside reasonable bounds. These are then saved in an Excel file alongside the full Monte Carlo sample.

To visualise the central tendency and the spread of the capacity distributions for the different separation systems, three plotting functions are called. These are:

- `_plot_grouped_histogram_mc()`. Produces histograms of combined capacity for each mode
- `_plot_boxplot_mc()` creates boxplots of the same distributions for spread comparison
- `_plot_violins_mc()` produces violin plots .

An additional Monte Carlo tool, `cv_sweep_XXXX`, is used to study convergence. It runs up to `N_max` simulations, updates online estimates of mean and standard deviation using Welford's method, and records the coefficient of variation $\mathrm{CV} = \sigma/\mu$ as a function of the number of runs. This allows an evidence-based choice when setting the number of Monte Carlo iterations to be ran.

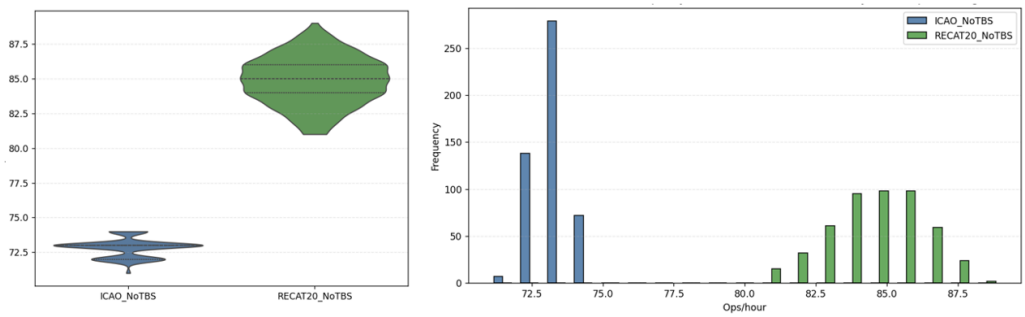

Figure 5.6: Monte Carlo violin & histogram plots (example)

5.2.8. Envelope Sweep

To produce the classical "Capacity Envelope" plot, the simulator performs envelope sweeps in which the share of arrivals is varied gradually from 0 to 1. In these experiments, the total number of operations N_{total} is fixed, and for each target arrival ratio p a corresponding number of arrivals $n_{\text{arr}} = \text{round}(pN_{\text{total}})$ and departures $n_{\text{dep}} = N_{\text{total}} - n_{\text{arr}}$ is used. For each such pair, a Monte Carlo experiment is carried out and the mean capacity is recorded. This is implemented in the function `sweep_arrival_ratio_XXXX()`.

For each value of p in `p_grid`, the function sets `n_arr` and `n_dep` as described, and for each mode model constructed via `_build_mode_model_for_run()` runs `_simulate_once_for_mode()` a number of times. The function computes, for each mode and each p, the mean and standard deviation of the combined, arrival-only and departure-only capacities. All these results are returned as a DataFrame and optionally saved to Excel.

The envelope is then visualised by plotting mean arrival capacity against mean departure capacity for all values of p. The function `sweep_arrival_ratio_segregated()` creates scatter plots of these points, coloured by mode. When applied to the different separation systems, these plots yield capacity envelopes that summarise the arrivals–departures trade-offs for each scheme.

5.2.9. Other Analyses: Coefficient of Variation and Sensitivity Studies

Beyond basic Monte Carlo statistics and capacity envelopes, the program includes several sensitivity analysis routines that explore how capacity changes with key parameters. The first family of analyses focuses on the sensitivity of runway system capacity to headwind (with and without TBS).

The function `sweep_headwind_icao_notbs_vs_tbs()` loops over a grid of headwind values and, for each value, builds ICAO modes with and without TBS using `_build_mode_model_for_run()`. For each headwind and each mode, it runs a fixed number of Monte Carlo iterations, collects capacities, and then plots the mean combined, arrivals and departures capacities as a function of headwind. In addition, it computes and plots the percentage improvement in total capacity of TBS over no TBS as a function of headwind., which provides a quantitative measure of the benefit of TBS under different wind conditions.

The second family of analyses examines the effect of the proportion of heavy aircraft in the fleet. The function `build_icao_mix_trade_M_to_H()` constructs ICAO fleet mixes in which medium aircraft are progressively replaced by heavy aircraft.

Similarly, `build_recat_mix_trade_D1_to_B1B2()` constructs RECAT mixes where certain classes are traded in a consistent way. These mixes are then used in `sweep_heavy_tradeoff_icao_vs_recat_notbs()`, which runs and plots the resulting capacities as functions of the heavy share. The last step computes the percentage capacity gain of RECAT-EU-PWS over ICAO and plots it against the heavy share.

Other sensitivity analysis, focused in varying runway geometric and distance parameters, such as DMIN and DMAP are also performed.

Finally, to test the sensitivity of RECAT-EU-PWS to changes in fleet mix undetectable by ICAO, a more focused sensitivity analysis is implemented in `sweep_recat_mix_only_with_icao_reference_notbs()`. Here the ICAO mix `mix_icao` is kept fixed, while only certain RECAT-EU-PWS classes (D1, E1, E2, among others) are varied.

The function `_lerp_mix()` is used to interpolate between two RECAT-EU-PWS mixes, meanwhile the other function `build_recat_mix_D1_E1_E2_sweep()` defines the specific variation pattern for D1/E1/E2. For each interpolated mix, the function `sweep_recat_mix_only_with_icao_reference_notbs()` runs Monte Carlo simulations and compares the RECAT capacities with the fixed ICAO reference, plotting capacity as a function of the share of a particular class (for example, E2 being ATR72 operations). This allows the impact of specific fleet composition changes on capacity to be quantified.

6

Scenarios

In order to properly validate the developed runway capacity simulation model, it is applied to a range of representative operational scenarios. This enables the assessment of whether the model can simulate realistic runway performance under representative conditions.

Five airports have been selected as case studies to capture a broad spectrum of operational contexts, including differences in traffic mix, runway layout, procedures, and size. All selected airports are among the busiest in Spain. This also provides a methodological advantage, as *Ingeniería y Economía del Transporte, S. M. E., M. P., S. A.* has extensive operational knowledge, data availability, and expertise within these scenarios.

Alicante, Palma de Mallorca, Barcelona and Madrid are used primarily to validate the runway capacity model in airports with heterogeneous winds and fleet compositions. Tenerife Norte and Palma de Mallorca are additionally employed to examine the RECAT-EU-PWS behavior of the model and its ability to capture potential shifts in peak runway capacity resulting from small variations in traffic mix.

- **Alicante - Elche [LEAL]** → Single Mixed Runway
- **Tenerife Norte - Los Rodeos [GCXO]** → Single Mixed Runway
- **Palma de Mallorca - Son Sant Joan [LEPA]** → Segregated Parallel Runway System
- **Barcelona - El Prat [LEBL]** → Crossing Runway System
- **Madrid - Barajas [LEMD]** → Converging / Diverging Runway System

Figure 6.1: Selected airport scenarios

Table 6.1: Five busiest airports in Spain by passenger traffic (AENA,2025 [46])

Airport	Annual passengers	Aircraft movements
Madrid-Barajas [LEMD]	68,179,054	430,616
Barcelona-El Prat [LEBL]	57,483,036	360,786
Palma de Mallorca [LEPA]	33,806,427	246,486
Malaga [LEMG]	26,760,549	186,990
Alicante [LEAL]	19,950,394	126,081

Madrid, Barcelona, Palma de Mallorca, and Alicante rank first, second, third, and fifth in Spain in annual passenger traffic [46], and are also positioned 5th, 7th, 16th, and 30th in Europe, respectively [47]. Their inclusion ensures that the model is validated in high-demand environments where runway capacity is an important operational constraint. Additionally, all selected airports have recently recorded traffic growth between approximately 2% and 8%, further emphasizing the importance of reliable capacity assessment.

Although handling lower passenger and traffic volumes (around 8 million passengers annually), Tenerife Norte has been included due to its distinctive turboprop heavy fleet mix. This specific traffic composition introduces operational effects that can significantly influence separation requirements and runway throughput, making it particularly suitable for analyzing the model's sensitivity to fleet mix variations.

This chapter introduces the five selected airports and provides a detailed analysis of their main operational characteristics in order to support the validation of the runway capacity model. Key aspects such as traffic mix, runway configurations and geometrical factors are examined to ensure that the scenarios considered accurately reflect real-world conditions.

6.1. Alicante - Elche Airport

Alicante - Elche Airport (LEAL) is located on Spain's southeast Mediterranean coast and is an important gateway for leisure and low-cost traffic. Operations are characterized by concentrated demand peaks associated with tourism flows and a relatively homogeneous short to medium-haul fleet.It is the busiest single runway airport in Spain, both in terms of passenger traffic and flight operations, operating its runway in mixed mode.

The airport´s reference temperature is 31ºC, with an elevation of 43m and operates under an ICAO category 4C.

Runway system and operational configuration

As mentioned in previous sections, Alicante operates with a single runway in a 10-28 orientation, which operates in mixed mode. Table 6.2 shows the runway´s declared distances.

Table 6.2: Alicante runway declared distances [48]

RWY Designator	TORA	TODA	ASDA	LDA
10	3,000	3,000	3,000	3,000
28	3,000	3,000	3,000	3,000

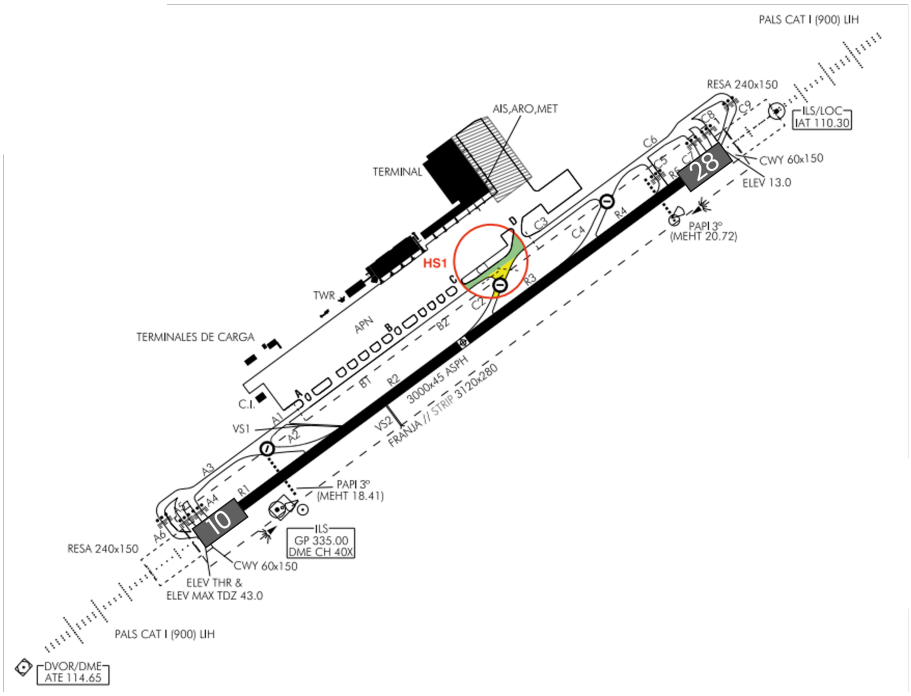

Figure 6.2: Alicante airport [48]

Regarding the operating mode, the airport's preferential configuration is the east configuration (departures and arrivals on runway 10), which accounted for approximately 75% of operations in 2025. The remaining operations used the west configuration (departures and arrivals on runway 28). As such, the eastern configuration will be utilized to model Alicante.

Table 6.3: Alicante 2025 configurations

RWY	Configuration	Utilisation
10	EAST	75.2%
28	WEST	24.8%

Traffic characteristics and peak periods

Alicante Airport is predominantly served by medium-sized (M and D1 category) aircraft, reflecting the nature of its route network. The vast majority of flights operate on short- to medium-haul routes within Europe, where single-aisle aircraft provide the most efficient balance between capacity and operating costs.

Table 6.4: Alicante 2025 aircraft distribution

Aircraft ICAO Code	ICAO WTC	RECAT-EU-PWS	Occurence
B738	M	D1	**36.5%**
B38M	M	D1	**20.5%**
A320	M	D1	**17.8%**
A20N	M	D1	**5.8%**
A319	M	D1	**5.8%**
A21N	M	D1	**2.9%**
A321	M	D1	**2.2%**
CRJX	M	E1	**2.1%**
BCS3	M	D1	**0.7%**
B733	M	E1	**0.5%**

Shown in Table 6.26, the aircraft with the highest number of operations is the Boeing 737-800 and 737-8, which combined total 57% of movements in 2025. It is mainly operated by airlines such as Ryanair, Norwegian, Jet2.com and TUI.

This is followed by the Airbus A320 and A320neo families (A319, A320, A321 and A320neo and A321neo) operated by airlines such as Vueling and easyJet. Together, these aircraft represented around 35% of operations in 2023.

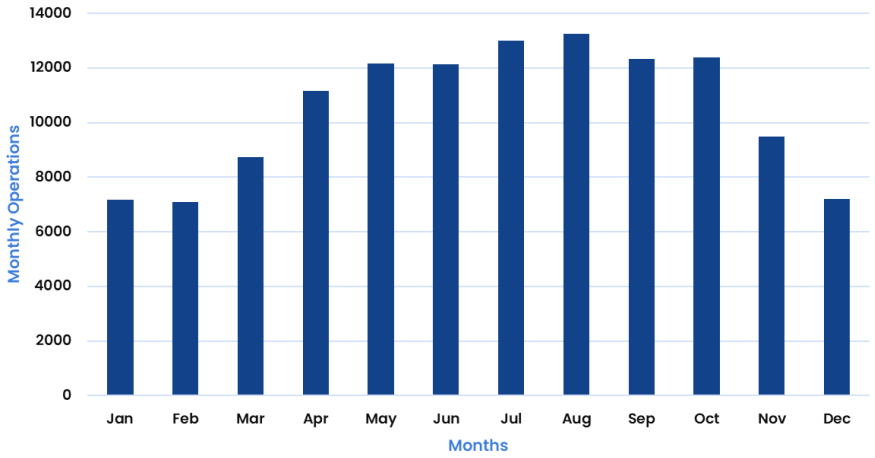

Figure 6.3: Alicante 2025 monthly operations

A moderate seasonal traffic pattern can be observed in Figure 6.3, primarily driven by Alicante´s strong dependence on tourism. Demand increases progressively from spring and reaches its peak during the summer months, particularly in July and August, almost duplicating low-season volumes.

Therefore, runway performance should be evaluated with particular emphasis on peak periods, which more accurately represent the airport's operational constraints than annual averages.

To characterize peak demand conditions, an average traffic mix was computed based on the five hours with the highest number of operations:

Table 6.5: Alicante 2025 peak hour flight schedule

Aircraft	ICAO	RECAT-EU-PWS	Occurence
B738	M	D1	**30.1%**
B38M	M	D1	**20.4%**
A320	M	D1	**19.4%**
A319	M	D1	**8.7%**
A321	M	D1	**3.9%**
A20N	M	D1	**2.9%**
CRJX	M	E1	**2.9%**
E295	M	D	**2.9%**
AT72	M	E2	**2.9%**
C680	M	F1	**2.9%**
GA	L	F3	**2.9%**

This fleet mix is then mapped to both ICAO and RECAT-EU-PWS wake turbulence categories, which are inputs to the simulation model.

Table 6.6: Alicante 2025 WTC peak hour flight schedule

ICAO		RECAT-EU-PWS	
Category	**Occurrence**	**Category**	**Occurrence**
L	2.9%	D1	85.4%
M	97.1%	D	2.9%
H	0.0%	E1	2.9%
		E2	2.9%
		F1	2.9%
		F3	2.9%

Geometric constraints

Additional inputs to the simulation model relate to airport-specific operational and geometric constraints. Parameters described in chapter 4, such as the common arrival path, ‚missed approach distance, mixed mode distance and SID allocation, are particularly relevant, as they directly influence aircraft separation requirements and runway throughput. The communications buffer, $\bar{c}$ is assumed to be 12 seconds.

The SID allocation has been obtained through an extensive analysis of the 2025 flight schedule, and is shown in Table 6.8 and highlighted in Figure A.1. A clear dominance of route MITOS3A can be observed, with 83% of the departures taking this standard instrument departure route. Other routes exist, but add up to less than 1% and have been neglected.

Table 6.7: Alicante runway 10 operational parameters

Parameter	Length [NM]
D_A	**6.02**
D_{MAP}	**0.72**
D_{MM}	**0.0**

Table 6.8: Alicante runway 10 SID allocation 2025

SID Utilized	Occurrence [%]
MITOS3A	83
ASTRO4A	11
CATON4A	3
MAGAL3A	2

Given that air traffic control at Alicante Tower is operated by the privately owned ANSP SkyWay rather than by state-owned ENAIRE, the SID departure separation matrix could not be obtained. As such, it will be assumed to be the same as Palma de Mallorca. The ROTs were derived from ENAIRE information.

Table 6.9: Alicante same SIDs DBS matrix

Follower → Leader ↓	R	C	M	L
R	80	60	60	60
C	120	105	105	90
M	180	105	105	90
L	240	240	240	120

Table 6.10: Alicante different SIDs DBS matrix

Follower → Leader ↓	R	C	M	L
R	60	60	60	60
C	120	90	90	90
M	120	90	90	90
L	180	180	180	90

These matrices were derived from the airport successive departure requirements specified in the agreement between the Area Control Center (ACC) and the Tower (TWR) [49]. In this context, *R* denotes *rapid* aircraft, *C* refers to *Citation-type* aircraft, while *M* and *L* indicate *medium* and *slow* aircraft, respectively.

To map these categories to ICAO Wake Turbulence Categories (WTC), it is assumed that Heavy (H) and Medium (M) correspond to *R* (rapid), whereas Light (L) corresponds to *C* (Citation-type). For RECAT-EU-PWS, the mapping presented below is applied.

1. **R** → A, A1, B, B1, B2, C, C1, C2, C3, C4, D, D1, E, E1, E3
2. **C** → F1, F2
3. **M** → E2
4. **L** → F3, F

Table 6.11: Alicante runway 10 ROTs

		Runway Occupancy Time [s]	
Group	**WTC**	**Arrivals**	**Departures**
ICAO	L	56.3	34.0
	M	53.6	47.1
	H	67.0	55.0
RECAT-EU-PWS	B1	70.3	50.0
	B2	65.3	50.0
	C2	62.2	50.0
	C4	61.9	50.0
	D	53.8	40.0
	D1	53.7	40.0
	E	60,7	35.3
	E1	49.4	35.3
	E2	50.5	35.3
	E3	49.4	35.3
	F1	52.8	30.0
	F2	48.6	30.0
	F3	53.6	30.0

6.2. Palma de Mallorca - Son Sant Joan Airport

Palma de Mallorca Airport (LEPA) is located on the island of Mallorca, in Spain's Balearic Islands and plays a strategic role in connecting the island with major European cities, particularly during the summer season. Similarly to Alicante, it is also a heavily touristic airport, with demand greatly influenced by international leisure travel and strong seasonal peaks associated with holiday traffic. Palma de Mallorca Airport is Spain's third busiest airport in terms of passenger traffic and aircraft movements, especially during peak season. It operates two parallel runways in a segregated mode configuration, assigning one runway to arrivals and the other to departures. The airport´s reference temperature is 31ºC, with an elevation of 8m.

Runway system and operational configuration

Palma operates two parallel runways in a 06-24 orientation. Table 6.12 presents the runway declared distances.

Table 6.12: Palma runway declared distances [50]

RWY Designator	TORA	TODA	ASDA	LDA
06L	3,270	3,330	3,270	3,270
24R	3,270	3,330	3,270	3,200
06R	3,000	3,000	3,000	2,590
24L	2,590	2,590	3,000	3,000

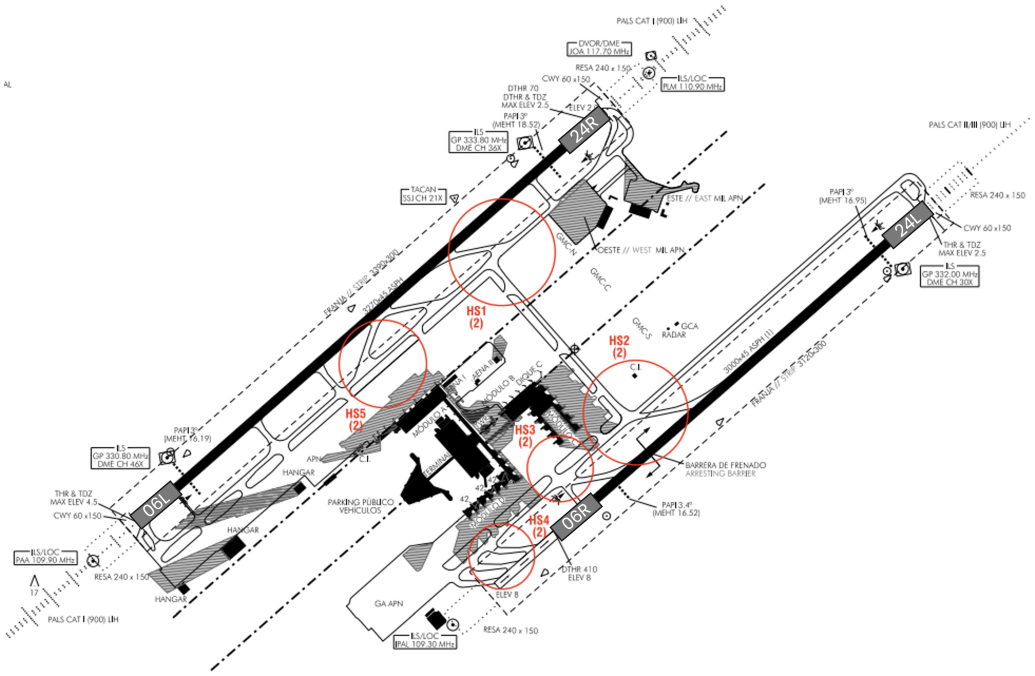

Figure 6.4: Palma de Mallorca airport [50]

The most used configuration is the western configuration (24R used for departures, 24L for arrivals), which accounted for approximately 70% of operations in 2025. 27% operations used the eastern configuration (06L departures, 06R arrivals). The remaining 3% of operations, used the 06R mixed mode, which was only active on very specific circumstances. As such, the western configuration is selected to model Palma´s segregated parallel runways.

Table 6.13: Palma 2025 configurations

RWY	Configuration	Utilisation
24L & 24R	WEST	69.8%
06R & 06L	EAST	27.0%
24R	MIXED	3.2%

Traffic characteristics and peak periods

Palma is predominantly served by medium-sized (M and D1 category) aircraft. The vast majority of flights operate on short- to medium-haul routes within Europe.

Table 6.14: Palma 2025 aircraft type distribution

Aircraft	ICAO	RECAT-EU-PWS	Occurence
A320	M	D1	**29.4%**
B738	M	D1	**23.2%**
B38M	M	D1	**9.2%**
A319	M	D1	**6.0%**
AT76	M	D1	**5.3%**
A20N	M	D1	**4.0%**
A321	M	D1	**3.7%**
CRJX	M	E1	**3.2%**
A21N	M	D1	**2.6%**
B753	M	E1	**0.9%**

The top 10 aircraft types are dominated by the Airbus A320 and A320neo families (45%), along with the Boeing 737-800 and 737 MAX 8 (34%), operated by airlines such as Vueling, Iberia Express, and Ryanair. The ATR 72-600 and CRJ-1000, account for roughly 8% of movements, primarily serving Air Nostrum routes for island connections and Spain's eastern coast.

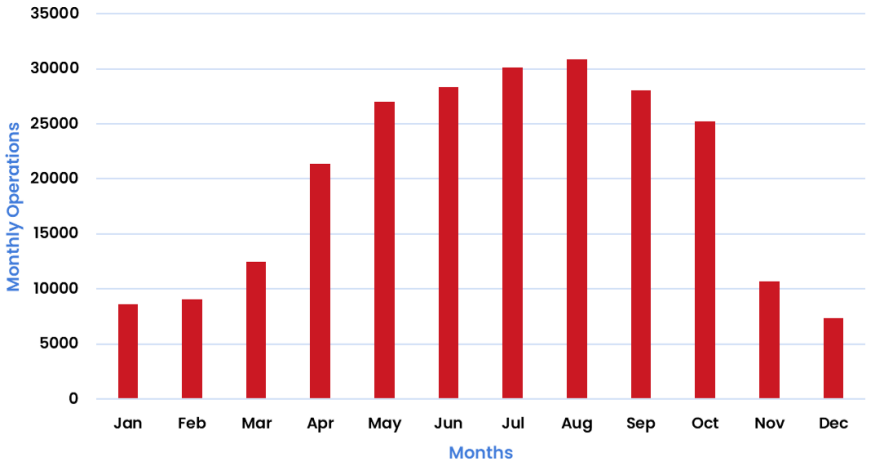

Figure 6.5: Palma 2025 monthly operations

A highly seasonal traffic pattern can be observed in Figure 6.5, where peak-month volumes reach up to four times those of the low season. This fluctuation is largely driven by Palma's strong dependence on tourism. Demand rises steadily from spring to fall, culminating in the summer months, especially July and August, when leisure travel is at its highest. In contrast, traffic declines during the winter period, due to the drop in tourist activity.

To characterize peak demand conditions, two average traffic mixes were computed based on the ten hours with the highest number of operations.

Table 6.15: Palma peak hour 1 flight schedule

Aircraft	ICAO	RECAT-PWS	Occurence
A320	M	D1	**31.9%**
B738	M	D1	**20.2%**
CRJX	M	E1	**8.4%**
B38M	M	D1	**5.9%**
A321	M	D1	**5.9%**
AT76	M	E2	**5.9%**
A20N	M	D1	**5.1%**
E295	M	D	**3.8%**
A319	M	D1	**3.5%**
E190	M	E1	**3.2%**
B788	H	B2	**1.9%**
C510	L	F3	**1.8%**
CR2	M	E3	**0.9%**
C56X	M	F2	**0.9%**

Table 6.16: Palma peak hour 2 flight schedule

Aircraft	ICAO	RECAT-PWS	Occurence
A320	M	D1	**19.7%**
B738	M	D1	**17.6%**
B38M	M	D1	**9.2%**
A20N	M	D1	**7.5%**
B752	H	C4	**6.8%**
AT76	M	E2	**6.8%**
B788	H	B2	**5.1%**
A333	H	B2	**5.1%**
CRJX	M	E1	**5.0%**
A21N	M	D1	**4.8%**
B763	H	C2	**3.4%**
CRJ2	M	E3	**3.4%**
E190	M	E1	**3.4%**
C510	L	F3	**1.7%**

This fleet mix is then mapped to both ICAO and RECAT-EU-PWS wake turbulence categories, which are inputs to the simulation model.

Table 6.17: Palma WTC peak hour 1 flight schedule

ICAO		RECAT-EU-PWS	
Category	**Occurrence**	**Category**	**Occurrence**
L	1.8%	B2	1.9%
M	96.3%	D	3.8%
H	1.9%	D1	72.5%
		E1	11.6%
		E2	5.9%
		E3	0.9%
		F2	0.9%
		F3	1.8%

Table 6.18: Palma WTC peak hour 2 flight schedule

ICAO		RECAT-EU-PWS	
Category	**Occurrence**	**Category**	**Occurrence**
L	1.7%	D1	58.8%
M	78.9%	B2	10.2%
H	19.4%	E1	8.4%
		E2	6.8%
		C4	5.8%
		C2	3.4%
		E3	3.4%
		F3	1.7%

Geometric constraints

Additional inputs to the simulation model relate to airport-specific operational and geometric constraints. Parameters described in chapter 4, such as the common arrival path, missed approach distance, minimum distance, intersection parameters and SID allocation, are particularly relevant, as they directly influence aircraft separation requirements and runway throughput. The communications buffer, $\bar{c}$ is assumed to be 12 seconds.

The SID allocation has been obtained through an extensive analysis of the 2025 flight schedule, and is shown in Table 6.20 and highlighted in Figure A.1. The procedures applied by air traffic controllers indicate that certain SIDs are operationally grouped and managed as a single unit. Accordingly, three SID "blocks" are defined. Block "NORTH" comprises DRAGO, GALAT, and ESPOR; Block "SOUTH" includes NELUX and BAVER; and Block "EAST" consists of PTC, ISTER, MORSS, and MEROS.

Table 6.19: Palma 24L operational parameters

Parameter	Length [NM]
D_A	**6.07**
D_{MAP}	**1.0**
D_{MIN}	**0.0**

Table 6.20: Palma 24R SID allocation 2025

SID Utilized	Occurrence [%]
NORTH	49.1
WEST	32.1
EPAMA	9.2
SOUTH	7.7

The SID Departure separation matrices, both for same and different SIDs are presented below:

Table 6.21: Palma same SIDs DBS matrix

Follower → Leader ↓	**R**	**C**	**M**	**L**
R	80	60	60	60
C	120	105	105	90
M	180	105	105	90
L	240	240	240	120

Table 6.22: Palma different SIDs DBS matrix

Follower → Leader ↓	**R**	**C**	**M**	**L**
R	60	60	60	60
C	120	90	90	90
M	120	90	90	90
L	180	180	180	90

These matrices were derived from the airport successive departure requirements specified in the agreement between the Area Control Center (ACC) and the Tower (TWR) [49]. In this context, R denotes rapid aircraft, C refers to Citation-type aircraft, while M and L indicate medium and slow aircraft, respectively.

To map these categories to ICAO Wake Turbulence Categories (WTC), it is assumed that Heavy (H) and Medium (M) correspond to R (rapid), whereas Light (L) corresponds to C (Citation-type). For RECAT-EU-PWS, the mapping presented below is applied.

1. **R** → A, A1, B, B1, B2, C, C1, C2, C3, C4, D, D1, E, E1, E3
2. **C** → F1, F2
3. **M** → E2
4. **L** → F3, F

Table 6.23: Palma 24R & 24L ROTs

		Runway Occupancy Time [s]	
Group	**WTC**	**Arrivals**	**Departures**
ICAO	L	46.3	34.0
	M	44.1	47.1
	H	55.1	55.0
RECAT-EU-PWS	B1	59.5	50.0
	B2	55.2	50.0
	C2	52.6	50.0
	C4	52.4	50.0
	D	45.5	40.0
	D1	45.4	40.0
	E	51.4	35.3
	E1	41.8	35.3
	E2	42.7	35.3
	E3	41.8	35.3
	F1	44.7	30.0
	F2	41.1	30.0
	F3	45.3	30.0

6.3. Barcelona - El Prat Airport

Barcelona–El Prat Airport (LEBL) is located approximately 15 km southwest of Barcelona, in Catalonia, and serves as the main international gateway to northeastern Spain. It provides extensive connectivity to major european cities and a wide range of long-haul destinations.

Although tourism represents a significant share of its traffic, the airport also handles substantial business and connecting flows, resulting in a more balanced year-round demand profile with less pronounced seasonality. Barcelona–El Prat is Spain's second busiest airport in terms of passenger traffic and aircraft movements. It operates two parallel runways in a segregated mode configuration and a third one crossing both segregated runways, although the three runways are never active at the same time.The reference temperature is 29ºC, with an elevation of 4m.

Runway system and operational configuration

El Prat features two parallel runways in a 06-24 orientation and a third crossing runway 02-20. Table X presents the runway declared distances.

Table 6.24: Barcelona runways declared distances [51]

RWY Designator	TORA	TODA	ASDA	LDA
06L	3,352	3,412	3,352	2,922
24R	3,352	3,412	3,352	3,352
06R	2,660	2,720	2,660	2,660
24L	2,660	2,720	2,660	2,660
02	2,528	2,600	2,528	2,528
20	2,528	2,588	2,528	-

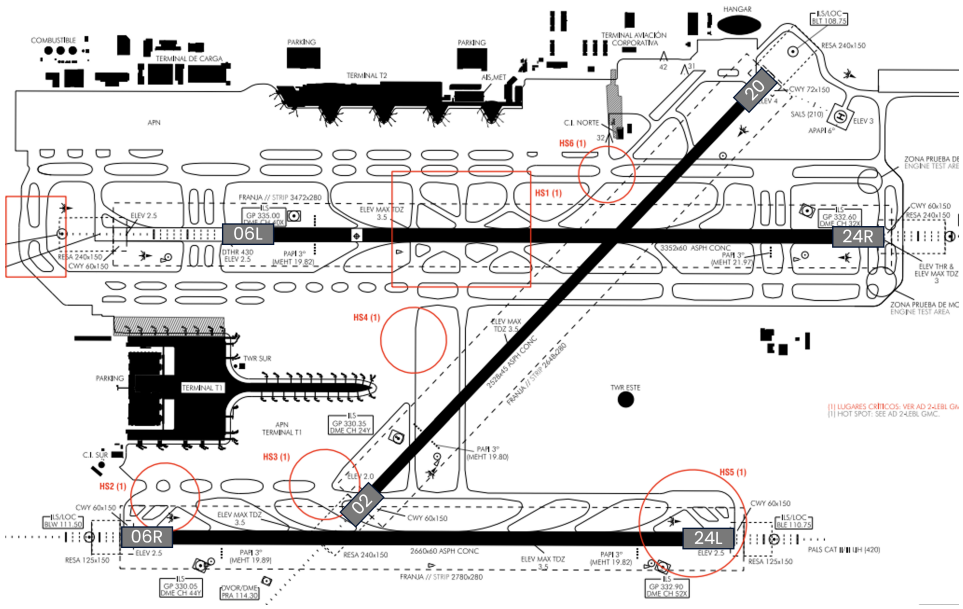

Figure 6.6: Barcelona - El Prat [51]

Due to noise abatement procedures implemented to mitigate noise in neighboring towns, Barcelona–El Prat operates under two differentiated modes: daytime operations (07:00–23:00) and nighttime operations (23:00–07:00).

During daytime, the preferential configuration is the western configuration, accounting for approximately 68% of total operations, with departures on RWY 24L and arrivals on RWY 24R. The eastern configuration (departures on RWY 06R and arrivals on RWY 06L) is non-preferential and used roughly 16% of cases.

At night, the preferential setup is the crossing-runway configuration, with arrivals on RWY 02 from the sea and departures on RWY 06R towards the sea, representing about 13% of operations. When this configuration is unavailable, both arrivals and departures operate on RWY 24L, accounting the remaining 3%.

Given that segregated runway operations were previously modelled for Palma de Mallorca Airport in section 6.2, Barcelona´s preferential night configuration with crossing runways will be used to validate the intersecting runway model.

Table 6.25: Barcelona 2025 configurations

RWY	Configuration	Mode	Utilisation
24L & 24R	WEST	Day Pref.	68.0%
06R & 06L	EAST	Day Non Pref.	15.7%
02 & 06R	CROSSING	Night Pref.	13.4%
24L	MIXED	Night Non Pref.	2.8%

Traffic characteristics and peak periods

The top 10 aircraft types are largely dominated by the Airbus A320 and A320neo families (64%), followed by the Boeing 737-800 and 737 MAX 8 (22%), primarily operated by airlines such as Vueling, Iberia, and Ryanair. The ranking is completed by three long-haul aircraft: the Boeing 787-8, Boeing 787-9, and Airbus A330-200.

Table 6.26: Barcelona 2025 flight schedule

Aircraft	ICAO	RECAT-EU-PWS	Occurence
A320	M	D1	**33.6%**
B738	M	D1	**16.5%**
A321	M	D1	**11.5%**
A20N	M	D1	**7.4%**
A319	M	D1	**6.7%**
B38M	M	D1	**5.2%**
A21N	M	D1	**4.3%**
B789	H	B2	**1.4%**
A332	H	B2	**0.9%**
B788	H	B2	**0.9%**

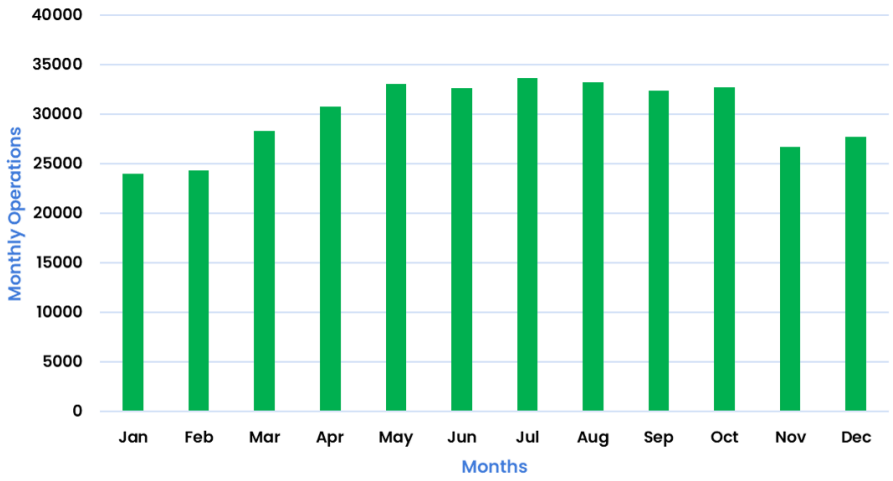

Figure 6.7: Barcelona 2025 monthly operations

A moderate seasonal traffic pattern can be observed in Figure 6.7, with peak-month volumes reaching up to 25%

above low-season levels. Demand increases steadily from January to April and remains relatively stable between May and October.

To characterize peak demand conditions, an average computed based on the five hours with the highest number of operations, only when the crossing Runways (02& 06R) are in use

Table 6.27: Barcelona 02 & 06R peak hour flight schedule

Aircraft	ICAO	RECAT-EU-PWS	Occurrence
A320	M	D1	**31.2%**
B738	M	D1	**19.0%**
A321	M	D1	**12.0%**
A319	M	D1	**6.1%**
B38M	M	D1	**5.4%**
B788	H	B2	**3.8%**
A20N	M	D1	**3.1%**
B77L	H	B1	**3.0%**
A333	H	B2	**2.9%**
B789	H	B2	**2.9%**
B764	H	C2	**2.3%**
AT43	M	E2	**1.5%**
BCS3	M	D1	**1.5%**
CRJX	M	E1	**1.5%**
A359	H	B1	**0.8%**
BE20	L	F3	**0.8%**
C55B	L	F3	**0.8%**
C510	L	F3	**0.8%**
PC12	L	F3	**0.8%**

This fleet mix is then mapped to both ICAO and RECAT-EU-PWS wake turbulence categories, which are inputs to the simulation model.

Table 6.28: Barcelona 02&06R 2025 WTC peak hour flight schedule

ICAO		RECAT-EU-PWS	
Category	**Occurrence**	**Category**	**Occurrence**
L	3.2%	B1	3.8%
M	81.1%	B2	9.6%
H	15.7%	C2	2.3%
		D1	78.3%
		E1	1.5%
		E2	1.5%
		F3	3.2%

Geometric constraints

Additional inputs to the simulation model relate to airport-specific operational and geometric constraints. Parameters described in chapter 4, such as the common arrival path, missed approach distance, minimum distance and SID allocation, are particularly relevant, as they directly influence aircraft separation requirements and runway throughput. The communications buffer, $\bar{c}$ is assumed to be 12 seconds. Modelling Barcelona's 02 and 06R as intersecting runways is a design choice. It is considered that $R_{A,int}$ represents the runway occupancy time of an arriving aircraft until a secured landing, approximately 1200 m from the threshold. $R_{D,int}$ represents the equivalent for a departing aircraft; it is the time taken until the aircraft crosses the arrival path of runway 02.

The SID allocation has been obtained through an extensive analysis of the 2025 flight schedule, and is shown in Table 6.30 and highlighted in Figure A.3 . The procedures applied by air traffic controllers indicate that

certain SIDs are operationally grouped and managed as a single unit. Accordingly, two SID "blocks" are defined. Block "NORTHWEST" comprises OLOXO1R, NATPI2R, GRAUS3R and LOBAR4R; Block "SOUTH" includes LARPA4R, SENIA5R, DUNES4R and LOTOS3R.

Table 6.29: Barcelona 02&06R operational parameters

Parameter	Value
D_A	**6.0 NM**
D_{MAP}	**1.0 NM**
D_{MIN}	**2.0 NM**
$R_{A,int}$	**18 s**
$R_{D,int}$	**23 s**

Table 6.30: Barcelona 02&06R SID allocation 2025

SID Utilized	Occurrence [%]
NORTHWEST	34.7
SOUTH	26.8
DALIN4R	14.6
AGENA4R	12.7
DIPES1R	10.9

The SID Departure separation matrices, both for same SID and different SID are presented below:

Table 6.31: Barcelona same SIDs DBS matrix

Follower → **Leader ↓**	**R**	**NR+**	**NR-**	**HP**	**LP**
R	90	60	60	130	90
NR+	180	90	60	220	180
NR-	240	240	120	280	240
HP	90	60	60	130	90
LP	110	60	60	150	110

Table 6.32: Barcelona different SIDs DBS matrix

Follower → **Leader ↓**	**R**	**NR+**	**NR-**	**HP**	**LP**
R	60	60	60	100	60
NR+	120	60	60	160	120
NR-	180	180	90	220	180
HP	60	60	60	100	60
LP	80	60	60	120	80

These matrices were derived from the airport successive departure requirements specified in the agreement between the Area Control Center (ACC) and the Tower (TWR) [52]. In this context, R denotes jet aircraft; NR+ refers to fast non-jet aircraft; and NR- refers to slow non-jet aircraft. The categories HP and LP indicate high-performing jets (primarily business jets) and low-performing jet aircraft (citation-type), respectively.

To map these categories to ICAO Wake Turbulence Categories (WTC), it is assumed that Heavy (H) and Medium (M) correspond to R, whereas Light (L) corresponds to NR-. For RECAT-EU-PWS, the mapping presented below is applied.

1. **R** → A, A1, B, B1, B2, C, C1, C2, C3, C4, D, D1, E, E1, E3
2. **NR+** → E2
3. **HP** → F1, F
4. **LP** → F2
5. **NR-** → F3

Table 6.33: Barcelona 02 & 06R ROTs

		Runway Occupancy Time [s]	
Group	**WTC**	**Arrivals**	**Departures**
ICAO	L	51.7	34.0
	M	51.9	47.1
	H	59.7	55.0
RECAT-EU-PWS	A1	70.8	50.0
	B1	58.7	50.0
	B2	60.0	50.0
	C2	58.8	50.0
	C3	62.4	50.0
	C4	63.1	50.0
	D	47.7	40.0
	D1	48.2	40.0
	E	51.2	35.3
	E1	45.3	35.3
	E2	44.6	35.3
	E3	45.1	35.3
	F	45.9	30.0
	F1	54.1	30.0
	F2	48.1	30.0
	F3	49.5	30.0

6.4. Madrid - Barajas Airport

Madrid–Barajas Airport (LEMD) is located approximately 12 km northeast of Madrid city, in the Community of Madrid, and serves as the main international gateway to Spain. It provides extensive connectivity to major European cities and a strong network of long-haul routes, particularly to South and Central America.

Although business and connecting traffic represent a large share of its activity (as it functions as a primary hub to Iberia and Air Europa) the airport also handles significant leisure demand, resulting in a stable year-round traffic profile with moderate seasonality. Adolfo Suárez Madrid–Barajas is Spain's busiest airport in terms of passenger traffic and aircraft movements. It operates four runways arranged in two independent pairs that allow simultaneous segregated operations, with some interdependencies between them. The reference temperature is 34ºC, with an elevation of 609m.

Runway system and operational configuration

Barajas features four exclusive runways in total, arranged in two pairs of parallel runways. When the northern runways are used for departures, the southern runways handle arrivals, and vice versa. Within each runway pair, the runways are independent, with independent approaches and departures (implemented in 2023 under the AMBAR project)

The only remaining dependency occurs between arriving runway 32R and departing runway 36L in the northern configuration, or between arriving runway 18L and departing runway 14R in the southern configuration. These operate as open-V runways, with potential missed-approach interference.

Table 6.34: Madrid runway declared distances [53]

RWY Designator	TORA	TODA	ASDA	LDA
14L	3,500	3,800	3,500	-
32R	-	-	-	3,000
14R	3,988	4,210	3,988	-
32L	-	-	-	3,060
18L	-	-	-	3,000
36R	3,500	3,800	3,500	-
18R	-	-	-	3,365
36L	4,179	4,609	4,179	-

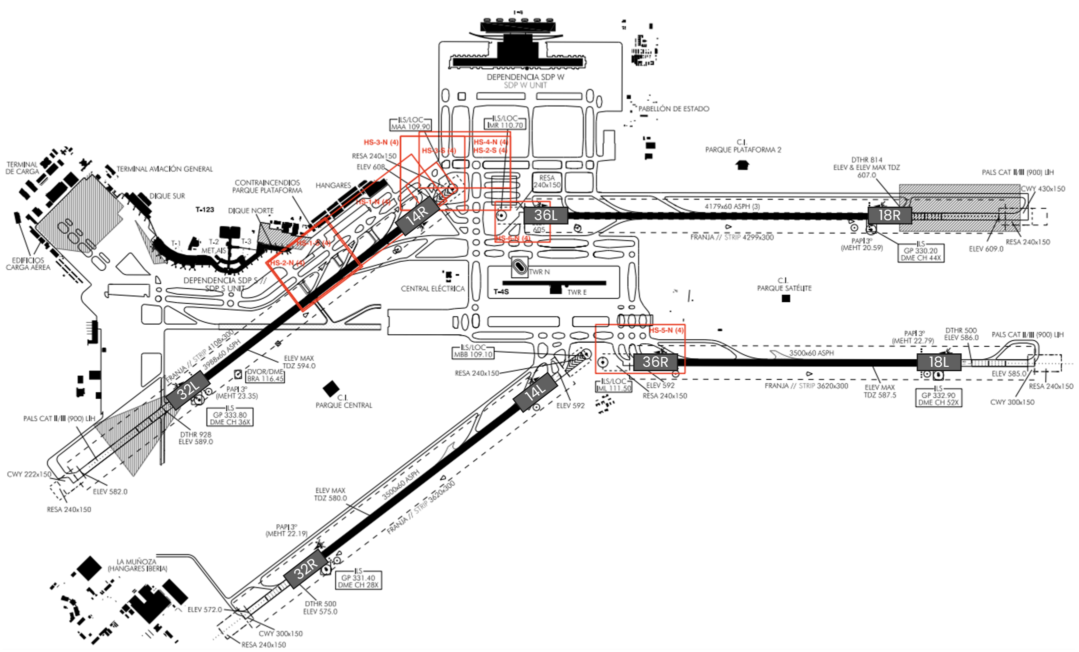

Figure 6.8: Madrid - Barajas [53]

The northern configuration uses runways 32L and 32R for arrivals and runways 36L and 36R for departures, and it is utilized approximately 74% of the time. The southern configuration, which uses runways 14R and 14L for departures and 18R and 18L for arrivals, is used during the remaining 26% of operations. Departing and arriving traffic is assigned to one of the two runways according to its origin or destination. Being the most utilized, the northern configuration will be used to model Madrid´s runway system capacity.

Table 6.35: Madrid 2025 configurations

Configuration	Arrivals RWY	Departures RWY	Utilisation
NORTH	32L & 32R	36L & 36R	73.7%
SOUTH	14R & 14L	18R & 18L	26.2%

Traffic characteristics and peak periods

The top 10 aircraft types are dominated by the Airbus A320 and A320neo families (40%),and the Boeing 737-800 and 737 MAX 8 (23%), primarily operated by airlines such as Iberia, Air Europa and Ryanair. The CRJ1000 shows around 10% of operations (Iberia Air Nostrum)The ranking is completed by two long-haul aircraft: the Boeing 787-9 and Airbus A350-900.

Table 6.36: Madrid 2025 top 10 aircraft types

Aircraft	ICAO	RECAT-EU-PWS	Occurence
B738	M	D1	**19.9%**
A320	M	D1	**14.9%**
CRJX	M	E1	**9.6%**
A20N	M	D1	**8.2%**
A21N	M	D1	**6.9%**
A321	M	D1	**6.3%**
B789	H	B2	**4.4%**
A359	H	B2	**3.6%**
A319	M	D1	**3.6%**
B38M	M	D1	**3.0%**

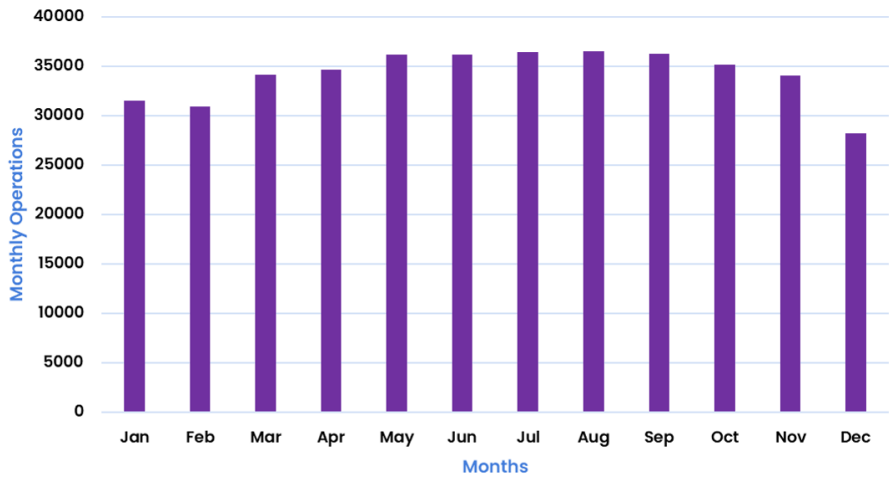

Figure 6.9: Madrid 2025 monthly operations

A moderate seasonal traffic pattern can be observed in Figure 6.7, with peak-month volumes reaching up to 29% above low-season levels. Demand increases steadily from January to April and remains relatively stable between May and September.

To characterize peak demand conditions, an average computed based on the five hours with the highest number of operations, when the northern configuration is in use.

Table 6.37: Madrid 2025 peak hour flight schedule

Aircraft ICAO Code	ICAO	RECAT-EU-PWS	Occurrence
B738	M	D1	**17.6%**
CRJX	M	E1	**13.6%**
A320	M	D1	**13.0%**
A21N	M	D1	**5.7%**
A321	M	D1	**5.3%**
A20N	M	D1	**5.0%**
B789	H	B2	**4.6%**
AT76	M	E2	**4.6%**
A332	H	B2	**4.5%**
B788	H	B2	**3.9%**
A359	H	B1	**3.3%**
A319	M	D1	**3.3%**
B38M	M	D1	**2.6%**
A333	H	B2	**2.4%**
CRJ2	M	E3	**2.0%**
B752	H	C4	**1.7%**
B77W	H	B1	**1.1%**
E190	M	E1	**1.1%**
C25B	L	F3	**1.8%**
B744	H	B1	**0.7%**
B764	H	C2	**0.7%**
C56X	M	F2	**1.4%**

This fleet mix is then mapped to both ICAO and RECAT-EU-PWS wake turbulence categories, which are inputs to the simulation model.

Table 6.38: Madrid 2025 WTC peak hour flight schedule

ICAO		RECAT-EU-PWS	
Category	**Occurrence**	**Category**	**Occurrence**
L	1.8%	B1	5.2%
M	75.2%	B2	15.3%
H	23.0%	C2	0.7%
		C4	1.7%
		D1	52.6%
		E1	14.7%
		E2	4.6%
		E3	2.0%
		F2	1.5%
		F3	1.8%

Geometric constraints

Parameters described in chapter 4, such as the common arrival path, missed approach distance, minimum distance and SID allocation, are particularly relevant, as they directly influence aircraft separation requirements and runway throughput. The communications buffer, $\bar{c}$ is assumed to be 12 seconds.

As previously explained, arrivals on runway 32R interact with departures on runway 36L, since a missed approach could conflict with a departing aircraft on the latter. To avoid this, the *"Área de Bloqueo"* procedure is used. It defines a forbidden window such that, if the arriving aircraft is within it, no departure clearance can be issued until the arrival vacates the area. This blocked area extends from 1 NM before the 32R threshold to the point where the arrival is considered to have a secured landing, 1200 m beyond the threshold along the runway.

The other departing runway (36R) and the other arriving runway (32L) are completely independent and present no additional interdependencies. For simplicity, these can therefore be assumed to operate as segregated independent runways, with no dependencies between them.

The SID allocation has been obtained through an extensive analysis of the 2025 flight schedule, and is shown in Table 6.40 and highlighted in Figure A.4 and Figure A.5.

Table 6.39: Madrid runway operational parameters

Parameter	Conv/Div 32R & 36L	Segregated 32L & 36R
D_A	**4.94 NM**	**4.75 NM**
D_{MAP}	**1.17 NM**	**1.15 NM**
D_{MIN}	**1.0 NM**	-
$R_{A,com}$	$R_A/3$	-

Table 6.40: Madrid departure runways SID allocation 2025

SID Utilized	36R [%]	36L [%]
PINAR3R	55.8	-
RBO3R	26.4	-
NANDO2R	14.5	-
VTB1R	1.2	-
CCS5W	0.8	-
CCS6L	-	27.4
SIE6L	-	18.5
ZMR7L	-	12.2
VTB6L	-	10.8
BARDI7L	-	9.3
CCS4N	-	6.7
PINAR3N	-	5.5
NANDO3N	-	2.5
RBO3N	-	2.3
BARDI3N	-	1.3
SIE2N	-	1.2
ZMR2N	-	0.9
VTB2N	-	0.9

The SID Departure separation matrix, is presented below:

Table 6.41: Madrid SIDs DBS matrix

Follower → Leader ↓	R	H+	H-	F
R	60	60	60	90
H+	180	60	60	180
H-	180	180	90	180
F	60	60	60	90

These matrices were derived from the airport successive departure requirements specified in the agreement between the Area Control Center (ACC) and Barajas Tower (TWR) [54]. In this context, R denotes jet aircraft; H+ refers to fast non-jet aircraft; and H- refers to slow non-jet aircraft. The category F indicate high-performing jets (primarily business jets).

To map these categories to ICAO Wake Turbulence Categories (WTC), it is assumed that Heavy (H) and Medium (M) correspond to R, whereas Light (L) corresponds to a combination between H- and F. For RECAT-EU-PWS, the mapping presented below is applied.

1. **R** → A, A1, B, B1, B2, C, C1, C2, C3, C4, D, D1, E, E1, E3
2. **H+** → E2
3. **H-** → F3, F
4. **F** → F1 & F2

Table 6.42: Madrid ROTs

		Runway Occupancy Time [s]		
Group	**WTC**	**32L Arrivals**	**32R Arrivals**	**Departures**
ICAO	L	51.7	59.3	34.0
	M	51.9	56.0	47.1
	H	61.8	70.3	55.0
RECAT-EU-PWS	A1	59.9	70.9	50.0
	B1	60.2	69.0	50.0
	B2	62.9	70.8	50.0
	C2	64.8	67.9	50.0
	C3	61.6	68.3	50.0
	C4	53.9	63.1	50.0
	D	52.7	54.3	40.0
	D1	52.8	57.3	40.0
	E	51.2	59.3	35.3
	E1	46.6	46.5	35.3
	E2	46.4	53.7	35.3
	E3	52.1	56.7	35.3
	F	50.1	57.6	30.0
	F1	54.1	58.3	30.0
	F2	48.9	56.7	30.0
	F3	50.7	58.4	30.0

6.5. RECAT-EU-PWS Case Studies

This section presents a set of case studies to evaluate the behaviour of the RECAT-EU-PWS model under different traffic mixes. The airports of Tenerife Norte and Palma de Mallorca are analysed to assess the model's sensitivity to traffic composition and its ability to capture variations in peak runway capacity caused by small changes in fleet mix, undetectable by ICAO categorization.

Particular attention is given to scenarios with a high proportion of turboprop operations, as this aircraft type can constrain sequencing efficiency and reduce achievable runway throughput.

The objective is to verify that the methodology reproduces realistic operations while enabling an individual assessment of how different aircraft categories affect runway capacity and delay metrics, illustrating the operational implications of RECAT-EU-PWS in practical situations.

6.5.1. Tenerife Norte

Tenerife Norte, commonly known as Los Rodeos, is located on the Spanish island of Tenerife, in the Canary Islands archipelago. The airport mainly serves inter-island traffic within the Canary Islands, together with a limited number of domestic mainland connections. The Island´s southern airport, Tenerife Sur, handles the majority of international and holiday traffic. Its operations are largely dominated by ATR72 aircraft, resulting in a relatively homogeneous but performance-limited traffic mix.

Operating a single mixed runway, the runway system is not capacity- constrained, with peak hourly operations reaching 26-27 [55], well below the limit for single runways. Operational data shows that runway 30 is used for 78.8% of operations under the western configuration, while the remaining 21.2% use runway 12 (eastern configuration).

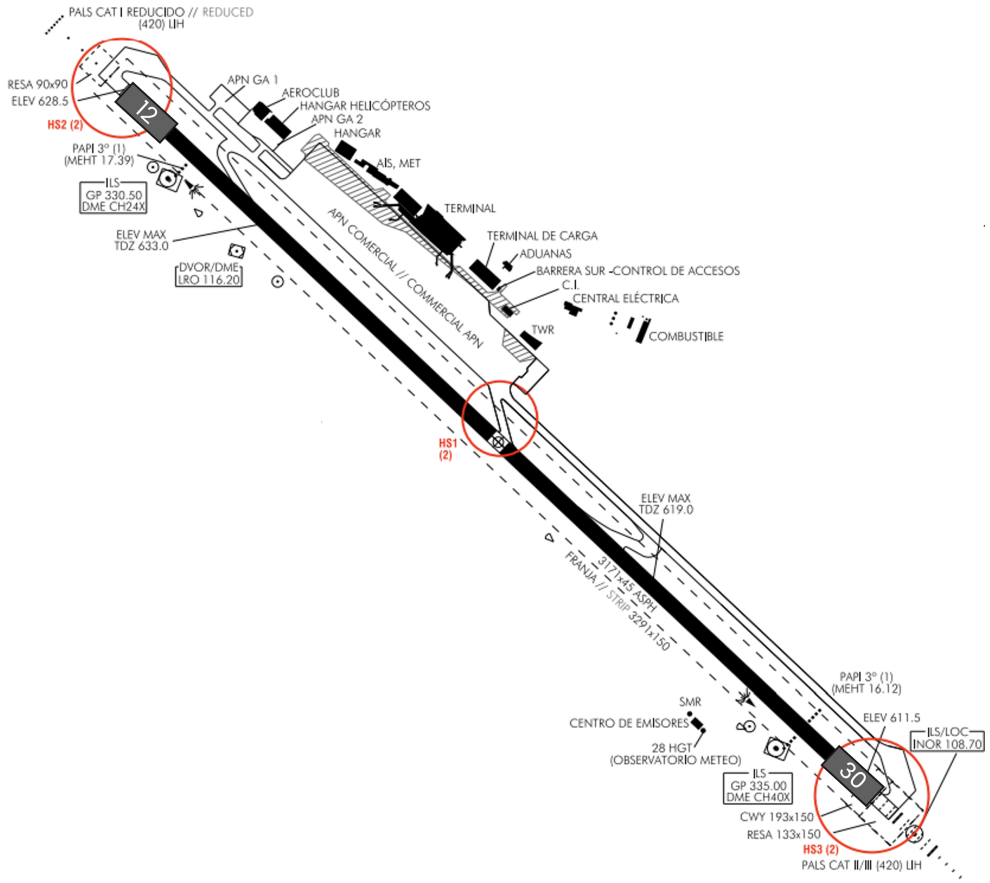

Figure 6.10: Tenerife Norte Los Rodeos [56]

The airport´s peak schedule, derived from multiple peak values is shown below:

Table 6.43: Tenerife Norte peak hour fleet mix

Aircraft	ICAO	RECAT-EU-PWS	Occurrence
AT76	M	E2	**57.7%**
A320	M	D1	**10.3%**
B738	M	D1	**10.3%**
E295	M	D	**10.3%**
CN35	M	E3	**5.2%**
B752	H	C4	**2.1%**
B788	M	B2	**2.1%**
SIRA	M	F3	**2.1%**

Table 6.44: Tenerife Norte ICAO & RECAT-EU-PWS fleet mix

ICAO		RECAT-EU-PWS	
Category	%	Category	%
L	2.1%	B2	2.1%
M	93.8%	C4	2.1%
H	4.2%	D	10.3%
		D1	20.6%
		E2	57.7%
		E3	5.2%
		F3	2.1%

Table 6.45: Tenerife Norte runway operational parameters

Parameter	Length [NM]
D_A	**6.9**
D_{MAP}	**1.0**
D_{MIN}	**0.0**

Table 6.46: TFN Runway 30 SID allocation 2025

SID Utilized	Occurrence [%]
ARACO2J	26.9
GDV4J	24.7
KORAL7J	15.8
VASTO5J	12.3
HIE4J	8.1
LALTO1J	6.2

The entirety of the ATR flights during the peak hour corresponds to inter-island services, operated by Binter (hub carrier) and Canaryfly. These flights mainly serve the islands of Gran Canaria and La Palma, which constitute the core trunk routes of the network. It is reasonable to assume that, in a hypothetical future scenario, part of these services could experience a fleet transition, progressively phasing out the ATR72 in favour of Binter's newer aircraft type, the Embraer E295.

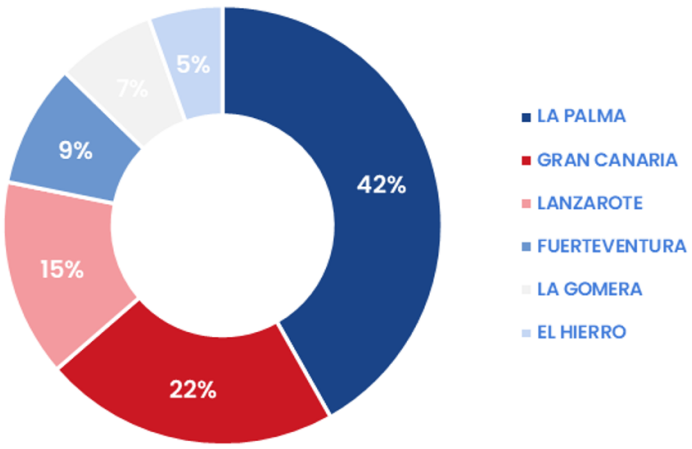

Figure 6.11: Tenerife ATR72 Route Share

Based on this hypothesis, three future scenarios are constructed in which ATR72 and E295 operations are interchanged. From the perspective of ICAO wake turbulence categories, both aircraft remain within category M and therefore no change occurs. However, differences do arise in the RECAT-EU-PWS categorisation. These scenarios are presented in Table 7.21 as high turboprop operations (HTO), medium turboprop operations (MTO) and low turboprop operations (LTO).

Table 6.47: Tenerife Norte RECAT-EU-PWS scenarios

RECAT-EU-PWS	HTO	MTO	LTO
B2	2.0	2.0	2.0
C4	2.0	2.0	2.0
D1	20.8	25.9	30.9
D	10.0	20.1	30.0
E2	57.8	42.6	27.7
E3	5.1	5.1	5.1
F3	3.3	3.3	3.3

The effect of these different RECAT-EU-PWS scenarios on peak capacity is presented in chapter 7.

Table 6.48: Tenerife Norte runway 30 ROTs

		Runway Occupancy Time [s]	
Group	**WTC**	**Arrivals**	**Departures**
ICAO	L	87.8	34.0
	M	56.9	47.1
	H	108.8	55.0
RECAT-EU-PWS	B2	108.9	50.0
	C2	103.7	50.0
	C4	77.9	50.0
	D	58.7	40.0
	D1	58.7	40.0
	E	66.2	35.3
	E1	53.9	35.3
	E2	55.1	35.3
	E3	53.9	35.3
	F1	57.7	30.0
	F2	53.1	30.0
	F3	70.9	30.0

6.5.2. Palma de Mallorca

The Palma de Mallorca airport scenario, modelled as a pair of segregated runways is already described above, in section 6.2.

The airport´s fleet mix corresponding to the peak hours with most turboprop operations, derived from multiple peak values is shown below:

Table 6.49: Palma ATR heavy peak hour fleet mix

Aircraft ICAO Code	%
A320	**27.7%**
AT76	**21.4%**
B738	**9.2%**
B38M	**7.7%**
A321	**6.2%**
A20N	**6.2%**
CRJX	**6.2%**
B788	**3.1%**
A319	**3.1%**
B752	**3.1%**
BE20	**1.5%**
A332	**1.5%**
LJ35	**1.5%**

Table 6.50: Palma ICAO & RECAT-EU-PWS fleet mix

ICAO		RECAT-EU-PWS	
Category	**%**	**Category**	**%**
L	0.0%	B2	4.6%
M	92.3%	C4	3.1%
H	7.7%	D1	60.1%
		E1	6.2%
		E2	21.4%
		F2	1.5%
		F3	1.5%

Shifting the focus to Palma de Mallorca, a comparable situation to Tenerife Norte can be analysed. During the identified ATR-heavy peak, the airport handles approximately 66 operations per hour, with around 14 operations corresponding to ATR72 aircraft (about 21% of the traffic). These operations are mainly performed by Iberia Regional and Air Europa and primarily serve short regional routes within Spain and the Balearic Islands. However, some of these routes are also frequently operated by jet aircraft Palma - Alicante (B738), Palma - Menorca (CRJX), and Palma - Valencia (B738/CRJX)) make Palma a suitable case to study how replacing turboprop operations may influence runway capacity.

To analyse the potential operational impact, three future scenarios are defined in which certain ATR72 operations are progressively phased out and replaced by the B737-800 and CRJX. The substitution is applied gradually, representing increasing levels of fleet transition from turboprop to regional jet operations on the abovementioned services.These scenarios are presented in Table 7.22 as high turboprop operations (HTO), medium turboprop operations (MTO) and low turboprop operations (LTO).

Table 6.51: Palma RECAT-EU-PWS scenarios

RECAT-EU-PWS	HTO	MTO	LTO
B2	4.6	4.6	4.6
C4	3.1	3.1	3.1
D1	60.1	66.3	72.5
E1	6.2	9.3	12.4
E2	21.4	12.1	2.8
F2	1.5	1.5	1.5
F3	1.5	1.5	1.5

6.6. Speed Profiles

In the previous sections, the runway occupancy times (ROTs) for each airport were presented. It is important to note that these values were obtained using different sources and methodologies depending on whether arrivals or departures were considered.

Arrival ROTs were extracted from the ENAIRE operational database, which contains recorded arrival runway occupancy times for every operation at Madrid, Barcelona, and Palma de Mallorca during the 2023–2025 period. The observations were grouped according to the ICAO or RECAT-EU-PWS categories, and the average ROTs for the categories were computed. This procedure provides runway-level occupancy times and therefore allows differences between individual runways to be captured. For example, Table 6.42 shows that Madrid's runway 32R generally presents higher ROT values than runway 32L in most category of aircraft.

In contrast, no equivalent operational dataset was available for departure runway occupancy times. Consequently, departure ROTs were taken from Lamers (2016) [23], where values are derived and documented in detail in the corresponding thesis.

Similarly to the runway occupancy times, the average arrival speeds of the common approach path were calculated for the scenarios in this study and then averaged. Departure speeds were also taken from Lamers (2016) [23] as a reference. Using the relationship between arrival and departure speeds established in that work, equivalent departure speeds were derived accordingly. However, they are not used in the simulations presented in this chapter, as the Specific Matrix Method (subsection 4.3.2) is applied instead of the Common Path Method (subsection 4.3.1)
.

Table 6.52: Scenario arrival and departure velocities

		Velocities [kts]	
Group	**WTC**	**Arrivals**	**Departures**
ICAO	L	141.6	156.2
	M	152.2	175.9
	H	153.5	188.8
RECAT-EU-PWS	A1	149.0	185.7
	B1	151.5	186.4
	B2	154.6	190.1
	C2	154.8	190.4
	C4	139.2	171.2
	D	145.8	168.5
	D1	153.9	177.9
	E	136.5	157.8
	E1	146.6	169.3
	E2	137.2	158.6
	E3	149.0	172.2
	F	140.6	156.2
	F1	139.8	161.6
	F2	146.3	161.4
	F3	140.8	155.3

7

Results, Verification and Validation

7.1. Verification and Validation

Verification and Validation are the two key processes used to measure and establish confidence in numerical and simulation models. The definitions used below are obtained from the 1998 AIAA guide [57].

Verification is the process by which it is determined that the model implemented accurately represents the developer´s conceptual description and solution to the model. It can be divided into code verification, where the focus is on the identification and removal of errors in the code, and calculation verification, which involves quantification of errors introduced during application of the code in a specific simulation.

Validation is the process of determining the extent to which a model is an accurate representation of real world data, from the perspective of use of the model.

The runway dependency calculations implemented in the model are based on the formulation presented in the thesis by Van der Klugt [21]. As this methodology has already undergone prior testing and validation, the focus of the present work is not the re-derivation of these relationships, but to use these as a base to build on top for the purpose of the investigation.

Verification

Code verification was performed through four complementary approaches.

In first place, a systematic visual inspection of the code, parameters, and data structures was conducted. This involves checking matrices, input data, and parameters with respect to existing literature to ensure that no incorrect constants, units, and indexing are introduced in the simulation.

Second, a visual inspection of simulations was carried out. Individual run results were exported to spreadsheets for easier inspection. Gantt charts, like the one shown in Figure 7.1 for arrival and departure operations were created for a simulation run, allowing for verification of sequencing, timing and possible runway conflicts.

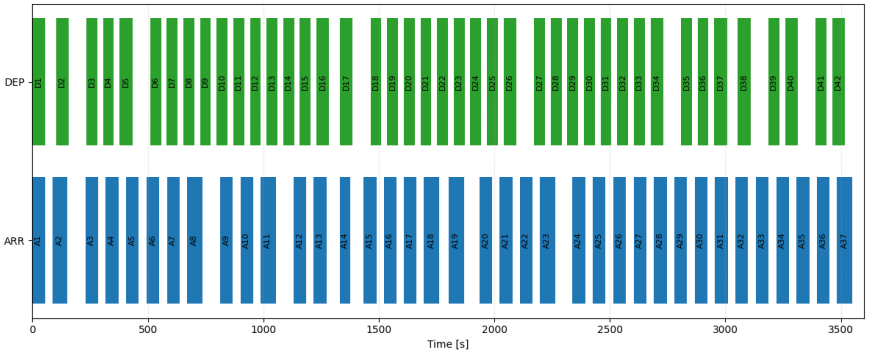

Figure 7.1: Single run operations Gantt chart (example)

A third verification method is the use of verification functions. These are special functions designed to recalculate some of the simulation results by using the same variables from a simulation run. These reconstructed simulation results are then compared with original simulation results. This process of backward calculation from simulation results to original variables, and then to simulation results, allows for the verification of mathematical correctness of implemented equations, independent of other simulation processes.

Fourth, the model outputs have been compared against results produced by RCAP 1.0 and ENAIRE's runway capacity simulation software, the *Programa de Investigación de Capacidad de Pistas* (PICAP). Being a consolidated and previously validated capacity model, agreement between both tools provides confidence that the fundamental operational calculations are correctly implemented. To support this comparison, the runway capacity envelope was computed following the same methodology presented in the previous section.

Calculation verification focuses on quantifying numerical uncertainty introduced by the stochastic nature of the simulation. Because the model relies on Monte Carlo simulations, insufficient numbers of runs may introduce statistical error in the estimated performance indicators.

Convergence analyses were performed by evaluating the coefficient of variation of peak hourly capacity as a function of the number of Monte Carlo iterations. The required number of runs was selected once the coefficient of variation stabilized below an acceptable threshold, ensuring statistically reliable estimates of runway system capacity.

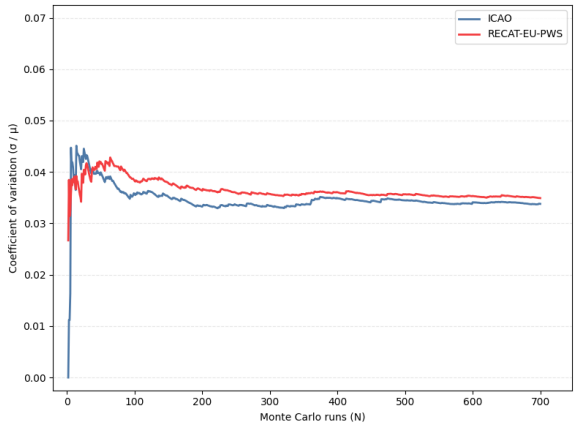

Figure 7.2: Coefficient of variation. Single runway

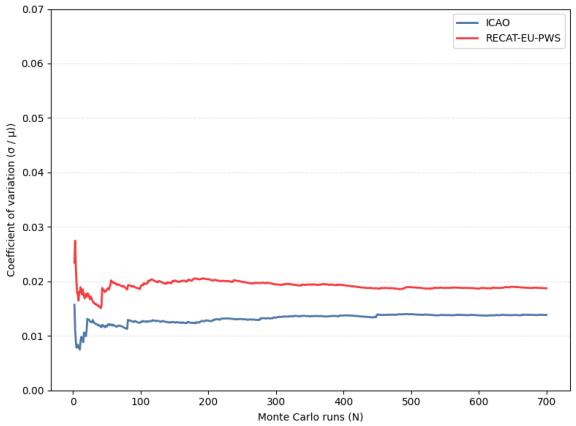

Figure 7.3: Coefficient of variation. Segregated runways

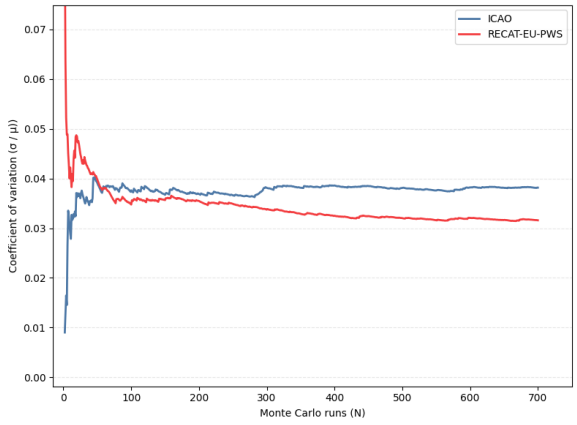

Figure 7.4: Coefficient of variation. Intersecting runways

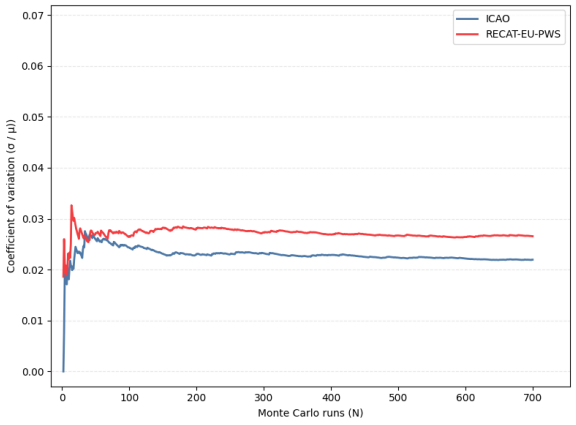

Figure 7.5: Coefficient of variation. Converging runway

Across the four scenarios, the coefficient of variation varies rapidly during the first Monte Carlo iterations and then gradually stabilises as the number of runs increases. This indicates that initially, a large sampling variability is

observed, which is reduces progressively as more samples are included. In all cases, the curves become effectively stable at approximately 500 simulation runs, suggesting that this number of iterations provides a good balance between computation times and statistical robustness.

For most scenarios, the RECAT-EU-PWS configuration stabilizes at a slightly higher coefficient of variation than the ICAO configuration. This means that, under this scheme, the simulated peak hourly capacity exhibits greater inherent variability between runs, which could be due to the increased sensitivity of operations to stochastic traffic sequencing, as a larger set of aircraft categories, with distinct speeds, runway occupancy times, and separations,is considered instead of only three categories. The exception is the intersecting runways case, where RECAT-EU-PWS stabilizes at a lower coefficient of variation than ICAO, indicating more consistent capacity outcomes for that specific operational configuration. This suggests that, for this scenario, the new wake scheme reduces operational variability rather than amplifying it.

Validation

The validation was carried out by comparing the simulated capacity envelopes with the observed hourly runway throughput from 2025 operations across the selected scenarios. This comparison aims to validate whether the model presents a realistic representation of runway performance capability. Visual representations of the comparison are shown in the following sections.

In some cases, observed capacity values may fall well below the capacity envelope. Airports may be operating below their maximum runway capacity, and movements may be restricted due to reasons outside the runway system, e.g., terminal capacity, stand availability, gate restrictions, or air traffic control restrictions in the surrounding airspace.

For this reason, it was also decided to compare the outputted capacity envelopes with those generated by RCAP 1.0, and, where applicable, to the peak capacity estimated by ENAIRE's runway capacity simulation software, the *Programa de Investigación de Capacidad de Pistas* (PICAP)

7.2. Single Runway

As previously explained in chapter 6, the single runway in mixed mode is modelled using Alicante airport´s runway 10 in mixed mode.

7.2.1. Assumptions

Before presenting the results, the assumptions taken to model this situation have to be explained. Depending on which, the result can see itself greatly influenced by each.

Runway 10 in mixed mode operations is modelled. The arrival Runway Occupancy times are derived from ENAIRE data. It is assumed that a Specific Matrix method is used to model SID dependencies, and as such the departure velocities are irrelevant, and departure ROTs are not the limiting factor, which instead is this DBS SID matrix. These two, however, have been derived from the previous thesis written by Lamers [23]. The geometric values, such as D_A and D_{MAP} have been obtained from navigation charts specific to Alicante runway 10. More information, such as the SIDs used, the ICAO and RECAT-EU-PWS traffic mix and the SID DBS matrix can be found in section 6.2.

Table 7.1: Assumptions made modelling Alicante

Parameter	Symbol	Value
Mode of Operation		Mixed
Departure ROT	R_D	Calculated from *Lamers, 2016* [23]
Arrival ROT	R_A	ENAIRE database
Departure Velocity	V_D	Calculated from *Lamers, 2016* [23]
Arrival Velocity	V_A	ENAIRE database
SID Logic Used		Specific Matrix Method
SIDs Modelled		LEAL 10
Common Approach Path	D_A	6.01 NM
Missed Approach Point	D_{MAP}	0.72 NM
Headwind TBS Scenario		25 kts
Headwind RECAT-EU-PWS Scenario		7 kts
Minimum Radar Separation		3 NM

7.2.2. Capacity Metrics

Arrivals TBS Deployment

As previously explained, headwind affects negatively the maximum throughput capacity of a runway system. The results below show the effect of applying TBS upon arrivals in a moderate-high headwind of 25kts and its effect on capacity metrics.

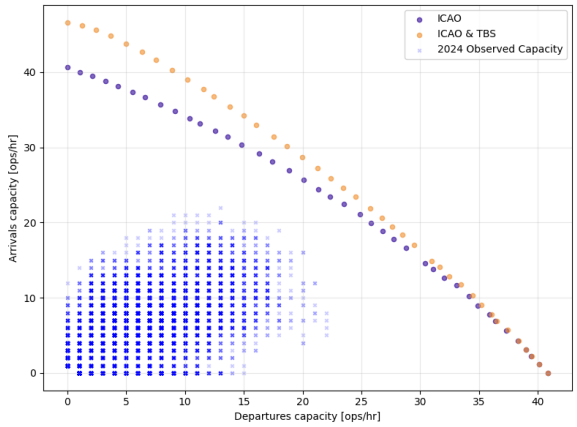

Figure 7.6: Capacity envelope (ICAO vs ICAO&TBS). LEAL 10

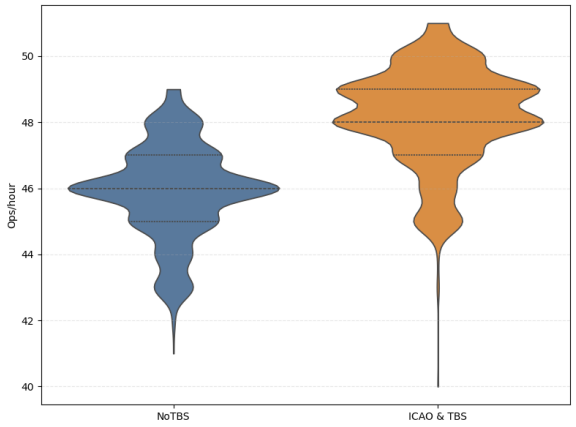

Figure 7.7: Capacity distribution (ICAO vs ICAO&TBS). LEAL 10

Applying TBS shifts the simulated capacity envelope outward versus the ICAO (Figure 7.6), achievable arrival throughput for the same departure rate. The benefit is strongest in arrivals dominated conditions and progressively diminishes as operations become departure dominant (which makes sense as TBS is applied exclusively for arrivals). The arrivals-only capacity sees the greatest benefit, growing from 41 to 46 ops/h. Under balanced operations, peak capacity can increase from 46 to 48. Under a departures-only regime both modes remain with 41.

The ICAO only peak-capacity distribution is centred at around 46 ops/hr and exhibits a wider spread, with a noticeable lower tail extending to approximately 43–44 ops/hr. In contrast, the ICAO & TBS distribution is shifted upward, clustering around 48–49 ops/hr, and although a thin lower tail remains, most outcomes are concentrated near the higher peak rates.

Given that the above plots show that the implementation of Time-Based Separation for arrival operations can increase peak hourly capacity, the next question concerns the influence of headwind on runway performance. Specifically, how does runway capacity vary as a function of headwind, and to what extent can TBS mitigate the capacity loss associated with increasing headwind conditions.

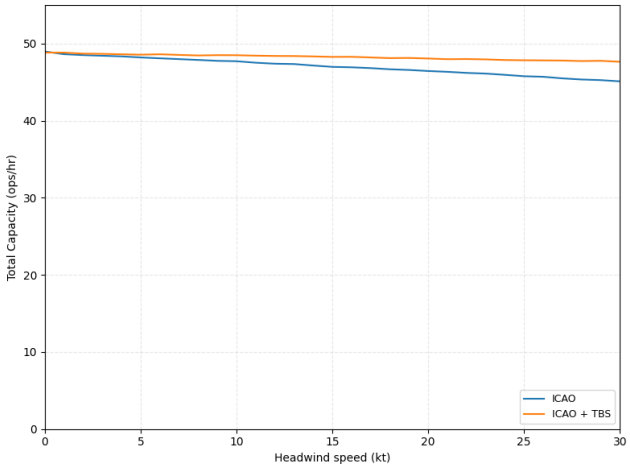

Figure 7.8: Total capacity as a function of headwind speed. ICAO vs ICAO&TBS. LEAL 10

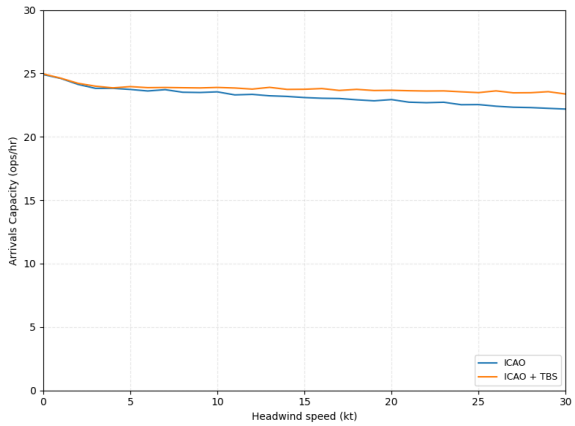

Figure 7.9: Arrival capacity as a function of headwind speed. ICAO vs ICAO&TBS. LEAL 10

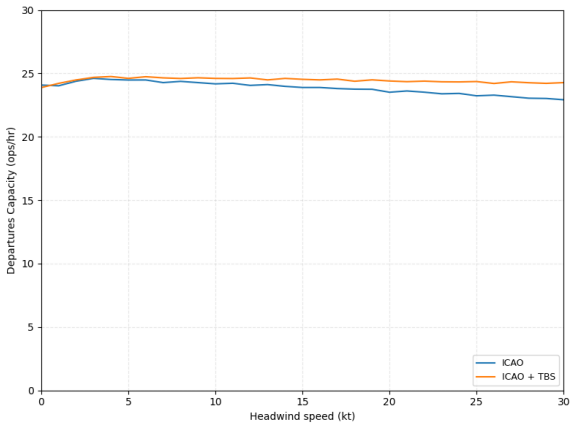

Figure 7.10: Departure capacity as a function of headwind speed. ICAO vs ICAO&TBS. LEAL 10

Figures 7.8–7.10 show the reduction in runway capacity with increasing headwind, with total throughput decreasing from 48 ops/h (25 arrivals, 23 departures) to 44 ops/h (21 arrivals, 23 departures). Under TBS, this capacity loss is partially mitigated, maintaining a total capacity of 47 ops/h, with 23 arrivals and 24 departures. This improvement when using TBS can be seen in Figure 7.11, in which the benefit varies from 0% up to 6%. Although

departures are not directly governed by time-based separation, they vary indirectly through arrival–departure interactions in mixed-mode operations, as small changes in arrival spacing can determine whether an additional departure can be accommodated or not. Realistic capacity gains begin to be observed at a headwind of 12 kts.

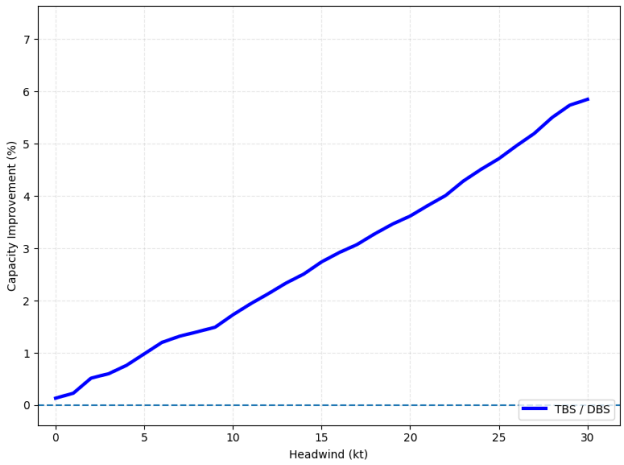

Figure 7.11: TBS capacity improvement as a function of headwind. LEAL 10

RECAT-EU-PWS Deployment

To model the deployment of RECAT-EU-PWS categorisation versus ICAO, an average headwind of 7 kts is assumed.

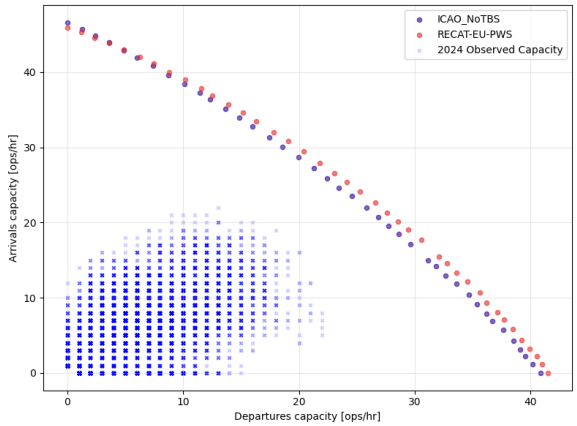

Figure 7.12: Capacity envelope (ICAO vs RECAT-EU-PWS). LEAL 10

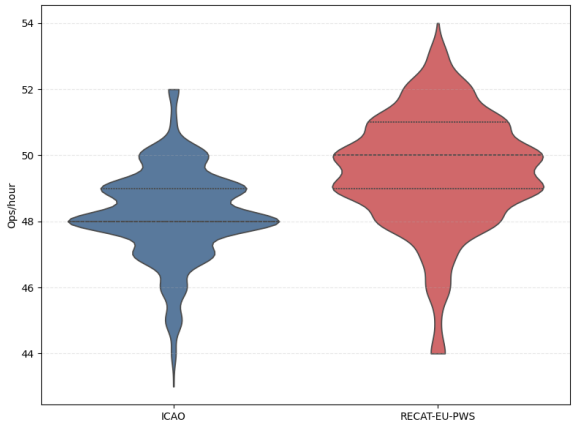

Figure 7.13: Peak capacity distribution (ICAO vs RECAT-EU-PWS). LEAL 10

Changing to a RECAT-EU-PWS wake categorisation scheme can increase peak hourly capacity from 48 ops/h to 50. This increase is more notable in the point were arrivals and departures are balanced. At the departures only point, an increase of 1 operation can be attained, from 41 to 42 departures, and the arrivals-only point remains unchanged with around 46 arrivals. The ICAO distribution is centered lower and has a more pronounced lower tail, In contrast, RECAT-EU-PWS is centred higher with most of the density concentrated at these higher values, although a lower tail remains.

The ICAO only peak-capacity distribution is centred at around 46 ops/hr and exhibits a wider spread, with a noticeable lower tail extending to approximately 43–44 ops/hr. In contrast, the ICAO & TBS distribution is shifted upward, clustering around 48–49 ops/hr, and although a thin lower tail remains, most outcomes are concentrated near the higher peak rates.

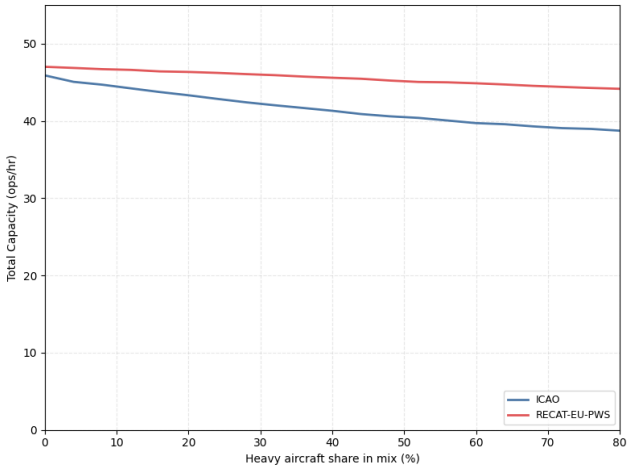

Figure 7.14: Total capacity as a function of proportion of heavy aircraft. ICAO vs RECAT-EU-PWS. LEAL 10

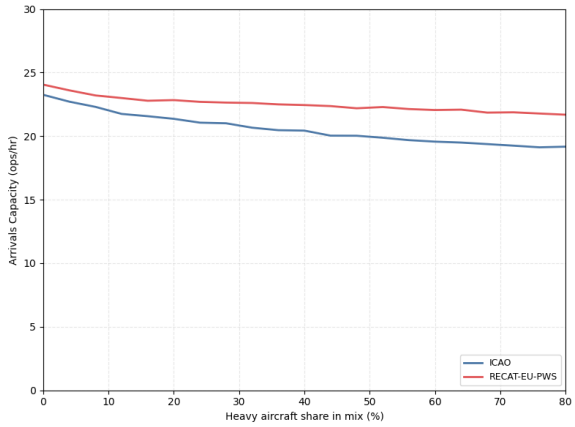

Figure 7.15: Arrival capacity as a function of proportion of heavy aircraft. ICAO vs RECAT-EU-PWS. LEAL 10

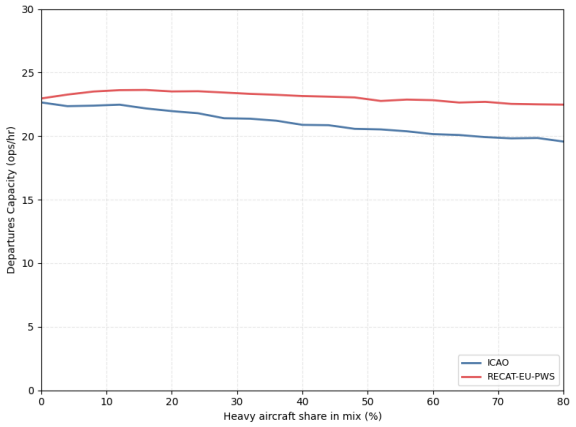

Figure 7.16: Departure capacity as a function of proportion of heavy aircraft. ICAO vs RECAT-EU-PWS. LEAL 10

From Figures 7.14–7.16 one can interpret that as the presence of heavy aircraft in the mix mostly B1 and B2 aircraft in RECAT-EU-PWS) increases, capacity logically decreases, and ARR-ARR and DEP-DEP separations become greater. As heavy % increases from 0% to 80%, ICAO peak capacity progresses from 46 ops (23 ARR, 23 DEP) to 39 (19 ARR, 20 DEP). The behavior of RECAT-EU-PWS is notably less pronounced, varying from 4 ops (24 ARR, 23 DEP) to 44 (22 ARR, 22 DEP).

The percentage change evolution is shown in Figure 7.17. When the heavy-aircraft share is negligible, most limiting pairs are $M \rightarrow M$ under ICAO and $D1 \rightarrow D1$ under RECAT-EU–PWS; both are effectively constrained by the minimum radar separation (MRS), here set to 3 NM, hence the smallest capacity gain.

As the fleet mix approaches an even balance of Heavy and Medium aircraft, the dominant limiting interaction under ICAO becomes $H \rightarrow M$ at 5 NM, which maps in RECAT-EU–PWS primarily to $B1 \rightarrow D1$ or $B2 \rightarrow D2$, with separations of 4 NM and 3 NM, respectively, leading to a larger relative improvement.

Finally, when heavy aircraft represent approximately 70–80% of the sample, most pairs become $H \rightarrow H$ (ICAO 4 NM) and $B1/B2 \rightarrow B1/B2$ (RECAT-EU–PWS 3 NM), maintaining a measurable but smaller incremental advantage as both regimes approach the MRS floor.

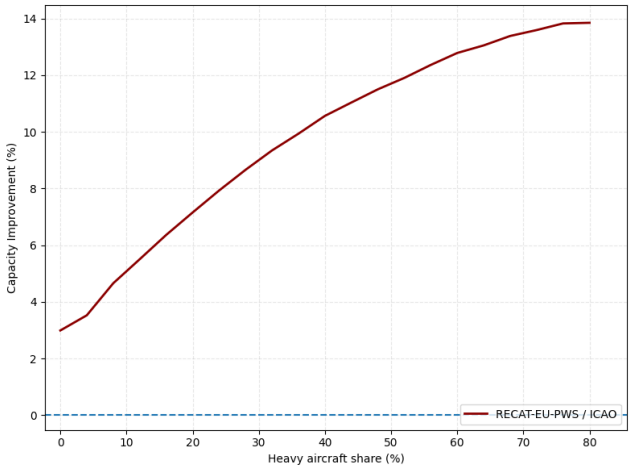

Figure 7.17: RECAT-EU-PWS capacity improvement as a function of heavy aircraft proportion. LEAL 10

7.2.3. Comparison with other models

As part of the validation procedure, the capacity envelopes produced by the model developed in this thesis, from now onwards, ARCAS (Airport Runway Capacity Analysis Software) has been compared, in identical conditions to that generated by van der Klugt in his thesis [21], RCAP 1.0.

Additionally, to strengthen the validation, results were compared against the peak capacity estimates produced by ENAIRE's runway capacity simulation software, the *Programa de Investigación de Capacidad de Pistas* (PICAP). While the underlying assumptions are broadly similar, the simulation conditions are not identical to those used in ARCAS and RCAP 1.0. The PICAP comparison is therefore included only as an orientative check.

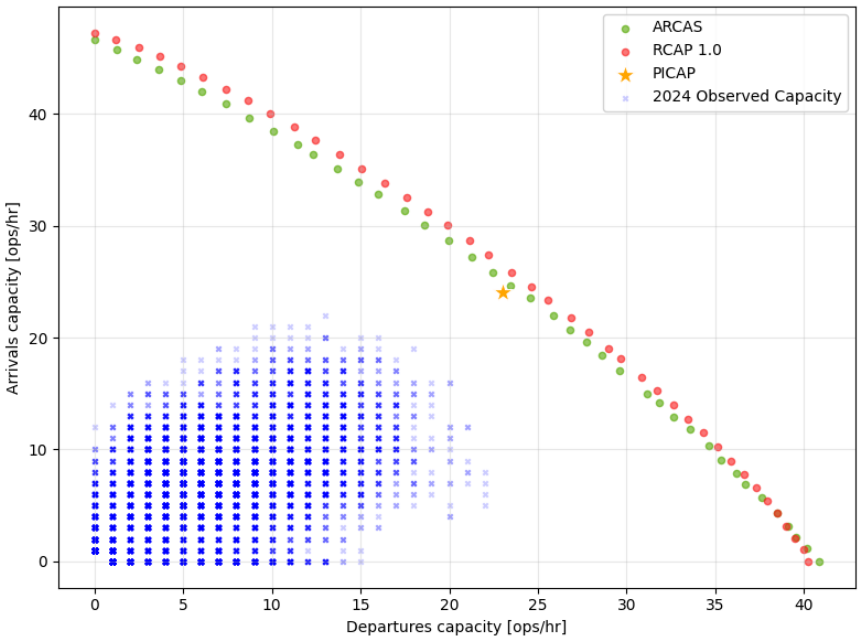

Figure 7.18: Validation of capacity envelope against RCAP 1.0 & PICAP. LEAL 10

The two modelled envelopes (ARCAS, in green, and RCAP 1.0, in red) are very close across the range, with RCAP 1.0 generally predicting slightly higher capacity than ARCAS, although at the arrivals-only and departures-only points both models converge to very similar values.

A single PICAP estimate is overlaid as an orange star at 23 departures/hr and 24 arrivals/hr, lying close to the

modelled envelopes. Finally, the 2024 observed capacity (blue points) form a dense cloud concentrated well below the envelope in the 0–20 departures/hr and 0–22 arrivals/hr range, with a maximum combined capacity of 37 ops/hr. This suggests that Alicante still has a margin to continue increasing the runway throughput without reaching peak capacity.

Table 7.2: Comparison of ARCAS, RCAP 1.0 & PICAP capacities. Alicante

	Peak / ARR / DEP	**Arrivals Only**	**Departures Only**
ARCAS	48.1 / 23.5 / 24.6	46.6	40.9
RCAP 1.0	49.1 / 24.5 / 24.6	47.2	40.3
% Change	2.08 / 4.25 / 0	1.29	-1.47
PICAP	47 / 23 / 24	-	-
% Change	-2.29 / -2.13 / -2.44	-	-

From Table 7.2 it can be observed that the simulated capacity results by the ARCAS model are in line with those outputted by RCAP 1.0 and PICAP, with a difference as high as 2% between models when calculating the peak runway capacity.

As shown in Figure 7.11 and Figure 7.17, meaningful capacity gains that would translate into a realistic increase in runway operational capacity would emerge at headwind levels of 12 to 13 kts for TBS, whereas for RECAT-EU-PWS they would occur at any proportion of heavy aircraft.

7.3. Parallel Runways

Palma de Mallorca airport's runways 24L and 24R are used to validate the parallel runways model in a segregated mode.

7.3.1. Assumptions

Before presenting the results, the assumptions taken to model this situation have to be explained. Depending on which, the result can see itself greatly influenced by each.considers two peak periods: one dominated by medium traffic and one with a more balanced mix of medium and heavy aircraft.

An average headwind of 7 kt is assumed for the RECAT-EU-PWS scenarios, whereas a strong headwind of 25 kt is applied in the TBS capacity envelope in order to illustrate the different system behaviour. The arrival ROTs have been obtained from specific ENAIRE data. It is assumed that the Specific Matrix method is used to model SID dependencies, and as such the departure velocities are irrelevant, and departure ROTs are not the limiting factor, which instead is this DBS SID matrix. These two, however, have been derived from the previous thesis written by Lamers [23]. The geometric values, such as D_A and D_{MAP} have been obtained from navigation charts specific to Alicante runway 10. More information, such as the SIDs used, the ICAO and RECAT-EU-PWS traffic mix and the SID DBS matrix can be found in section 6.2.

Table 7.3: Assumptions made modelling Palma

Parameter	Symbol	Value
Mode of Operation		Segregated de-coupled
Departure ROT	R_D	Calculated from *Lamers, 2016* [23]
Arrival ROT	R_A	ENAIRE LEPA database
Departure Velocity	V_D	Calculated from *Lamers, 2016* [23]
Arrival Velocity	V_A	ENAIRE LEPA database
SID Logic Used		Specific Matrix Method
SIDs Modelled		LEPA 24R
Common Approach Path	D_A	6.07 NM
Missed Approach Point	D_{MAP}	1.0 NM
Minimum Distance for DEP before ARR	D_{MIN}	0.0 NM
Headwind TBS Scenario		25 kts
Headwind RECAT-EU-PWS Scenario		7 kts
Minimum Radar Separation		3 NM

7.3.2. Capacity Metrics

Arrivals TBS Deployment
"M" Dominated Mix

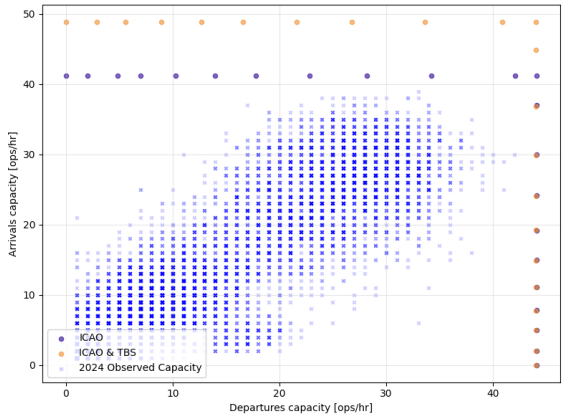

Figure 7.19: Capacity envelope (ICAO vs ICAO&TBS). LEPA 24R&24L

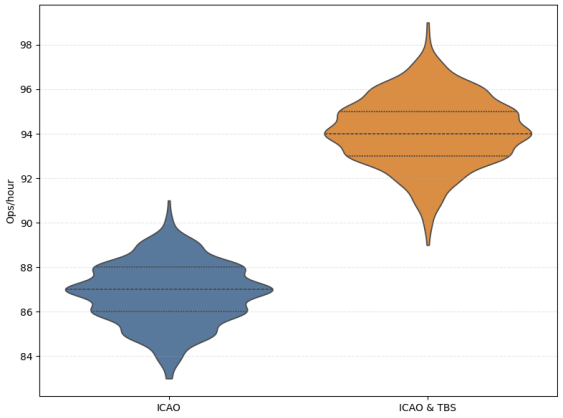

Figure 7.20: Peak capacity distribution (ICAO vs ICAO&TBS). LEPA 24R&24L

Palma de Mallorca, having two segregated completely independent runways, shows no interaction at all between arrivals and departures, meaning that both runways can operate at their peak capacity without affecting the other. In this case, departures are completely unchanged with the implementation of TBS, which makes sense due to the independence of operations. At a headwind of 25kts, implementing TBS implies a capacity jump of 85 (41 ARR 44 DEP) to 93 movements per hour (49 ARR 44 DEP). From it can be concluded that both distributions show a comparable spread (similar overall width and tail extent), however, and as expected ICAO & TBS shows a behavior clearly shifted upward, with a higher central tendency.

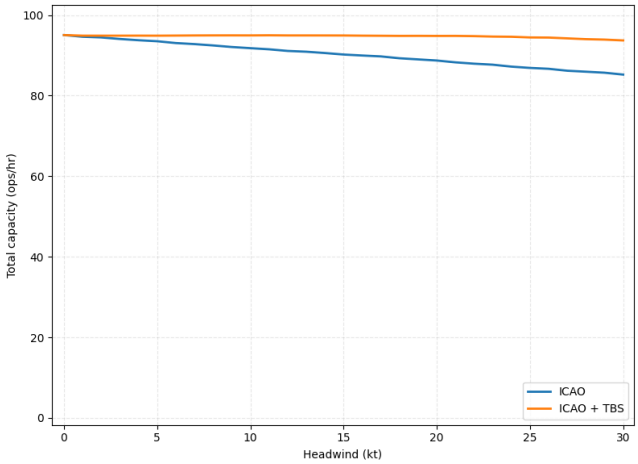

Figure 7.21: Total capacity as a function of headwind speed. ICAO vs ICAO&TBS. LEPA 24R&24L

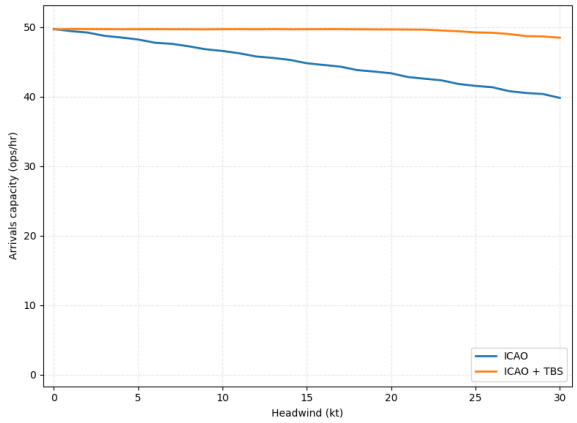

Figure 7.22: Arrival capacity as a function of headwind speed. ICAO vs ICAO&TBS. LEPA 24R&24L

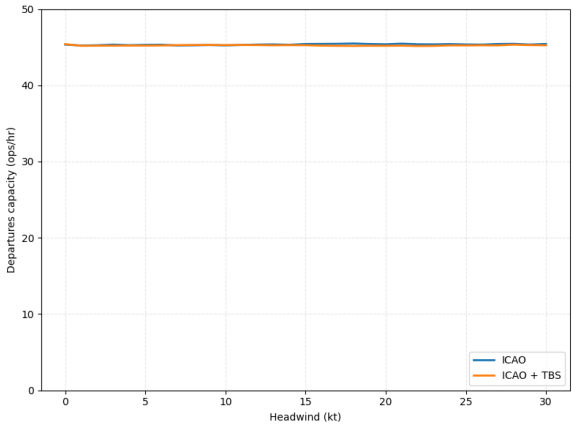

Figure 7.23: Departure capacity as a function of headwind speed. ICAO vs ICAO&TBS. LEPA 24R&24L

Figures 7.21–7.23 show the reduction in runway capacity with increasing headwind, with total throughput decreasing from 94 ops/h (49 ARR 45 DEP) to 85 ops/h (40 ARR 45 DEP). Under TBS, this capacity loss is greatly neutralised, maintaining a total capacity of 93 ops/h, with 48 arrivals and 45 departures. This improvement when using TBS can be seen in Figure 7.24, in which realistic capacity gains start to occur at 4 kts of headwind.

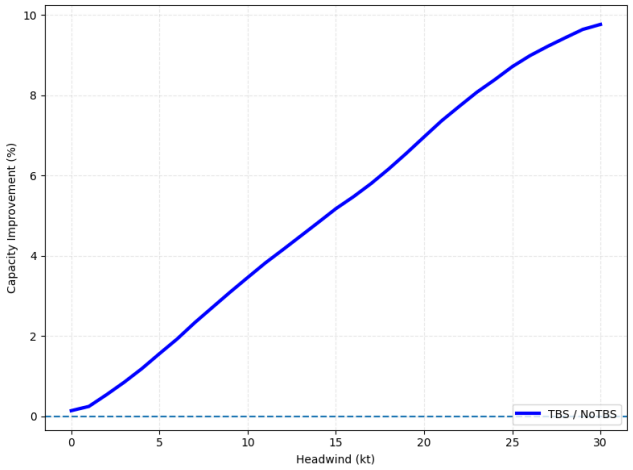

Figure 7.24: TBS capacity improvement as a function of headwind. LEPA 24R&24L

"Balanced" Mix

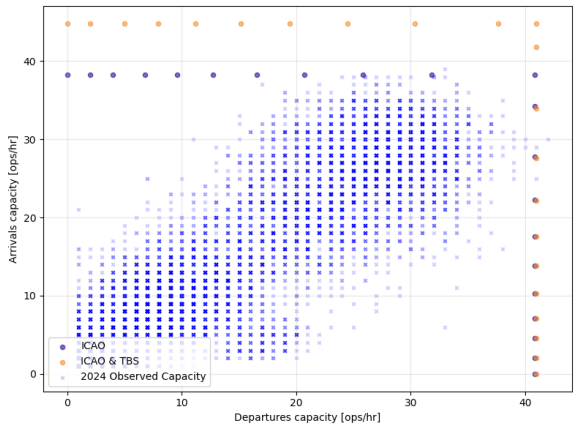

Figure 7.25: Capacity envelope (ICAO vs ICAO&TBS). LEPA 24R&24L

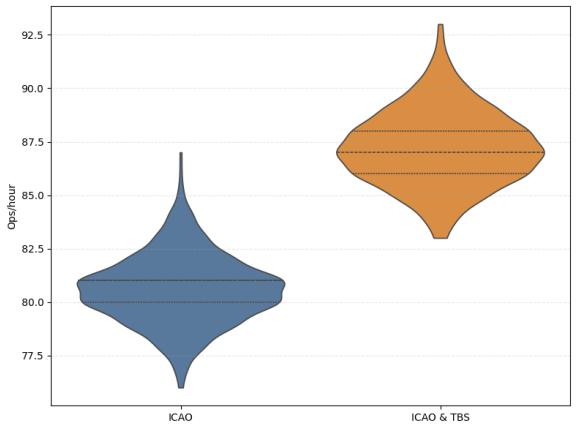

Figure 7.26: Peak capacity distribution (ICAO vs ICAO&TBS). LEPA 24R&24L

Considering a traffic mix with a heavier proportion of Heavy-type aircraft (B2 mainly in RECAT-EU-PWS), implementing TBS implies a capacity jump of 79 (41 ARR 44 DEP) to 93 movements per hour (49 ARR 44 DEP). From it can be concluded that both distributions show a comparable spread (similar overall width and tail extent), however, and as expected ICAO & TBS shows a behavior clearly shifted upward, with a higher central tendency.

Given that the above plots show that the implementation of Time-Based Separation for arrival operations can increase peak hourly capacity, the next question concerns the influence of headwind on runway performance. Specifically, how does runway capacity vary as a function of headwind, and to what extent can TBS mitigate the capacity loss associated with increasing headwind conditions.

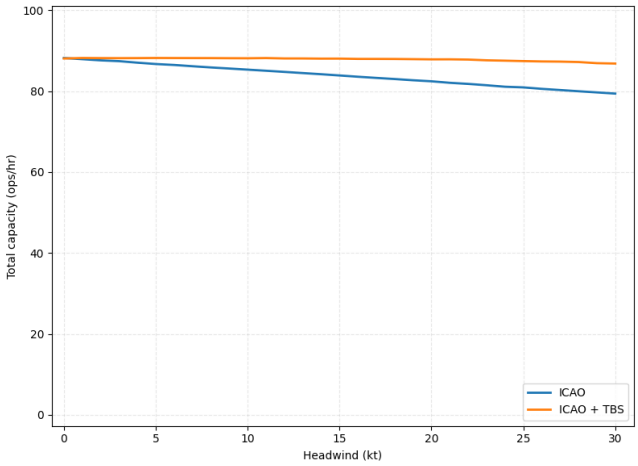

Figure 7.27: Total capacity as a function of headwind speed. ICAO vs ICAO&TBS. LEPA 24R&24L

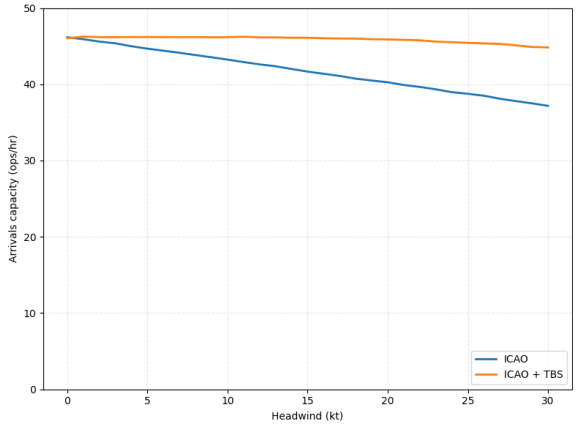

Figure 7.28: Arrival capacity as a function of headwind speed. ICAO vs ICAO&TBS. LEPA 24R&24L

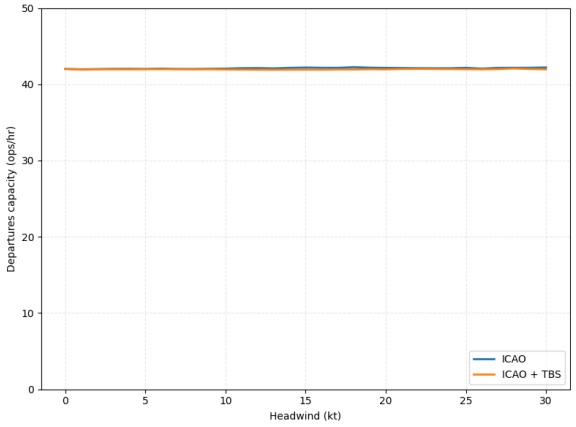

Figure 7.29: Departure capacity as a function of headwind speed. ICAO vs ICAO&TBS. LEPA 24R&24L

Figures 7.27–7.29 show the reduction in runway capacity with increasing headwind, with total throughput decreasing from 88 ops/h (46 ARR 42 DEP) to 79 ops/h (37 ARR 42 DEP). Under TBS, this capacity loss is greatly neutralised, maintaining a total capacity of 87 ops/h, with 45 arrivals and 42 departures. This improvement when using TBS can be seen in Figure 7.30, in which realistic capacity gains start to occur at 4 kts of headwind.

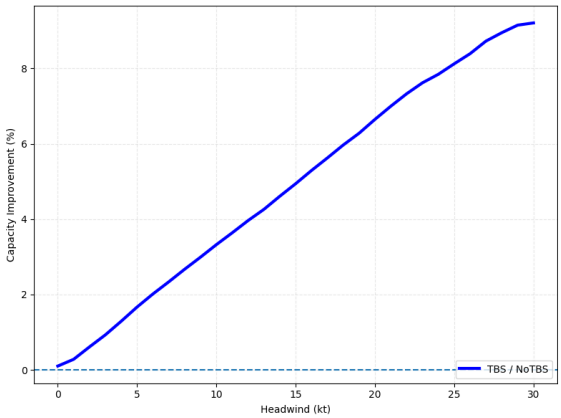

Figure 7.30: TBS capacity improvement as a function of headwind. LEPA 24R&24L

RECAT-EU-PWS Deployment

SAs shown below, capacity varies with the proportion of heavy aircraft in the traffic mix. In the first scenario, implementing RECAT-EU–PWS slightly reduces departure capacity relative to ICAO, driven by the increased variability in departure separations introduced by the finer separation scheme (20 categories rather than 3). This is also reflected in Figure 7.31, where the RECAT distribution exhibits a lower central tendency due to a longer lower tail, despite a similar upper tail to ICAO. The results are summarized in Table 7.4 below.

Table 7.4: Capacity metrics by traffic mix and separation scheme

	M Dominated			**Balanced**		
	Total	ARR	DEP	Total	ARR	DEP
ICAO	91	47	44	84	43	41
RECAT	90	47	43	88	46	42

"M" Dominated Mix

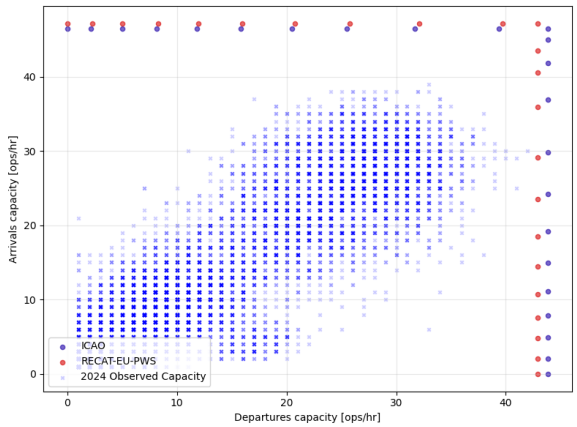

Figure 7.31: Capacity envelope (ICAO vs RECAT-EU-PWS). LEPA 24R&24L

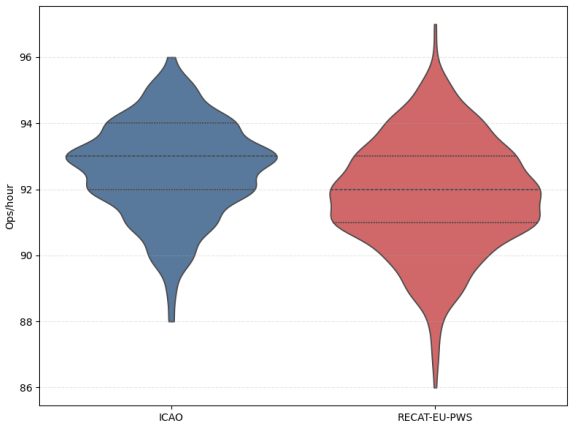

Figure 7.32: Peak capacity distribution (ICAO vs RECAT-EU-PWS). LEPA 24R&24L

"Balanced" Mix

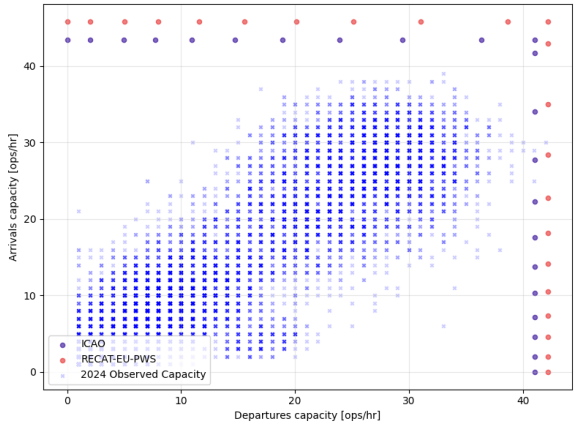

Figure 7.33: Capacity envelope (ICAO vs RECAT-EU-PWS). LEPA 24R&24L

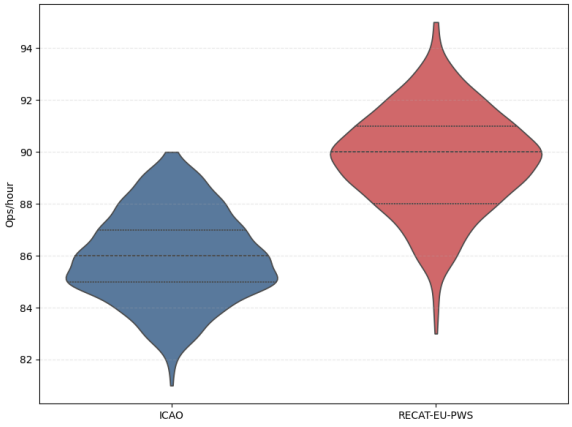

Figure 7.34: Peak capacity distribution (ICAO vs RECAT-EU-PWS). LEPA 24R&24L

The behavior exhibited by the previous capacity envelopes can be better explained through the following sensitivity analysis.

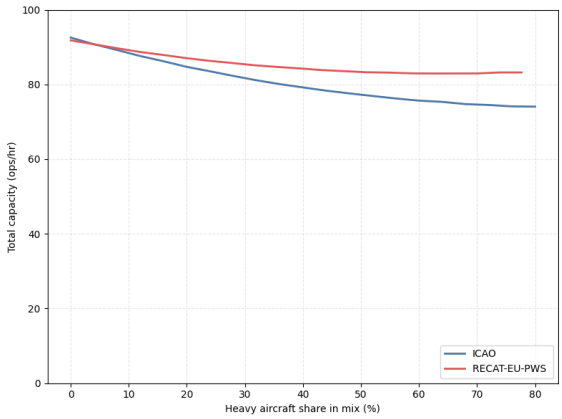

Figure 7.35: Total capacity as a function of proportion of heavy aircraft. ICAO vs RECAT-EU-PWS. LEPA 24R&24L

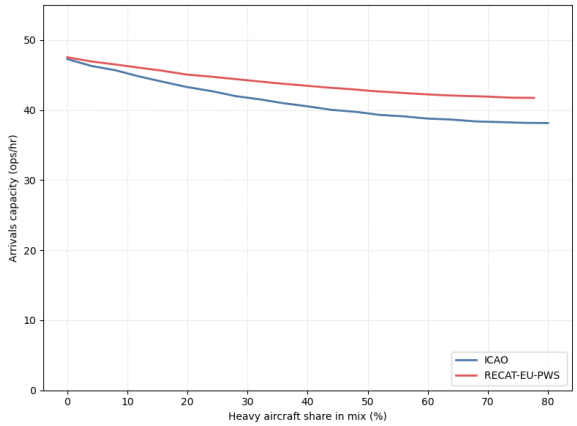

Figure 7.36: Arrival capacity as a function of proportion of heavy aircraft. ICAO vs RECAT-EU-PWS. LEPA 24R&24L

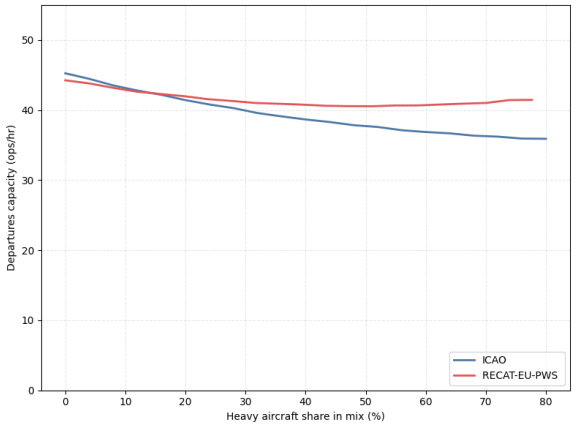

Figure 7.37: Departure capacity as a function of proportion of heavy aircraft. ICAO vs RECAT-EU-PWS. LEPA 24R&24L

From Figures 7.35–7.37 one can interpret that as the presence of heavy aircraft in the mix mostly B1 and B2 aircraft in RECAT-EU-PWS) increases, capacity logically decreases, and ARR-ARR and DEP-DEP separations become greater. When no Heavy aircraft are in the traffic sample, ICAO produces 93 ops/h (48 ARR 45 DEP), while RECAT-EU-PWS, 92 ops/h (48 ARR 44 DEP). As the percentage of heavy aircraft increases, both schemes see a decrease in total capacity, although ICAO´s is much more pronounced. Both schemes offer the same capacity at aroun 4-5% of H, and beyond, RECAT-EU-PWS outperforms ICAO until the endpoint, where, at 80% of heavy aircraft, ICAO outputs 74 operations, of which 38 are arrivals and 36 departures, while RECAT-EU-PWS gives 85, with 42 arrivals and 43 departures. The evolution in benefit of using RECAT-EU-PWS instead of ICAO can also be seen in Figure 7.38, where realistic capacity gains begin at around 11% of heavy aircraft in the fleet.

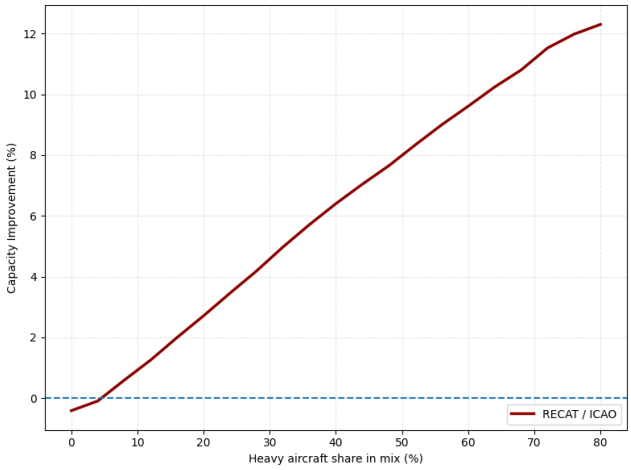

Figure 7.38: RECAT-EU-PWS capacity improvement as a function of heavy aircraft proportion. LEPA 24R&24L

7.3.3. Comparison with other models

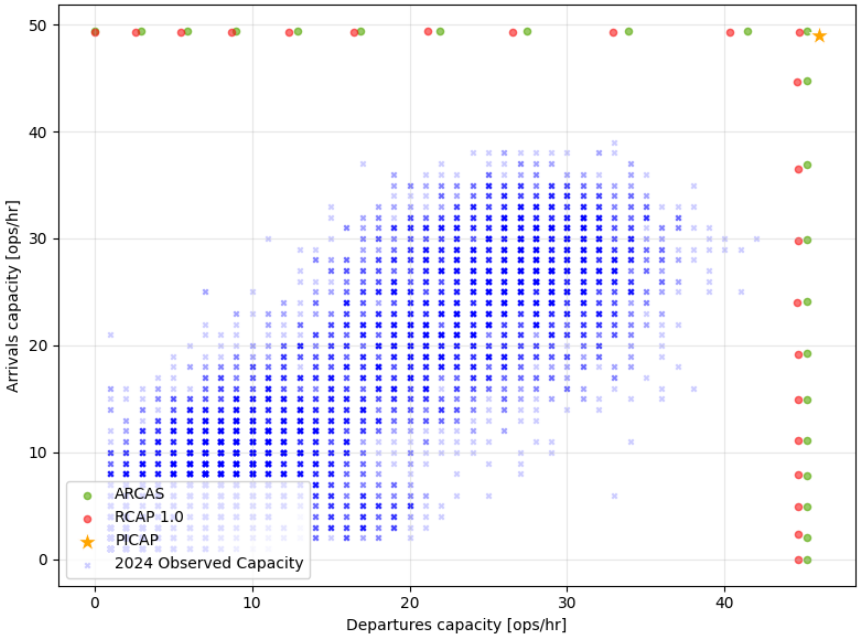

Figure 7.39: Validation of Capacity Envelope against RCAP 1.0 & PICAP. LEPA 24R&24L

The two modelled envelopes (ARCAS, in green, and RCAP 1.0, in red) are very close across the range, with identical arrivals performance, and ARCAS producing estimates slightly higher than RCAP 1.0

A single PICAP estimate is overlaid as an orange star at 46 departures/hr and 49 arrivals/hr, lying close to the modelled envelopes.Finally, the 2024 observed capacity (blue points) forms a dense cloud below the theoretical envelope, spanning up to 42 departures/hr and 38 arrivals/hr, with the highest-density region concentrated around mid values. The maximum observed combined throughput is approximately 70-75 ops/hr, indicating that while Palma de Mallorca operates closer to its capacity frontier than Alicante, typical observed operations still remain below the theoretical peak capacity limit.

Table 7.5: Comparison of ARCAS, RCAP 1.0 & PICAP capacities. Palma de Mallorca

	Combined	**Arrivals**	**Departures**
ARCAS	94.6	49.4	45.2
RCAP 1.0	94.0	49.3	44.7
% Change	-0.6	-0.2	-1.1
PICAP	95	49	46
% Change	0.4	1.2	1.8

Table 7.5 above shows highly consistent results across the three models, with peak-capacity variations of less than 1%.

7.4. Intersecting Runways

7.4.1. Assumptions

Before presenting the results, the assumptions taken to model this situation have to be explained. Depending on which, the result can see itself greatly influenced by each.

Runways 02 & 6R are modelled in intersecting A+D are modelled. It is assumed that a Specific Matrix method is used to model SID dependencies, and as such the departure velocities are irrelevant, and departure ROTs are not the limiting factor, which instead is this DBS SID matrix. These two, however, have been derived from the previous thesis written by Lamers [23]. The geometric values, such as D_A and D_{MAP} have been obtained from navigation charts specific to Barcelona runway 02 and 6R. More information, such as the SIDs used, the ICAO and RECAT-EU-PWS traffic mix and the SID DBS matrix can be found in section 6.2.

Table 7.6: Assumptions made modelling Barcelona

Parameter	Symbol	Value
Mode of Operation		Intersecting
Departure ROT	R_D	Calculated from *Lamers, 2016* [23]
Arrival ROT	R_A	ENAIRE Database
Departure Velocity	V_D	Calculated from *Lamers, 2016* [23]
Arrival Velocity	V_A	ENAIRE Database
SID Logic Used		Specific Matrix Method
SIDs Modelled		LEBL Rwy 06R
Common Approach Path	D_A	6.0 NM
Missed Approach Point	D_{MAP}	1.0 NM
Minimum Distance for DEP before ARR	D_{MIN}	2.0 NM
Intersection Arrival ROT	$R_{A,int}$	18s
Intersection Departure ROT	$R_{D,int}$	23s
Headwind TBS Scenario		25 kts
Headwind RECAT-EU-PWS Scenario		7 kts
Minimum Radar Separation		3 NM

7.4.2. Capacity Metrics

Arrivals TBS Deployment

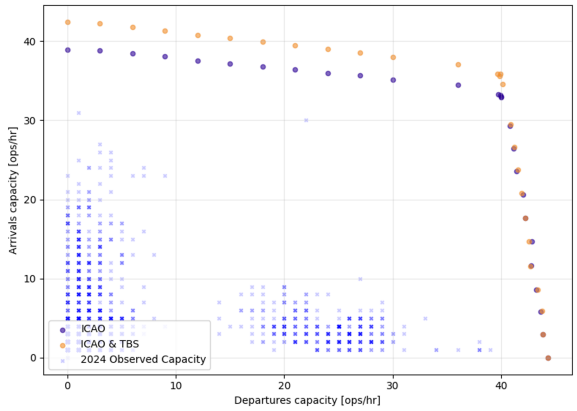

Figure 7.40: Capacity envelope (ICAO vs ICAO&TBS). LEBL 02 & 06R

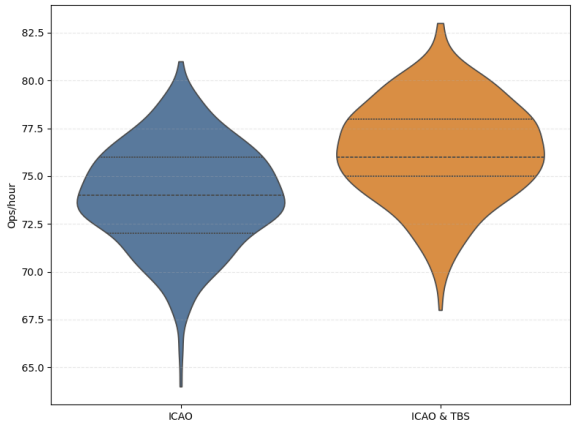

Figure 7.41: Peak capacity distribution (ICAO vs ICAO&TBS). LEBL 02 & 06R

Figure 7.40 shows the capacity envelope for Barcelona´s 02 & 06R runways. For 25 kts of headwind, it can be observed that the scenario´s peak capacity is 73 ops/h (33 arrivals, 40 departures) without TBS. When TBS is applied, this value climbs to 76 ops/h , adding three more arrivals. In arrivals only regime, the runway system can

accomodate 39 arrivals without TBS or 42 with it. The maximum number of departures remains constant for both modes, with 44 maximum operations. The trapezium-like shape suggests that, unlike in section 6.2, arrival and departure processes are coupled by the intersection constraint: their interaction is governed by the time-blocking windows defined by $R_{A,int}$, $R_{D,int}$, and D_{MIN}.

In Figure 7.41, the spreads appear to be broadly similar, but the TBS case concentrates more density at higher values and shows fewer low-capacity outcomes (a shorter tail and higher central tendency).

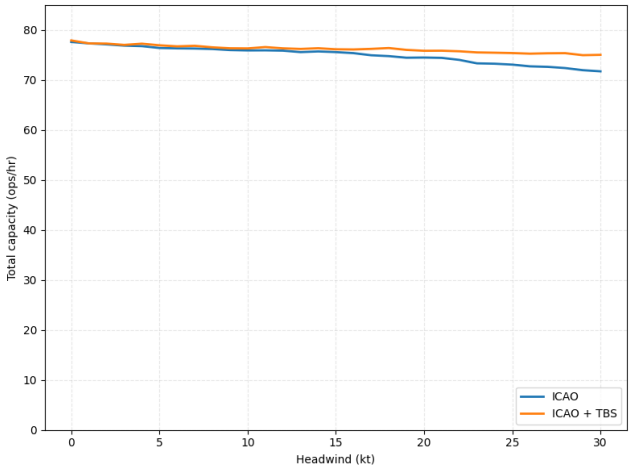

Figure 7.42: Total capacity as a function of headwind speed. ICAO vs ICAO&TBS. LEBL 02&06R

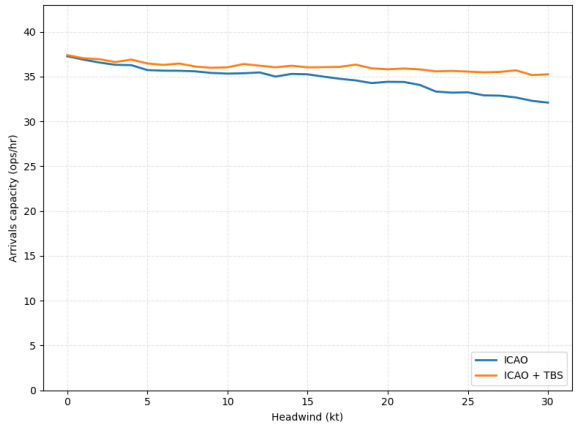

Figure 7.43: Arrival capacity as a function of headwind speed. ICAO vs ICAO&TBS. LEBL 02&06R

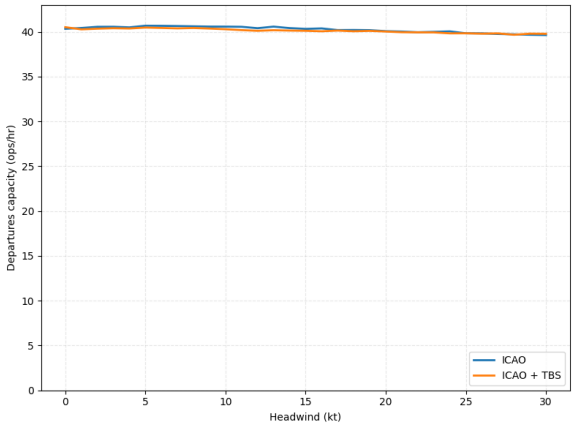

Figure 7.44: Departure capacity as a function of headwind speed. ICAO vs ICAO&TBS. LEBL 02&06R

Figures 7.42–7.44 show that as headwind increases the overall capacity reduces from 77 hourly movements (37 arrivals and 40 departures) to 72, of which 32 are arrivals. Under TBS, this capacity loss is greatly neutralised, maintaining a total capacity of 75 ops/h, with 35 arrivals and 40 departures. It can be concluded that arrivals are unaffected by TBS, not even indirectly through changes in forbidden windows. This improvement when using TBS can be seen in Figure 7.45, in which the benefit varies from 0% up to 4%, and realistic capacity gains appear at a headwind speed of around 15 kts.

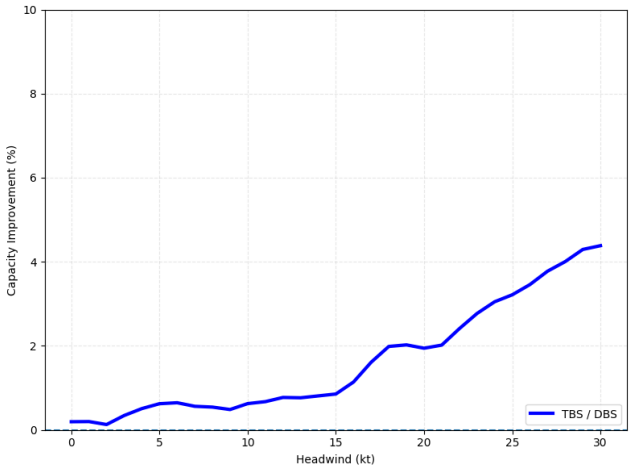

Figure 7.45: TBS capacity improvement as a function of headwind. LEBL 02&06R

RECAT-EU-PWS Deployment

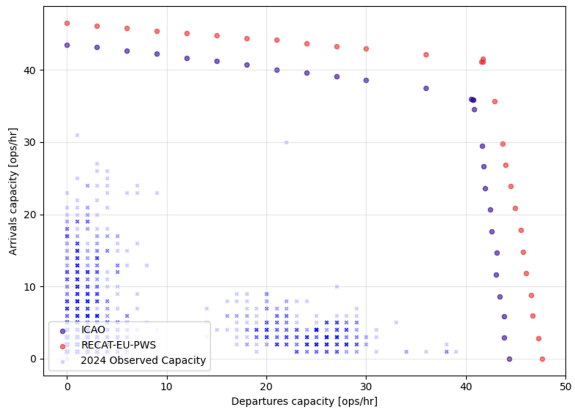

Figure 7.46: Capacity envelope (ICAO vs RECAT-EU-PWS). LEBL 02 & 06R

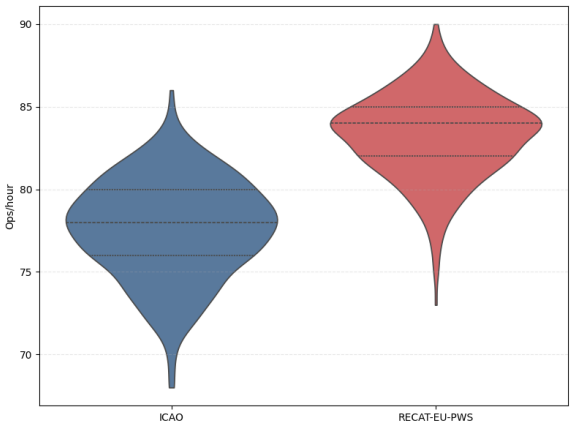

Figure 7.47: Peak capacity distribution (ICAO vs RECAT-EU-PWS). LEBL 02 & 06R

Changing to the RECAT-EU–PWS wake categorisation scheme increases peak hourly capacity from 77 ops/h (36 arrivals, 41 departures) under ICAO to 83 ops/h (41 arrivals, 42 departures). In addition, RECAT-EU–PWS expands the envelope and makes its boundary more gradual, indicating weaker coupling between arrivals and departures. This is consistent with the smaller envelope angle under RECAT-EU–PWS (≈105°) compared to ICAO (≈115°): as the angle approaches 90°, the trade-off becomes less steep and the two flows behave more independently.

The ICAO distribution is centred lower, with most outcomes clustered in the high-70s to 80 ops/h and a longer lower tail indicating more frequent reduced peak-capacity cases. In contrast, RECAT-EU-PWS is shifted upward and concentrated around 83–85 ops/h.

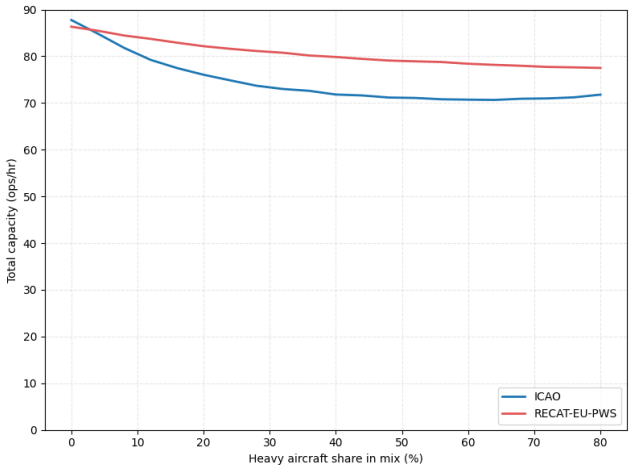

Figure 7.48: Total capacity as a function of proportion of heavy aircraft. ICAO vs RECAT-EU-PWS. LEBL 02&06R

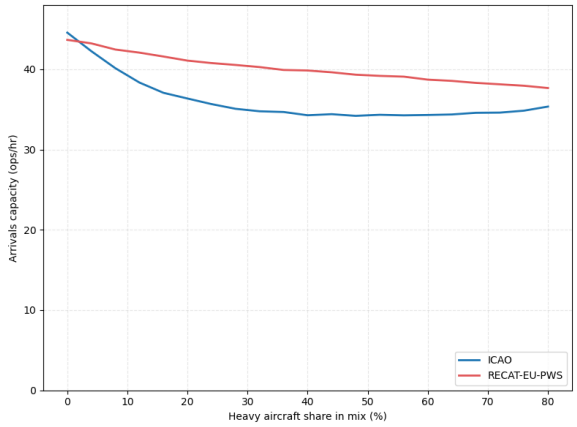

Figure 7.49: Arrival capacity as a function of proportion of heavy aircraft. ICAO vs RECAT-EU-PWS. LEBL 02&06R

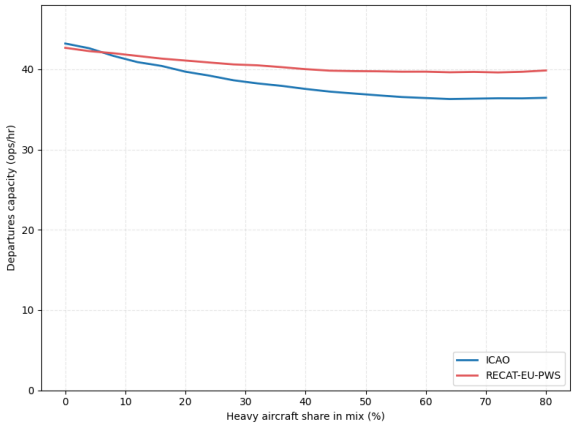

Figure 7.50: Departure capacity as a function of proportion of heavy aircraft. ICAO vs RECAT-EU-PWS. LEBL 02&06R

Looking at figures 7.48–7.50, it can be observed that as the presence of heavy aircraft in the traffic share increases, the total capacity for ICAO decreases steeply from 88 ops/h at first, then flattens into a long, shallow decline, reaching a clear minimum of 71 ops/h, and finally shows a slight uptick toward the end reaching 72 ops/h.

In the RECAT-EU-PWS scenario, capacity declines more gradually with a smooth slope that steadily flattens from 86 to 78 ops/h. Until a 4% share of heavy aircraft in the mix, ICAO outperforms RECAT-EU-PWS in capacity.

The variation in RECAT-EU–PWS capacity improvement is shown in Figure 7.51. The maximum gain occurs in the 45%–65% heavy-aircraft range, followed by a dip at higher shares. This decline does not indicate worse performance; it it shows a smaller improvement in the ICAO baseline as the proportion of heavy aircraft becomes very high. Beyond roughly 60% heavy traffic, the mix contains fewer $H \rightarrow M$ pairs and more $H \rightarrow H$ pairs, reducing the prevalence of 5 NM in-trail separations in favour of 4 NM separations under ICAO. The plot also shows that RECAT-EU-PWS implementation becomes viable in a scenario where the mix of heavy aircraft is 5% or higher.

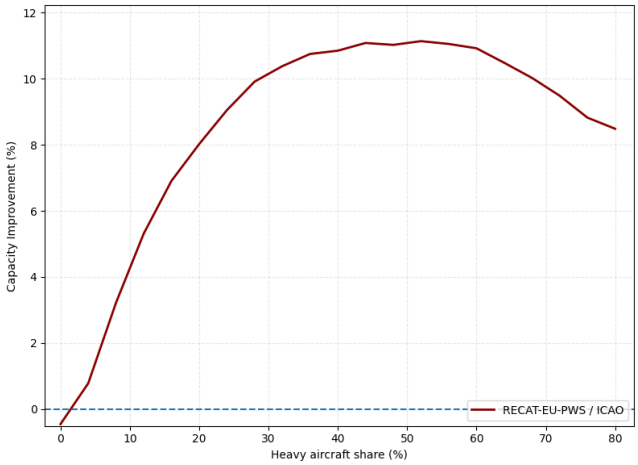

Figure 7.51: RECAT-EU-PWS capacity improvement as a function of heavy aircraft proportion. LEBL 02&06R

7.4.3. Comparison with other models

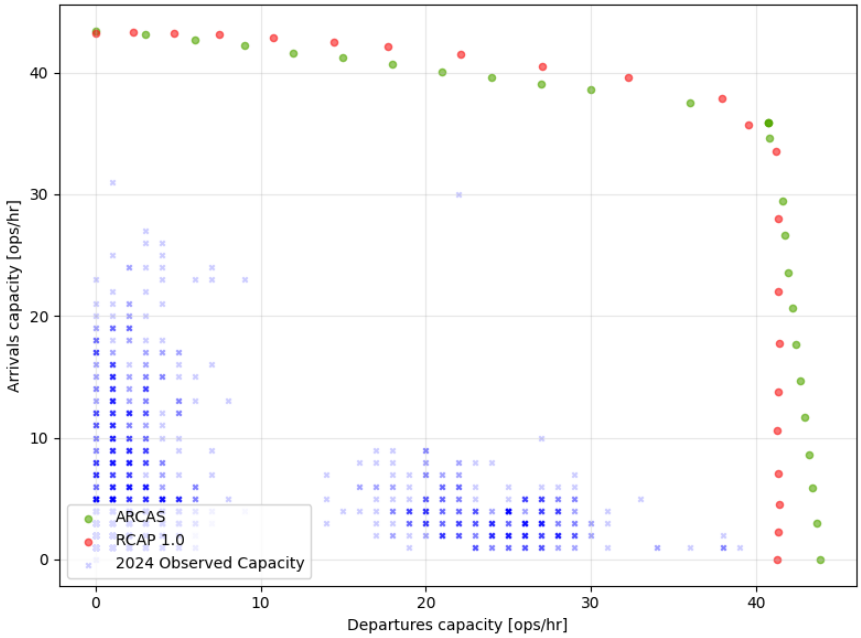

Figure 7.52: Validation of capacity envelope against RCAP 1.0 . LEBL 02&06R

The two modelled envelopes (ARCAS, in green, and RCAP 1.0, in red) output similar values across the range, with RCAP 1.0 generally predicting slightly higher arrival capacity and lower departures than ARCAS. There is a clear convergence in the arrivals-only point and also towards the peak capacity. However, as the arrivals only point is approximates, ARCAS generates increasingly different values from RCAP 1.0 .

No PICAP estimate is provided in this scenario as there isnt one available. Finally, the 2024 observed capacity (blue points) form two clouds, one in the 0-28 arrivals capacity and 0-9 departures, whilst the other in the 15-39 departures and 1-10 range. Only a few observations lie outside of these clouds, with a consistent 30 arrivals and 22 departures. These observed values might be surprising at first, as it suggests these runways operate in departures or arrivals heavy mode.

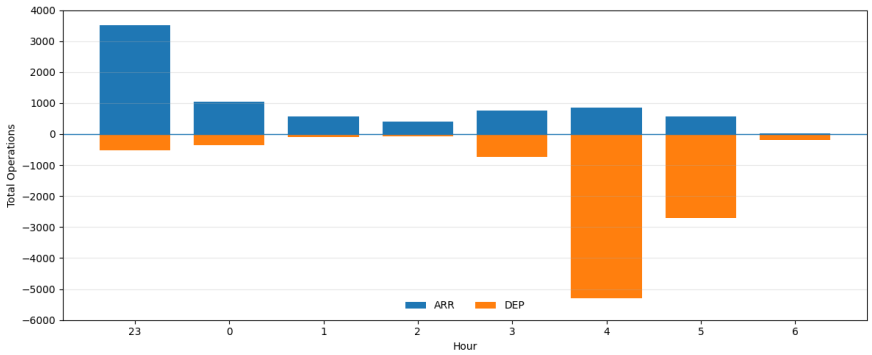

Figure 7.53: 02 & 06R operating hours arrival and departures distribution. Barcelona

In fact, Figure 7.53 validates the point made earlier on, and suggests that although runways 02 and 06R are designed to operate in an intersecting configuration, the vast majority of movements occur in strongly departure-biased or arrival-biased configurations. This can largely be explained by the operating window of this runway system, which is primarily at night, from 23:00 to 07:00. Within this period, distinct traffic "banks" can be identified: the last arrivals of the day into Barcelona, followed by a small number of overnight freighter arrivals, then early-morning transoceanic arrivals around 03:00–05:00, and finally the first departures of the day, including a pronounced departure peak around 04:00 as freighters depart.

Table 7.7: Comparison of ARCAS and RCAP 1.0 capacities. Barcelona

	Peak / ARR / DEP	**Arrivals Only**	**Departures Only**
ARCAS	76.6 / 35.9 / 40.7	43.4	43.9
RCAP 1.0	75.3 / 35.7 / 39.6	43.2	41.2
% Change	-1.7 / -0.55 / -2.7	-0.46	-6.15

Table 7.7 shows that RCAP 1.0 and ARCAS converge to very similar peak capacities, differing by less than 2%. The arrivals-only capacities are also closely aligned, with differences below 0.5%. The largest discrepancy appears in the departures-only capacity, with differences of up to 3 operations per hour. This may be attributed to differences in how the two models account for the effect of SIDs, as well as to the finer tuning of ARCAS in the Specific Matrix method.

7.5. Converging Diverging Runways

7.5.1. Assumptions

At Madrid–Barajas Airport, runways 32R and 36L can be classified as a converging–diverging runway pair. Although this section primarily focuses on the validation of converging runway operations using runways 32R and 36R, the ”bigger picture” of Madrid´s Capacity envelope, including all four runways operating, will be shown towards the end of the section. This inclusion allows the analysis to capture the overall capacity performance of the entire Madrid runway system.

Table 7.8: Assumptions made modelling Madrid Barajas

Parameter	Symbol	32R&36L	32L&36R
Mode of Operation		Open V A+D	Segregated de-coupled
Departure ROT	R_D	Calculated from *Lamers, 2016* [23]	
Arrival ROT	R_A	ENAIRE database	
Departure Velocity	V_D	Calculated from *Lamers, 2016* [23]	
Arrival Velocity	V_A	ENAIRE database	
SID Logic Used		Specific Matrix Method	
SIDs Modelled		LEMD 36L	LEMD 36R
Common Approach Path	D_A	4.94 NM	4.75 NM
Missed Approach Point	D_{MAP}	1.17 NM	1.15 NM
Minimum Distance for DEP before ARR	D_{MIN}	1.0 NM	-
Secured Touchdown ROT	$R_{A,com}$	$R_A/3$	-
Headwind TBS Scenario		25 kts	
Headwind RECAT-EU-PWS Scenario		7 kts	
Minimum Radar Separation		3 NM	

7.5.2. Capacity Metrics

Arrivals TBS Deployment

Figure 7.54 shows the capacity envelope for Madrid´s 36L & 32R runways. For 25 kts of headwind, it can be observed that the scenario´s peak capacity is 71 ops/h (35 arrivals, 36 departures) without TBS. The use of TBS can increase throughput by an arrival and a departure, up to 73. The arrivals only capacity varies from 36 to 38, while the departures only capacity is 40 for both cases. This slight tradeoff in departures and arrivals observed in the graph suggests that, unlike in section 6.2, arrivals and departures are coupled to some extent by the missed approach constraint: their interaction is governed by the time-blocking windows defined by $R_{A,com}$ and D_{MIN}.

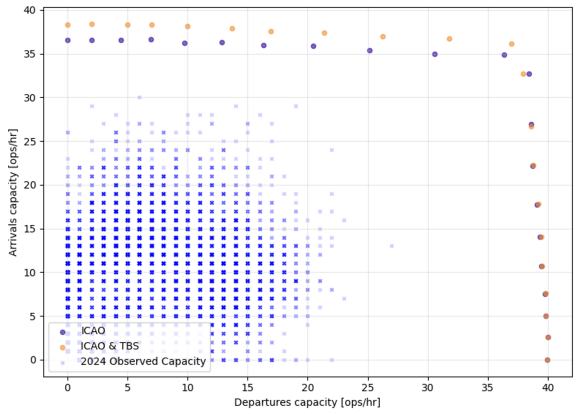

Figure 7.54: Capacity envelope (ICAO vs ICAO&TBS). LEMD 32R & 36L

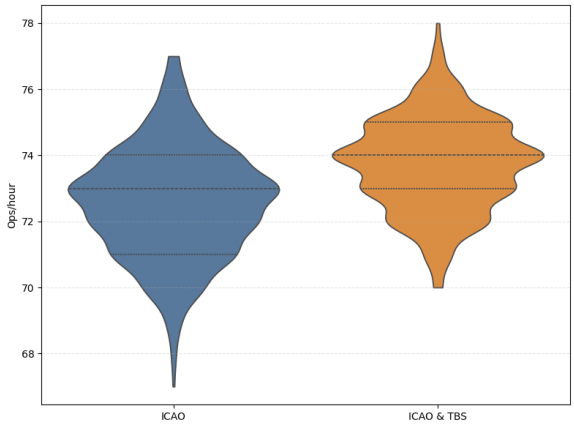

Figure 7.55: Peak capacity distribution (ICAO vs ICAO&TBS). LEMD 32R&36L

In Figure 7.55, ICAO & TBS violin plot shows not only a higher central behavior, with higher median and

quartiles, but also shows a smaller spread than ICAO, which has a longer lower tail, caused by a poor performing sequencing combination in the montecarlo runs.

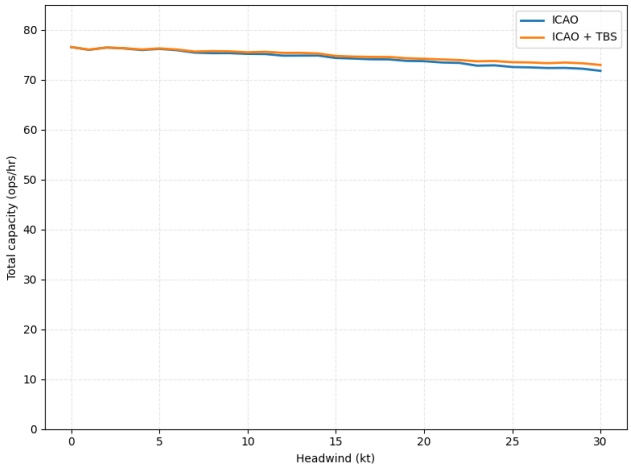

Figure 7.56: Total capacity as a function of headwind speed. ICAO vs ICAO&TBS. LEMD 32R&36L

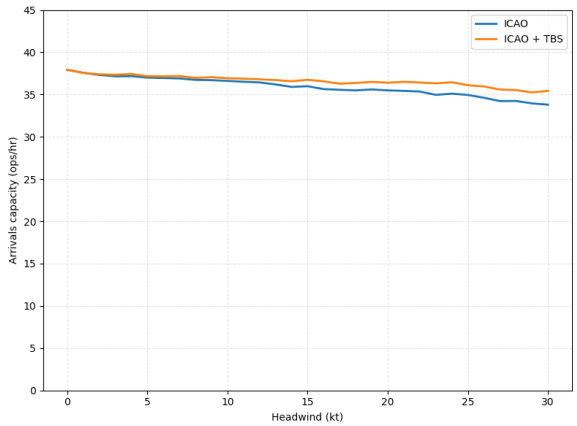

Figure 7.57: Arrival capacity as a function of headwind speed. ICAO vs ICAO&TBS. LEMD 32R&36L

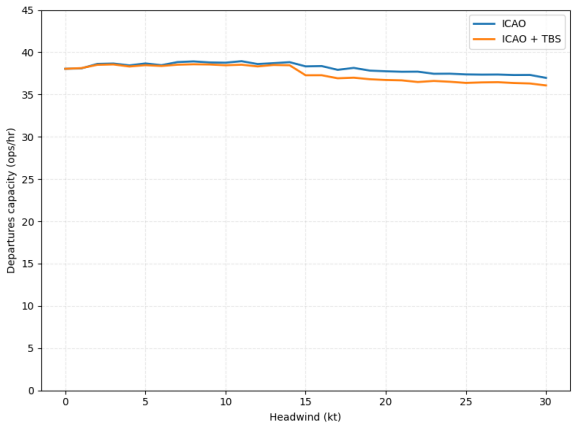

Figure 7.58: Departure capacity as a function of headwind speed. ICAO vs ICAO&TBS. LEMD 32R&36L

Figures 7.56–7.58 show that as headwind increases, the overall capacity reduces from 76 hourly movements (38 arrivals and departures) to 72, of which 34 are arrivals. Under TBS, this capacity loss is slightly mitigated, maintaining a total capacity of 73 ops/h, with 36 arrivals and 37 departures.

TBS does not directly reduce departure capacity. Instead it modifies arrival separations and indirectly reshapes the time windows in which departures cannot be accommodated. Consequently, the lower number of departures observed under strong headwinds with TBS indicates that, in those conditions, the optimizer finds it ”cheaper” to schedule an additional arrival than to insert a departure. The improvement when using TBS can be seen in Figure 7.59, in which the benefit varies from 0% up to 1.5%. Only at headwinds equal or greater than 25 kts would TBS make an operational difference in realistic conditions.

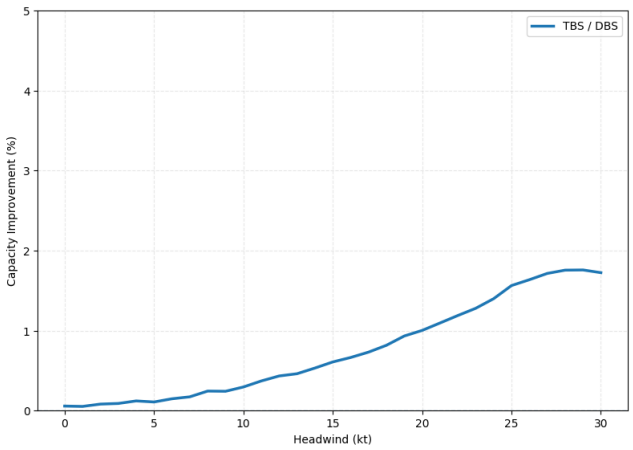

Figure 7.59: TBS capacity improvement as a function of headwind. LEMD 32R&36L

RECAT-EU-PWS Deployment

Changing to the RECAT-EU–PWS wake categorisation scheme increases peak hourly capacity from 75 ops/h (37 arrivals, 38 departures) under ICAO to 77 ops/h (38 arrivals, 39 departures).

The ICAO distribution is centred lower, with most outcomes clustered in the 74-77 range. In contrast, RECAT-EU-PWS is shifted upward and concentrated around 76-79 ops/h. Both distributions share the same minimum operations per hour. However, the RECAT-EU-PWS distribution is shifted toward higher values than ICAO, with more probability mass concentrated above the ICAO central range.

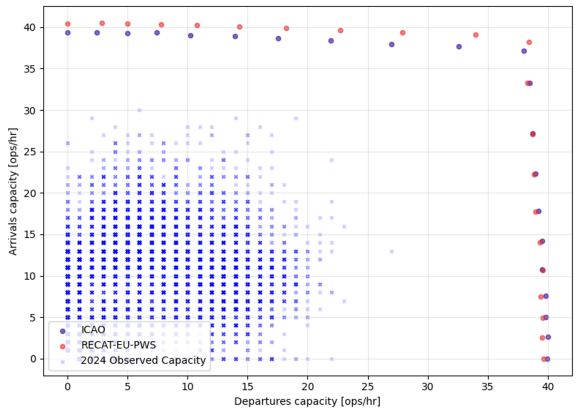

Figure 7.60: Capacity envelope (ICAO vs RECAT-EU-PWS). LEMD 32R & 36L

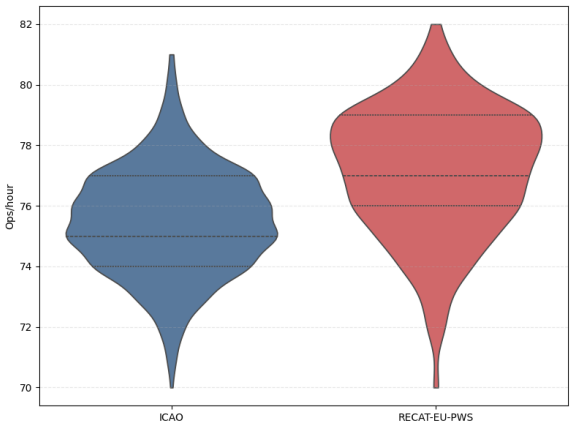

Figure 7.61: Peak capacity distribution (ICAO vs RECAT-EU-PWS). LEMD 32R & 36L

From Figures 7.62–7.64 one can interpret that as the presence of heavy aircraft in the mix increases, capacity decreases. When no Heavy aircraft are in the traffic sample, ICAO produces 83 ops/h (40 ARR 43 DEP), while RECAT-EU-PWS, 83 ops/h (41 ARR 42 DEP). As the percentage of heavy aircraft increases, both schemes see a decrease in total capacity, although ICAO´s is much more pronounced. At 80% of heavy aircraft, ICAO outputs 68 operations, of which 36 are arrivals and 32 departures, while pairwise RECAT gives 75, with 32 arrivals and 43 departures. Notice how for arrivals capacity at around 56% ICAO performs better than RECAT. This variation of performance in arrivals and departure responds to the ”greedy” performande of the rollout optimiser, which selects the operations based on a lookahead horizon selecting the ones which give the higher density. The evolution in benefit of using this scheme instead of ICAO can also be seen in Figure 7.65, and follows a very similar trend to the evolution presented insection 7.4. It shows that RECAT-EU-PWS provides a realistic increase in capacity when heavy aircraft suppose a 5% in the traffic mix or more.

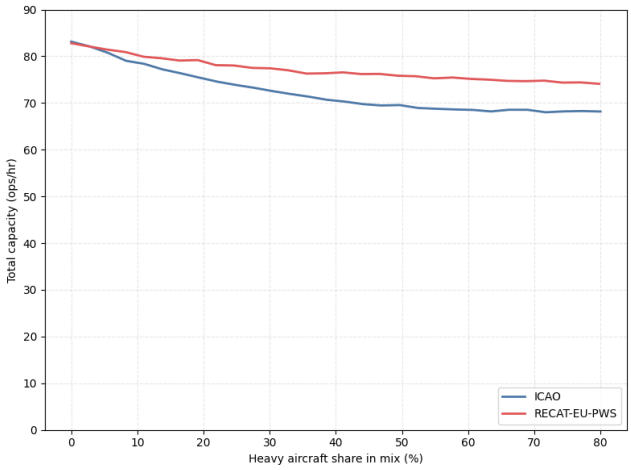

Figure 7.62: Total capacity as a function of proportion of heavy aircraft. ICAO vs RECAT-EU-PWS. LEMD 32R&36L

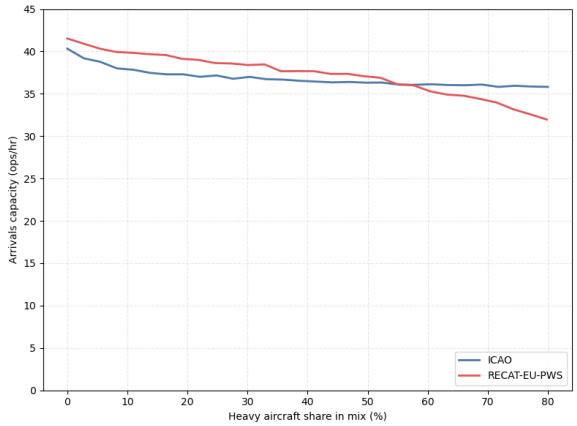

Figure 7.63: Arrival capacity as a function of proportion of heavy aircraft. ICAO vs RECAT-EU-PWS. LEMD 32R&36L

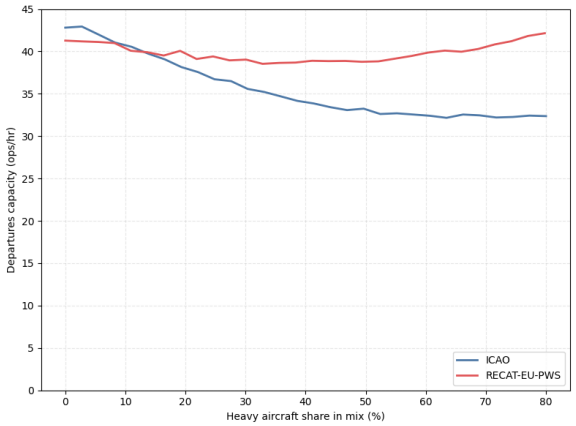

Figure 7.64: Departure capacity as a function of proportion of heavy aircraft. ICAO vs RECAT-EU-PWS. LEMD 32R&36L

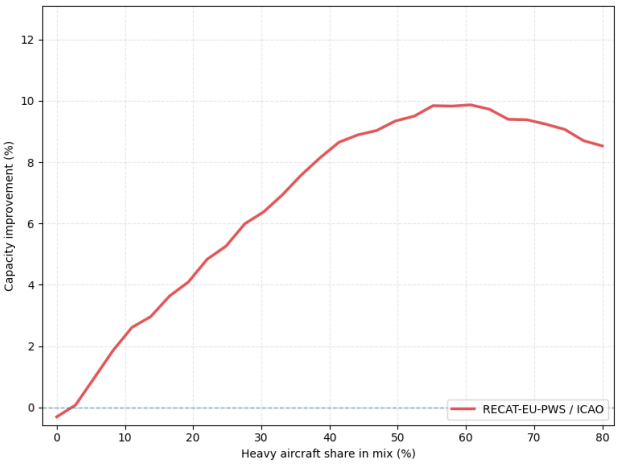

Figure 7.65: RECAT-EU-PWS capacity improvement as a function of heavy aircraft proportion. LEMD 32R&36L

Complete Runway System Envelopes

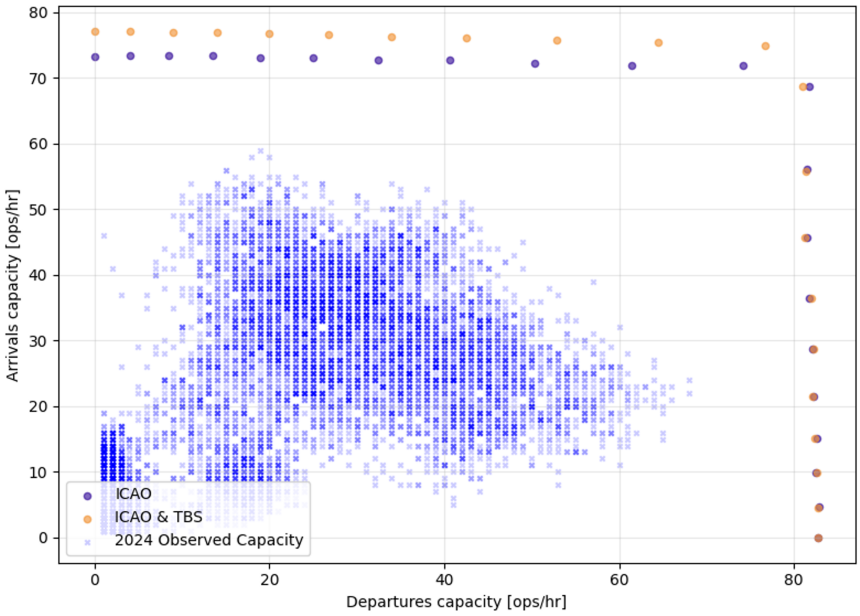

Figure 7.66: Capacity envelope (ICAO vs ICAO & TBS). LEMD all runways

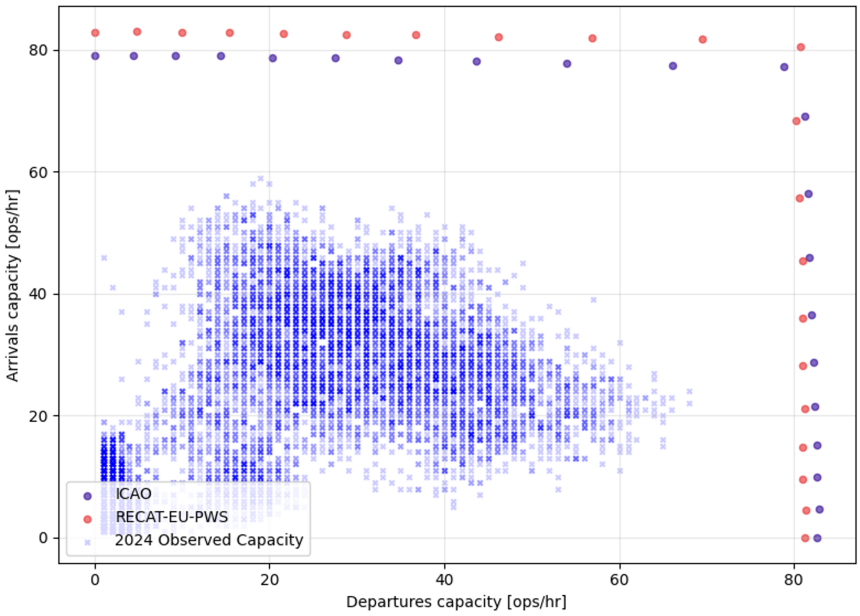

Figure 7.67: Capacity envelope (ICAO vs RECAT-EU-PWS). LEMD all runways

When combined with Madrid´s other runways (36R and 32L), the above envelopes are formed. Figure 7.66 shows that under 25 kts of headwind the total capacity can be increased from 146 (72 ARR 74 DEP) to 151 (75 ARR 77 DEP) ops/h.

The implementation of RECAT-EU-PWS could increase throughput from 155 (77 arrivals, 78 departures) to 161, with 80 arrivals and 81 departures.

7.5.3. Comparison with other models

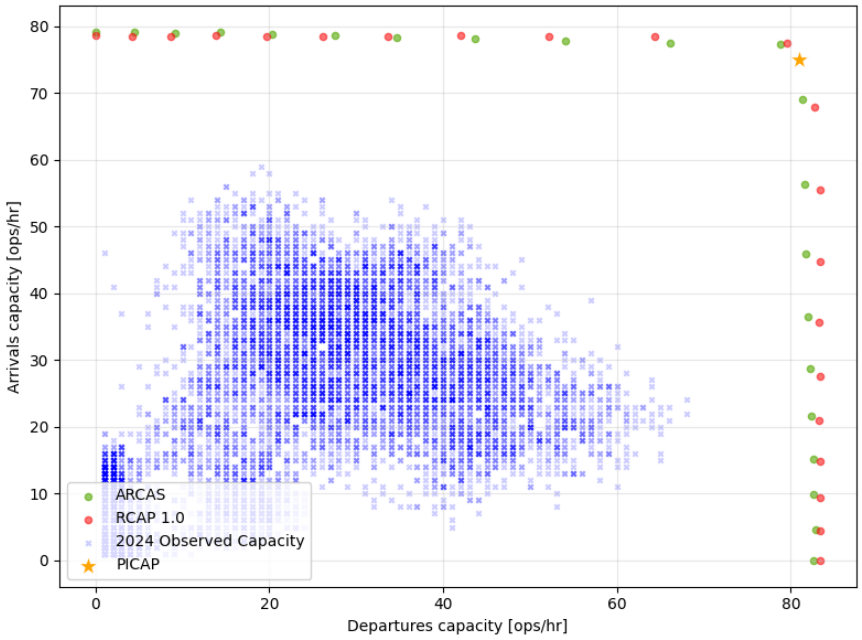

Figure 7.68: Validation of Capacity Envelope against RCAP 1.0 & PICAP. Madrid

The two modelled envelopes ARCAS and RCAP 1.0 are very close across the range, with RCAP 1.0 generally predicting slightly higher capacity than ARCAS, although at the arrivals-only and departures-only points both models converge to very similar values.

A single PICAP estimate is overlaid as an orange star at 81 departures/hr and 75 arrivals/hr, lying close to the modelled envelopes. Finally, the 2024 observed capacity (blue points) form a dense cloud concentrated well below the envelope in the 0–70 departures/hr and 0–60 arrivals/hr range, with a maximum combined capacity reaching around 100 ops/hr, quite below the theoretical peak capacity limit.

Table 7.9: Comparison of ARCAS, RCAP 1.0 & PICAP capacities. Madrid

	Peak / ARR / DEP	Arrivals Only	Departures Only
ARCAS	156.0 / 77.2 / 78.8	79.0	82.6
RCAP 1.0	157.0 / 77.5 / 79.5	78.5	83.3
% Change	0.64 / 0.39 / 0.88	0.63	0.85
PICAP	156 / 75 / 81	-	-
% Change	0 / -2.85 / 2.79	-	-

Table 7.9 above shows highly consistent results across the three models, with peak-capacity variations of less than 1%.

7.6. Scenario Deployment

Now that all four scenarios have been tested, producing capacity envelopes, violins plots, and metrics to analyze the effectiveness of TBS and RECAT-EU-PWS across different parameters.

In this section, a quick comparison of threshold values at which in each runway configuration does the implementation of TBS and RECAT-EU-PWS make sense from the operational perspective (ability to increase by at least one slot the peak hourly capacity of the selected runway configuration)

7.6.1. TBS Deployment

The previous four sections have shown that the effectiveness of TBS in increasing peak capacity under adverse wind conditions depends primarily on two factors: (i) the headwind profile at each airport, including its speed, direction, and frequency of occurrence, and (ii) the runway geometry in use.

This leads to an important practical question: *at what headwind level does TBS begin to generate significant capacity gains at a given airport?* To address this, Figure 7.69 summarizes the results of the sensitivity analyses carried out for each runway layout, showing how variations in headwind affect the efficiency of TBS. The detailed results for each case were presented in the previous subsections.

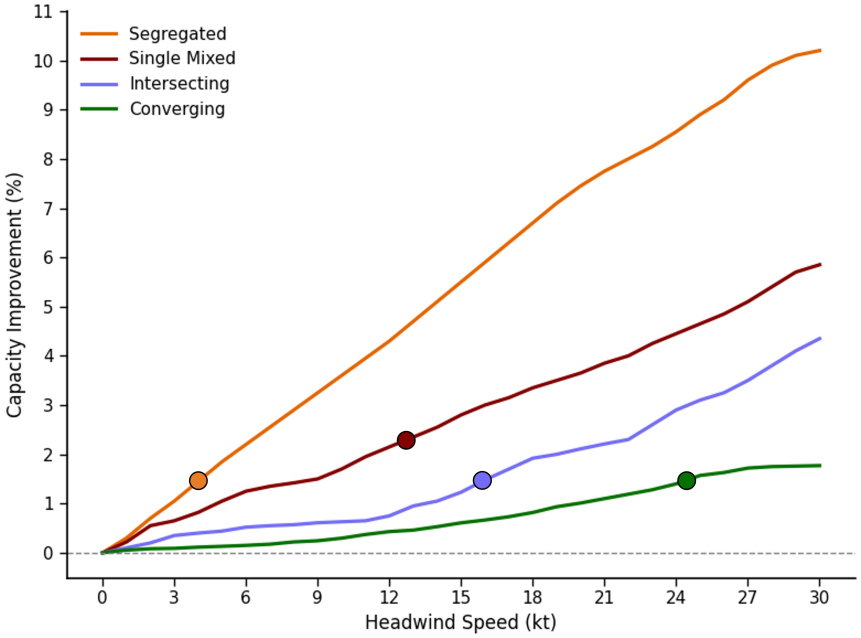

Figure 7.69: TBS capacity improvement as a function of headwind speed for each runway layout

Figure 7.69 highlights the different behaviour of TBS across the runway layouts considered. The circles on each curve indicate the headwind threshold beyond which TBS begins to produce meaningful capacity gains. These threshold values are approximately 4 kt for segregated runways, 12 kt for single mixed-mode operations, 15 kt for intersecting runways, and 25 kt for the converging runway scenario.

These results indicate that TBS is only operationally justified when headwind speeds exceed the corresponding threshold values. The next step, therefore, is to compare, for each of the four scenarios, the frequency with which these headwind conditions occur under the selected runway configurations. For this purpose, METAR data were obtained from the AENA Master Plans for Madrid, Barcelona, Palma de Mallorca, and Alicante airports.

First, a medium-level analysis is performed to find out the occurences at which the headwind at each scenario occurs, during the busy season (May to October) over the last ten years.

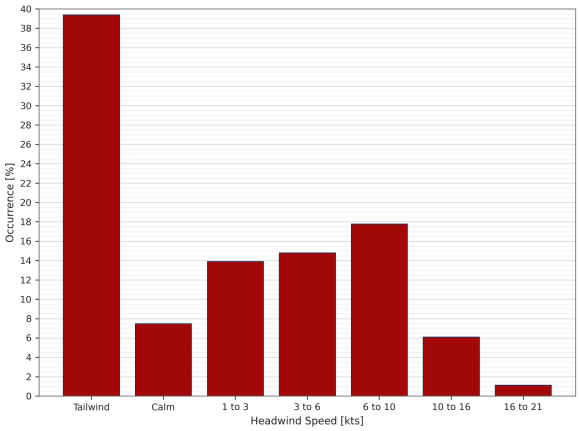

Figure 7.70: Headwind distribution for Alicante, runway 10 (10-year historical series)

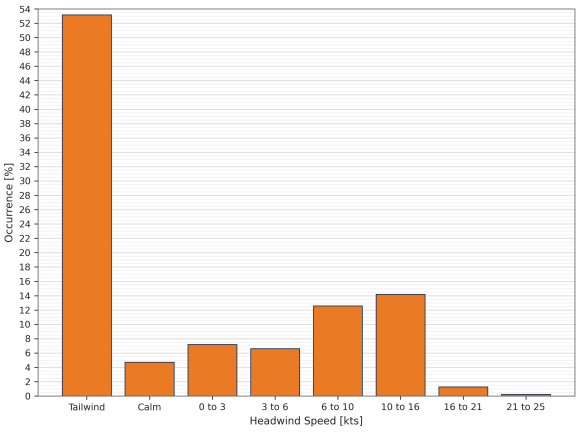

Figure 7.71: Headwind distribution for Palma, runways 24R and 24L (10-year historical series)

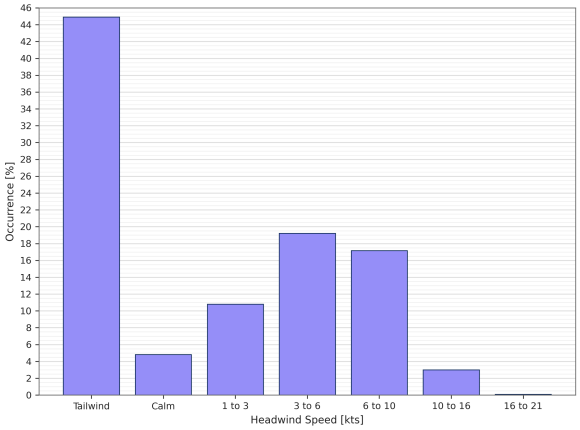

Figure 7.72: Headwind distribution for Barcelona, runway 02 (10-year historical series)

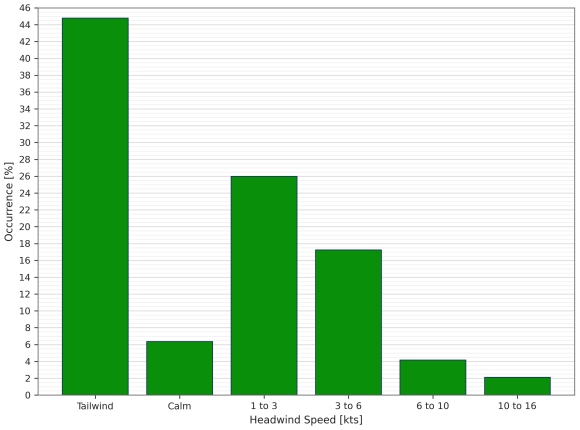

Figure 7.73: Headwind distribution for Madrid, runways 32L and 32R (10-year historical series)

For Alicante, shown in Figure 7.70, the relevant threshold corresponds to the single mixed-mode case, which requires a headwind of at least 12 kt. The proportion of observations meeting or exceeding this threshold is approximately 7.1%.

For Palma de Mallorca, which represents the segregated runway scenario, the threshold is 4 kt. As shown in Figure 7.71, headwinds at or above this value occur in approximately 34.1% of observations.

For Barcelona's intersecting runway configuration, the threshold is 15 kt. According to Figure 7.72, headwinds of this magnitude or higher occur in approximately less than 1% of observations.

For Madrid's converging runway configuration, the threshold is 25 kt. As shown in Figure 7.73, the proportion of observations at or above this value is also below 1%.

Based on these results, the implementation of TBS appears to be technically viable at Palma de Mallorca, unlikely to be viable at Madrid and in Barcelona's intersecting configuration, and potentially worthy of further evaluation at Alicante. According to capacity and traffic forecasts, Alicante is expected to exceed its sustainable capacity within the next two years, while Palma de Mallorca is expected to do so within the next five years. By contrast, Madrid and Barcelona's intersecting configuration remain well below both their peak and sustainable capacity limits.

The conclusions of the medium-level analysis suggest that TBS deployment could be technically viable at Palma de Mallorca and warrants further evaluation at Alicante. By contrast, Barcelona's runways 02 and 06R, together with Madrid's runways 32R and 36L, appear to be highly unviable candidates.

Accordingly, a high-level analysis was carried out for Palma de Mallorca and Alicante. For both airports, peak hours over the last five years were matched directly with wind data, resulting in more than 200 headwind samples in each case. This approach ensures that the analysis only considers periods in which the highest runway throughputs were actually recorded.

The results are presented below:

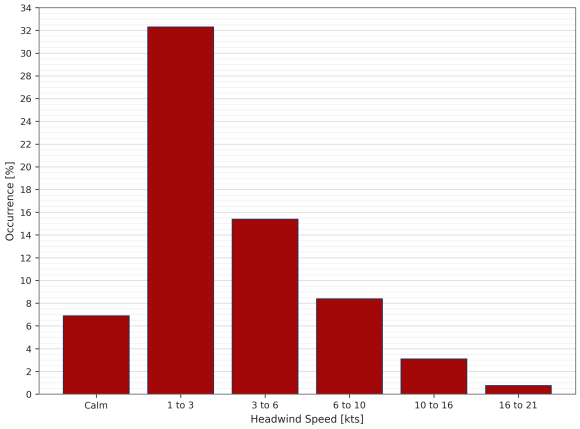

Figure 7.74: Headwind distribution at peak hours for Alicante, runway 10 (10-year historical series)

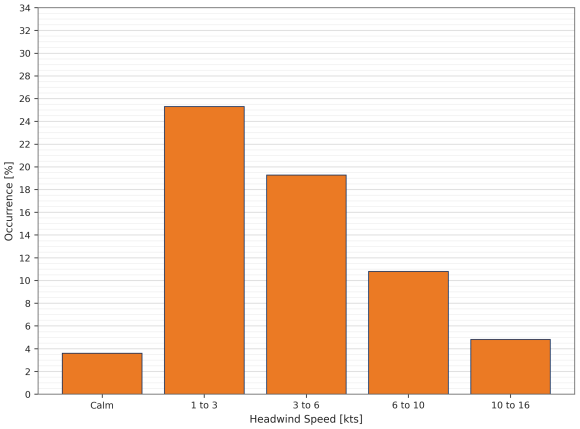

Figure 7.75: Headwind distribution at peak hours for Palma, runways 24R and 24L (10-year historical series)

At this higher level of analysis, it can be observed that in Alicante the headwind exceeds the threshold in only 3.1% of peak-hour cases, which suggests that TBS implementation is not viable.

By contrast, the situation in Palma de Mallorca is different. There, headwind exceeds the required threshold in 33.7% of peak-hour cases, which suggests that TBS implementation could become viable once the runway system approaches saturation in the coming years.

7.6.2. RECAT-EU-PWS

The previous sections also demonstrate that the effectiveness of RECAT-EU-PWS in increasing peak capacity depends primarily on two factors: (i) the traffic mix composition at each airport, particularly the proportion, and (ii) the runway geometry in use.

This leads to an important practical question: *under what traffic mix conditions does RECAT-EU-PWS begin to generate significant capacity gains at a given airport?* To address this, Figure 7.76 summarizes the results of the sensitivity analyses carried out for each runway layout, showing how variations in traffic mix composition affect the efficiency of RECAT-EU-PWS. The detailed results for each case were presented in the previous subsections.

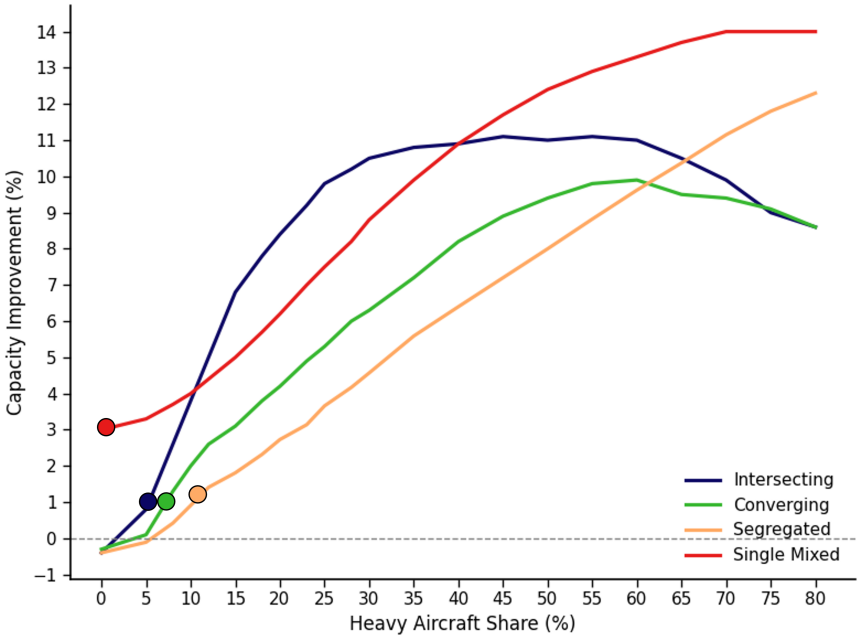

Figure 7.76: RECAT-EU-PWS capacity improvement as a function of traffic mix composition for each runway layout

Figure 7.76 highlights the different behaviour of RECAT-EU-PWS across the runway layouts considered. The circles on each curve indicate the traffic mix threshold beyond which RECAT-EU-PWS begins to produce meaningful capacity gains. These threshold values vary depending on the runway layout and reflect the minimum proportion of favourable traffic mix conditions required for the procedure to deliver operational benefits.

For Alicante, the relevant threshold corresponds to the single mixed-mode case, which delivers capacity gains straight away, without the presence of heavy aircraft.

For Palma de Mallorca, which represents the segregated runway scenario, the threshold is 11 to 12% of heavy aircraft in the fleet mix. However, Palma´s average fleet mix during peak hours is at 2%, which would provide insufficient capacity gains.

For Barcelona's intersecting runway configuration, the threshold is 5%. As shown in chapter 6, the average fleet mix at peak conditions corresponds to a 15%.

For Madrid's converging runway configuration, the threshold is 5 to 6 percent. Having an average proportion of 23% heavy aircraft, RECAT-EU-PWS deployment in Madrid is feasible both for a converging configuration and for the segregated configuration.

7.7. Delay

Beyond quantifying how capacity changes translate into utilisation differences, a secondary question in this thesis is whether the implementation of TBS or RECAT-EU-PWS can help in delay reduction during realistic operational settings. To adress this, information written in subsection 2.4.6 and section 4.6.

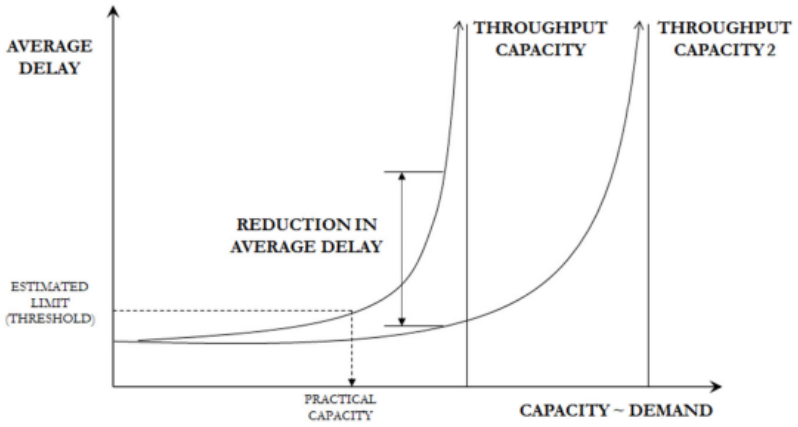

Figure 7.77: Variation in delay by capacity increase [43]

Accordingly, the delay analysis focuses on the airports where capacity constraints and runway-system characteristics suggest that procedural changes could meaningfully affect congestion. The case studies include Madrid (LEMD), Alicante (LEAL), and Palma de Mallorca (LEPA). Barcelona (LEBL) is not included in the delay-mitigation assessment because results in the preceding sections indicate that it operates well below capacity and under a very specific night configuration that rarely resembles that of an intersecting nature.

For each airport, the analysis reports the estimated delay reduction for each scenario comparison and presents the observed annual departure and arrival delay distribution, which combined with the average delays have been obtained from the EUROCONTROL ANS database [58]. Arrival delay is assumed to be the ASMA delay, the additional time spent by aircraft on the arrival flow in the arrival sequencing and metering area. The capacity-related departure delay is assumed to be the additional taxi-out time, which is the difference between the expected time-to-taxi from the gate to the runway threshold. More than 90% of this delay occurs precisely when holding short for the runway [45].

For each scenario, runway utilisation ρ is computed using total operations (arrivals plus departures). Using the queueing-based heavy-traffic relationship in Equation 2.4 together with the comparative formulation in Equation 4.54, the relative delay effect implied by the capacity change is estimated and reported in the tables below. In addition, using each airport's flight schedule, the average departure delay per operation is derived and its distribution is analysed across the 50 busiest hours, providing an empirical view of delay patterns to complement the utilisation-based comparative results.

7.7.1. Alicante

From Table 7.10 and Table 7.11 it can be concluded that the implementation of TBS reduces runway utilisation by increasing the maximum throughput of the runway, which reduces delay by 16-17% during high headwinds. Additionally, the implementation of RECAT-EU-PWS can reduce capacity delay in the 8 to 9% range.

Alicante Airport Delay Assessment

Table 7.10: ICAO vs ICAO&TBS

	RWY Utilisation U		Δ Delay
	ICAO	ICAO&TBS	
ARR	0.81	0.77	-16.3%
DEP	0.81	0.77	-16.8%
TOTAL	0.81	0.77	-16.5%

Table 7.11: ICAO vs RECAT-EU-PWS

	RWY Utilisation U		Δ Delay
	ICAO	RECAT-EU-PWS	
ARR	0.77	0.75	-8.8%
DEP	0.77	0.75	-8.2%
TOTAL	0.77	0.75	-8.5%

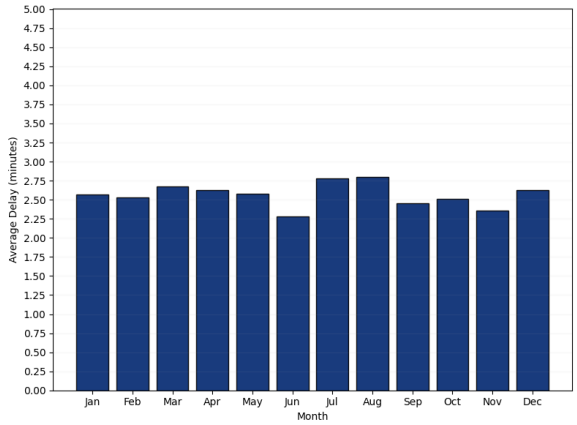

Figure 7.78: Monthly distribution of arrival delays in 2025. Alicante

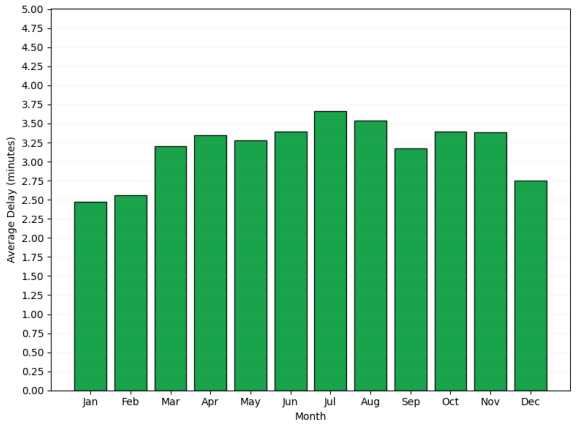

Figure 7.79: Monthly distribution of departure delays in 2025. Alicante

Figure 7.78 above shows the monthly average arrival delay in Alicante during 2025 as a bar chart. Arrival delays are fairly stable throughout the year (roughly 2.3–2.8 minutes), with a small dip around June and a modest peak in July–August before easing into autumn.

Figure 7.79 above shows the monthly average departure delay in Alicante during 2025. Departure delays are consistently higher and more seasonal, rising from January–February levels (2.5–2.6 minutes) to a clear summer peak around July (3.7 minutes), then gradually declining toward December.

The average arrivals delay in these observations amounts to 2.57 minutes. The implementation of RECAT-EU-PWS could reduce this departure delay by 8.8% to 2.34 minutes.

On the other hand, the departures delay could be reduced from 3.23 to 2.97 minutes.

7.7.2. Palma de Mallorca

Tables 7.12–Table 7.15 show that in the M-dominated scenario in Palma the implementation of TBS reduces arrival delay by 49% during high headwinds. In the balanced scenario, the arrivals delay is reduced by 65%. Being segregated independent runways, TBS has no effect in departures, as such no effect on departure delay.

Additionally, as the implementation of RECAT-EU-PWS reduces departures capacity in the dominated scenario, it can increase departure delay by 43%. The reasons behind this result are already explained in previous subsections. When moving to the Balanced scenario, arrivals delay can be reduced by 22% and departures by 23%.

Palma de Mallorca Airport Delay Assessment

Table 7.12: ICAO vs ICAO&TBS

	RWY Utilisation U		Δ Delay
	ICAO	ICAO&TBS	
ARR	0.85	0.71	-48.8%
DEP	0.86	0.86	0.0%
TOTAL	0.86	0.78	-34.4%

Table 7.13: ICAO vs RECAT-EU-PWS

	RWY Utilisation U		Δ Delay
	ICAO	RECAT-EU-PWS	
ARR	0.74	0.74	0.0%
DEP	0.86	0.88	17.3%
TOTAL	0.80	0.81	4.7%

Table 7.14: ICAO vs ICAO&TBS

	RWY Utilisation U		Δ Delay
	ICAO	ICAO&TBS	
ARR	0.92	0.78	-64.5%
DEP	0.93	0.93	0%
TOTAL	0.92	0.85	-49.8%

Table 7.15: ICAO vs RECAT-EU-PWS

	RWY Utilisation U		Δ Delay
	ICAO	RECAT-EU-PWS	
ARR	0.81	0.76	-22.2%
DEP	0.93	0.9	-23.2%
TOTAL	0.87	0.83	-23.2%

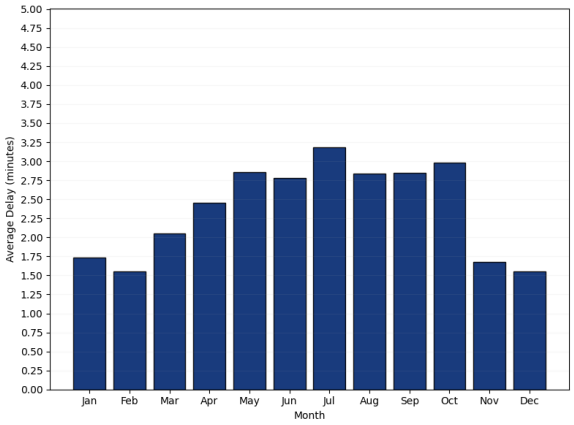

Figure 7.80: Monthly distribution of arrival delays in 2025. Palma de Mallorca

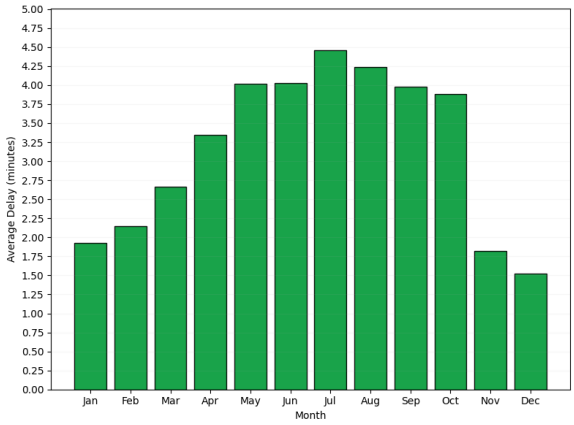

Figure 7.81: Monthly distribution of departure delays in 2025. Palma de Mallorca

Figure 7.80 above shows the monthly average arrival delay in Mallorca during 2025 as a bar chart. Arrival delays remain fairly steady across the year (around 2.3–2.8 minutes), with a small dip in June and a slight rise in July–August before easing into autumn.

Figure 7.81 shows that departure delays are consistently higher and more seasonal, increasing from January–February (2.5–2.6 minutes) to a summer peak around July (about 3.6–3.7 minutes), then gradually declining toward December.

The average arrivals delay in these observations amounts to 2.65 minutes. The implementation of RECAT-EU-PWS would not affect departure delay in the first scenario, and in the second it would reduce it by 8.8% to 2.1 min.

On the other hand, the departures delay, currently at 3.64 minutes, would increase to 4.27 minutes under the first scenario, and decrease to 2.79m.

7.7.3. Madrid

From Table 7.16 and Table 7.17 it can be concluded that the implementation of TBS reduces delay by 7% during high headwinds. Additionally, the implementation of RECAT-EU-PWS can reduce capacity delay in the 5 to 6% range.

Madrid Airport Delay Assessment

Table 7.16: ICAO vs ICAO&TBS

	RWY Utilisation U		Δ Delay
	ICAO	ICAO&TBS	
ARR	0.65	0.63	-7.0%
DEP	0.66	0.64	-7.1%
TOTAL	0.66	0.63	-7.0%

Table 7.17: ICAO vs RECAT-EU-PWS

	RWY Utilisation U		Δ Delay
	ICAO	RECAT-EU-PWS	
ARR	0.61	0.59	-5.5%
DEP	0.63	0.60	-5.9%
TOTAL	0.62	0.60	-5.7%

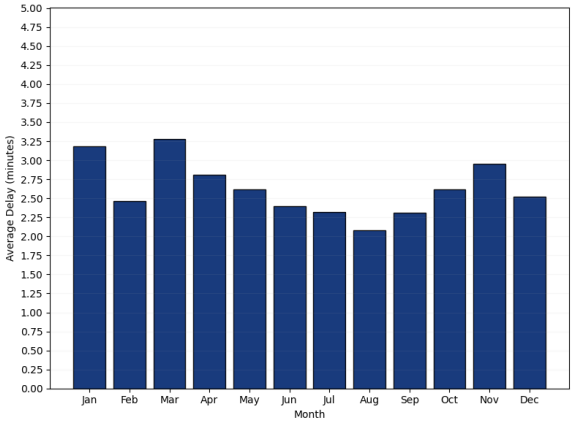

Figure 7.82: Monthly distribution of arrival delays in 2025. Madrid

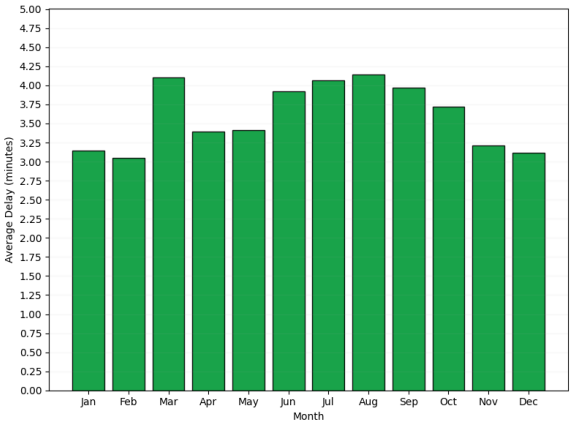

Figure 7.83: Monthly distribution of departure delays in 2025. Madrid

Figure 7.82 above shows the monthly average arrival delay in Madrid during 2025 as a bar chart. Arrival delays are fairly stable throughout the year (roughly 2.3–2.8 minutes), with a small dip around June and a modest peak in July–August before easing into autumn.

Figure 7.83 above shows that departure delays are consistently higher and more seasonal, rising from January–February levels (2.5–2.6 minutes) to a clear summer peak around July (3.7 minutes), then gradually declining toward December.

The average arrivals delay in these observations amounts to 2.63 minutes. The implementation of RECAT-EU-PWS could reduce this departure delay by 8.8% to 2.49 minutes.

On the other hand, the departures delay could be reduced from 3.62 to 3.4 minutes.

7.8. Sensitivity Analyses

In the previous airport specific sections, sensitivity analyses were conducted to quantify (i) the extent to which the implementation of Time Based Separation (TBS) can reduce the resulting capacity loss. In the RECAT-EU-PWS analysis, an additional sensitivity analysis examined the effect of varying the proportion of heavy aircraft in the traffic mix on runway capacity, with results compared between the ICAO and RECAT-EU-PWS schemes.

In this section, additional scenario-based sensitivity analyses are presented to assess the impact of runway operational parameters on capacity. Specifically, the analyses examine the effects of D_{MAP} (missed approach point), D_{MIN} (latest permissible departure point prior to an arrival), headwind, proportion of heavy aircraft in traffic mix, runway occupancy times, and point of intersection, each factor where applicable.

This analysis is not only done to demonstrate that the implemented model is robust and results vary as expected, but also as an identification on which are the limiting factors, or ”bottlenecks” in the operation of each runway configuration.

The missed approach point distance D_{MAP} is of relevance as it directly enters the runway-availability time separation constraint. Changes in D_{MAP} modify the latest point at which a go-around could be initiated and therefore alter the minimum separation required to ensure the runway is vacated in time. This sensitivity study is conducted in all four scenarios, with a variation of this distance between 0.3 NM and 1.5 NM to quantify the effects....

The effect of runway occupancy times (ROT) are included in the study because they define the time an aircraft remains, or ”occupies” a runway before it becomes available for the next operation. In practice, ROT is often not the primary limiting factor in RSC, as wake- and radar-based separations usually exceed ROT, which the runway is vacated before the next aircraft reaches the relevant spacing point. A sensitivity analysis is therefore useful to identify when this assumption holds and under what conditions ROT becomes the limiting factor. This study is performed on all scenarios and departure and arrival ROTs are varied percentually from -40% to 40% of their nominal values.

The D_{MIN} parameter is of high importance in operations where runways are coupled in some sort to each other, as it directly defines part of the ”blocking area” where a departure forbids an arrival. This constraint is used in intersecting, converging diverging and segregated parallel runways. Given that the scenario used in this thesis for parallel segregated runways features two de-coupled runways, the study on the effect of this parameter is performed only in intersecting and converging runways case. This parameter is varied from 0 to 4NM and capacity results at each point are noted down.

In intersecting runway operations, the point of intersection, or point of crossing of both runways is relevant to the capacity analysis. The closer it is to the departure and arrival thresholds, the higher the capacity. As such, it becomes interesting to investigate the exact relation between the arrival ROT, $R_{D,int}$, the departures ROT, $R_{D,int}$ and total capacity of a runway system. Both parameters are varied simultanously across the full runway occupancy times, on a two-dimensional sensitivity analysis.

Lastly, the sensitivity analyses for the effect of headwind and composition of heavy aircraft on the fleet mix are already described in sections 7.2-7.4, but will be taken into account in the summary towards the end of this section.

7.8.1. Single Mixed Runway

The single mixed runway scenario is utilized as a base to vary two parameters in addition to the already explored headwind and heavy aircraft share: ROT and D_{MAP}, shown in the figures below.

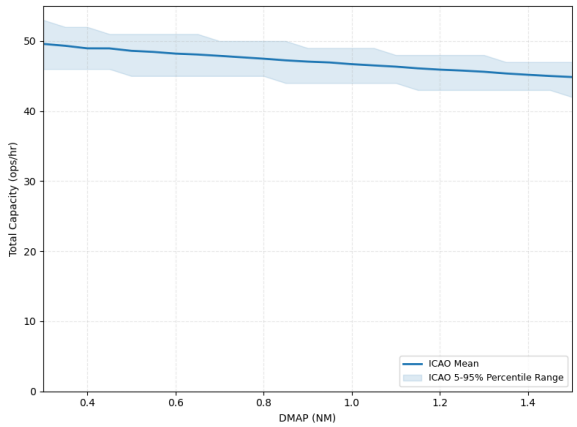

Figure 7.84: Total capacity as a function of D_{MAP}. Single Mixed runways

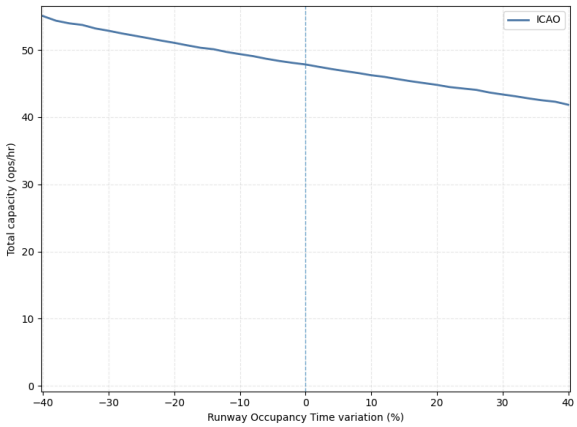

Figure 7.85: Total capacity as a function of ROT. Single Mixed runways

Figure 7.84 shows the continuos but smooth capacity decay when varying D_{MAP}, which changes from 50 mov/hr to 45 mov/hr. Complementarily, Figure 7.85 shows how varying ROT from it´s nominal values can affect capacity, varying from 55 ops/h in the low end, 48 ops/h in nominal values, and 42 ops/h in the highest ROTs of the range.

Shown in XXX, headwind also affects capacity, where an increase from o to 30 kts signifies the decay of 8.3% of the peak capacity. Varying the share of heavy aircraft from 0 to 80% implied a further reduction in capacity of 15.2%. It can be concluded that all four parameters become limiting in this scenario, as small variations lead to direct changes in capacity.

7.8.2. Parallel Segregated Runway

The parallel segregated runway scenario is also used as a base to vary two parameters in addition to the already explored headwind and heavy aircraft share: ROT and D_{MAP}, shown in the figures below.

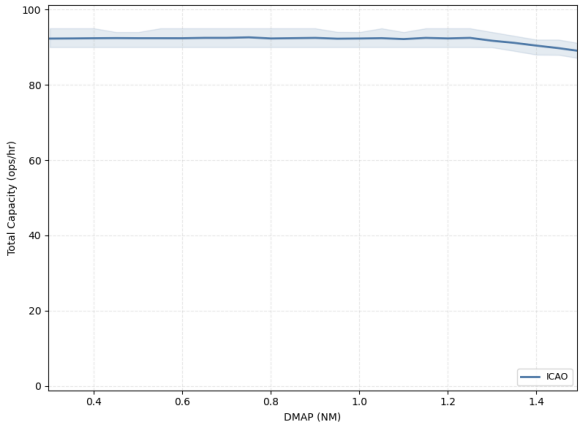

Figure 7.86: Total capacity as a function of D_{MAP}. Parallel segregated runways

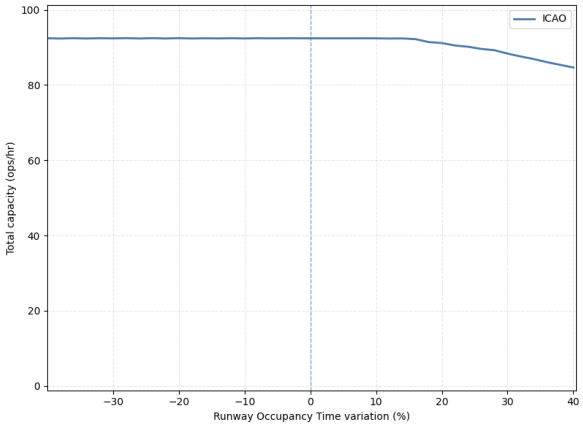

Figure 7.87: Total capacity as a function of ROT. Parallel segregated runways

Figure 7.86 shows a constant capacity of 92 ops/hr, which only begins to be limited at a D_{MAP} value of 1.25 and higher, reaching 89 ops/hr at 1.5 NM. Considering the nominal value of the parameter in Palma being 1.0 NM, it can be concluded that capacity is not limited by the missed approach distance. Complementarily, Figure 7.87 shows how varying ROT from it´s nominal values can affect capacity. Again, it can be observed how capacity remains unchanged through most of the varied ROTs at a capacity of 92 hourly movements. Only when ROT is increased beyond 16% it begins to be limiting, reaching 85 operations at 40% of ROTs. Considering the nominal ROT values, it can be concluded that this parameter is also not capacity limiting in this specific scenario.

Headwinds and heavy aircraft mix are capacity limiting, with capacity decreases of 9.6% and 20.4% respectively.

7.8.3. Intersecting Runway

Besides testing headwind, heavy aircraft share, D_{MAP} and ROT, the intersecting scenario characterised by Barcelona´s 02 & 06R assessed the interactions of D_{MIN} and point of intersection of the runways.

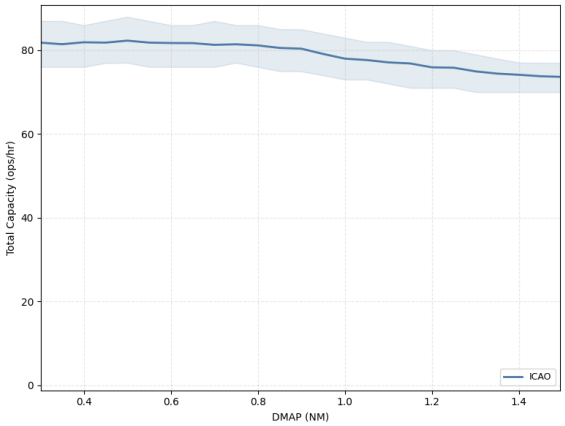

Figure 7.88: Total capacity as a function of D_{MAP}. Intersecting runways

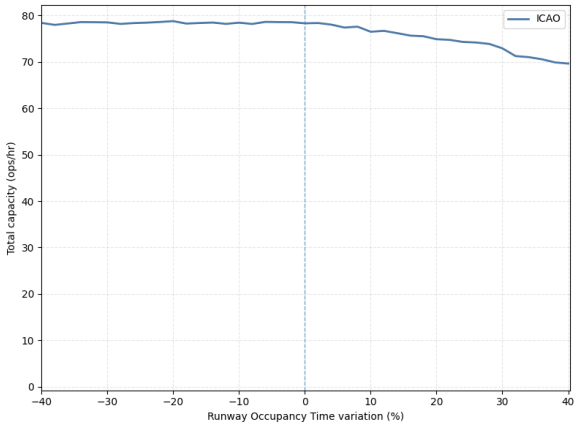

Figure 7.89: Total capacity as a function of ROT. Intersecting runways

Figure 7.88 shows a constant capacity of 82 ops/hr, which only begins to be slightly limited at a D_{MAP} value of 0.8 NM and higher, reaching 73 ops/hr at 1.5 NM. Considering the nominal value of the parameter in Barcelona being 1.0 NM, it can be concluded that capacity is slightly limited by the missed approach distance. Complementarily, Figure 7.89 shows how capacity remains constant through most of the varied ROTs at a capacity of 78 hourly movements. Only when ROT is increased beyond 3% it begins to be limiting, reaching 70 operations at 40% of ROTs. Considering the nominal ROT values, it can be concluded that this parameter is not capacity limiting in this specific scenario, but on the edge of becoming.

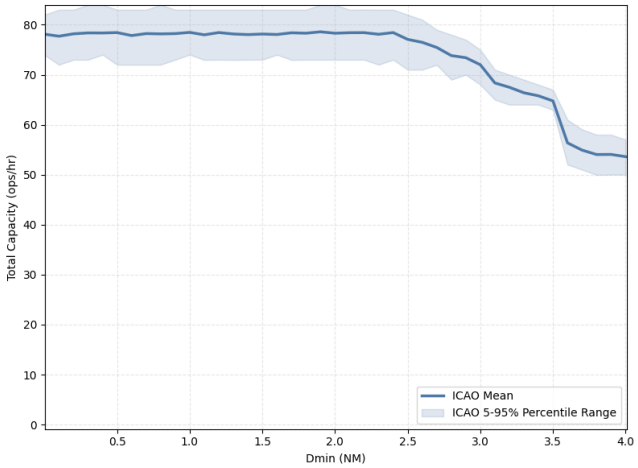

Figure 7.90: Total capacity as a function of D_{MIN}. Intersecting runways

Figure 7.90 shows that D_{MIN} remains at a constant peak capacity of 78 mov/hr as the parameter is varied from 0 to 2.4 NM, thus it is not capacity limiting until that point. As it increases beyond that value, capacity starts varying from 78 ops/h down to 54 at 4 NM, following an irregular decline.

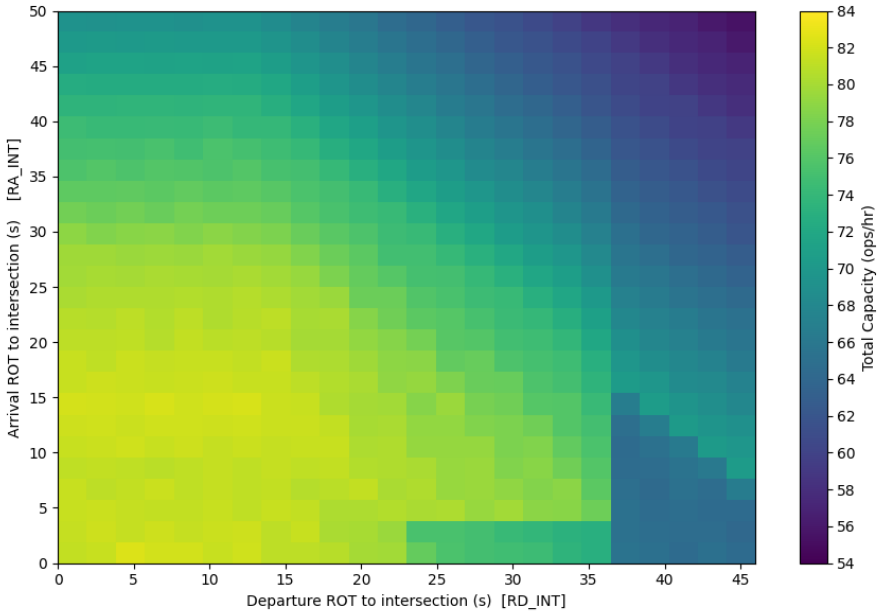

Figure 7.91: Total capacity as a function of intersection location. Intersecting runways

Results in Figure 7.91 show that there exists an inversely proportional relationship between the runway occupancy time to the intersection (ROT) and the total capacity. In particular, the lowest values of ROT are related to the highest capacities, reaching 82 to 84 operations per hour for the bottom-left region of the heatmap. However, when $R_{A,int}$ and $R_{D,int}$ increase, the capacities decrease uniformly. The darkest region of the heatmap, located at the top-right, related to the intersection that is farthest from the thresholds, indicates that the capacities decrease to 54-58 operations per hour, which represents decrease of 25 to 30 operations compared to the optimal case.

The low-capacity pocket observed on the bottom right of the plot is interesting, as capacity becomes particularly constrained when the departure ROT grows beyond 35 s. This suggests that a longer departure-related interaction with the intersection can dominate the bottleneck.

Headwinds and heavy aircraft mix are capacity limiting, with capacity decreases of 6.5% and 18.2% respectively.

7.8.4. Converging Runway

Madrid´s 36L & 32R runways are used to test the parameters for a converging runway scenario. Besides headwind and traffic mix, D_{MAP}, D_{MIN} and ROT are assessed.

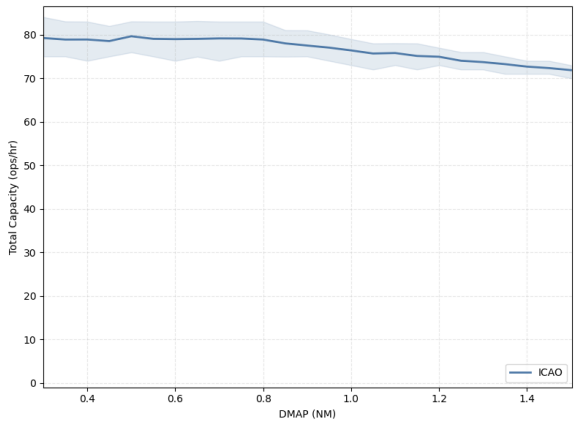

Figure 7.92: Total capacity as a function of D_{MAP}. Converging runways

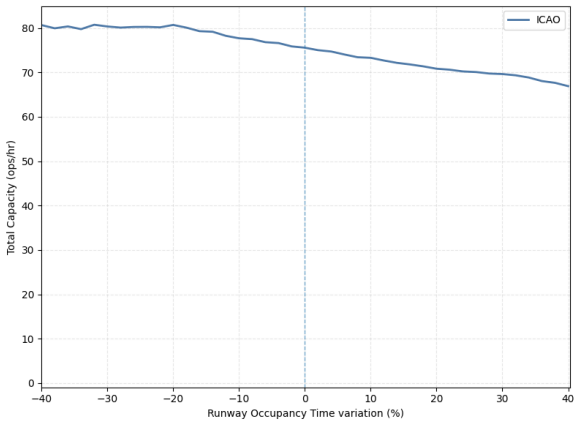

Figure 7.93: Total capacity as a function of ROT. Converging runways

Figure 7.92 shows an approximately constant capacity of 79 ops/hr until a D_{MAP} value of 0.8 NM, where it begins to be capacity limiting with a continuous smooth decay to 72 ops/hr at 1.5 NM. Considering the nominal value of the parameter in Madrid being around 1.2 NM, it can be concluded that capacity is limited by the missed approach distance. Additionally, Figure 7.93 shows how capacity remains constant at 80 ops/hr through the range of 40 to 20% reduction in ROTs. At this point, it begins to be limiting, linearly decreasing to 76 ops/hr at nominal conditions and 67 ops/hr at maximum 40% extra ROTs.

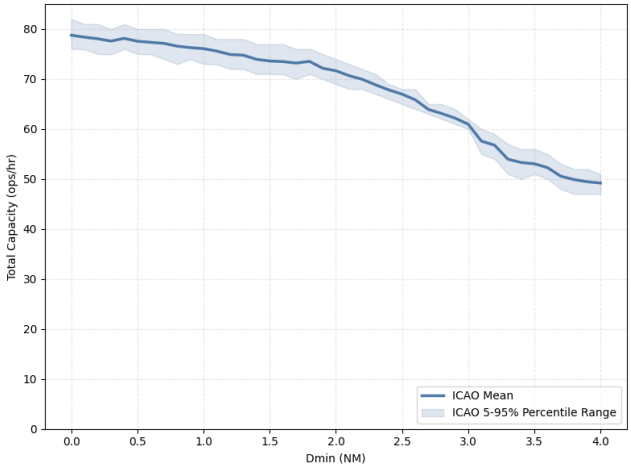

Figure 7.94: Total capacity as a function of D_{MIN}. Converging runways

Figure 7.94 shows that mean total capacity decreases monotonically with increasing D_{MIN}, with a relatively smooth decay and a noticeably steeper reduction beyond approximately 2.5-3 NM. Headwind and heavy aircraft ratio are again limiting factors, with capacity decreases of -5.3% and 18.1% respectively in their given ranges.

7.8.5. KPI Analysis

As previously explained, one of the aims of this section is to identify, per runway layout scenario, what are the runway capacity bottlenecks.

To do so, results from the sensitivity analysis are obtained and evaluated using two author-developed key performance indicators. These are the Capacity Limitation Indicator (CLI) and the Operational Bottleneck Indicator (OBI).

CLI is defined as the maximum percentage reduction in peak capacity induced by each parameter over the entire range. The resulting scores are normalized within each scenario in order to identify the critical factors. This KPI may be interpreted as a stress test, as it captures the full extent of capacity variation across the entire parameter range, irrespective of the practical realism of the values considered.

OBI is defined as the maximum realistic capacity loss with respect to the baseline parameter ranges. As such, it represents a more scenario-specific KPI, providing a less general but more practically grounded measure than CLI.

Table 7.18: CLI scores by scenario and parameter

Parameter	Mixed	Segregated	Intersecting	Converging
Intersection	–	–	10.0	–
D_{MIN}	–	–	8.9	10.0
HVY%	10.0	10.0	5.5	5.1
Headwind	5.5	4.7	2.0	1.5
D_{MAP}	4.0	0.8	2.3	1.9
ROT	9.6	1.9	3.1	3.3

CLI results shown in Table 7.18 indicate that the most critical capacity drivers vary substantially across runway configurations. In the Mixed scenario, the highest sensitivity is associated with heavy aircraft mix (10.0), closely followed by ROT (9.6), indicating that both fleet mix and runway occupancy time have a strong impact on peak capacity when the full explored parameter range is considered. In the Segregated scenario, the proportion of heavy aircraft is again the dominant factor (10.0), while all other parameters show comparatively limited influence, with HW reaching 4.7 and the remaining parameters staying below 2.0.

For the Intersecting configuration, the intersection constraint emerges as the main limiting factor (10.0), followed by D_{MIN} (8.9), showing that intersection-related parameters dominate, as expected, the stress test response in this case. The influence of heavy mix is still noticeable (5.5), but clearly secondary, while headwind, D_{MAP}, and ROT remain of relatively minor importance. In the converging scenario, D_{MIN} is the critical parameter (10.0), with heavy aircraft proportion also showing a relevant effect (5.1), whereas the remaining parameters have only modest contributions. Again, this result is expected as it is the runway time-blocking rules that cause the bottleneck.

Overall, the capacity limitation indicator confirms that, when the entire explored range is considered, fleet composition is the dominant driver in the more conventional Mixed and Segregated scenarios, while intersection and runway-blocking related constraints become the key limiting factors in the more operationally constrained Intersecting and Converging configurations.

Table 7.19: OBI scores by scenario and parameter

Parameter	Mixed	Segregated	Intersecting	Converging
Intersection	–	–	10.0	–
D_{MIN}	–	–	2.3	10.0
HVY%	10.0	10.0	4.8	6.5
Headwind	9.5	8.1	1.6	2.1
D_{MAP}	4.7	0.0	1.9	0.7
ROT	3.6	0.0	0.5	1.6

On the other hand, the OBI results shown in Table 7.19 provide a more scenario specific view by focusing only on realistic parameter variations around the baseline. Under this metric, heavy mix remains the dominant factor in the mixed and segregated scenarios, reaching the maximum normalized score of 10.0 in both cases. In the mixed configuration, Headwind also appears as a highly relevant driver (9.5), while D_{MAP} and ROT have a more limited effect. In the Segregated scenario, headwind is again the second most influential parameter (8.1), whereas D_{MAP} and ROT have no practical impact within the realistic ranges considered.

For the Intersecting configuration, the point of intersection remains the most critical factor (10.0), but unlike in the CLI results, the effect of D_{MIN} becomes much smaller (2.3), indicating that its strong stress-test influence is not equally pronounced within realistic operating conditions. The remaining parameters all show comparatively low scores, with heavy mix reaching 4.8 and ROT only 0.5. In the Converging scenario, D_{MIN} becomes the dominant factor again (10.0), while the heavy mix shows a strong contribution (6.5), and Headwind, D_{MAP}, and ROT remain secondary.

Overall, the OBI results suggest that, under realistic variations, traffic mix is the most consistently important driver of capacity across scenarios, while some parameters that appeared important in the CLI assessment, such as D_{MIN} and ROT, lose relative importance in favour of headwind and heavy aircraft mix when the analysis is restricted to plausible operating ranges. With respect to CLI: whereas CLI identifies the parameters with the greatest theoretical potential to degrade capacity, OBI highlights those that are most likely to matter in practice.

7.9. Other Analyses

Additional analyses, such as evaluating the effect of implementing a 2.5 NM minimum radar separation and assessing the impact of changing runway configurations while keeping all other parameters constant, are presented in the following section.

7.9.1. Minimum Radar Separation

The minimum radar separation (MRS), selected as 3 NM, can become a binding constraint on both the RECAT-EU-PWS and ICAO wake turbulence arrival separation matrices. In practice, this means that any wake-based separation value below 3 NM is effectively "floored" up to 3 NM. As a result, runway throughput may be limited by the radar minimum rather than by the wake separation scheme itself.

This effect is particularly relevant at airports where a high proportion of operations involve aircraft pairs whose wake-based requirement would otherwise be smaller than the imposed MRS. In such cases, the potential benefits of adopting more specific wake categories can be "lost" because many sequences end up operating at the same minimum spacing regardless of the underlying wake minima.

For this reason, it is useful to investigate how capacity changes when the MRS is reduced from 3 NM to 2.5 NM. Conceptually, lowering the MRS relaxes the hard lower bound applied to the arrival separation matrices, allowing those "floored" aircraft pairings to be spaced more tightly. The overall gain will depend on the share of floored pairs in the traffic mix, how often they occur in typical sequencing, and whether other constraints (such as runway occupancy time, approach speed control, or procedural limitations) become limiting once the MRS is reduced.

This sensitivity will be examined at the two most capacity dense airports in the scenarios considered: Alicante and Palma de Mallorca, with input parameters described in chapter 6 including an average headwind of 7 kts.

Alicante

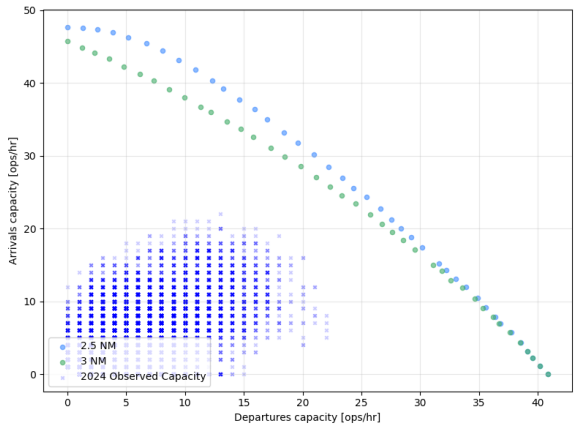

Figure 7.95: Capacity envelope (MRS 3 vs 2.5NM). LEAL 10

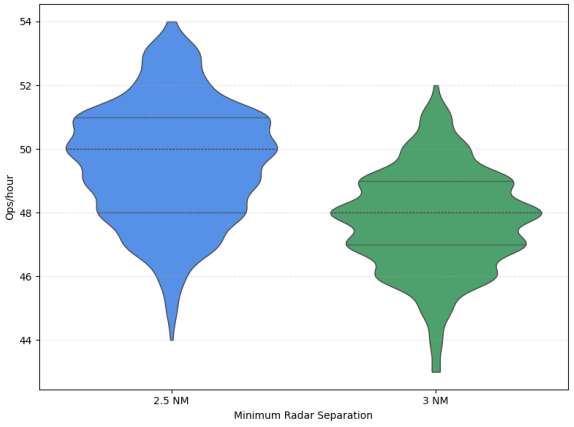

Figure 7.96: Peak capacity distribution (MRS 3 vs 2.5NM). LEAL 10

A hypothetical implementation of the 2.5 NM MRS could imply Alicante´s peak balanced capacity jumping from 47 to 50 hourly operations. Figure 7.95 shows the shift in the capacity envelope, which becomes especially evident as the arrivals ratio nears unity. The difference in spread and variability is shown in Figure 7.96. Shifting to a 2.5 surveillance minima shifts upwards the central values, although results in a slightly more dispersed distribution.

Palma

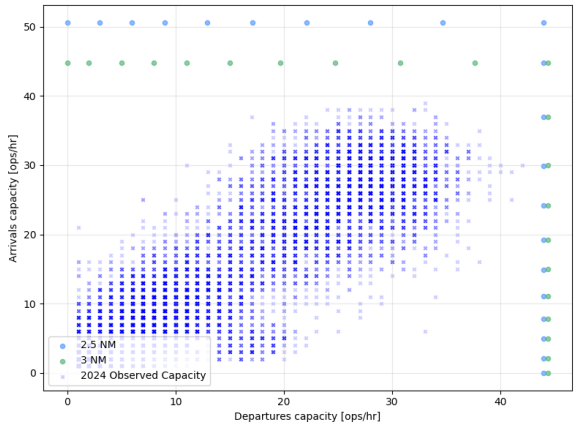

Figure 7.97: Capacity envelope (MRS 3 vs 2.5NM). LEPA 24R&24L

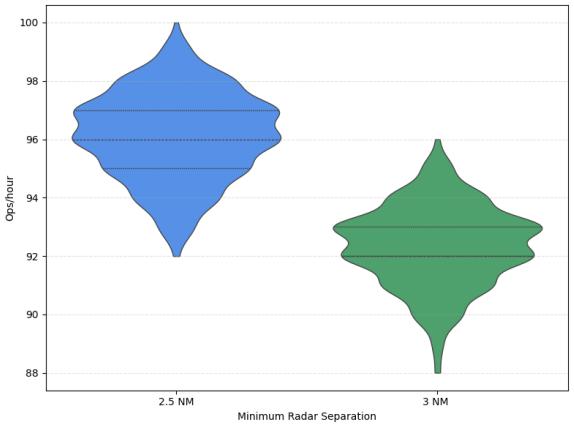

Figure 7.98: Peak capacity distribution (MRS 3 vs 2.5NM). LEPA 24R&24L

Similarly, Figure 7.97 displays when using the 2.5 NM surveillance minima, Palma de Mallorca increases by 5 arrivals from 89 ops/hr to 94. The violin plots in Figure 7.98 show that the change in surveillance minima logically increases the central values and shifts the distribution upwards, but does not alter significantly the variability.

7.9.2. Mode of Operation

To investigate the effect of runway layout and operating mode on airside performance, a set of simulations was carried out using an identical scenario in terms of traffic demand, weather conditions, runway-occupancy times (ROTs), and SID constraints. This corresponds to to Madrid Barajas converging-diverging runway pair (32R&36L) and can be found in section 6.4. The only variable changed between runs was the runway geometry/mode of operation: a single mixed runway (like Alicante), parallel segregated operations (like Palma de Mallorca), intersecting runways (like Barcelona), and a converging/diverging (C/D) configuration.

The capacity plots (Figures 7.99–7.100) show a clear separation between the single runway and the multiple-runway configurations. Being a mixed runway, the tradeoff between Arrivals and departures is strong. As departures increase, the Arrival capacity drops almost linearly, which keeps total capacity relatively flat around the low 40s.

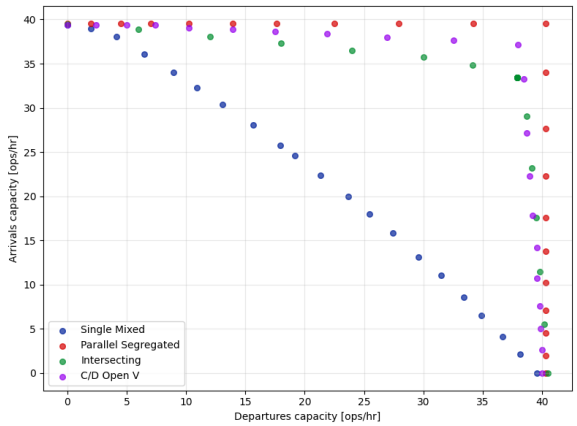

Figure 7.99: Mode of operation comparison: Capacity envelope

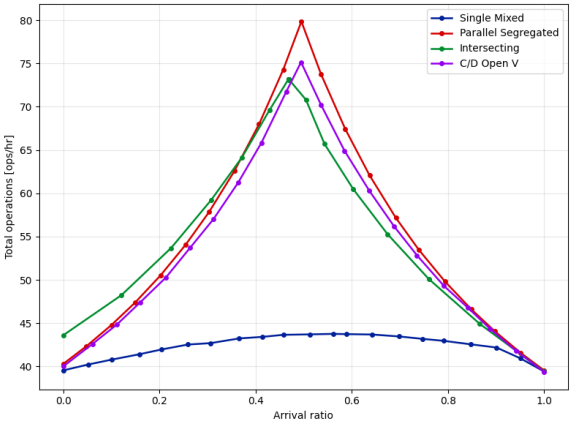

Figure 7.100: Mode of operation comparison: Capacity - Arrival ratio

By contrast, and expected as they use two runways, the remaining three configurations (segregated, intersecting and Open V) sustain high throughput along a wide range of demand values, producing a peak capacity near a

balanced arrival ratio of 0.5 . Being independent, the segregated operations achieve the highest capacity, with a peak around 80 ops/hr. The converging / diverging open v configuration achieves slightly lower values, due to the blocking distance and arrival ROT, with around 75 ops/hr, slightly followed by the intersecting case, with around 73 hourly operations. In this last case, the peak capacity is achieved at a slightly higher departure-biased ratio than the other configurations. All four configurations converge to similar departures-only and arrivals-only throughput.

The violin plots confirm the performance ranking seen before and add a dimensión in variability and spread of the simulations.

Figure 7.101 shows that for total capacity, parallel segregated outperforms the other modes with the highest central values around 83 ops/hr and a tight distribution. Intersecting and C/D Open V configurations sit lower in the mid-70s ops/h range, with C/D Open V slightly higher than intersecting.

The arrivals distribution in Figure 7.102 show a stronger disonance, with parallel runway maintaining the highest and consistent distribution. Intersecting shows the lowest median arrivals and the widest spread, with a long lower tail. C/D Open V is intermediate, with a higher center than intersecting and consistent variability.

Lastly, the departures modes shown in Figure 7.103 are closer than for arrivals, but parallel segregated still has the highest central tendency. Intersecting is slightly lower, while C/D Open V tends to be lowest and more dispersed, implying departures in that configuration are more affected by the runway geometry/coordination constraints than arrivals.

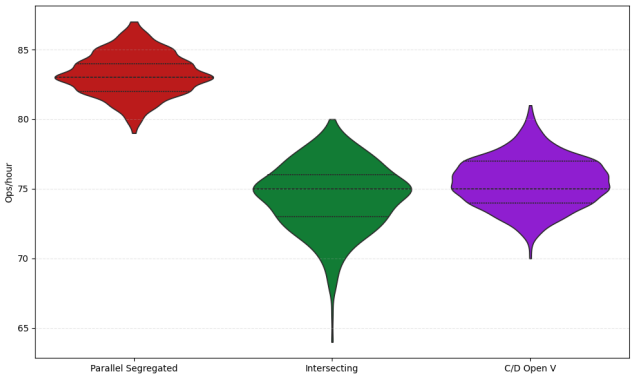

Figure 7.101: Mode of operation comparison: Total distribution

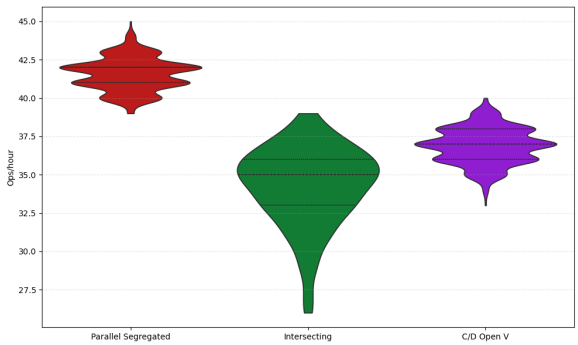

Figure 7.102: Mode of operation comparison: Arrivals distribution

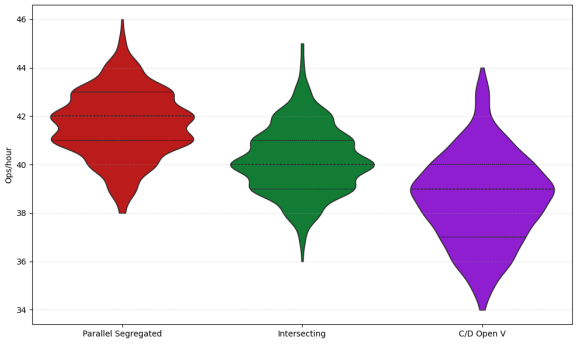

Figure 7.103: Mode of operation comparison: Departures distribution

7.10. RECAT-EU-PWS Case Studies

In order to identify whether RECAT-EU-PWS can be used as tool in airport planning to evaluate how specific changes in aircraft demand distribution affect peak capacity, and as explained in section XX, two similar scenarios have been set up. For Tenerife-Norte and for Palma de Mallorca, varying fleet mixes composed by different degrees of ATR72 are utilized. This aircraft is pàrticularly interesting when talking about runway capacity, as even though it is a Medium type aircraft, it tends to have slower approach speeds and typically requires longer separations in standard instrument departure matrices.

7.10.1. Scenario 1: Tenerife-Norte

Tenerife Norte is an airport known for a very high number of ATR operations. This makes it an ideal candidate for the study. The assumptions used to model this airport are shown below in Table 7.20.

Table 7.20: Assumptions made modelling Tenerife Norte

Parameter	Symbol	Value
Mode of Operation		Mixed
Departure ROT	R_D	Calculated from *Lamers, 2016* [23]
Arrival ROT	R_A	ENAIRE database
Departure Velocity	V_D	Calculated from *Lamers, 2016* [23]
Arrival Velocity	V_A	ENAIRE database
SID Logic Used		Specific Matrix Method
SIDs Modelled		GCXO 30
Common Approach Path	D_A	6.9 NM
Missed Approach Point	D_{MAP}	1.0 NM
Headwind TBS Scenario		25 kts
Headwind RECAT-EU-PWS Scenario		7 kts
Minimum Radar Separation		3 NM

Table 7.21: Tenerife Norte RECAT-EU-PWS scenarios

RECAT-EU-PWS	HTO	MTO	LTO
B2	2.0	2.0	2.0
C4	2.0	2.0	2.0
D1	20.8	25.9	30.9
D	10.0	20.1	30.0
E2	57.8	42.6	27.7
E3	5.1	5.1	5.1
F3	3.3	3.3	3.3

As explained in subsection 6.5.1, the above table shows the three future scenarios in which ATR72 is slowly traded off with other M type aircraft, mainly the Embraer E2 and Boeing 737-800.

Figure 7.104 shows the expected result: the ICAO scheme is unable to capture the changes in demand reflected in Table 7.21, as these all occur within the same Medium category. The peak balanced capacity is calculated to be around 45 ops/h, with a maximum of 39 arrivals and 41 departures.

However, as shown in Figure 7.105, all three RECAT-EU-PWS plots shift inwards. This shift indicates that the fine-tuning introduced by this scheme is effective and enables more realistic reproduction of specific traffic combinations.

The envelope demonstrates that increasing the proportion of ATR72 aircraft in the fleet causes the plot to shift inwards, with the greatest impact observed on departure capacity. At 28% ATR share, the peak balanced capacity is 46 operations per hour, with arrivals-only and departures-only capacities at 40 operations per hour each. When the ATR proportion increases to 43%, these capacities decrease to 45, 39, and 38 operations per hour, respectively.

At 58% ATR share, corresponding to the actual peak hours flight schedule, the maximum capacity is 44 operations per hour, with arrivals-only and departures-only capacities of 40 and 36 operations per hour, respectively.

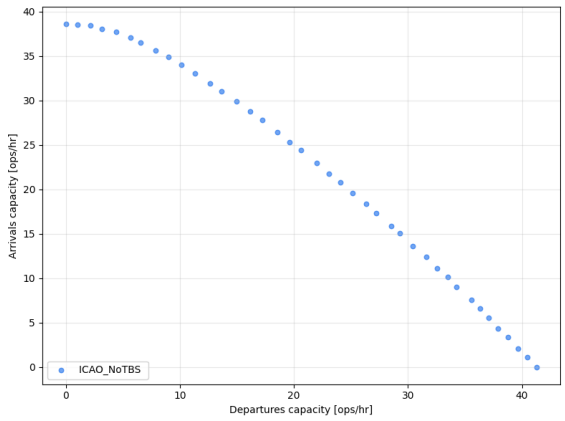

Figure 7.104: Capacity envelope. ICAO

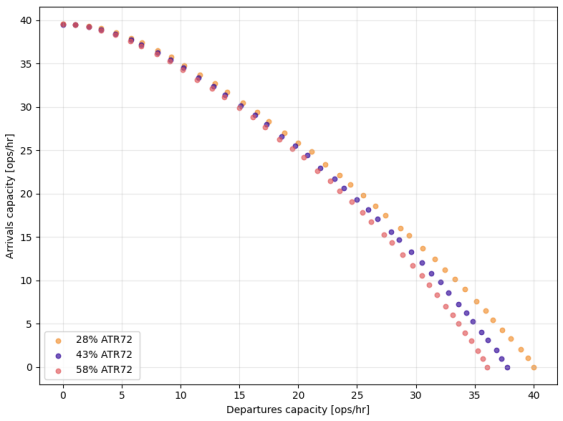

Figure 7.105: Capacity envelope. RECAT-EU-PWS 3 cases

The violin plot presented in Figure 7.106 supports the previously discussed results. As the proportion of ATR aircraft in the mix increases, central values decrease. Aditionally, the spread of the distribution becomes slightly larger, and the highest density in each distribution shifts to a lower proportion, which confirms the decrease runway performance associated with ATR operations.

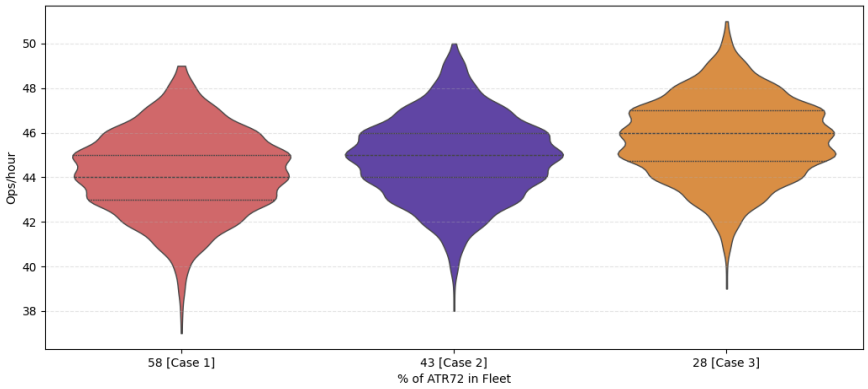

Figure 7.106: Capacity distribution. RECAT-EU-PWS scenarios

The exact variation in runway capacity with ATR operations can be also displayed in the form of a continuous graph, as shown in Figure 7.107. While ICAO remains entirely stable at 45 ops/hr, RECAT-EU-PWS outputs a peak capacity of 48 ops/hr at 0% of ATR operations. As this variable increases to 80%, RECAT-EU-PWS scheme decreases almost linearly to 44 ops/hr. This shows that the RECAT-EU-PWS scheme can be used as a tool to detect the effects of small changes in traffic demand.

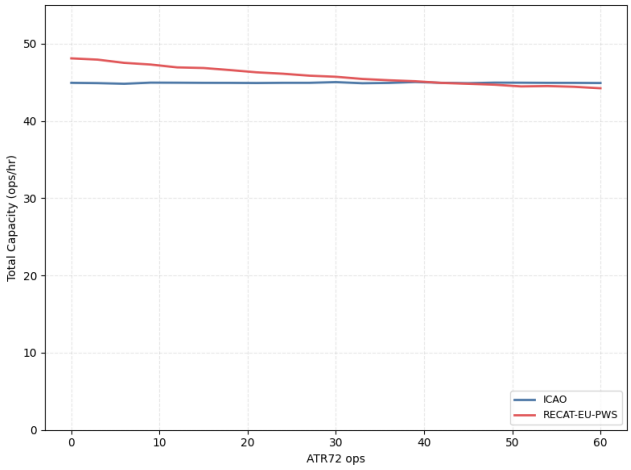

Figure 7.107: Total Capacity as a function of turboprop share. ICAO vs RECAT-EU-PWS. GCXO 30

7.10.2. Scenario 2: Palma de Mallorca

The assumptions regarding the airport´s mode of operation and numerical input values can be found in XX. As for the case scenarios simulated, they originate during ATR-heavy peaks (explicar mas....)

Explained in subsection 6.5.2, three future scenarios (HTO, MTO and LTO) are generated in which ATR72 operations are slowly traded off with other Medium type aircraft.

Table 7.22: Palma RECAT-EU-PWS scenarios

RECAT-EU-PWS	HTO	MTO	LTO
B2	4.6	4.6	4.6
C4	3.1	3.1	3.1
D1	60.1	66.3	72.5
E1	6.2	9.3	12.4
E2	21.4	12.1	2.8
F2	1.5	1.5	1.5
F3	1.5	1.5	1.5

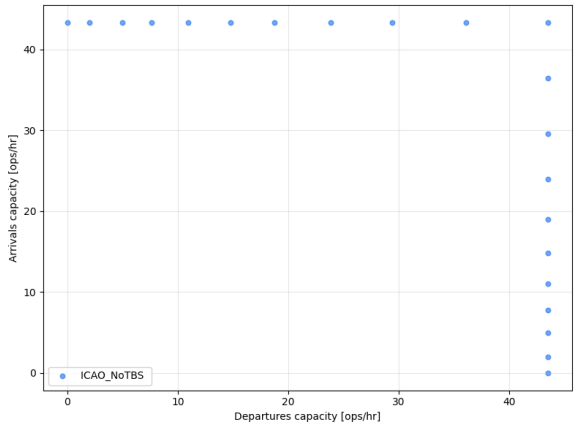

Figure 7.108: Capacity envelope. ICAO

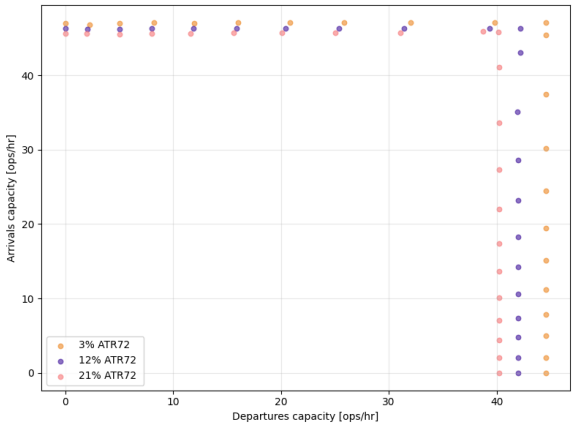

Figure 7.109: Capacity envelope. RECAT-EU-PWS 3 cases

Figure Figure 7.108 shows the expected result: the ICAO scheme cannot capture demand changes in **??**, since all of them fall within the same Medium category. The peak capacity is about 87 ops/h, with 43 arrivals and 44

departures.

The envelope in **??** demonstrates that as the ATR72 share increases in the fleet, the plot shifts inward, mainly affecting departures capacity. With 3% ATR, peak capacity is 92 ops/hr; with 47 arrivals and 45 departures. At 12% , capacities drop to 88, 46, and 42 hourly operations, respectively. Lastly, at 21% of ATR traffic, the maximum capacity is 86 ops/hr, with 46 arrivals and 40 departures.

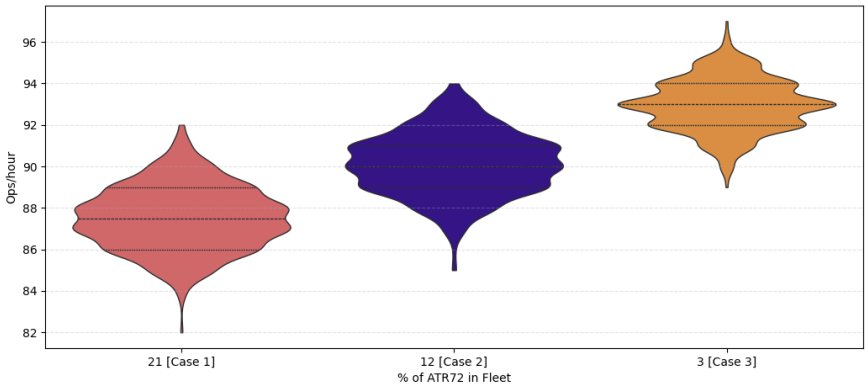

Figure 7.110: Capacity distribution. RECAT-EU-PWS scenarios

Figure 7.110 again shows that a greater proportion of ATR operations not only lowers the central values, but also elongates the spread of distributions.

The exact variation in runway capacity with ATR operations can also be displayed in the form of a continuous graph, as shown in Figure 7.111. While ICAO remains entirely stable at 48 ops/hr, RECAT-EU-PWS outputs a peak capacity of 51 ops/hr at 0% of ATR operations. As this variable increases to 80%, the RECAT-EU-PWS scheme decreases almost linearly to 46 ops/hr. This shows that the RECAT-EU-PWS scheme can detect the effects of small changes in traffic demand.

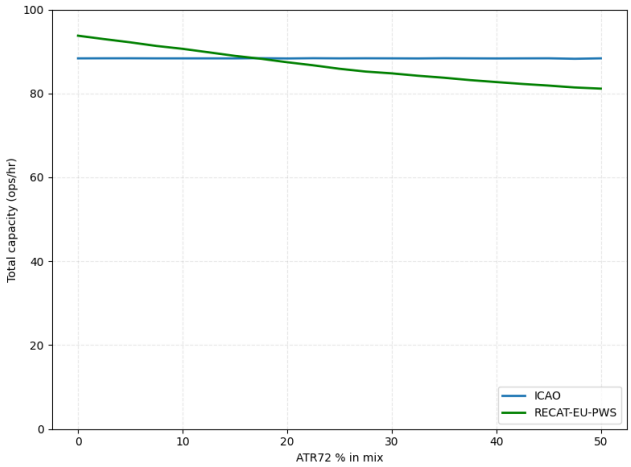

Figure 7.111: Total capacity as a function of turboprop share. ICAO vs RECAT-EU-PWS. LEPA 24R&24L

8

Conclusions and Recommendations

In this final chapter, the reader is presented with the concluding findings of the thesis regarding the implementation of arrival time–based separation (TBS) and pairwise RECAT (RECAR-EU-PWS).

Rather than focusing solely on the selected airports, a broader and more generalized perspective is developed based on the range of scenarios analyzed. The limitations of the proposed model and the overall research are then discussed, leading to recommendations for future academic work. Finally, key considerations for potential real world deployment are examined, providing an overview of the next steps in advancing this field.

8.1. Thesis Conclusions

The objective of this master's thesis was initially conceived as the development of a new runway capacity model capable of estimating peak runway capacity for multiple runway configurations under varying traffic mixes and weather conditions.

The literature review presented in chapter 2 first outlines the historical development of runway capacity estimation models and then provides an extensive analysis of the main factors affecting runway capacity, namely aircraft separation requirements, runway layout and mode of operation, aircraft characteristics, and weather conditions. In addition, several measures aimed at increasing runway capacity are examined, including Time Based Separation (TBS) in strong headwind conditions, as well as the implementation of RECAT and RECAT-EU-PWS.

The research gap identified in this study is clear: at present, there is no openly available macro-level analysis of the capacity gains that can be expected from the implementation of TBS and, separately, RECAT-EU-PWS. Accordingly, the research question of this thesis is formulated as follows:

Research Question

To what extent can the implementation of Time Based Separation and the wake categorisation scheme RECAT-EU-PWS increase an airport´s peak runway capacity?

To answer the main and sub-research questions, this thesis developed ARCAS, *Airport Runway Capacity Assessment Software*, a Discrete Event Simulation model in Python to analyse peak runway capacity. The model is based on the runway dependency logic established in previous RCAP research by van der Klugt [22] and Lamers [23], but re-implements this logic in a flexible and modular simulation framework. Building on this foundation, the model incorporates stochastic aircraft sequence generation, new SID logic, multiple runway layouts, and alternative separation concepts, including RECAT-EU-PWS, and Time Based Separation. Embedded within a Monte Carlo framework the simulation model is capable of calculating peak runway capacities, capacity envelopes for any runway, multiple sensitivity analyses and of course quantifying the potential capacity gains resulting from the implementation of TBS and RECAT-EU-PWS.

The verification process provided confidence that the simulation model was implemented correctly and operated as intended. This was achieved through a combination of systematic code inspection, visual examination of

simulation outputs, the use of dedicated verification functions to reproduce selected results independently, and direct comparison with other models, such as RCAP 1.0 and PICAP under identical input conditions. In addition, calculation verification addressed the stochastic nature of the model by means of convergence analyses based on the coefficient of variation of peak hourly capacity. Across the considered scenarios, the results showed that the Monte Carlo estimates stabilised at around 500 simulation runs, indicating that the capacity estimates are statistically reliable.

The validation results likewise support the suitability of the model for the purposes of this thesis. By comparing simulated capacity envelopes with observed runway throughput from 2025 operations, the model was shown to provide a realistic macro-level representation of runway system performance, with maximum deviation of peak capacities being 2%. At the same time, the validation exercise highlighted that observed traffic levels do not necessarily coincide with the theoretical capacity frontier, since actual airport operations may be constrained by factors beyond the runway system itself. Overall, these results indicate that the model is sufficiently credible for analysing relative differences in runway capacity and for supporting the assessment of the potential benefits of TBS and RECAT-EU-PWS.

Alicante was used as the reference case for a single mixed runway, Palma de Mallorca for segregated parallel runways, Barcelona for an intersecting runway configuration, and Madrid for a converging/diverging runway system with partial interdependence between arrival and departure flows. In addition, Tenerife Norte and Palma de Mallorca were used as specific RECAT-EU-PWS case studies to analyse the effect of changes in fleet composition, particularly in scenarios with a significant proportion of turboprop operations. This combination of scenarios made it possible to evaluate the model across different operational contexts and to apply the sensitivity analyses and implementation assessments to representative runway layouts.

The main findings obtained from the sensitivity analyses showed that the factors affecting runway capacity, and therefore the dominant operational bottlenecks, vary considerably across runway configurations. In the single mixed and parallel segregated scenarios, the principal capacity drivers were associated with traffic composition and weather, with the proportion of heavy aircraft consistently emerging as the most significant source of capacity loss and headwind also exerting an important influence. In these more conventional layouts, parameters such as D_{MAP} and runway occupancy time were only limiting under specific conditions, and in the segregated case their practical effect remained relatively small. In contrast, for intersecting and converging runway systems, the main bottlenecks were linked to runway geometry and inter-runway operational coupling. In the intersecting configuration, the location of the runway crossing proved to be the most critical determinant of capacity, while in the converging case D_{MIN} became the dominant limiting factor due to its direct role in defining runway-blocking constraints. These results, obtained through parameter variation and quantified using KPI´s, confirm that runway capacity cannot be explained by a single generic bottleneck, but must instead be understood as the outcome of interacting operational, geometric, and traffic-related constraints whose relative importance depends on the specific runway layout under consideration.

Regarding the effectiveness of TBS across the analysed scenarios, it was found that its technical viability as a means of increasing peak runway capacity under adverse headwind conditions depends mainly on two factors: runway geometric layout and the airport-specific wind profile. For the selected case studies, realistic capacity gains were found to emerge at headwind values of approximately 12 kts in single mixed-mode operations, 4 kts in parallel segregated runway systems, 15 kts in intersecting runway configurations, and 25 kts in converging runway layouts. This demonstrates that the effectiveness of TBS is strongly configuration-dependent and cannot be generalised across airports. Consequently, any assessment of whether TBS should be implemented at a given airport must combine these threshold values with local wind conditions, particularly with the frequency and intensity of runway-specific headwind conditions, in order to determine whether meaningful peak capacity gains can be expected in practice.

Similarly, it was found that the technical viability of RECAT-EU-PWS implementation depends mainly on two factors: runway geometry and the traffic mix during peak hour conditions, particularly the proportion of heavy aircraft. Since RECAT-EU-PWS is based on a recategorisation of wake vortex separation minima, its potential benefits depend directly on the composition of traffic and therefore do not materialise equally across all runway configurations. In single mixed-mode operations, capacity gains are observed across the entire analysed range of heavy-aircraft shares, indicating immediate technical viability. In the parallel segregated scenario, by contrast, meaningful gains only begin to appear when the proportion of heavy aircraft exceeds approximately 11%. For intersecting and converging runway layouts, the corresponding thresholds are lower, at around 5% for both cases. The effectiveness of RECAT-EU-PWS cannot be generalised across airports, but must instead be assessed in

relation to both runway configuration and local fleet composition in order to determine whether its implementation is likely to work in a specific scenario.

Overall, the deployment assessment shows that TBS is most justified at Palma de Mallorca, where the required headwind threshold is relatively low and occurs frequently enough to make implementation technically viable. By contrast, TBS appears difficult to justify at Alicante, Barcelona and particularly at Madrid, where the required headwind conditions occur too rarely to produce consistent benefits. For RECAT-EU-PWS, the conclusions are different: Alicante, Barcelona, and Madrid appear to be suitable candidates, as their traffic mix conditions are compatible with meaningful capacity gains, while Palma de Mallorca does not currently justify implementation given its low proportion of heavy aircraft. These conclusions become more relevant in light of capacity forecasts, which indicate increasing pressure in Alicante and Palma, while the converging and crossing configurations of Madrid and Barcelona´respectively are to remain significantly below their peak and sustainable capacities.

The delay analysis confirmed that delay increases non-linearly as demand approaches runway capacity, meaning that even small capacity gains from TBS or RECAT-EU-PWS can lead to meaningful delay reductions under congested conditions. At the same time, the results underline that delay is not a function of capacity alone, but of the relationship between capacity and demand. As such, the practical benefit of these procedures is greatest in scenarios where the runway system operates close to saturation, while their effect is naturally more limited when sufficient spare capacity already exists.

The RECAT-EU-PWS case studies further indicate that the scheme can be used as a valuable tool for airport planning, since it captures the sensitivity of peak runway capacity to changes in fleet composition with a level of detail that the ICAO categorisation cannot provide. In both Tenerife Norte and Palma de Mallorca, higher shares of turboprop traffic were shown to reduce peak capacity, especially for departures, whereas ICAO-based estimates remained unchanged because these variations occur within the same broad wake category. This highlights that RECAT-EU-PWS offers not only a finer categorisation system, but also a more realistic representation of operational bottlenecks linked to aircraft mix. Consequently, it may provide airport planners and authorities with a useful basis for scenario analysis, peak-hour planning, and the assessment of how future changes in demand distribution could affect runway capacity.

8.2. Recommendations for future academic work

This thesis focuses mainly on the implementation of two runway throughput optimisation SESAR solutions, namely TBS and RECAT-EU-PWS using the 20-category wake turbulence scheme. However, the current modelling framework could be further extended in several directions to enhance its fidelity and applicability.

The first recommendation for future work lies in extending the current categorical implementation of the 20 wake turbulence categories towards more refined approaches. While this thesis focuses on a fixed categorical application of RECAT-EU-PWS, alternative implementations exist that allow for greater flexibility and precision. In particular, it can also be applied on a pairwise basis, and a procedural implementation for selected aircraft type pairs3weeeee. Moving in this direction would effectively bridge the gap between categorical and full aircraft representation. In reality, aircraft differ significantly in terms of approach speed profiles, deceleration capabilities, runway occupancy times, and wake vortex generation. Accounting for these differences could still allow for an even more accurate estimation of separations and runway throughput, particularly in mixed fleet environments where variability within categories such as “Medium” or “Heavy” can otherwise lead to conservative spacing and infrautilisation of runway capacity.

In addition to this, future research could investigate the implementation of other SESAR solutions such as ROCAT, which focuses on optimising separations based on Runway Occupancy Time rather than wake turbulence. While RECAT-EU-PWS enhances runway throughput by refining wake turbulence separation minima, it does not address situations where ROT becomes the limiting constraint. In such cases, ROCAT provides a complementary approach by deriving distance based spacing minima from locally observed ROT data, typically characterised per runway, per aircraft type and even per airline. The incorporation of ROCAT into the modelling framework would make possible to capture scenarios in which runway occupancy, rather than wake turbulence, is the limiting constraint. This would enable a more comprehensive representation of operational constraints, particularly in scenarios where reduced wake separations shift the bottleneck towards ROT. Furthermore, ROCAT can also be implemented in multiple ways, including procedural, category based, or more advanced leader-wise (iROT) approaches supported by separation delivery tools..

Another important extension concerns the modelling of wake vortex behaviour under a wider range of meteorological conditions, particularly crosswind scenarios. The current study primarily considers headwind conditions in the application of Time-Based Separation, as these are most directly linked to variations in ground speed and approach spacing. However, crosswinds also have a significant influence on wake vortex transport and decay, often accelerating lateral displacement and reducing wake persistence. Incorporating crosswind effects into a wake vortex model could allow for a more realistic representation of wake behaviour and its impact on separation requirements. Also related to wind conditions is the interaction between headwind and ROTs, and whether its effect can be modelled and implemented onto the model.

Furthermore, the impact of future aircraft fleet evolution represents a relevant direction for continued research. The composition of the global fleet is expected to change significantly over the coming decades, with the introduction of new-generation aircraft that could feature advanced aerodynamics and more efficient propulsion systems. These changes could alter wake vortex characteristics as well as operational parameters such as approach speeds and runway occupancy times.

With regards to the scope and generalisability, this thesis work applies ARCAS to several Spanish airport case studies and shows that benefits are highly configuration-dependent. Future work could extend the validation of the model to a broader set of European airports using data of equal or higher quality. This is particularly relevant for the intersecting-runway case. While the airport selected in this thesis provides a valid scenario for initial testing, the results discussion already indicated that Barcelona´s crossing configuration differs in important ways from that of a more typical intersecting-runway system. It would therefore be advisable to validate the model against additional airports with more representative intersecting operations, such as Hamburg Airport (EDDH) or Warsaw Chopin Airport (EPWA).

Another potential extension would be to investigate the integration between upstream arrival sequencing and runway-based separation optimisation, particularly through the integration of Point Merge procedures with Time-Based Separation. While the present work focuses on runway throughput once aircraft are established in the approach stream, Point Merge provides a structured method for sequencing and metering arrivals in the terminal manoeuvring area before they reach final approach. Combining these concepts in the model would allow the assessment of how improved upstream flow organisation influences the effectiveness of TBS at the runway threshold. In particular, Point Merge could reduce sequence instability, vectoring, and tactical controller interventions, thereby providing a more orderly and predictable arrival stream for TBS delivery. This would make it possible to analyse whether part of the capacity gain attributed to TBS depends not only on the separation logic itself, but also on the quality of arrival pre-sequencing upstream.

Finally, the scope of the model could be extended towards a more holistic representation of the airport system. While this thesis focuses on runway capacity, it is well understood that the runway is only one component of a larger, interconnected system that includes taxiways, apron operations, and terminal processes. Increases in runway throughput may shift bottlenecks to other parts of the system, such as taxiway congestion or stand availability. Future work could therefore integrate these subsystems into a unified gate-to-gate simulation environment, enabling the analysis of a system wide performance instead of isolated runway metrics.

A final recommendation for future work concerns the availability and quality of detailed input data. Throughout the development and testing of the simulation model, multiple datasets were used, and the results obtained from high-fidelity data differed significantly from those generated in earlier iterations based on simpler and less specific inputs. Although the datasets used in this thesis are of generally high quality, some specific parameters could not be obtained directly, particularly departure runway occupancy times and speeds had to be derived or recalculated from previous studies. The direct availability of such parameters from high-quality local operational data would directly improve the precision and reliability of the simulation results further.

8.3. Future Deployment considerations

This thesis work focused on the technical viability of implementing RECAT-EU-PWS and Time-Based Separation (TBS) in order to improve runway capacity performance. However, a positive outcome from the technical point of view does not necessarily imply that implementation is feasible in practice. It may be the case that, even if a specific airport shows clear benefits from these concepts, other constraints prevent their deployment. In particular, the economic and operational viability of such implementations must also be considered.

Given that this analysis lies beyond the scope of the present work, the level of detail is intentionally limited. Nev-

ertheless, it is important to highlight that the future deployment of RECAT-EU-PWS and TBS must be addressed across the three classical decision-making levels of Air Traffic Management, namely the strategic, tactical, and operational levels. In the context of this work, the strategic level refers to airspace and procedure design, the tactical level to flow control, and the operational level to vectoring and real-time control actions.

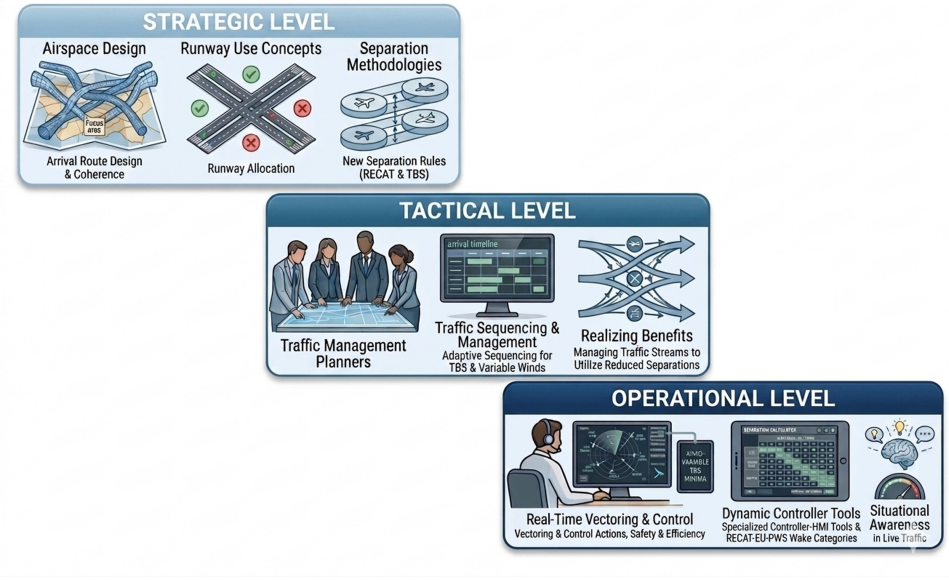

Figure 8.1: Strategic, Tactical and Operational decision-making levels

At the strategic level, the main concern is whether RECAT-EU-PWS and TBS can be incorporated into the design of the airspace and the associated operational procedures. This includes assessing whether the structure of arrival routes, runway use concepts, and separation methodologies can accommodate these new concepts in a coherent and efficient way.

At the tactical level, the focus shifts to flow control. In this case, the potential benefits of reduced separations can only be realized if traffic streams are planned, sequenced, and managed in a way that allows them to be effectively used. This is especially relevant for TBS, since runway throughput may vary depending on wind conditions and therefore requires traffic management strategies capable of adapting to changing circumstances.

At the operational level, implementation directly affects vectoring and real-time control actions. Controllers must apply the required separations in live traffic conditions while maintaining safety, efficiency, and situational awareness. TBS requires the use of separation minima that vary according to real-time wind conditions rather than fixed distance-based values, while RECAT-EU-PWS increases the number of wake turbulence categories and therefore the number of possible leader–follower combinations to be considered during runway operations.

In addition to this distinction by decision-making level, future deployment must also be examined from three complementary perspectives: regulatory, personnel, and systems. These dimensions interact across the strategic, tactical, and operational levels and together determine whether implementation is feasible in practice.

From a regulatory perspective, the feasibility of implementing RECAT-EU-PWS and TBS must be assessed in light of the existing frameworks at both European and national levels. Initiatives led by organizations such as EUROCONTROL already provide guidance and methodologies for the deployment of both concepts, and TBS has already been operationally implemented at some airports globally. However, local regulatory approval may still be required, and adaptations may be necessary to comply with state-specific ATM regulations, certification processes, and safety assessment requirements. The time and complexity associated with obtaining such approval can therefore become a limiting factor.

From a personnel perspective, both concepts introduce additional complexity into air traffic control tasks and therefore require significant adaptation by controllers and other operational staff. Implementation would require additional training, simulator-based instruction, procedural updates, and human factors evaluations. Controller workload, situational awareness, and acceptance of the new procedures are critical elements, since they directly

affect the successful integration of these concepts into day-to-day ATM practice. If the perceived complexity is too high, or if the benefits are not clearly evident to operators, resistance to implementation may arise. Therefore, effective change management and gradual integration strategies are essential.

From a systems perspective, significant challenges arise in the integration of these concepts into existing ATM tools and controller interfaces. The implementation of TBS implies that separation expressed in distance is no longer constant, but instead varies continuously as a function of wind conditions. This requires the development and validation of support tools capable of presenting such dynamic separations in an intuitive and operationally usable way. Possible solutions include the use of dynamic distance targets, predicted spacing indicators, and the Final Target Distance Indicator (FTDi) [59].

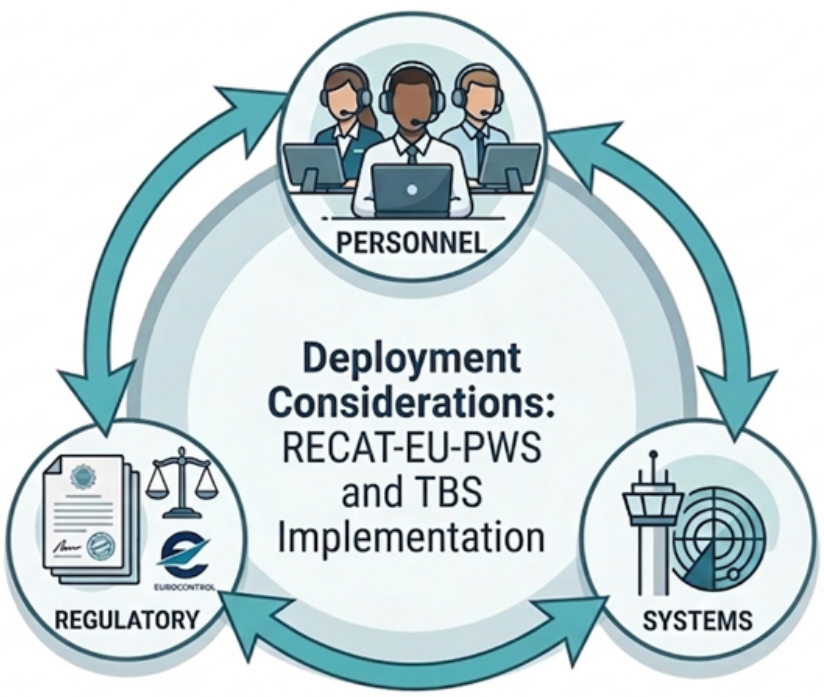

Figure 8.2: Deployment considerations

For RECAT-EU-PWS, the challenge lies in presenting information related to a larger number of aircraft categories, effectively increasing the complexity from a small set of ICAO wake categories to a more detailed classification, without overloading the controller. Systems must be capable of automatically identifying aircraft categories and calculating the required separations in real time. At the same time, the Human-Machine Interface must remain clear and simple. This may require the use of abstraction techniques such as color coding, simplified labels, or decision-support tools that provide the required separation directly, without requiring the controller to interpret complex category combinations.

In addition, the implementation of both concepts must ensure compatibility with existing ATM infrastructure, including surveillance systems, flight data processing systems, and coordination tools. Depending on the level of technological maturity of the airport, these upgrades may also represent a significant investment, thereby linking system-related considerations to longer-term infrastructure planning and funding decisions.

In conclusion, while RECAT-EU-PWS and TBS demonstrate clear potential for increasing runway capacity, their deployment in real-world environments will also depend on a broader system-wide vision. Such deployment must be considered across the strategic, tactical, and operational levels of ATM, while also taking into account regulatory, personnel, and systems-related issues. A comprehensive evaluation of these factors is therefore essential to determine whether implementation is not only technically viable, but also operationally and economically feasible.

References

[1] ACI EUROPE. *Position Paper on Airport Capacity*. Tech. rep. Position Paper. Brussels, Belgium: ACI EUROPE, Nov. 2019.

[2] R. de Neufville and A.R Odoni. *Airport Systems Planning, Design and Management*. 2nd ed. ISBN:978-0-07-177058-3. McGraw Hill Education, 2013.

[3] R.M. Horonjeff et al. *Planning and Design of Airports*. 5th. McGraw-Hill Professional, 2010. ISBN: 9780071446419.

[4] A. Blumstein. "The Landing Capacity of a Runway". In: *Operations Research* 7.6 (1959), pp. 752–763. DOI: 10.1287/opre.7.6.752.

[5] G.F Newell. "Airport Capacity and Delays". In: *Transportation Science* 13.3 (1979), pp. 201–241. DOI: 10.1287/trsc.13.3.201.

[6] Federal Aviation Administration. *Airport Capacity and Delay*. Advisory Circular AC 150/5060-5. Washington, D.C.: Federal Aviation Administration, 1983. DOI: 10.21949/1513590.

[7] Transportation Research Board, Engineering National Academies of Sciences, and Medicine. *Evaluating Airfield Capacity*. Ed. by Leigh Fisher. Washington, DC: The National Academies Press, 2012. ISBN: 978-0-309-25873-9. DOI: 10.17226/22674.

[8] E.P Gilbo. "Airport capacity: Representation, Estimation, Optimization". In: *IEEE Transactions on Control Systems Technology* 1.3 (1993), pp. 144–154. DOI: 10.1109/87.251882.

[9] M. Bazargan, K.Fleming, and P. Subramanian. "A simulation study to investigate runway capacity using TAAM". In: vol. 2. Jan. 2003, 1235–1243 vol.2. ISBN: 0-7803-7614-5. DOI: 10.1109/WSC.2002.1166383.

[10] A. Kim and M. Hansen. "Validation of Runway Capacity Models". In: *Transportation Research Record: Journal of the Transportation Research Board* 2177 (Dec. 2010), pp. 69–77. DOI: 10.3141/2177-09.

[11] M. Hansen. "Post-Deployment Analysis of Capacity and Delay Impacts of an Airport Enhancement: Case of a New Runway at Detroit". In: *Air Traffic Control Quarterly* 12 (Oct. 2004), pp. 339–365. DOI: 10.2514/atcq.12.4.339.

[12] A. Kim, S.A. Rokib, and L. Yi. "Refinements to a Procedure for Estimating Airfield Capacity". In: *Transportation Research Record: Journal of the Transportation Research Board* 2501 (Oct. 2015), pp. 18–24. DOI: 10.3141/2501-03.

[13] K. Chen et al. "Understanding the capacity of airport runway systems". In: *Transportation Research Part C: Emerging Technologies* 173 (2025), p. 104998. ISSN: 0968-090X. DOI: 10.1016/j.trc.2025.104998.

[14] P. Di Mascio, G. Rappoli, and L. Moretti. "Analytical Method for Calculating Sustainable Airport Capacity". In: *Sustainability* 12.21 (2020). ISSN: 2071-1050. DOI: 10.3390/su12219239.

[15] D.A. Lee, C. Nelson, and G. Shapiro. *The Aviation System Analysis Capability Airport Capacity and Delay Models*. NASA Contractor Report, RTOP 538-04-14-02, NAS2-14361. Apr. 1998.

[16] R. Kicinger et al. "Airport Capacity Prediction Integrating Ensemble Weather Forecasts". In: June 2012. DOI: 10.2514/6.2012-2493.

[17] W.L. Cheung et al. "Dynamic capacity and variable runway configurations in airport slot allocation". In: *Computers Industrial Engineering* 159 (2021), p. 107480. ISSN: 0360-8352. DOI: 10.1016/j.cie.2021.107480.

[18] B. Bubalo and J. Daduna. "Airport capacity and demand calculations by simulation—the case of Berlin-Brandenburg International Airport". In: *NETNOMICS Economic Research and Electronic Networking* 12 (Oct. 2011), pp. 161–181. DOI: 10.1007/s11066-011-9065-6.

[19] P.C. Kuzminski. "An improved runwaySimulator — Simulation for runway system capacity estimation". In: Apr. 2013, pp. 1–11. ISBN: 978-1-4673-6251-1. DOI: 10.1109/ICNSurv.2013.6548575.

[20] C. Wang, X. Zhang, and X. Xu. “Simulation Study on Airfield System Capacity Analysis Using SIMMOD”. In: vol. 1. Oct. 2008, pp. 87–90. DOI: 10.1109/ISCID.2008.70.

[21] J. van der Klugt et al. “Calculating capacity of dependent runway configurations: A discrete-event simulation approach for analysing the effect of aircraft sequencing”. In: Aug. 2013. ISBN: 978-1-62410-225-7. DOI: 10.2514/6.2013-4353.

[22] J. van der Klugt. “Calculating Capacity of Dependent Runway Configurations”. Master’s Thesis. Delft University of Technology, Nov. 2012.

[23] M.F Lamers. “Enhanced Runway Capacity at Airports with Complex Runway Layouts”. Master’s Thesis. Delft University of Technology, June 2016.

[24] “Airport Capacity”. In: *Airport Engineering*. John Wiley Sons, Ltd, 2011. Chap. 7, pp. 234–296. ISBN: 9780470950074. DOI: 10.1002/9780470950074.ch7.

[25] M.C. Gelhausen, D. Wilken, and P. Berster. *Airport Capacity Constraints and Strategies for Mitigation: A Global Perspective*. ISBN:9780128126585. London: Academic Press / Elsevier, 2019.

[26] International Air Transport Association. *Airport Development Reference Manual*. 11th ed. ISBN: 978-92-9229-853-1. Montreal: International Air Transport Association, 2019.

[27] EUROCONTROL. *Performance Review Report: An Assessment of Air Traffic Management in Europe during the Calendar Year 2019*. Brussels: EUROCONTROL, 2020.

[28] J. Banks et al. *Discrete-Event System Simulation*. 5th ed. ISBN:978-0-13-815037-2. Prentice Hall, 2009.

[29] International Civil Aviation Organization. *Manual on Simultaneous Operations on Parallel or Near□Parallel Instrument Runways (SOIR), Doc 9643*. Technical Manual. ISBN:978-92-9258-911-0. International Civil Aviation Organization, 2020.

[30] *Commission Implementing Regulation (EU) 2017/373*. https://eur-lex.europa.eu/legal-content/EN/TXT/PDF/?uri=OJ:L:2017:062:FULL. Official Journal of the European Union, L 62, 8 March 2017, pp. 1–126. 2017.

[31] M.A. Stamatopoulos, K.G. Zografos, and A.R. Odoni. “A decision support system for airport strategic planning”. In: *Transportation Research Part C: Emerging Technologies* 12.2 (2004), pp. 91–117. ISSN: 0968-090X. DOI: 10.1016/j.trc.2002.10.001.

[32] United States Air Force. *Aircrew Quick Reference to the METAR and TAF Codes*. Washington, D.C., Mar. 2011. URL: https://skybrary.aero/sites/default/files/bookshelf/1543.pdf.

[33] J.D Anderson Jr. *Introduction to Flight*. 8th ed. New York: McGraw-Hill Education, 2016. ISBN: 978-0-07-802767-3.

[34] Federal Aviation Administration. *Wake Turbulence (AIM Chapter 7, Section 4)*. Aeronautical Information Manual. Air Traffic Plans and Publications. Aug. 2025. URL: https://www.faa.gov/air_traffic/publications/atpubs/aim_html/chap7_section_4.html.

[35] International Civil Aviation Organization (ICAO). *Procedures for Air Navigation Services – Air Traffic Management (PANS-ATM), Doc 4444*. Sixteenth. ISBN:978-92-9258-081-0. International Civil Aviation Organization. Montréal, Quebec, Canada, 2016.

[36] Luchtverkeersleiding Nederland (LVNL). *Voorschriften Dienst Verkeersleiding*. [Regulations for Air Traffic Services; Dutch]. Luchtverkeersleiding Nederland. Schiphol, The Netherlands, 2012.

[37] V. Treve and F. Rooseleer. *RECAT-EU: European Wake Turbulence Categorisation and Separation Minima on Approach and Departure*. Tech. rep. Brussels, Belgium: EUROCONTROL, 2024.

[38] Austro Control GmbH. *Aeronautical Information Circular A 06: Implementation of RECAT-EU Wake Turbulence Separation Scheme*. 2018.

[39] F. Rooseleer. *RECAT-EU-PWS Solution: Optimised Wake Turbulence Categorisation and static Pair-Wise Separation (S-PWS) Minima on Approach and Departure*. Tech. rep. Brussels, Belgium: EUROCONTROL, 2023.

[40] F. Rooseleer and S. Neshevski. *Guidelines on Time-Based Separation (TBS) with Optimised Runway Delivery (ORD) for Final Approach*. Tech. rep. GUID-196. ISBN:978-2-87497-127-3. EUROCONTROL, 2024.

[41] EUROCONTROL. *Enhancing Airside Capacity, the Complete Guide*. Technical Report. Eurocontrol, 2003.

[42] N.P Meijers. “Data-Driven Predictive Analytics of Runway Occupancy Time for Improved Capacity at Airports”. Master’s Thesis. MASSACHUSETTS INSTITUTE OF TECHNOLOGY, Feb. 2020.

[43] A. Rodriguez-Sanz and L. Rubio Andrada. “An empirical analysis of airport capacity evaluation: insights regarding air traffic design hours”. In: *Journal of Physics: Conference Series* 2526.1 (2023), p. 012095. DOI: 10.1088/1742-6596/2526/1/012095.

[44] J.F.C Kingman. “The single server queue in heavy traffic”. In: *Mathematical Proceedings of the Cambridge Philosophical Society* 57.4 (1961), pp. 902–904. DOI: 10.1017/S0305004100036094.

[45] INECO. *Conversation with Javier Vázquez Capitán, Project Manager in Runway Capacity, Operations & ANSP’s*. Meeting, January 29th, 2026. Jan. 2026.

[46] AENA. *Tráfico de pasajeros, operaciones y carga en la red de Aena: Datos provisionales. Diciembre de 2025*. Tech. rep. Statistical report. Madrid, Spain: AENA, Dec. 2025.

[47] AirServiceOne. *EATS European Airport Traffic Statistics 2025*. Tech. rep. 29065343. European Airport Traffic Statistics report. Online: AirServiceOne, Aug. 2025. URL: https://cdn.airserviceone.com/wp-content/uploads/2025/08/29065343/EATS-European-Airport-Traffic-Stats-2025-28-Aug-2580.pdf (visited on 02/10/2026).

[48] ENAIRE. *Aeronautical Information Publication (AIP) España: AD 2-LEAL Alicante–Elche Miguel Hernández*. 2025.

[49] ENAIRE. *Carta de Acuerdo entre Palma TACC (LECP) y Palma de Mallorca TWR (LEPA)*. Letter of Agreement, Internal document. 2023.

[50] ENAIRE. *Aeronautical Information Publication (AIP) España: AD 2-LEPA/LESJ Palma de Mallorca*. AIRAC Amendment, effective 27-Nov-2025. 2025.

[51] ENAIRE. *Aeronautical Information Publication (AIP) España: AD 2-LEBL 1 BARCELONA/Josep Tarradellas Barcelona-El Prat*. 2025.

[52] ENAIRE. *LoA entre LECB y LEBL*. Letter of Agreement, Internal document. 2023.

[53] ENAIRE. *Aeronautical Information Publication (AIP) España: AD 2-LEMD 1 MADRID/Adolfo Suarez Madrid-Barajas*. 2025.

[54] ENAIRE. *LoA entre MADRID ACC y MADRID-BARAJAS TWR*. Letter of Agreement, Internal document. 2023.

[55] Performance Review Commission. *Airport Capacity Imbalance*. Technical Note. Brussels, Belgium: EUROCONTROL, Oct. 2020.

[56] ENAIRE. *Aeronautical Information Publication (AIP) España: AD 2-GCXO 1 TENERIFE NORTE/Ciudad de La Laguna*. 2025.

[57] American Institute of Aeronautics and Astronautics. *Guide for the Verification and Validation of Computational Fluid Dynamics Simulations*. Tech. rep. AIAA-G-077-1998. ISBN:1-56347-285-6. Reston, VA: American Institute of Aeronautics and Astronautics, 1998.

[58] EUROCONTROL. *ANS Performance Database*. EUROCONTROL. n.d. URL: https://ansperformance.eu/data/ (visited on 03/05/2026).

[59] EUROCONTROL. *Guidelines on Final Target Distance Indicator (FTDi) for Distance-Based Separation on Final Approach*. Edition 1.0, accessed 2026-03-21. Brussels, Belgium: EUROCONTROL, Oct. 2024.

[60] ENAIRE. *AIP España AD 2-LEAL SID RWY 10*. 2023.

[61] ENAIRE. *AIP España AD 2-LEPA/LESJ SID 4*. 2023.

[62] ENAIRE. *AIP España AD 2-LEBL SID 5*. 2023.

[63] ENAIRE. *AIP España AD 2-LEMD SID 5 MADRID/Adolfo Suárez Madrid - Barajas*. 2025.

[64] ENAIRE. *AIP España AD 2-LEMD SID 7 MADRID/Adolfo Suárez Madrid - Barajas*. 2025.

[65] ENAIRE. *AIP España AD 2-GCXO SID 2*. 2025.

A

Charts and Tables

A.1. SID Navigation Charts

Alicante - Elche

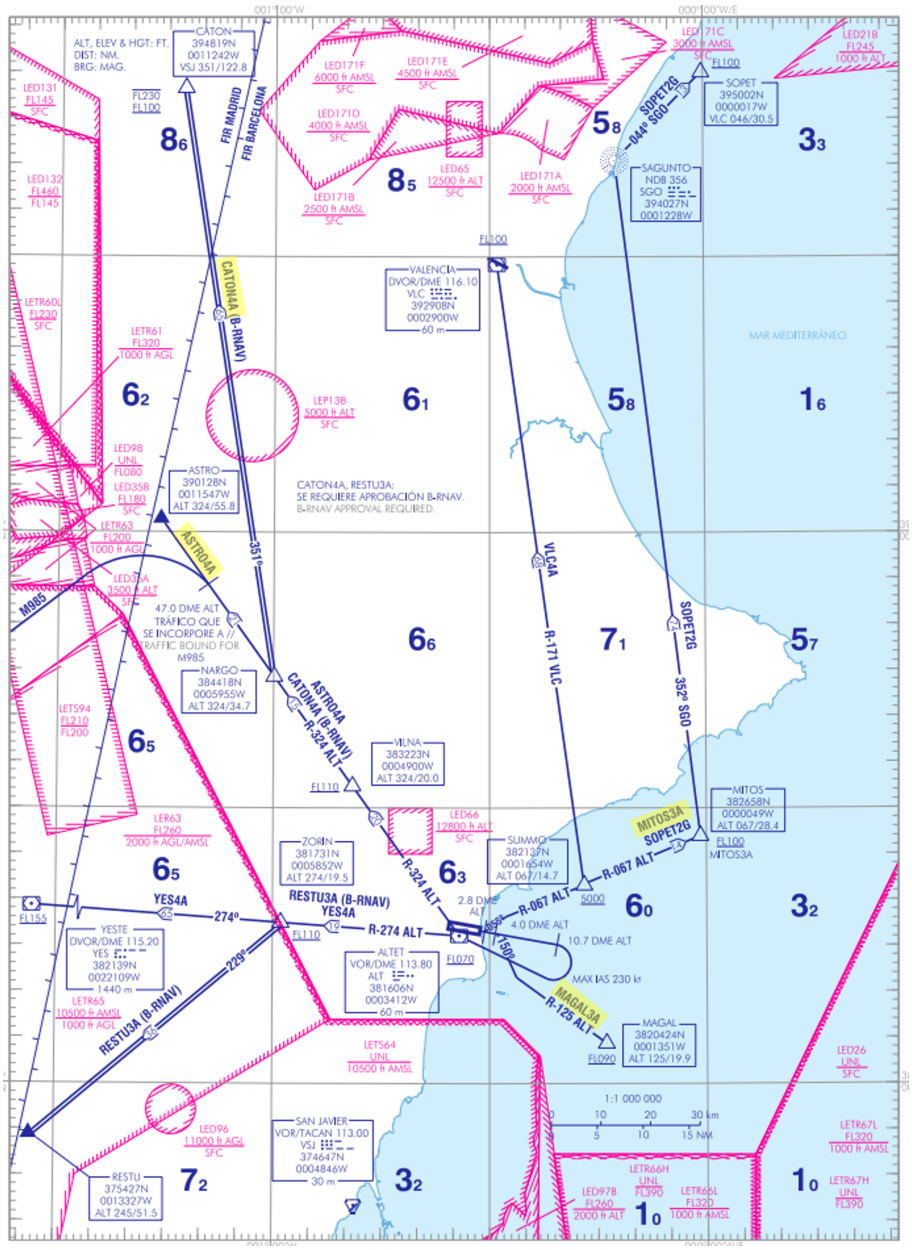

Figure A.1: LEAL Runway 10 SID Routes [60]

Palma de Mallorca - Son Sant Joan

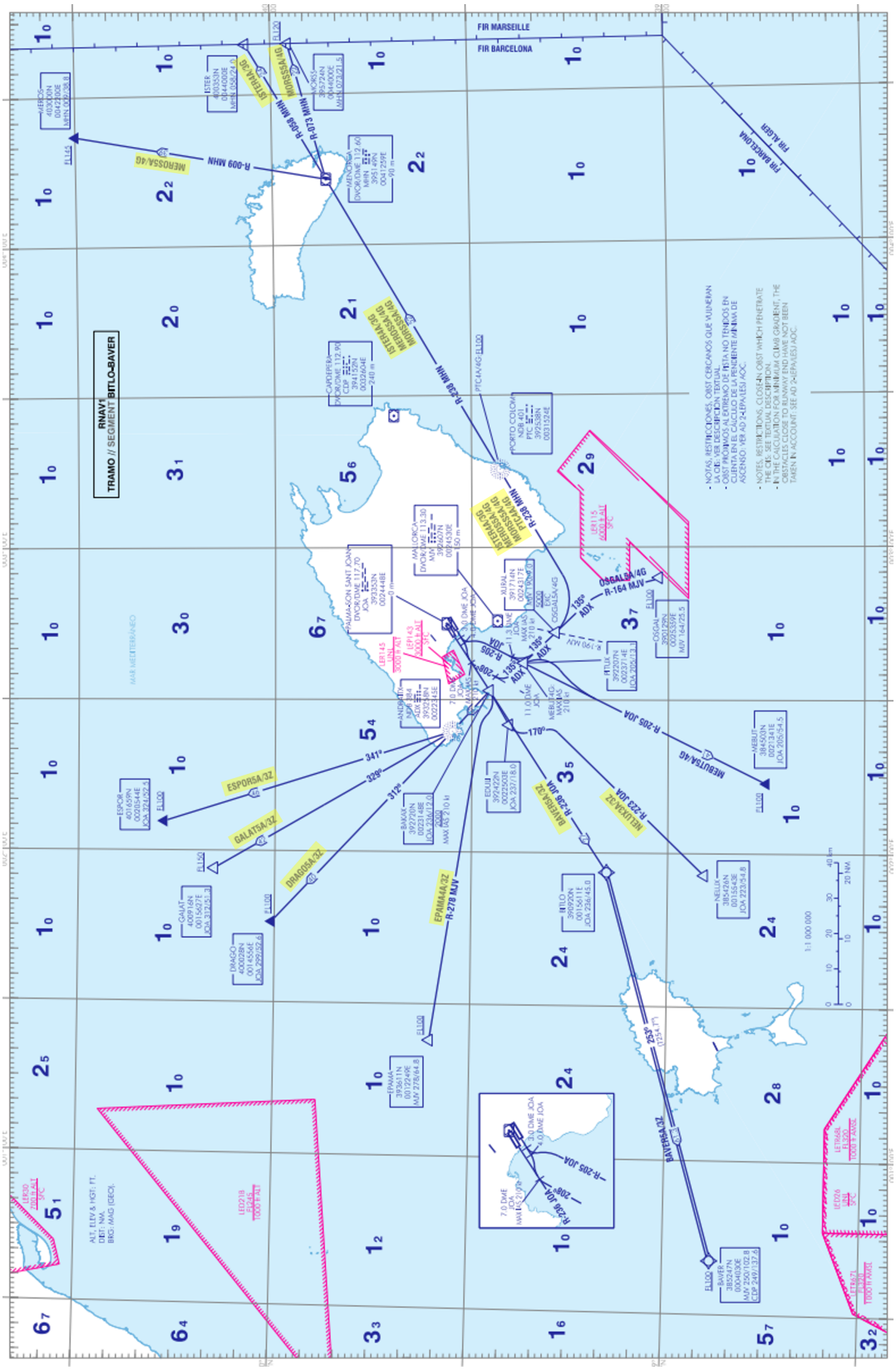

Figure A.2: LEPA Runway 24R SID Routes [61]

Barcelona - El Prat

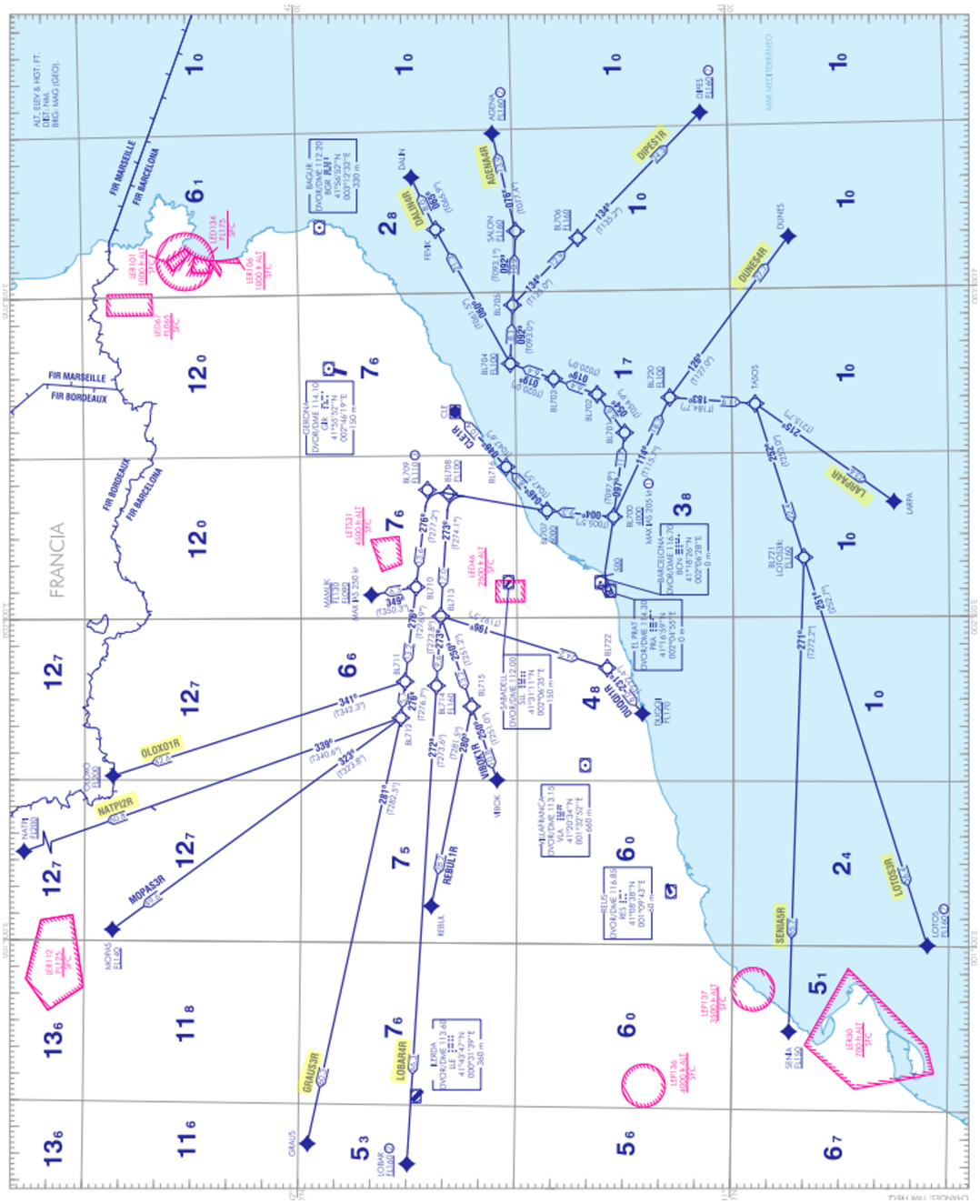

Figure A.3: LEBL Runway 06R SID Routes [62]

Madrid - Barajas

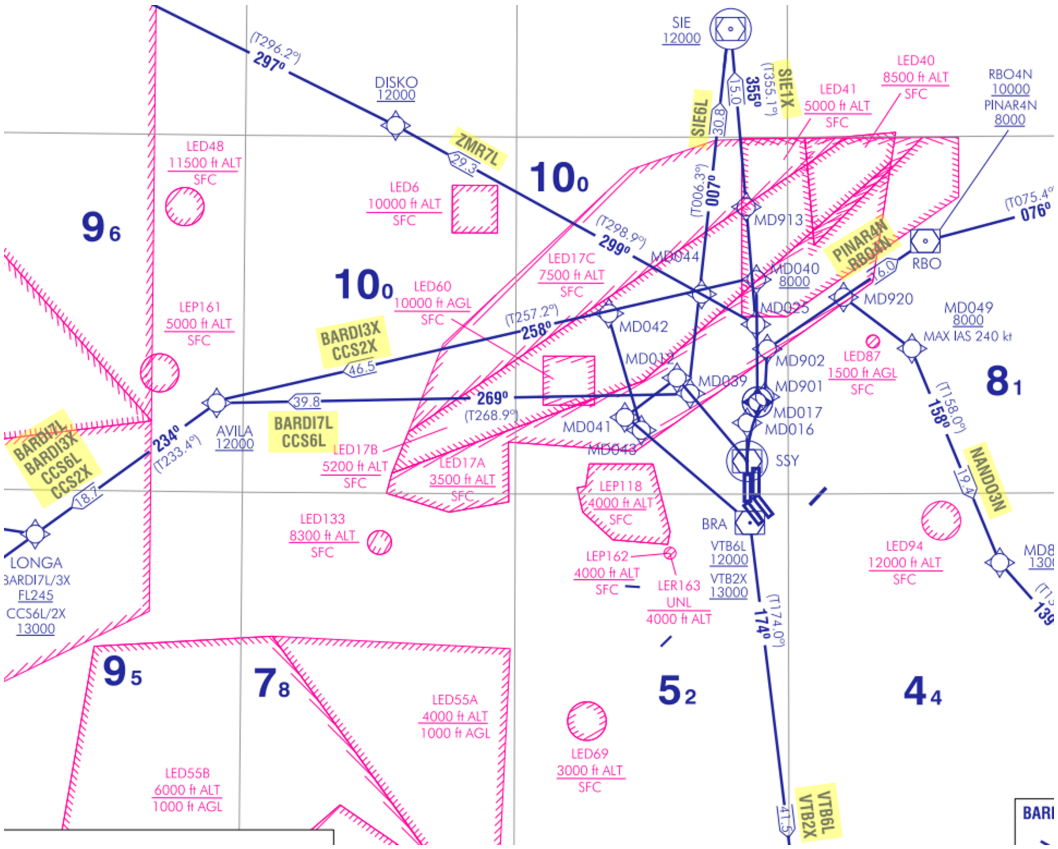

Figure A.4: LEMD Runway 36L SID Routes [63]

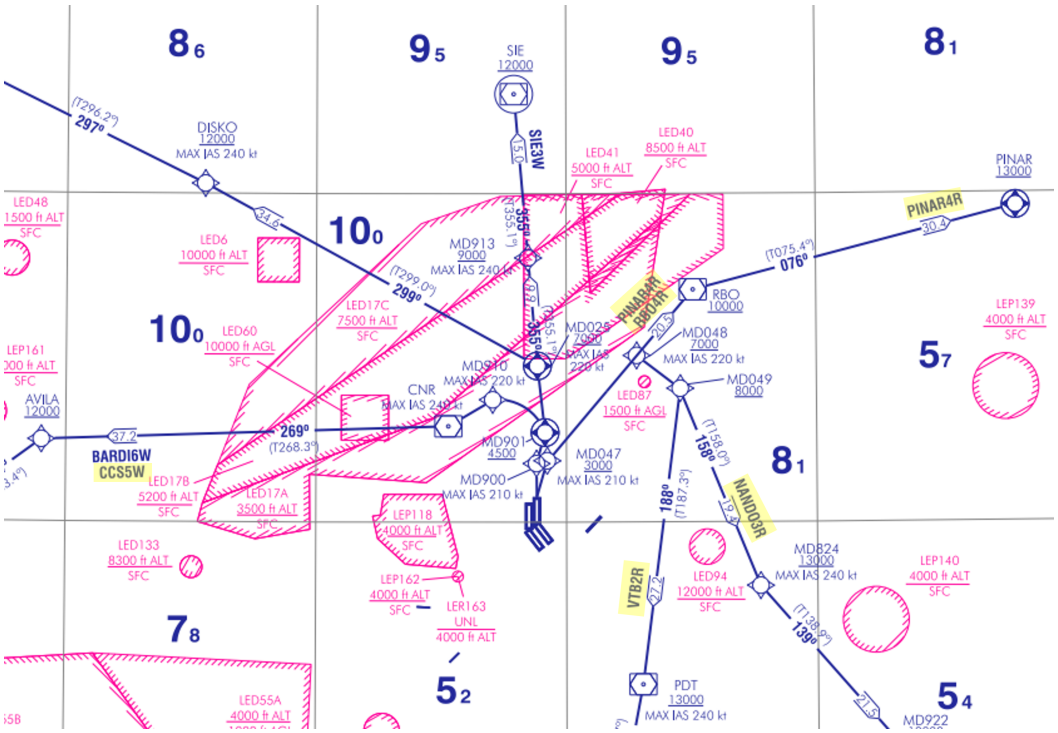

Figure A.5: LEMD Runway 36R SID Routes [64]

Tenerife Norte

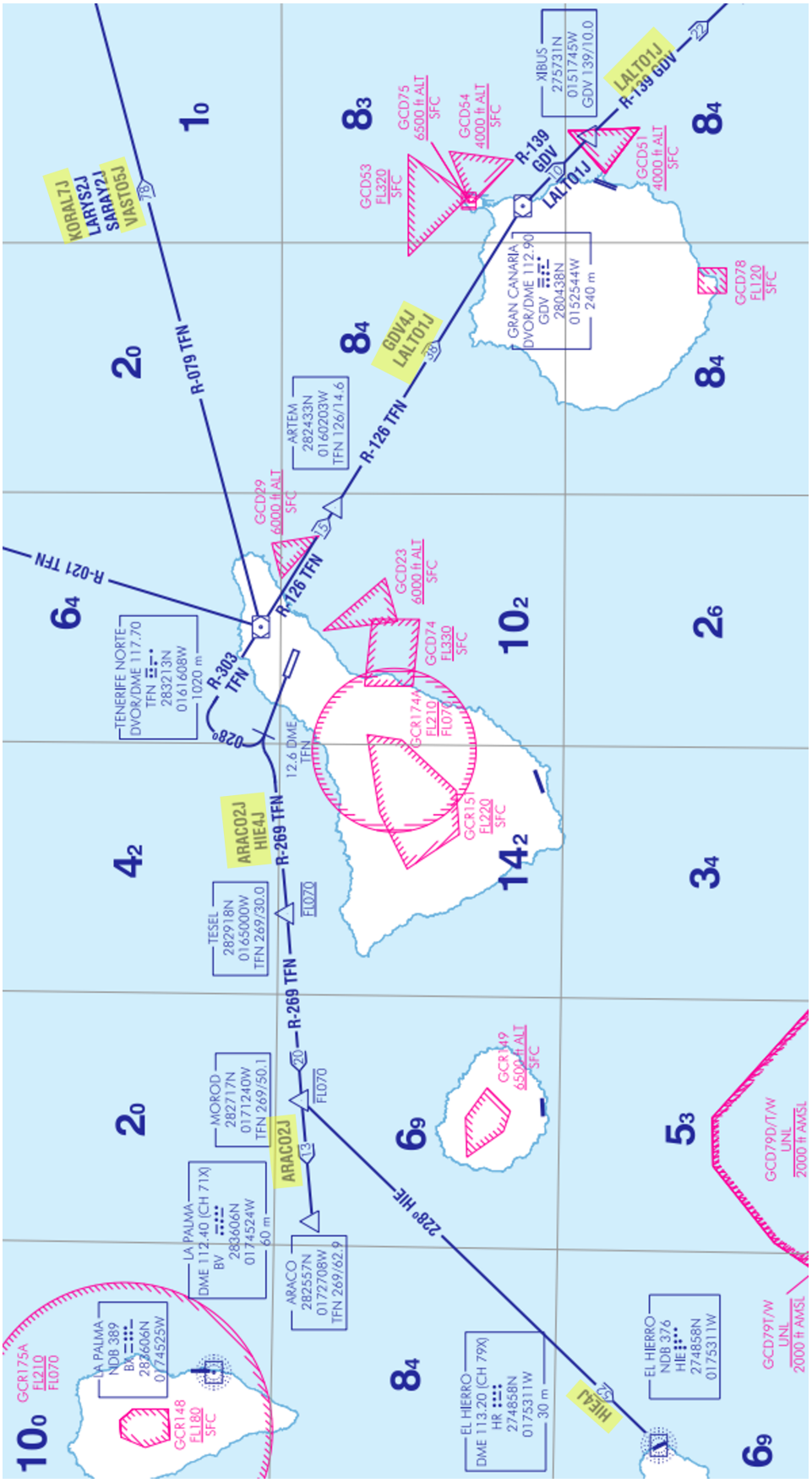

Figure A.6: GCXO Runway 30 SID Routes [65]

A.2. RECAT-EU-PWS Aircraft Categorisation

Table A.1: RECAT-EU-PWS complete categorisation [39]

A	A1	B	B1	B2	C	C1	C2	C3	C4
A124	A388	A337	A359	A332	A400	DC10	762	A306	752
		C5M	A35K	A333	AN70	MD11	763	A30B	753
		AN22	A345	A338	B701		764	A310	
			A346	A339	B720		IL76	IL62	
			741	A342	C135		IL86		
			742	A343	C17		L101		
			743	788	T204				
			744	789					
			748	78X					
			77L	772					
			77W	773					
				IL96					

D	D1	E	E1	E2	E3	F	F1	F2	F3
C919	A319	C700	CRX	AT76	CR2	A149	C680	C56X	B350
DC6	A320	F15	CR9	AT46	CL60	B407	E120	LJ35	C25A
E290	A321	F18H	CR7	DH8A	CN35	S76	D328	G150	C550
E295	A20N	F22	E170	DH8C	E135	S96	SF34	H25B	PA34
	A21N	F35	E190	DH8D	E145			PC24	PC12
	722	SU17	E195	FA7X	F2TH			LJ35	C180
	737	SU27	733	SB200	F900			LJ40	BE33
	738		734					LJ45	P28T
	739		735					LJ55	DA40
	B38M		GLEX					LJ60	
	BCS1		SU95						
	BCS3								
	MD88								
	MD90								
	TU154								

B

Planning

Proper planning prevents poor performance. With this principle in mind, this master's thesis has been structured to ensure a smart and efficient approach to answering the research questions and sub-research questions introduced in chapter 3.

To achieve this objective, the work has been divided into several work packages (WPs), each designed to address specific sub-research questions and collectively contribute to answering the main research question. section B.1 outlines the six primary work packages, detailing their respective objectives, required inputs, expected outcomes, and associated tasks.

WP0 focuses on the literature review, recompiling all necessary background information on runway capacity, the current state of the art, and the identification of existing research gaps. WP1 involves the development of the simulation model and is the main programming component of this thesis. In this phase, the theoretical foundations established in WP0 are integrated to construct a working discrete event simulation (DES) model for runway capacity analysis.

WP2 is dedicated to the selection of relevant scenarios, which are used both for model verification and validation, as well as for addressing the research questions. These scenarios are executed in WP3, where results are deeply analyzed, and the model undergoes verification and validation. WP4 encompasses the final stages of the thesis, including reporting, proofreading, and the preparation of a scientific paper. Finally, WP5 (closure package) includes code documentation and preparation for the greenlight meeting and thesis defense.

The Work Breakdown Structure (WBS), presented in section B.2, provides a hierarchical overview of all work packages, tasks, and subtasks. It illustrates the planned time allocation at varying levels of detail, offering a clear picture of the expected effort distribution throughout the project.

In addition, section B.3 presents the Gantt chart, which outlines the chronological sequence of all planned activities. It highlights key milestones such as the midterm and greenlight meetings, as well as task dependencies. The chart also incorporates scheduled vacation periods and buffer times to account for uncertainties.

Although the Gantt chart was developed at the early stages of the thesis, the planned timeline has been largely adhered to, with no significant delays. A minor deviation occurred in mid-February, when all simulation results had to be recomputed twice due to the availability of higher-quality input data, leading to improved accuracy. This issue was effectively managed by utilizing the allocated buffer time and dedicating additional effort during afternoons and weekends. In some cases, vacation and buffer periods were interchanged to maintain progress.

It is also important to note that this thesis was conducted under an 80% workload modality, where 80% of the time was dedicated to thesis work and the remaining 20% to company related projects. This distribution was accounted for during the planning phase and is reflected in both the Gantt chart and the WBS.

B.1. Work Packages

The workload for the thesis completion is divided into six primary work packages as illustrated in the Work Breakdown Structures (Figures B.1 B.2).

WP 0: Literature Review

Objective	Explore the state-of-the-art in runway system capacity, identify current methodology gaps, and define the research framework.
Input	RSC methodology papers, documentation on capacity advancements, existing software documentation, and academic databases.
Exclusions	This package focuses on theoretical foundations and does not include the actual coding of the simulation model.
Tasks	As presented in Figure B.1, this involves a nominal review of RSC background (10 days) and historical methods (4 days). It requires identifying research gaps (5 days) to formulate specific research questions (3 days). The package concludes with the research proposal reporting (7 days) and presentation (3 days), alongside a 7 day technical preparation phase to select and understand the RSC software.
Outcome	A finalized research proposal and a selected software baseline for the implementation phase.

WP 1: Simulation Model

Objective	Construct and verify a comprehensive simulation environment capable of modeling various runway configurations and separation standards.
Input	Theoretical logic for runway operations, TBS and RECAT-EU-PWS documentation.
Exclusions	Real-world airport data integration is excluded here, as it is handled in WP 2.
Tasks	This package forms the technical core (Figure B.1), starting with Single Runway (10 days) and Depending Runway (25 days) model construction. It includes the implementation of Time-Based Separation (4 days), RECAT-EU-PWS logic (4 days), and SID sequencing logic (3 days). A 5 day period is allocated for code and calculation verification to ensure mathematical integrity.
Outcome	A robust, verified simulation engine ready for scenario-specific testing, a solid version of the methodology and simulation chapters in the thesis report, and a proper midterm review presentation.

WP 2: Scenarios Selection & Evaluation

Objective	Identify and preprocess real-world airport and necessary input data to create realistic simulation scenarios.
Input	Airport navigation charts, flight schedules, speed profiles, ATM data, ROT recordings.
Exclusions	The actual execution of these scenarios is reserved for WP 3.
Tasks	This package involves investigating real-life airports and making a selection decision (3 days). Following this, a 7 day data preprocessing phase is required to collect ROTs, speed profiles, process flight schedules and gather all remaining input information for the runway capacity simulation software. Finally, the scenario definitions are documented in the thesis report (3 days).
Outcome	A set of finalized, complete scenarios for running the simulation model with.

WP 3: Result Analysis, Verification & Validation

Objective	Execute simulations across multiple scenarios and validate the outputs against real-life performance data.
Input	The verified simulation model (WP 1) and the selected airport scenarios (WP 2).
Exclusions	Performance tuning of the core code is excluded; this package is strictly for testing and validation.
Tasks	As detailed in Figure B.2, this involves 18 days of model scenario simulations across the four selected airports and specific RECAT-EU-PWS case studies. A 6 day sensitivity analysis is performed on TBS, RECAT-EU-PWS and other parameters, followed by a 5-day validation phase comparing results to other simulators and real-life observations.
Outcome	A validated dataset and graphs of results demonstrating the performance and sensitivity of the implemented separation models and simulation model.

WP 4: Thesis Finalisation Phase

Objective	Synthesize the research findings into a formal thesis document and a scientific paper.
Input	Results from the simulation, validation data, and initial literature review drafts.
Exclusions	Final code documentation is handled in the Closure package (WP 5).
Tasks	This involves 6 days of R,V&V reporting and a 3 day draft finalization. Significant time is allocated for feedback implementation (4 days) and the write-up of conclusions (3 days). Additionally, a 15 day period is dedicated to drafting a scientific paper for publication.
Outcome	A complete, high-quality thesis document and a corresponding scientific paper.

WP 5: Closure

Objective	Finalize the technical documentation and prepare for the academic defense.
Input	The finalized thesis report and the developed simulation code.
Exclusions	Further technical development or modification of the simulation results is excluded.
Tasks	This final package includes code documentation (5 days) to ensure future usability, preparation for the Greenlight meeting (3 days), and a 9 day intensive preparation phase for the final defense.
Outcome	Successful completion of the Greenlight milestone and the final thesis defense.

B.2. Work Breakdown Structure

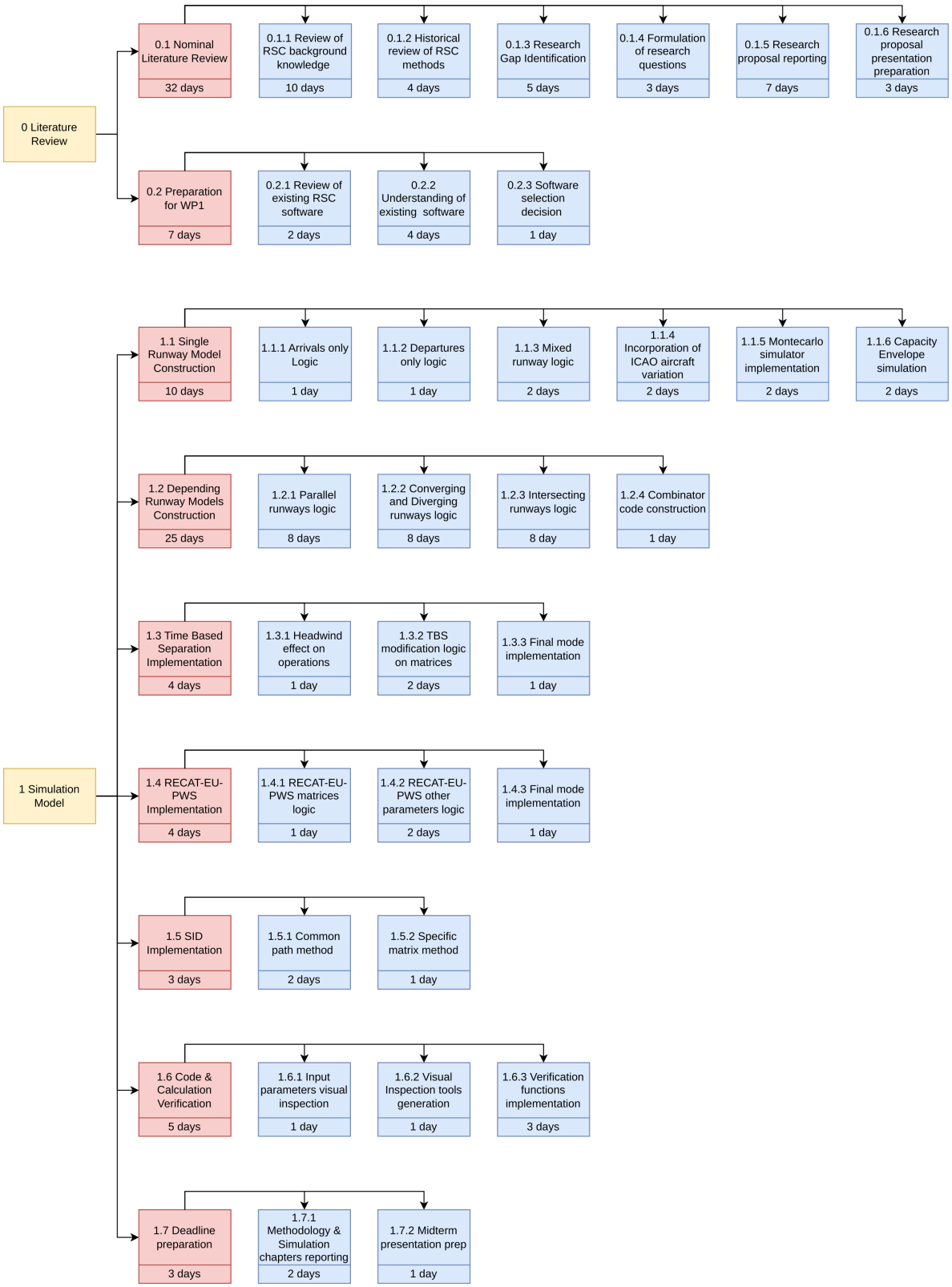

Figure B.1: Work packages 0 & 1 Breakdown Structure

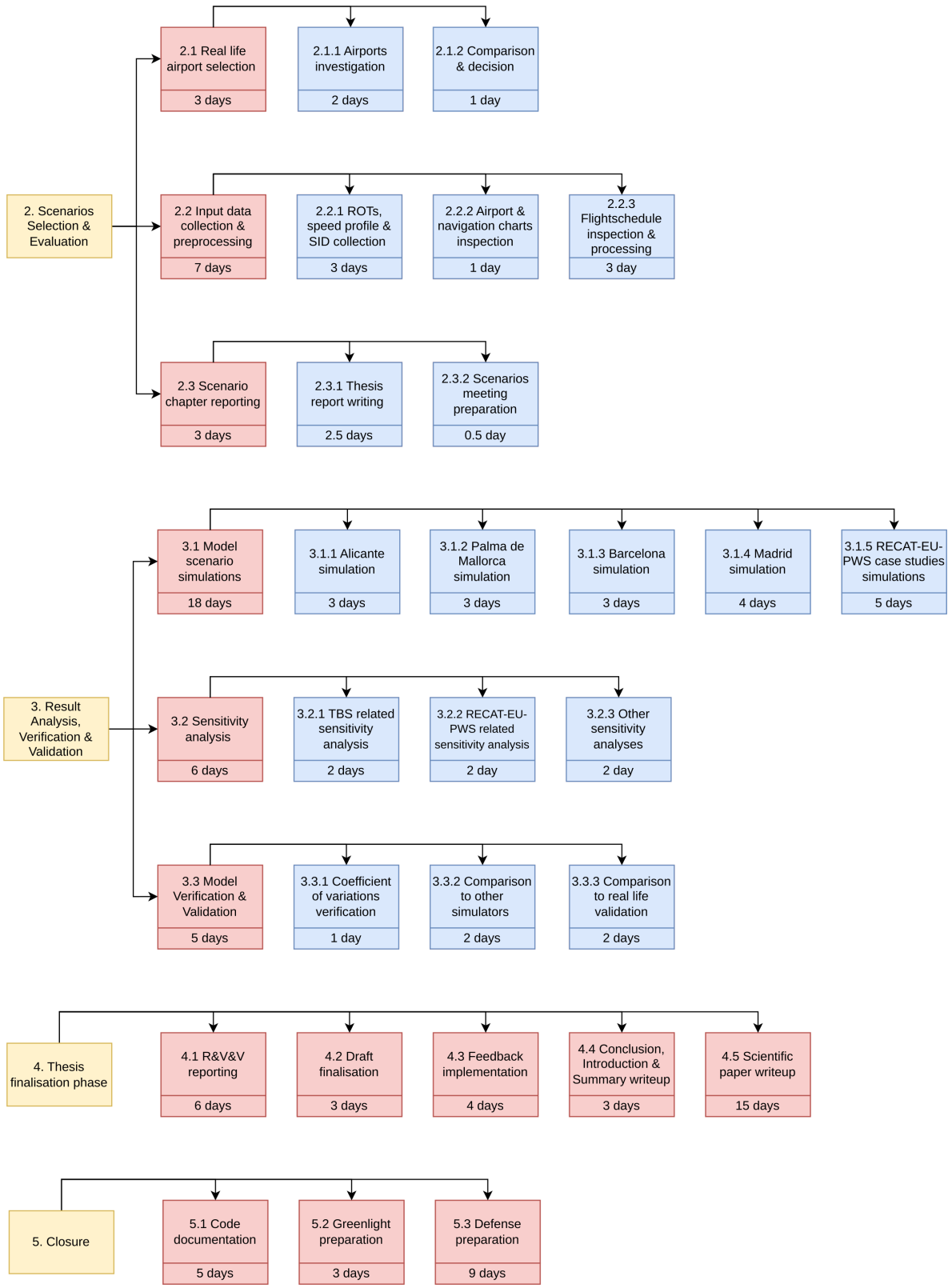

Figure B.2: Work packages 2,3,4 and 5 Breakdown Structure

B.3. Gantt Chart

Figure B.3: Final Gantt Chart

C

Technical Risk Assessment

Having established the project schedule and key deliverables, the next step is to identify the technical risks that may affect the successful completion of this Master's thesis (June 2025–May 2026). In this context, "technical" refers to the risks associated with data availability and quality, model implementation, verification and validation, computational reproducibility, and the robustness of results and conclusions. As with any research project, risks evolve over time; therefore, the risk register is treated as a living document and is reviewed at each major milestone (research proposal, mid-term review, draft hand-in, and final hand-in).

The risk register is presented in three parts. First, section C.1 identifies the main technical risks and summarises their cause, event, and effect. Second, section C.2 assigns each risk a numerical rating based on likelihood and impact. Finally, section C.3 defines mitigation strategies and assigns responsibility, after which residual likelihood and impact are estimated to assess the remaining exposure.

C.1. Risk Identification

The technical risks for this thesis are grouped into categories aligned with the project workflow:

- **DATA:** Risks related to obtaining, cleaning, and interpreting input datasets.
- **MODEL:** Risks related to implementing the methodology (algorithms, assumptions, parameterisation).
- **V&V:** Risks related to verification, validation, and benchmarking against reference methods/tools.
- **COMPUTE:** Risks related to computational resources, performance, and numerical stability.
- **COMMUNICATION:** Risks related to presenting results clearly and defensibly in the written thesis.

The identified technical risks are summarised in Table C.1.

Table C.1: Technical risks identification (Master's thesis, Jun 2025–May 2026)

ID	Name	Cause	Effect
R-DAT-01	Restricted data access / missing fields	Data not available due to licensing, confidentiality, or incomplete export	Scope reduction; weaker validation and reduced credibility of conclusions
R-DAT-02	Data quality issues (outliers, duplicates, time zones)	Inconsistent timestamps, encoding, airport identifiers, or aggregation rules	Erroneous results; additional time spent on cleaning and rework
R-DAT-03	Data loss (raw or processed datasets)	Insufficient backups, accidental deletion/overwrite, disk failure, or loss of access to shared drives	Rework of data pipeline and analyses; delays; potential loss of traceability and weakened results
R-MOD-01	Model implementation error	Coding mistakes, incorrect units, or misinterpretation of definitions	Invalid conclusions; loss of time during V&V stage
R-MOD-02	Sensitivity to assumptions / parameters	Strong dependence on chosen thresholds, distributions, or scenario settings	Low robustness; conclusions difficult to defend
R-VV-01	Insufficient verification and validation	Limited reference material, lack of ground-truth, or weak benchmarks	Reduced scientific quality; reviewer/supervisor concerns
R-VV-02	Misalignment between tools/benchmarks	Reference tools (e.g., legacy simulators or external benchmarks) use different assumptions	Confusing narrative; risk of misleading interpretation
R-COM-01	Computational bottlenecks	Large datasets, inefficient code, or heavy Monte Carlo/scenario runs	Delayed analysis and writing; fewer scenarios explored
R-COM-02	Reproducibility breakdown	Untracked code changes, missing seeds, environment drift, or poor documentation	Loss of confidence; time spent rerunning and debugging
R-COMM-01	Ambiguous or weak presentation of methods/results	Insufficient methodological clarity, missing limitations, or unclear figures/tables	Lower thesis quality; difficult defense and reduced impact

C.2. Risk Assessment

Given that different risks may affect the project in different ways, each risk is rated using a likelihood score (Probability of Occurrence) and an impact score (Severity of Consequences), each from 1 to 5. The overall risk rating will range in a 1-25 scale and is computed as:

$$\text{Risk rating} = \text{Likelihood} \times \text{Impact}. \tag{C.1}$$

Likelihood is expected to evolve throughout the thesis: for example, data-related risks are highest early (literature review/data acquisition), while reproducibility and communication risks peak near submission. 1 denotes very low probability and 5 denotes very high probability.

Impact is rated based on the potential severity of consequences for completion, scientific validity, and final deliverables. High-impact risks are those that can invalidate results, force major scope reduction, or prevent on-time submissions.

Table C.2: Initial technical risk ratings

ID	Likelihood (1–5)	Impact (1–5)	Rating (1–25)
R-DAT-01	3	5	15
R-DAT-02	4	4	16
R-DAT-03	3	5	15
R-MOD-01	3	5	15
R-MOD-02	3	4	12
R-VV-01	3	5	15
R-VV-02	2	3	6
R-COM-01	3	4	12
R-COM-02	4	4	16
R-COMM-01	3	4	12

C.3. Risk Mitigation

Mitigation strategies are grouped into four response types:

- **TREAT:** Reduce likelihood and/or impact through preventive actions.
- **TRANSFER:** Use third-party tools/expertise (e.g., supervisor feedback, institutional resources).
- **TERMINATE:** Avoid the risk by changing scope or approach to remove the failure mode.
- **TOLERATE:** Accept the risk where mitigation is impractical, while planning contingencies.

The mitigation plan in Table C.3 is aligned with the thesis timeline. In particular, data and definition lock-in is prioritised before September 2025 (proposal milestone), verification and validation is prioritised before December 2025 (mid-term), and reproducibility and writing quality are prioritised from January 2026 onwards.

Table C.3: Technical risks mitigation strategies and residual ratings

ID	Planned response
R-DAT-01	TREAT/TRANSFER: Confirm data access and permissions by December 2025; create a minimal viable dataset and a documented fallback (like a reduced scope airport set). Freeze data schema and definitions before the proposal milestone.
R-DAT-02	TREAT: Implement a reproducible data pipeline (unit tests for time zones, duplicates, airport IDs, and units); perform exploratory checks and summary statistics after every ingest; maintain a "data issues" log and cleaning rules appendix.
R-DAT-03	TREAT: Establish a robust backup strategy from project start: (i) keep raw data read-only and versioned, (ii) maintain at least two independent backups (local + cloud/institutional drive), (iii) automate weekly snapshots of the project directory (data, code, and outputs), and (iv) use checksums and a clear folder structure to prevent accidental overwrite. Perform a recovery drill once per semester to ensure backups are usable.
R-MOD-01	TREAT: Modularise code; add sanity checks (units, bounds, conservation constraints); validate intermediate outputs against hand calculations and toy examples; peer-review key functions with supervisor at the end of implementation stage.
R-MOD-02	TREAT: Run sensitivity analysis and report ranges rather than point estimates; justify parameter choices from literature; predefine scenarios and thresholds; include uncertainty discussion and limitations section.
R-VV-01	TREAT/TRANSFER: Plan V&V deliverables explicitly (verification suite + validation comparisons) by September 2025; validate against at least two reference points (e.g., observed operational envelopes and external benchmarks such as RCAP/PICAP where appropriate); document non-like-for-like assumptions.
R-VV-02	TREAT: Treat tool comparisons as "indicative" unless assumptions match; present harmonised conditions where possible and clearly label differences; avoid over-claiming; add a dedicated subsection explaining comparability and limitations.
R-COM-01	TREAT: Profile runtime early; cache intermediate results; run scenario batches overnight; restrict parameter grid to research questions; use vectorisation and efficient storage formats; prioritise "must-have" scenarios before April 2026.
R-COM-02	TERMINATE/TREAT: Use Git with tagged releases for milestones; lock environments (requirements file/conda); fix random seeds; automated re-run scripts; archive datasets and generated figures; perform a full clean rerun one month before hand-in.
R-COMM-01	TREAT/TRANSFER: Maintain a running thesis draft from January 2026; write methods while coding; enforce figure/table standards; schedule supervisor feedback cycles (draft chapter reviews) before Green Light and before final hand-in; include a limitations and reproducibility checklist.